https://doi.org/10.59761/RCR5136

BODIPY: synthesis, modification, and applications in sensing and biomedicine

Daniil V. Spector,[a] Daniil S. Abramchuk,[a] Vladislav V. Bykusov,[a] Anastasia O. Zharova,[a] Eva S. Egorova,[a] Alevtina S. Voskresenskaya,[a] Alexander R. Olovyanishnikov,[a] Ilia A. Kuzmichev,[b] Anna A. Bubley,[a] Roman L. Antipin,[a] Elena K. Beloglazkina,[a] Olga O. Krasnovskaya[a]

[a] *Lomonosov Moscow State University, Faculty of Chemistry, 119991 Moscow, Russia*
[b] *V.P.Serbsky National Medical Center for Psychiatry and Narcology, Ministry of Health of Russia, 119034 Moscow, Russia*

BODIPY chromophores (4,4-difluoro-4-bora-3a,4a-diaza-s-indacene) are one of the most versatile fluorophores which are commonly used in a variety of scientific fields. The combination of excellent photophysical properties with the possibility of easy chemical modification of structure, chemical and photostability determines the application of BODIPY in biomedicine, photocatalysis, analytical chemistry and materials science. This review summarizes approaches to the synthesis and modification of BODIPY, discussing both classical and recently-published synthetic and postfunctionalization approaches. An influence of BODIPY structure and various postfunctionalization methods on photophysical properties of the fluorophores and their potential applications in biomedicine, materials science and biosensorics are also discussed.
The bibliography includes 344 references.
Keywords: boron-dipyrromethenes, BODIPY, postmodification, photodynamic therapy, photothermal therapy, fluorescent probes, photocatalysis, J-aggregates.

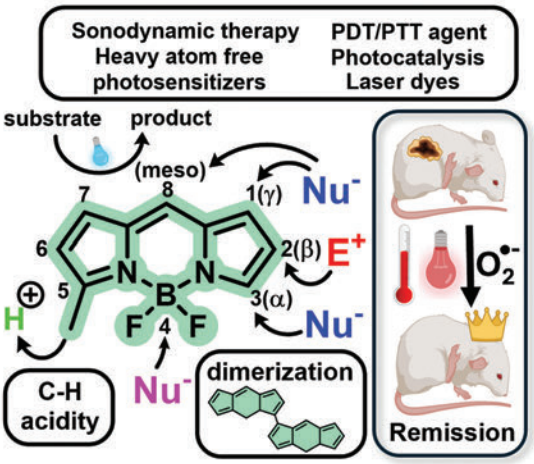

Contents

Received 4 June 2024

1. Introduction

Nowadays, 4,4-difluoro-4-bora-3a,4a-diaza-s-indacenes (BODIPY chromophores, or BDP) are considered to be a universal fluorophore scaffold. BODIPY derivatives are generally characterized by high fluorescence quantum yields, facile chemical modification, valuable photophysical properties, diverse array of chemical transformations, as well as exceptional optical and thermal stability.[1] Today, BODIPY-based dyes have a wide range of applications in various fields of scientific research — from biomedicine to materials science. These compounds are used as triplet photosensitizers,[2] agents for photodynamic (PDT) and photothermal (PTT) antitumor therapy,[3] as well as photocatalysts,[4] fluorescent labels for biomolecules,[5,6] photoremovable protecting groups[7] and light-harvesting systems.[8]

The BODIPY core is a deprotonated dipyrromethene ligand that coordinated with electron-deficient disubstituted boron atom, which is usually part of the BF_2 group[9,10] (Fig. 1). Formally, the negative charge is localized on the boron atom, while the positive charge is delocalized over the dipyrromethene system.[10] However, as the BODIPY molecule is weakly polar, the molecule is usually depicted without formal charges (see Fig. 1). Since the structure of the BODIPY core without substituents is similar to that of *s*-indacene, the numbering system of the BODIPY dyes is also analogous. The positions of the carbon atoms in the side rings of BODIPY are also named by analogy with pyrrole: thus, the α-position corresponds to atoms 3 and 5, the β-position — to atoms 2 and 6, and the γ-position — to atoms 1 and 7. Position 8 of the BODIPY core is also called the *meso*-position[10] (see Fig. 1).

A unique feature of BODIPY, which favorably distinguishes them from many other chromophores, is the ability to precisely tune its photophysical properties through various post-functionalization approaches.[10,11] For example, replacing the boron-bound fluorine with other nucleophile can lead to an increase in fluorescence quantum yields of BODIPY, improved chemical stability, increased water solubility.[12] In addition, it

D.V.Spector. PhD in Chemistry, Lead Engineer at the Organic Chemistry Department of Chemistry Faculty at Moscow State University. E-mail: danspector@yandex.ru
Current research interests: platinum-based anticancer agents, platinum(IV) prodrugs, photodynamic therapy agents, platinum(IV) coordination compounds with controlled photoactivation, boron-dipyrromethenes, riboflavin.
D.S.Abramchuk. PhD Student at the Organic Chemistry Department of Chemistry Faculty at Moscow State University.
E-mail: abr_daniil@mail.ru
Current research interests: boron-dipyrromethenes, tacrine, diagnostic agents for the diagnosis of Alzheimer's disease, optical probe, Alzheimer's disease therapy, copper-chelating organic compounds.
V.V.Bykusov. PhD Student at the Organic Chemistry Department of Chemistry Faculty at Moscow State University.
E-mail: vladbyk.2001@gmail.com
Current research interests: platinum-based anticancer agents, platinum(IV) prodrugs, photodynamic therapy agents, platinum(IV) coordination compounds with controlled photoactivation, boron-dipyrromethenes.
A.O.Zharova. MD Student at the Organic Chemistry Department of Chemistry Faculty at Moscow State University.
E-mail: moon17012003@gmail.com
Current research interests: platinum-based anticancer agents, platinum(IV) prodrugs, photodynamic therapy agents, platinum(IV) coordination compounds with controlled photoactivation, boron-dipyrromethenes, riboflavin.
E.S.Egorova. MD Student at the Organic Chemistry Department of Chemistry Faculty at Moscow State University.
E-mail: tigrbox23@gmail.com
Current research interests: platinum(IV) prodrugs, photodynamic therapy agents, organic synthesis, boron-dipyrromethenes
A.S.Voskresenskaya. MD Student at the Organic Chemistry Department of Chemistry Faculty at Moscow State University.
E-mail: margo.coyika762@gmail.com
Current research interests: boron-dipyrromethenes, tacrine, Alzheimer's disease.
A.R.Olovyanishnikov. MD Student at the Organic Chemistry Department of Chemistry Faculty at Moscow State University.
E-mail: dimethoxan@gmail.com
Current research interests: organic synthesis, boron-dipyrromethenes, tacrine, diagnostic and therapeutic agents for Alzheimer's disease.
I.A.Kuzmichev. Research Assistant at the Immunochemistry Laboratory of the V.P.Serbsky National Medical Research Center for Psychiatry and Narcology.
E-mail: ilyakuzmichev712@gmail.com
Current research interests: magnetic nanoparticles, polymeric nanoparticles and micelles, targeted drug delivery, surface modification of nanoparticles.
A.A.Bubley. Technician at the Organic Chemistry Department of Chemistry Faculty at Moscow State University.
E-mail: anka.bubley@yandex.ru
Current research interests: platinum-based anticancer agents, platinum(IV) prodrugs, photodynamic therapy agents, platinum(IV) coordination compounds with controlled photoactivation, boron-dipyrromethenes, riboflavin.
R.L.Antipin. PhD in Chemistry, Associate Professor at Organic Chemistry Department of Chemistry Faculty at Moscow State University.
E-mail: roman.antipin@gmail.com
Current research interests: synthesis, biologically active coordination compounds.
E.K.Beloglazkina. Doctor of Chemical Sciences, Professor at the Organic Chemistry Department of Chemistry Faculty at Moscow State University.
E-mail: beloglazki@mail.ru
Current research interests: coordination compounds, organic synthesis, biologically active coordination compounds.
O.O.Krasnovskaya. PhD in Chemistry, Senior Research Fellow at Organic.
E-mail: krasnovskayao@gmail.com
Current research interests: platinum(IV) prodrugs, organic synthesis, platinum-based anticancer agents, diagnostic and therapeutic agents for Alzheimer's disease.

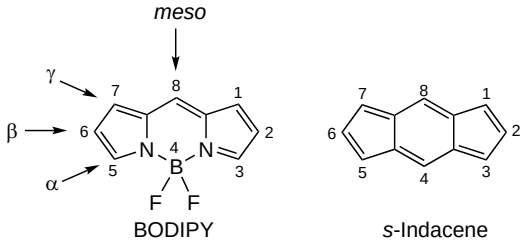

Figure 1. Atom numbering in BODIPY and *s*-indacene.

also opens up possibilities for the synthesis of light-harvesting systems.[12] Introduction of chiral substituents into BODIPY results in fluorophores with circularly polarized luminescence,[13] while conjugation of photoacceptor moiety to the BODIPY core paves the way for the formation of dyads, triads and other light-harvesting systems.[14] The introduction of heavy atoms into BODIPY promotes spin-orbit interaction and stabilization of the triplet state of fluorophores, which is widely used in the design of BODIPY-based PTT agents.[15] The presence of mesomeric donors in the BODIPY structure usually causes intramolecular charge transfer (ICT) and fluorescence quenching to occur in polar solvents; this phenomena is commonly used in the development of sensors for biomolecules, metal cations and pH changes, as well as for hypoxia diagnostics.[16,17]

The possibility of fine-tuning the physicochemical properties of BODIPY derivatives is attracting the attention of researchers, who are looking for new synthetic approaches and expanding the possibilities of the BODIPY core functionalising. A review of publications focused on these issues revealed a growing interest among specialists in both the discovery of new compounds and the modification of known synthetic methods. Thus, in 2023, new approaches were presented to the radical acylation of BODIPY,[18] the introduction of a cyano group into the core,[19] the use of photoexcitation of various derivatives to increase their reactivity,[20] and the modification of BODIPY at the boron atom with chalcogenophenes.[21] In 2024, methods for obtaining water-soluble carbohydrate derivatives,[22] BODIPY π-system expansion[23] and synthesis of fluorinated analogs were described;[24] reactions of electrophilic β-alkenylation[25] and soft electrochemical sulfonylation were studied;[26] new one-pot synthesis options for 3-substituted BODIPY were also presented.[27] Thus, the relevance of developing new approaches to the synthesis and modification of the BODIPY core is beyond doubt.

An important area of BODIPY application is the photocatalysis of various organic transformations. Thus, in 2021, BODIPY were used as photocatalysts for ion-radical addition to alkenes,[28] and in 2022, the BODIPY photocatalyzed Beckmann rearrangement was described.[29]

The enormous interest in BODIPY as highly stable fluorophores with valuable photophysical characteristics and the ability to fine-tune their photophysical properties has resulted in a large number of publications. Many works are devoted to the development of BODIPY-based agents for PTT and PDT,[30–33] for sonodynamic therapy[15] and photoacoustic imaging,[34] as well as fluorescent probes, which are used in the analysis of food objects, water, detection of biomolecules *in vitro* and *in vivo*.[35,36]

Various areas of BODIPY application are summarized in a number of review publications. In 2014 Ni and Wu[37] published a review on the synthesis and application of NIR-absorbing BODIPY (NIR — near infrared) as fluorescent pH-sensitive probes for bioimaging. In the same year, a review was published on the structural modifications of the BODIPY core that lead to a shift of the absorption maximum in electronic spectra towards the NIR region.[38] In 2019, Chen *et al.*[39] generalized the data on the development of triplet photosensitizers based on BODIPY and also summarized the structural factors contributing to internal conversion. A year later Poddar and Misra[40] published a review examining optoelectronic applications of BODIPY. In 2021, a review paper dedicated to the use of BODIPY as reporters of molecular processes in a living cell was published in the *Russian Chemical Reviews*[41] journal. In 2023, Wang *et al.*[42] presented a review on BODIPY-based photosensitizers, and Zhang *et al.*[43] summarized the data on photoactivated BODIPY for PALM (photoactivated localization microscopy). In addition, several reviews devoted to the synthesis and chemical properties of BODIPY were published. In 2007, Loudet and Burgess[9] published a fundamental and comprehensive analysis of the preparation and postfunctionalization of BODIPY and its derivatives, including aza-BODIPY and dipyrromethenes, and a year later Ulrich *et al.*[1] presented a brief overview of BODIPY functionalization methods and their applications. In 2019, a detailed review dedicated to the postfunctionalization of BODIPY was published by Boens *et al.*[10] In the same year, Clarke and Hall[44] published a review summarizing recent advances in the synthesis of BODIPY, and Nascimento *et al.*[45] summarized methods for the preparation of dipyrromethanes. Of recent work, a brief review from 2023 by Yadav and Misra[46] on the synthesis, functionalization of BODIPYs and their application as PDT agents is worth mentioning.

This review summarizes recent advances in the chemistry of boron-dipyrromethenes, including synthetic tools and methods and approaches for modifying of the BODIPY structure, as well as their various applications, including as sensors, antitumor agents, and optical materials. In particular, information is presented on the synthesis of the boron-dipyrromethene core and methods for its modification, such as reactions involving the BODIPY aromatic ring and CH-acid methyl groups as well as substituents at the boron atom. In addition, the influence of chemical transformations and structural factors on the photophysical properties of BODIPY are discussed in the context of their potential practical applications. The factors contributing to the increase in the effectiveness of the BODIPY derivatives as PDT and PTT agents are analyzed, and the most successful approaches to the design of antitumor agents based on them are noted. Particular attention is paid to the use of BODIPY as fluorescent sensors, and agents for cellular organelles visualization, for detecting specific environmental conditions and specific compounds, such as biothiols, acyl chlorides, hypochlorite anion, reactive oxygen species (ROS), Hg^{II} ions. Photophysical aspects of the fluorescence response are discussed.

Given the high interest in the use of BODIPY and their derivatives in biomedicine and optoelectronics, and taking into account the large number of publications on this topic in highly rated scientific journals, we believe that this review will be of interest to a wide range of specialists in organic and medicinal chemistry. The material published in the review may be useful both in choosing a strategy for the synthesis and functionalization of the BODIPY molecules, and in designing of the BODIPY derivatives with specific photophysical properties and biological activity for biomedical applications, among others.

Scheme 1

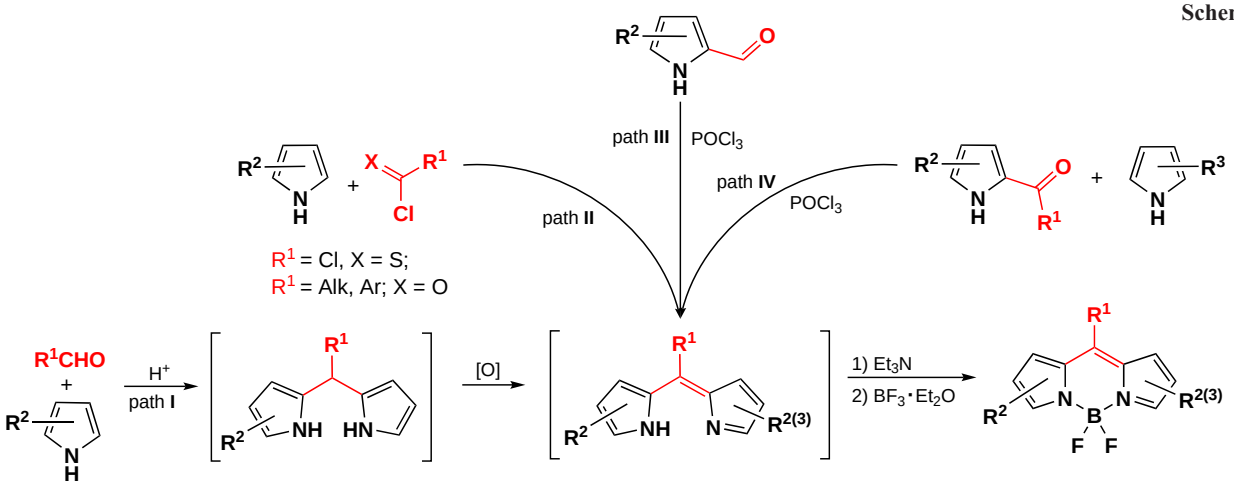

2. Methods of BODIPY derivatives preparation

Over the last few decades, studies devoted to the design of the BODIPY fluorophores have led to the development of a large number of diverse synthetic approaches that have opened the way to the preparation of boron dipyrromethenes with different structures and different photophysical properties (Scheme 1). The methods for synthesis of the BODIPY core can be divided into two main types: preparation of dipyrromethanes with subsequent oxidation (path I) or direct synthesis of dipyrromethenes formed from pyrroles and acyl chlorides (path II), by self-condensation of acylpyrroles in the presence of $POCl_3$ (path III) or *via* a reaction between acylpyrrole and pyrrole (path IV). Approaches **I** through **IV** are discussed in this section.

2.1. Synthesis from pyrroles and aldehydes

A common method for the synthesis of BODIPY is the condensation of aromatic aldehydes and pyrroles, described by Wagner and Lindsey[47] in 1996. Acid catalysis produces symmetric dipyrromethane, which is further oxidized by 2,3-dichloro-5,6-dicyano-1,4-benzoquinone (DDQ) and p-chloranil to form dipyrromethane. Further base action followed by complexation under the action of boron trifluoride etherate yields the target BODIPY fluorophores. α-Substituted pyrroles, such as 2,4-dimethylpyrrole, are commonly used to inhibit the polymerization side reaction.[48–50] In the case of unsubstituted pyrrole, the dipyrromethane production step is carried out directly in the pyrrole, after which the dipyrromethane is isolated and introduced into successive oxidation and complexation reactions (Scheme 2)†.[51–53] The alkyl derivatives of BODIPY, such as compound **1a**, are characterized by absorption maxima in the range of 490–500 nm, a Stokes shift of 5–10 nm, and bright fluorescence. It should be noted that the

Scheme 2

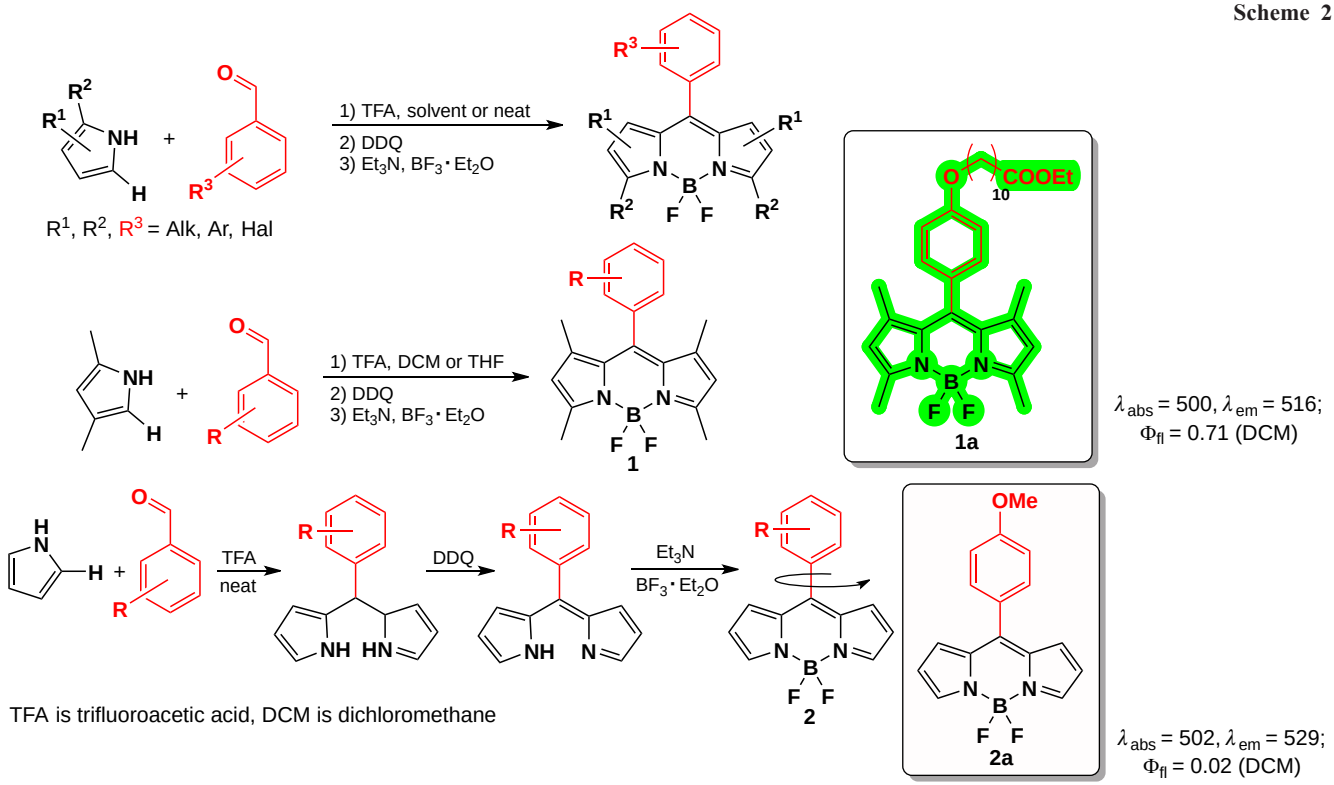

BODIPY derivative **2a** with free positions 1, 3, 5, and 7 exhibits almost no fluorescence due to the free rotation of the aryl substituent around the C–C bond. [54]

In 2024, Kang *et al.*[27] proposed the synthesis of meso-aryl-substituted 3-pyrrolyl-BODIPY by condensation of aromatic aldehyde with pyrrole in the presence of catalytic amounts of iodine as a weak Lewis acid[55] (Scheme 3). The key benefit of this approach is the potential for a one-pot synthesis, yielding 3-pyrrolyl-BODIPY **3** with an absorption maximum in the 580–600 nm spectral range.

Scheme 3

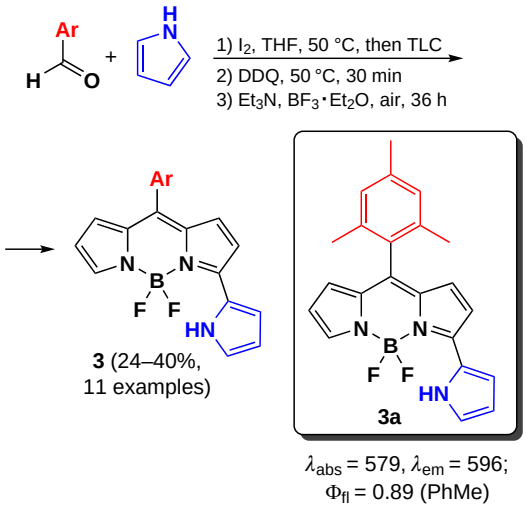

λ_{abs} = 579, λ_{em} = 596;
Φ_{fl} = 0.89 (PhMe)

Another method of one-pot synthesis of BODIPY with a red-shifted absorption maximum is the use of condensed pyrroles as starting material. Thus, a series of PDT-active BODIPY **4** was prepared by Yoon *et al.*[56] from various benzaldehydes and 6-methyl-4*H*-thieno[3,2-*b*]pyrrole (Scheme 4). Due to the presence of a condensed thiophene moiety, BODIPY **4** exhibited enhanced spin-orbit coupling (SOC) in combination with a reduced energy gap between the singlet and triplet states.

Zhao *et al.*[57] in 2022 synthesized a BODIPY-based fluorescent probe **5** for the detection of hypochlorous acid

Scheme 4

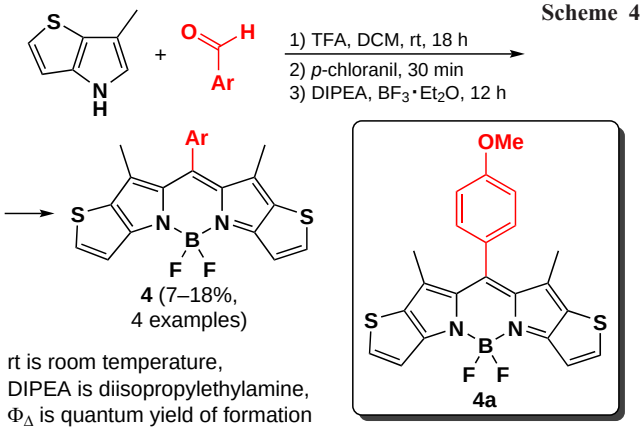

rt is room temperature,
DIPEA is diisopropylethylamine,
Φ_Δ is quantum yield of formation of active oxygen species

λ_{abs} = 564, λ_{em} = 579;
Φ_{fl} = 0.171, Φ_Δ = 0.89 (PhMe)

(Scheme 5). The fluorescence of BODIPY **5** was significantly suppressed due to photoinduced electron transfer (PET) from the electron-rich BODIPY core to the electron-deficient benzylpyridinium fragment (Φ_{fl} = 0.024). In the presence of HClO, the dimethylthiocarbamate fragment was cleaved off, resulting in an increase in fluorescence (Φ_{fl} = 0.51).

2.2. Synthesis from pyrroles and acid chloranhydrides or anhydrides

Condensation of pyrroles with carboxylic acid chloranhydrides or anhydrides is also widely used to obtain meso-substituted BODIPY **6**–**8**.[58] The advantage of this approach is that both aromatic[59] and aliphatic chloranhydrides,[60] as well as chloranhydrides of bidentate carboxylic acids,[61] can be used as substrates for BODIPY synthesis. In addition, cyclic anhydrides can serve as starting compounds, yielding BODIPYs with a meso-carboxylic group[62,63] (Scheme 6).

In 2020, Mhlongo *et al.*[64] proposed to use microwave (MW) radiation to carry out the condensation of pyrrole and glutaric anhydride, BODIPY **9** was obtained. The stage of dipyrromethene formation under these conditions took 15 min (Scheme 7).

Microwave irradiation was also used by Lama *et al.*[65] in 2022 for one-pot synthesis of BODIPY **10** from pyrroles and aromatic (*e.g.*, for **10a**) or aliphatic (for **10b**) chlorohydrides. The reaction was carried out under gentle heating in a minimal volume of

Scheme 5

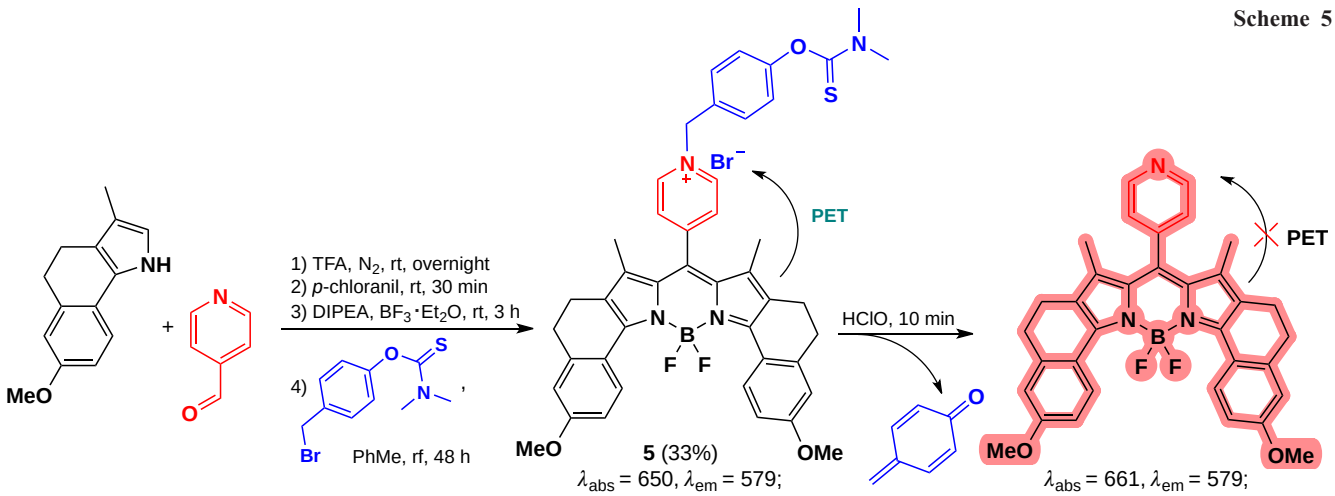

AcN is acetonitrile, PBS is phosphate-buffered saline

λ_{abs} = 650, λ_{em} = 579;
Φ_{fl} = 0.0241
(AcN–PBS (1:1))

λ_{abs} = 661, λ_{em} = 579;
Φ_{fl} = 0.5118
(AcN–PBS (1:1))

† Absorption (λ_{abs}) and emission (λ_{em}) maxima in the electronic spectra (in nm), as well as fluorescence quantum yield (Φ_{fl}) are given under the formulas of specific compounds; the solvent is indicated in brackets

Scheme 6

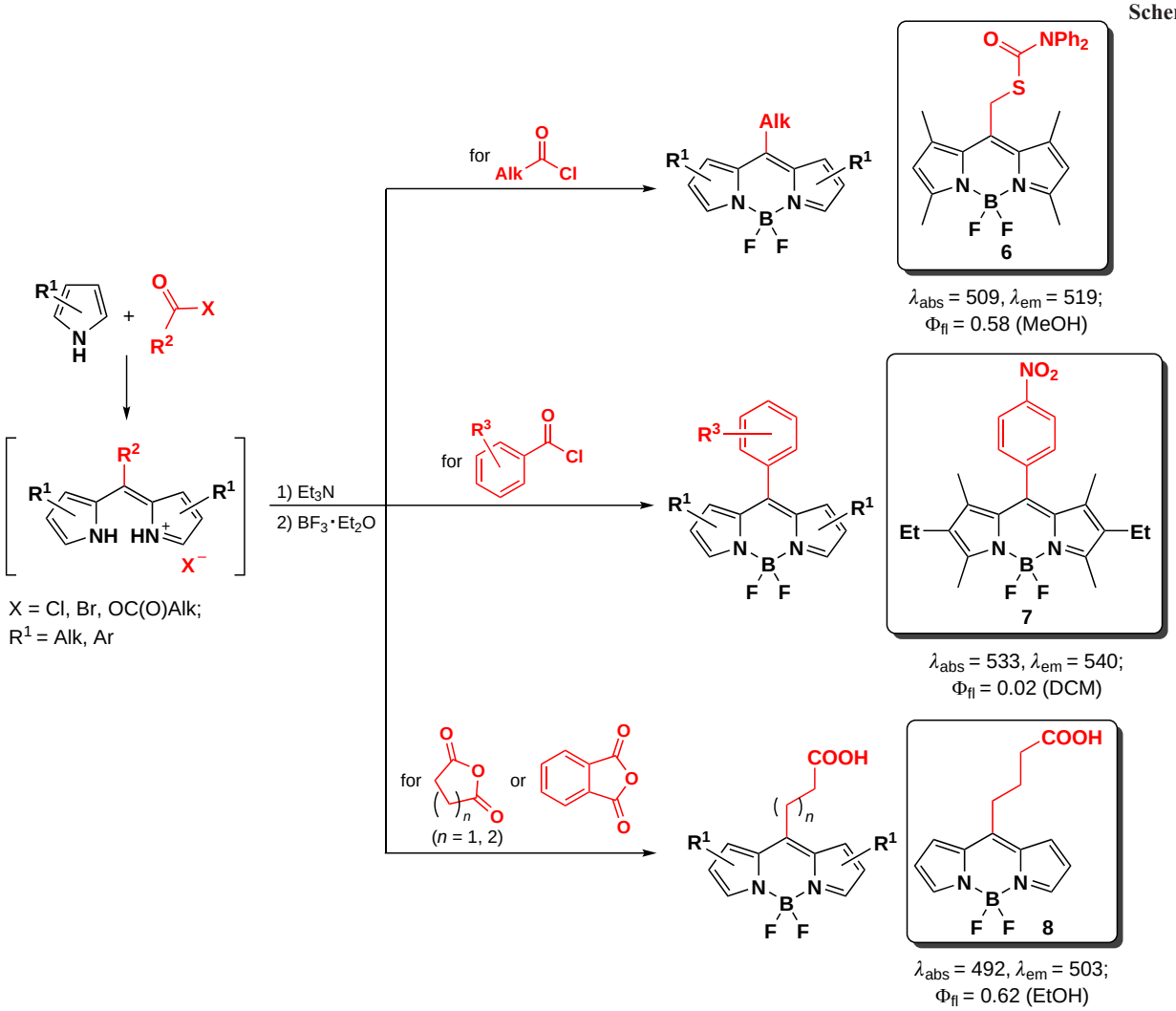

Scheme 7

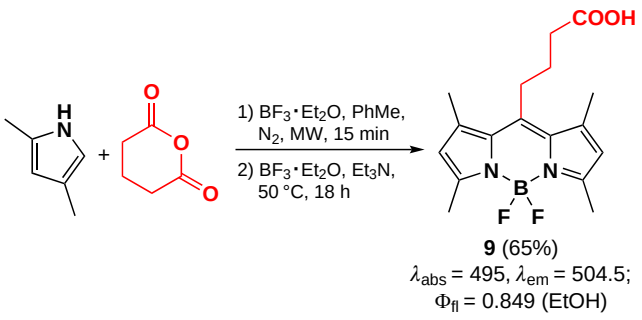

Scheme 8

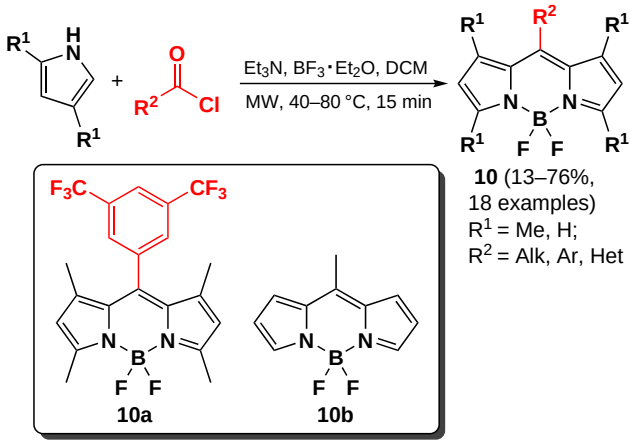

solvent, and the synthesis of BODIPY **10** in gram quantities was shown to be possible (Scheme 8).

2.3. Synthesis from acylpyrroles and pyrroles

Unsymmetrical BODIPY with two different pyrrole cycles can be synthesized by condensation of α-ketopyrroles with other pyrroles. When pyrrole-2-carbaldehyde is used as a starting reagent, BODIPY derivatives without a substituent at the meso-position are formed.[66–70] This method also allows the preparation of unsymmetrical BODIPY with a carboxyl group in one of the pyrrole cycles available for further functionalization.[71,72] When condensed pyrroles are used as substrates, the resulting BODIPYs are characterized by absorption in the NIR region and high molar absorption coefficients.[73–75] Another modification of this approach is the use of an α-iminium salt of a pyrrole, which can be obtained by the Wilsmeyer–Haack formylation, as the starting compound. It is worth noting that pyrroles[76] and their condensed analogs, particularly isoindole,[77] can be used as substrates for the formylation (Scheme 9).

Following this approach, in 2023 Spingler *et al.*[78] synthesized a series of highly active PTT agents **11** based on asymmetric

Scheme 9

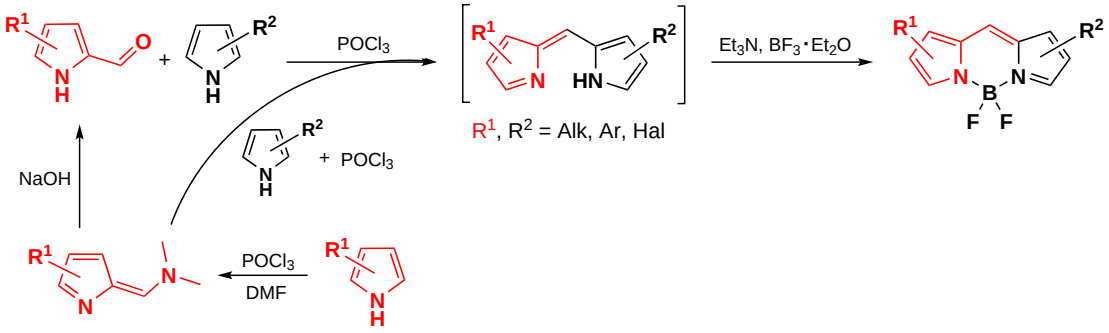

BODIPYs with a thiophene moiety at position 3. BODIPY **11a** was highly phototoxic in the nanomolar concentration range under NIR radiation at a wavelength of 630 nm (total irradiation dose 5 J cm^{-2}) (Scheme 10).

Scheme 10

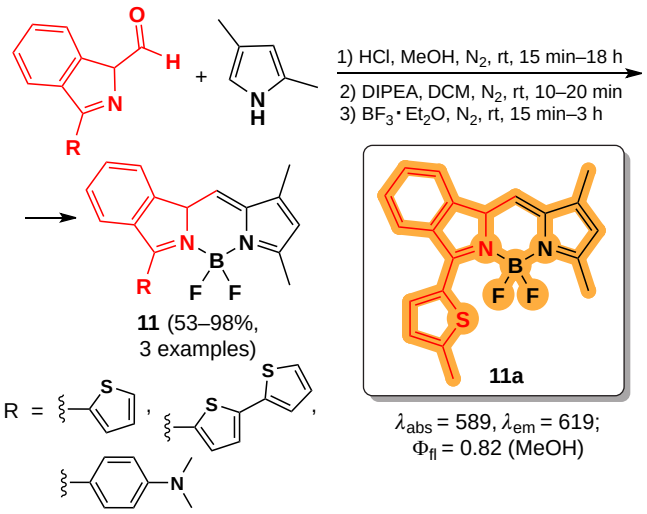

In 2024, Uriel *et al.*[22] have proposed an approach for the synthesis of BODIPY-based α-glycosides **12** formed by condensation of the corresponding α-glycosidopyrrole and 3,5-dimethylpyrrole-2-carbaldehyde. The BODIPY obtained, such as mannoside **12a**, exhibited bright fluorescence (Φ_{fl} = 0.7–1) in organic solvents, while the deacylated derivative **12b** showed fluorescence in aqueous media (Scheme 11).

Condensed BODIPY **13** was synthesized from 2,4-dimethylpyrrole and uracil -based pyrrole-2-carbaldehyde by Nagpal *et al.* in 2024.[23] (Scheme 12). The BODIPY **13** showed the ability to form singlet oxygen ($^1O_2$) upon irradiation and PDT activity on rat C6 glioblastoma cells.

2.4. $POCl_3$-catalyzed self-condensation of pyrrolcarbaldehydes

An attractive way to synthesize symmetric BODIPYs with unsubstituted meso-position is the self-condensation of pyrrolcarbaldehydes in the presence of $POCl_3$. This approach was developed by Wu and Burgess[79] in 2008 for the synthesis of a series of BODIPY **14** (Scheme 13). The resulting fluorophores exhibited absorption in the NIR region as well as a bright fluorescence (Φ_{fl} = 0.7–1). BODIPY **15** were obtained in a similar way from condensed and aryl-substituted pyrroles.[70,75]

Scheme 11

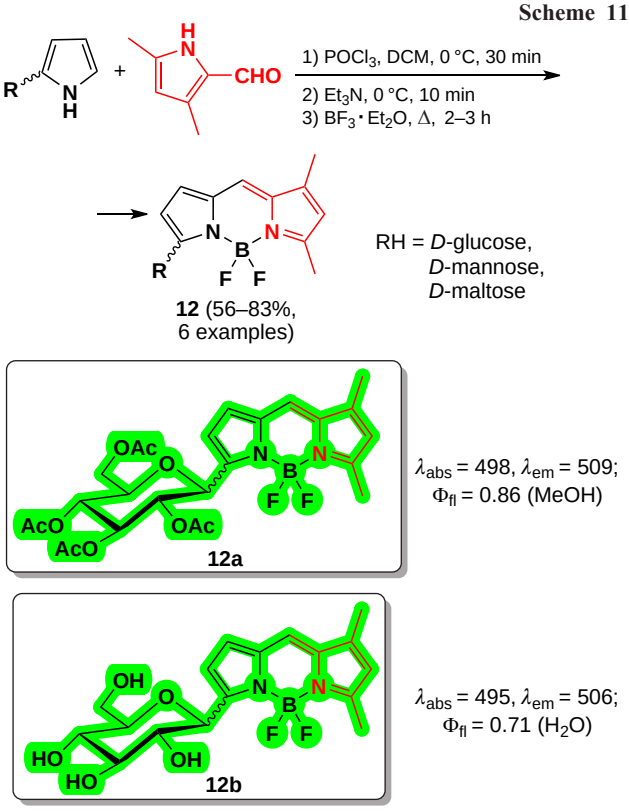

2.5. Preparation of 8-heteroatom-substituted BODIPYs

2.5.1. 8-Sulfanyl derivatives

8-Methylsulfanyl-BODIPYs can be obtained by using thiophosgene as the carbonyl component in condensation with pyrroles. Such BODIPYs are utilized as substrates in nucleophilic substitution and cross-coupling reactions.[10] Three 8-methylsulfanyl BODIPYs **16**, including the 3,5-dimethyl-8-methylsulfanyl-BODIPY **16a**, were synthesized for the first time in 2006 by Goud *et al.*[80] The authors first prepared a dipyrrolylthioketone from pyrrole and thiophosgene. then methylated it at the sulfur atom followed by a complexation reaction with $BF_3 \cdot Et_2O$ (Scheme 14). In the following work,[81] a series of other 8-methylsulfanyl-BODIPYs were synthesized, including BODIPY **16b** with methyl groups at positions 1, 3, 5, and 7. The emission suppression of the polymethyl derivative **16b** was observed due to the removal of the 8-SMe group from electronic coupling with the BODIPY core because of steric hindrance with the methyl groups at positions 1, 7.[81] In 2022, 1,3,5,7-tetramethyl-8-methylsulfanyl-BODIPY **16b** was used as a photocatalyst for Beckmann rearrangement and oxime

Scheme 12

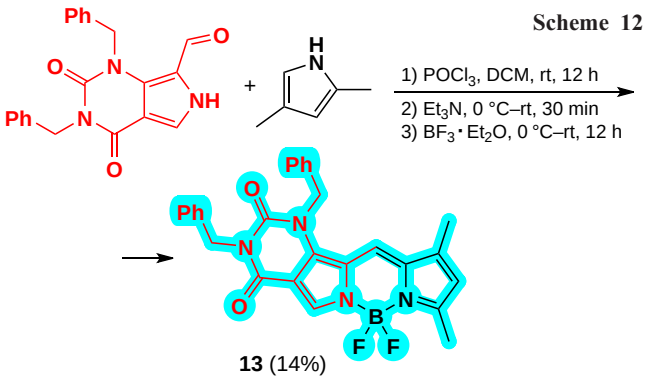

13 (14%)
λ_{abs} = 484, λ_{em} = 495;
Φ_{fl} = 0.095, Φ_D = 0.14 (AcN)

Scheme 13

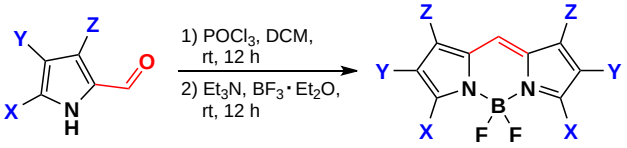

X, Y, Z = Alk, Ar, Cb;
Cb is carbocycle

14 (21–92%, 8 examples)

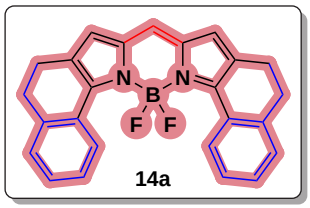

14a

λ_{abs} = 629, λ_{em} = 637;
Φ_{fl} = 0.78 (DCM)

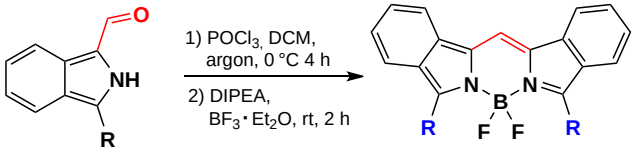

R = Ar, Het

15 (41–73%, 5 examples)

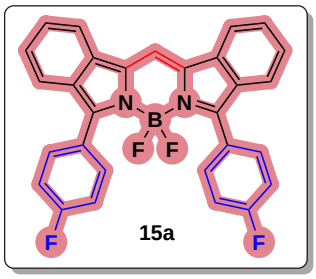

15a

λ_{abs} = 646, λ_{em} = 674;
Φ_{fl} = 0.78 (PhMe)

hydrolysis.[29] The SMe-group at the meso-position promotes intersystem crossing (ISC) and the formation of a triplet excited state in which such BODIPY reacts with an electron donor to form an anion radical.

2.5.2. 8-Halogen derivatives

In 2012. Leen *et al.*[82] described the synthesis of meso-chloro- (**17**) and meso-bromo-BODIPY (**18**) by reaction of dipyrrolyl ketone with phosphorus oxochloride or oxobromide followed by treatment with base and complexation with boron trifluoride esterate. A direct synthesis of 8-iodo-BODIPY **19** using this approach is not possible, but 8-iodo-BODIPY **19** can be obtained from 8-chloro-BODIPY **17** by the Finkelstein reaction with sodium iodide. The initial dipyrrolyl ketone can be synthesized by condensation of pyrrole with thiophosgene followed by oxidation with hydrogen peroxide[83] (Scheme 15). It should be noted that the nature of the halogen atom at the *meso*-position has a negligible effect on the absorption and emission wavelengths of resulted BODIPYs. Nevertheless, the decrease in the fluorescence quantum yields with increasing halide ion size is in good agreement with the 'heavy atom' effect. The

Scheme 15

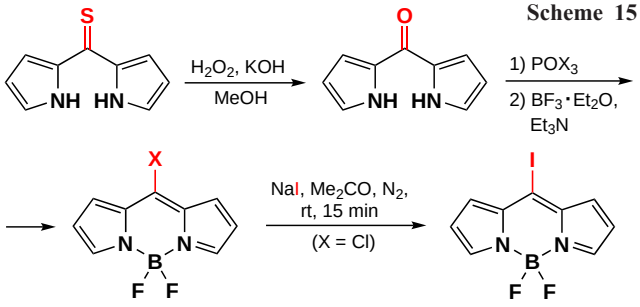

17, **18**

19 (66%)
λ_{abs} = 507, λ_{em} = 519;
Φ_{fl} = 0.16 (THF)

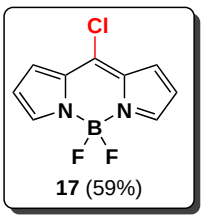

17 (59%)

λ_{abs} = 503, λ_{em} = 515;
Φ_{fl} = 0.72 (THF)

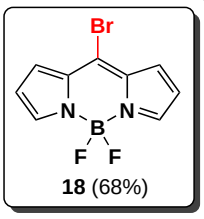

18 (68%)

λ_{abs} = 504, λ_{em} = 517;
Φ_{fl} = 0.50 (THF)

X = Cl, Br

Scheme 14

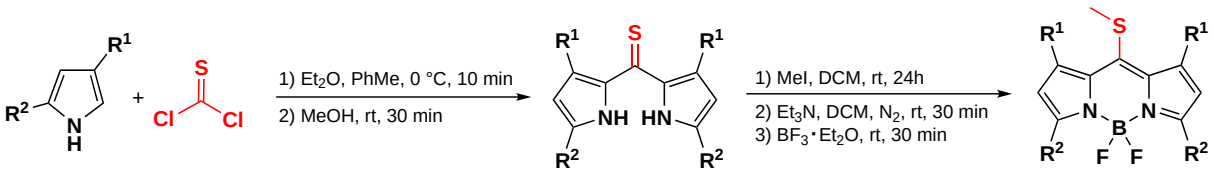

R^1, R^2 = Alk, H

16 (58–70%, 4 examples)

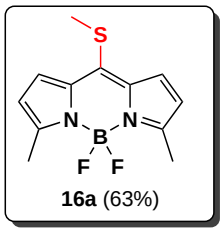

16a (63%)

λ_{abs} = 530, λ_{em} = 554;
Φ_{fl} = 0.37 (MeOH)

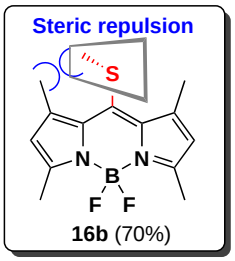

16b (70%)

λ_{abs} = 521, λ_{em} = 544;
Φ_{fl} = 0.006 (MeOH)

photophysical properties of halogen-containing BODIPYs are discussed in detail in Section 3.2.1.

2.6. Synthesis from pyrroles and orthoesters

A method for the synthesis of a BODIPY with a free meso-position **20** *via* the condensation of 2,4-dimethylpyrrole with an orthoester was described by Sekiya *et al.*[84] If triethylorthoacetate is used instead of an orthoester, 8-methyl-substituted BODIPY **21** is formed from 2-phenylpyrrole (Scheme 16).[85]

Scheme 16

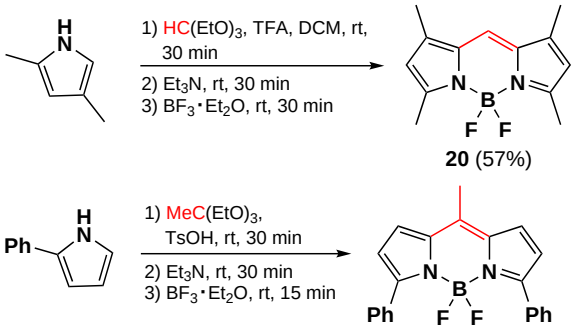

2.7. Synthesis of 8-trifluoromethyl-substituted BODIPYs

BODIPYs with a trifluoromethyl group at the *meso*-position are of particular interest due to the fact that the electron acceptor CF_3 group promotes aromatic nucleophilic substitution (SNAr) in the BODIPY core, greatly facilitating modification at positions 3 and 5.[86] When the CF_3 group is present at the meso-position, the absorption spectrum of the compounds shifts into the NIR region.[34] 8-trifluoromethyl-substituted BODIPYs with methyl groups at positions 1 and 7 are of interest as PTT agents because the absence of the CF_3-group rotation barrier leads to almost complete quenching of fluorescence and high photothermal efficiency.[34]

In 2008, Li *et al.*[86] proposed a method for the synthesis of *meso*-CF_3-BODIPY **22** from pyrrole and trifluoromethyl-oxymethanol. The condensation of the reagents under acidic conditions resulted in the formation of CF_3-substituted dipyrromethane, the subsequent oxidation of which and complexation with boron trifluoride etherate led to the target product (Scheme 17).

An alternative method for the synthesis of NIR-absorbing *meso*-CF_3-BODIPY **23a** and its analogs was published in 2011 by Sobenina *et al.*[87] The synthetic steps included the reduction

Scheme 17

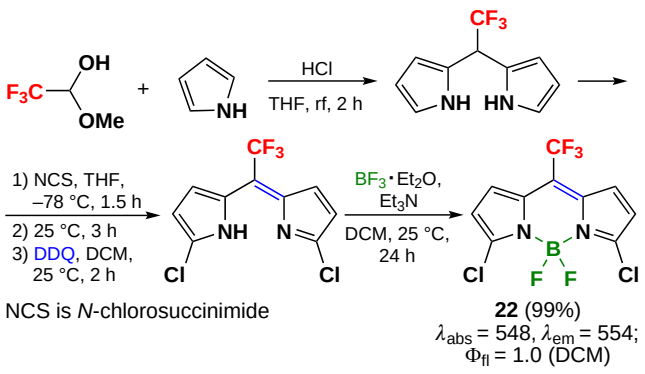

Scheme 18

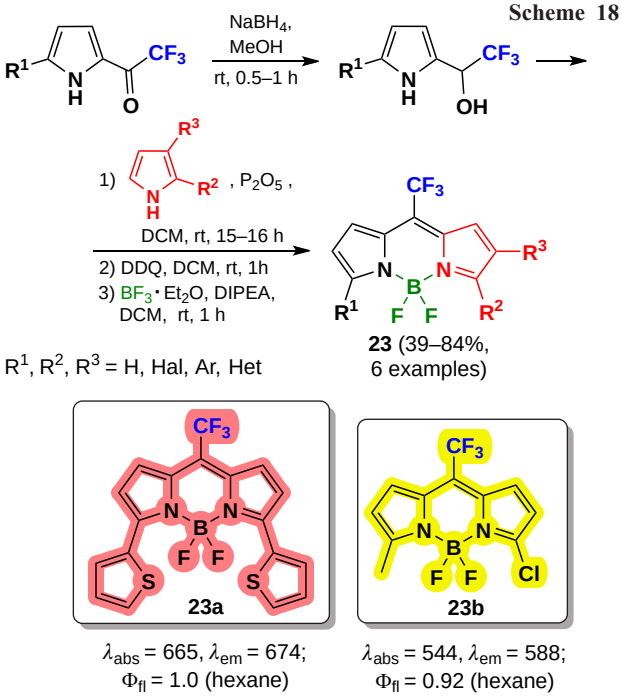

of 2-trifluoroacetylpyrroles to alcohols, with further condensation reaction with pyrroles yielding dipyrromethanes, followed by oxidation and complexation (Scheme 18). *Meso*-CF_3-BODIPYs were characterized by absorption maxima shifted to the red region of the spectrum as well as bright fluorescence ($\Phi_{fl} = 0.6–1$). Using this approach, Wang *et al.* 2022 synthesized a series of PTT active BODIPY dimers **23b** absorbing in the NIR(II)-region (see Section 3.6.10).[88]

In 2014 Choi *et al.*[89] synthesized 1,3,5,7-tetramethyl-8-CF_3-BODIPY **24** *via* condensation of ketopyrroles with pyrroles in the presence $POCl_3$ (Scheme 19). The high electonegativity of the CF_3 group leads to a significant decrease in the energy gap between the highest occupied (HOMO) and lowest unoccupied (LUMO) molecular orbitals compared to the *meso*-methyl-BODIPY.

It should be noted that BODIPY **24** demonstrated an extremely low fluorescence quantum yield (0.008) due to the

Scheme 19

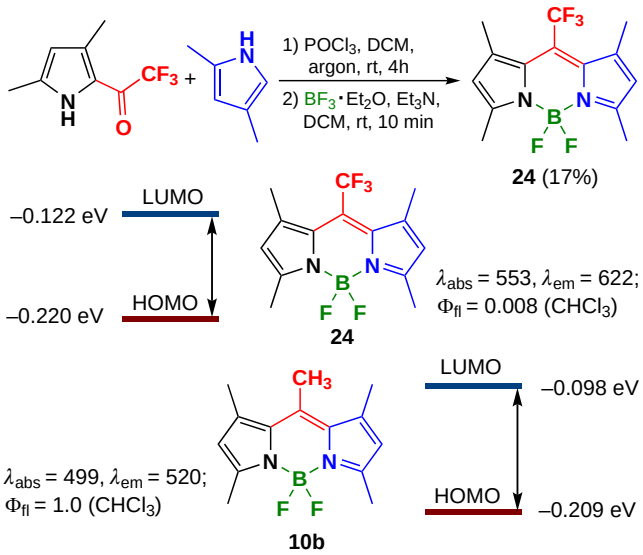

significant difference in the geometry of the ground (S_0) and first excited (S_1) singlet states. In addition, aggregation induced emission (AIEE) was observed for BODIPY **24**. Thus, as the water amount in BODIPY **24** solution increased from 0 to 99%, the formation of J-aggregates occurred, accompanied by a bathochromic shift and the appearance of a new absorption band at 626 nm with a 40-fold increase in fluorescence ($\Phi_{fl} = 0.06$). Importantly, under the same conditions, 8-methyl-BODIPY **10b** exhibited H-aggregation accompanied by a hypochromic shift and significant fluorescence quenching. The main difference between BODIPYs **24** and **10b** with trifluoromethyl and methyl substituents at the *meso*-position is the orientation of the dipoles with respect to the stacking axes. Although both of these compounds have a coplanar tilt of the dipole arrangement, the slip angle (q) is 36° for the CF_3 derivative and 65° for the methyl derivative, which, according to Kasha exciton theory, corresponds to the classical examples of J-type ($q < 54.7$) and H-type ($q > 54.7$) packing.[90] The formation of J- and H-aggregates of BODIPY is also discussed in Section 3.5.1.2.

In 2017, Jiang *et al.*[91] proposed a one-pot method for the synthesis of 8-CF_3-BODIPY **24** and **25** directly from α-unsubstituted pyrroles in the presence of 1 equiv. of trifluoroacetic acid and phenyltrichlorosilane ($PhSiCl_3$). The key step in this approach is the reaction of TFA and $PhSiCl_3$ with *in situ* chloranhydride formation (Scheme 20).

Scheme 20

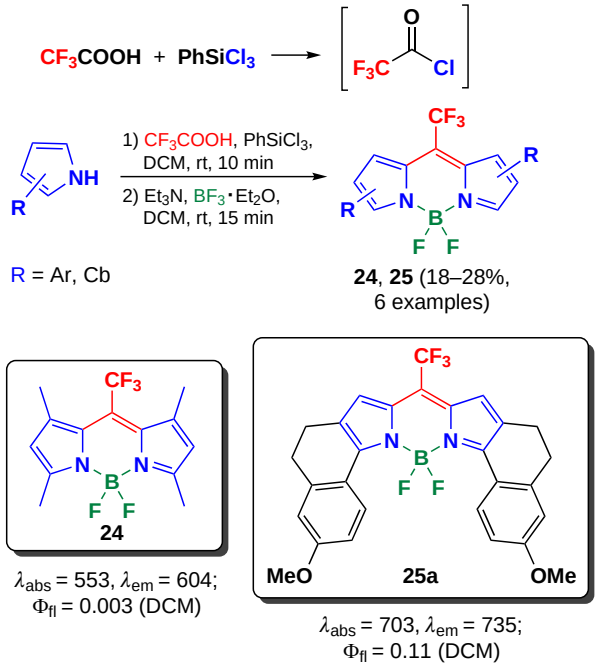

Following this approach, in 2020 Xi *et al.*[34] synthesized BODIPY **24** with a freely rotating meso-CF_3 group in the design of a highly efficient BODIPY-based PTT agents (Scheme 21).

Scheme 21

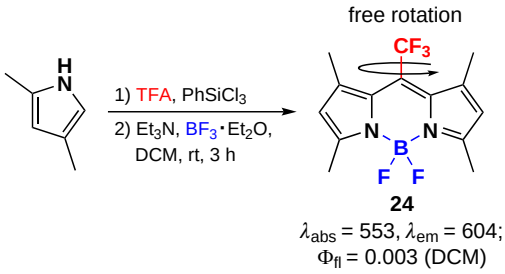

2.8. Preparation of boron-substituted BODIPYs

BODIPYs substituted at the boron atom are of great interest as fluorophores due to the fact that the introduction of substituents on the boron atom causes an increase in the Stokes shift and fluorescence quantum yields, increases the photostability and water solubility of the compounds, and allows the J-aggregation ability of BODIPY dyes to be controlled.[12,92,93] The main method of modification of boron atom in BODIPY is the nucleophilic substitution of fluoride anions. Section 3.7 is devoted to such reactions. Herein we discuss an alternative approach, the complexation of dipyrromethane with organoboron derivatives.

In 2009, Bonnier *et al.*[94] reported the synthesis of boron-substituted BODIPY **26** by complexation of dipyrromethene with perfluoroaryl borohalides such as $C_6F_5BF_2$ and $(C_6F_5)_2BCl$, as well as with perfluorinated 9-bromoborafluorene (Scheme 22). The resulting spiro-BODIPY **26** exhibited bright fluorescence due to the presence of a rigid chelating moiety. In 2017, Yuan *et al.*[95] proposed a method for the synthesis of boron-substituted BODIPY **27** by the reaction of dipyrromethene with various diaryl bromoboranes in the presence of a proton sponge (PS), 1,8-bis(dimethylamino)naphthalene. For BODIPY **27a** the fluorescence quenching due to the heavy atom effect was shown, while for the oxygen-containing BODIPY **27b** high fluorescence quantum yields and a large Stokes shift in the solid state were observed.

In 2019, Wang *et al.*[96] proposed a method for the synthesis of mono-β-aryl-substituted BODIPY **28** from organotrifluoroborates. The complexation of dipyrromethene with aryl-, vinyl-, and alkyltrifluoroborates was carried out in the presence of sodium carbonate as a base (Scheme 23). The photophysical properties of BODIPY **28** were identical to those of the BF_2-analogs.

In 2016, Saikawa *et al.*[13] synthesized boron-dipyrromethene macrocycles in which the boron atoms are coordinated by two nitrogen atoms and two oxygen atoms (N_2O_2) *via* the reaction of macrocyclic dipyrromethene with phenylboronic acid. By varying the amounts of phenylboronic acid, a mono- (**29**) or binuclear macrocycle (**30**) can be obtained (Scheme 24; the value of the circularly polarized luminescence is also given under structure 30, see Section 3.9 for details).

The fluorescence of mononuclear BODIPY **29** was almost completely suppressed by the PET effect, while for the binuclear complex **30** bright fluorescence ($\Phi_{fl} = 0.58$) was observed due to its rigid structure and the binding of the oxygen lone pair. X-ray diffraction analysis revealed a twisted configuration for the binuclear complex **30**, explaining the high circular polarization of the fluorescence ($\Phi_F|g_{lum}| = 5.3 \times 10^{-3}$) in the NIR band ($\lambda = 663$ nm). Fluorophores with high circular polarization are of interest due to the high emission resolution, which is important for bioimaging and organic electronics.[97]

2.9. Analysis of BODIPY core synthesis methods

The BODIPY core synthesis methods that were developed over the last three decades are now widely used. Given the large number of publications dedicated to these methods, it is reasonable to conclude that a specific method is optimized for solving specific tasks. Thus, the classical method of acid-catalyzed reaction of aromatic aldehydes with pyrroles[48,49,51,52,56] (see Section 2.1.) is a universal way to synthesise symmetric BODIPYs with an aromatic substituent at the *meso*-position. In contrast, symmetrical *meso*-alkyl derivatives of BODIPY are

Scheme 22

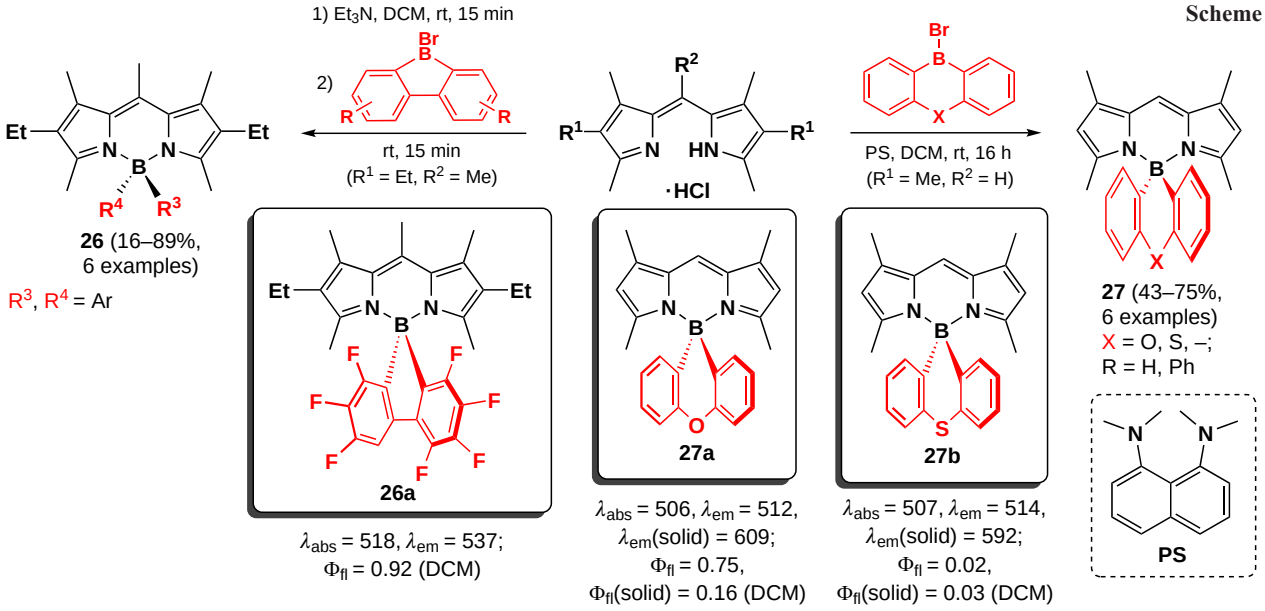

Scheme 23

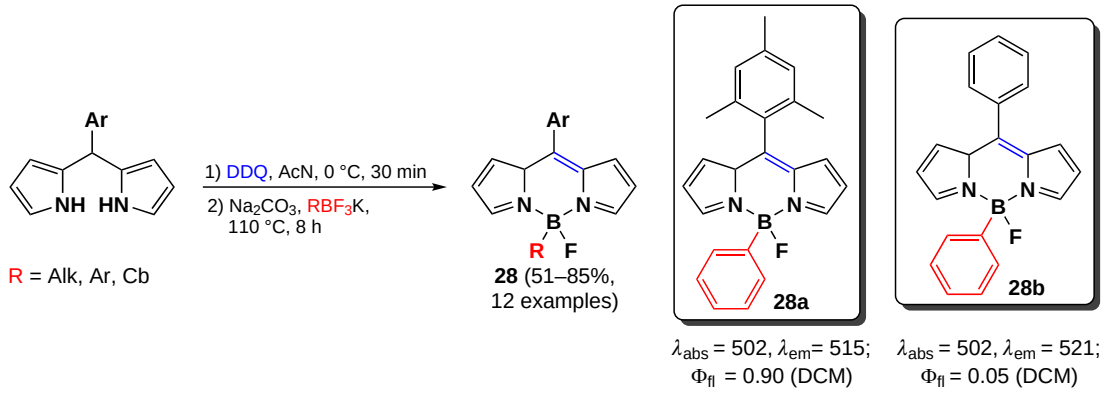

Scheme 24

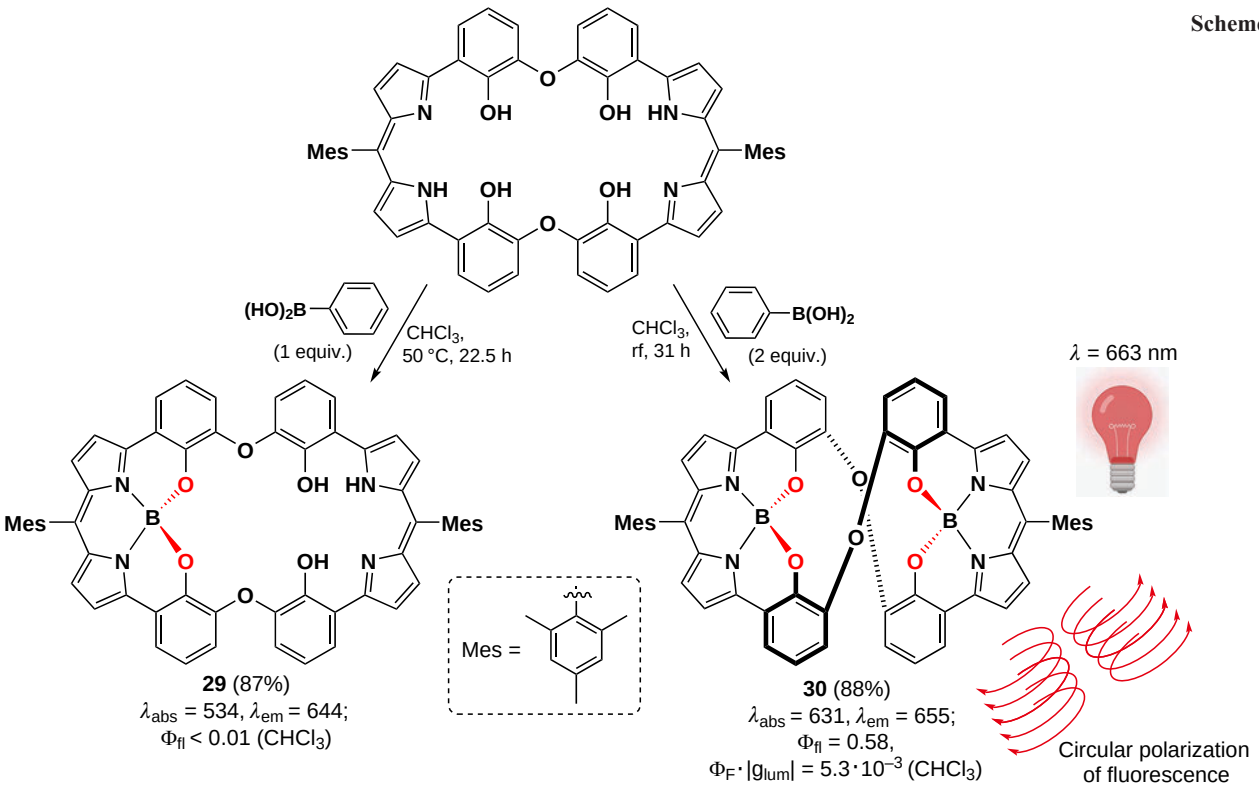

usially synthesized by reaction of acyl chlorides with pyrroles (see Section 2.2.).[60,63,65] A convenient method for the direct synthesis of symmetric NIR-absorbing BODIPYs is the $POCl_3$-catalyzed self-condensation of pyrroles (see Section 2.4),[70,79] but it is complicated by the low availability of pyrrolecarbaldehydes.

It is worth noting that the $POCl_3$-catalyzed condensation of acylpyrroles and pyrroles is the only method for the preparation of asymmetric BODIPYs with different substituents in the pyrrole scaffold (see Section 2.3).[66,71] The synthesis of BODIPY from two different scaffolds allows precise adjustment of the photophysical properties of the dyes and further selective functionalization of the pyrrole moieties.[22,78]

A number of approaches could be utilized for the synthesis of BODIPY with an unsubstituted *meso*-position, including the above-mentioned self-condensation of acylpyrroles and condensation of pyrroles with acylpyrroles (see Sections 2.3 and 2.4).[67,75] The use of orthoesters as reagents is also worth mentioning, as it yields *meso*-H-BODIPY from the available pyrroles with a high yield.[84]

A number of approaches leading to BODIPYs with specific *meso*-substituents should be mentioned. Thus, bis-(1H-pyrrol-2-yl)-methanethione is a key precursor for both the synthesis of 8-thioalkyl- (see Section 2.5.1)[80] and 8-halogen-BODIPY (see Section 2.5.2),[82] and to date no alternative approaches to the synthesis of *meso*-substituted BODIPYs have been developed. Among a number of methods leading to 8-CF_3-BODIPYs, a reaction based on the *in situ* formation of trifluoroacetyl chloride by reaction of $PhSiCl_3$ with TFA is worth mentioning.[91] This approach avoids the use of difficult-to-access CF_3-containing precursors, such as 2-trifluoroacetylpyrroles, and uses the common substrate for BODIPY synthesis, 2,4-dimethylpyrrole. (see Section 2.7.).

The replacement of the boron trifluoride etherate with other organoboron compounds in complexation of dipyrromethenes opens the way to the direct synthesis of boron-substituted BODIPYs.[94] Such derivatives have valuable properties, such as solid state fluorescence,[95] as well as high circular polarization emission.[13]

Thus, in order to obtain a BODIPY of a given structure, one can choose the optimal method among the many described in the literature.

3. BODIPY core modification methods and their products

3.1. Substitution reactions in the BODIPY core

Analysis of the mesomeric structures of BODIPY reveals that the electron density is unevenly distributed between the atoms in the BODIPY core (Fig. 2).[9,10] The electron density on carbon atoms in BODIPY decreases in the following series: positions 2 and 6 ≫ 1 and 7 > 3 and 5 ≫ 8. This sequence shows the change in regioselectivity in electrophilic substitution reactions and demonstrates the regioselectivity of nucleophilic substitution reactions in the reverse order. However, carbon atoms at positions 1 and 7 compared to positions 3 and 5 often exhibit less activity due to steric hindrance in the presence of a substituent at position 8.[98,99] Therefore, according to the electron density distribution in the BODIPY core and the influence of steric hindrance, the rate of electrophilic substitution reactions decreases from carbon atoms at positions 2 and 6, to C3 and C5, and lastly to positions 1 and 7.[10]

The resonance structure of the BODIPY core reveals that carbon atoms at positions 1, 3, 5, 7, and 8 are electron deficient, and thus can be involved in nucleophilic substitution reactions (Fig. 3). The rate of nucleophilic substitution reactions in BODIPY decreases from carbon atom at the *meso*-position, to less active C3 and C5, and to positions 1 and 7.[100] The decreased reactivity of carbon atoms at positions 1 and 7 compared to positions 3 and 5 is explained by their lower HOMO coefficients.[101]

3.2. Halogen substituted BODIPY

Synthesis of halogen-substituted BODIPYs could be conducted by several synthetic methods. The most common path involves electrophilic halogenation reactions (path I). Moreover,

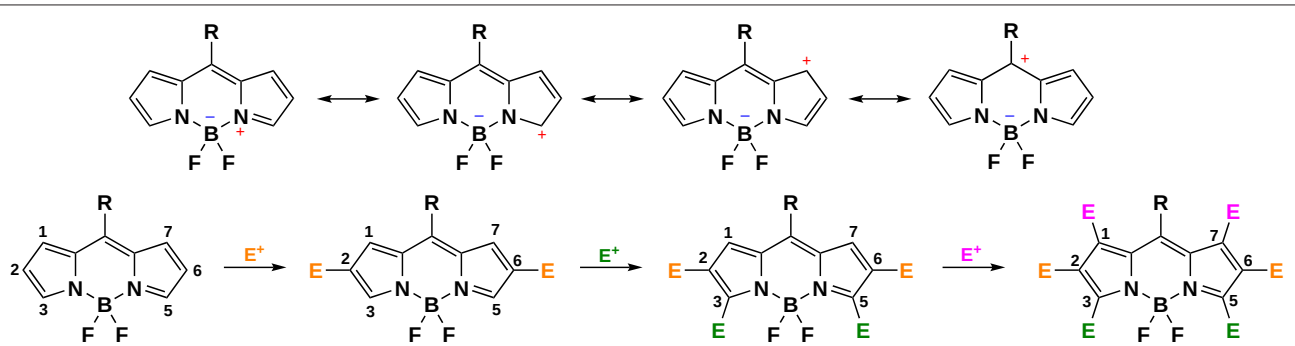

Figure 2. Regioselectivity in electrophilic substitution reactions in BODIPY.

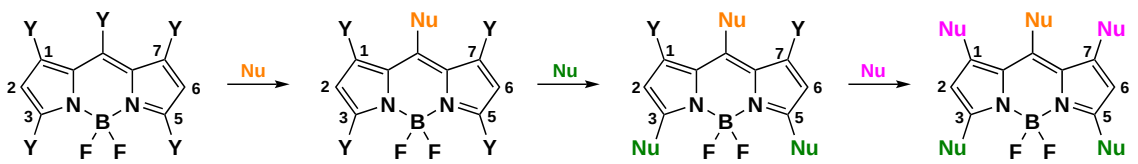

Figure 3. Regioselectivity in nucleophilic substitution reactions in BODIPY.

Scheme 25

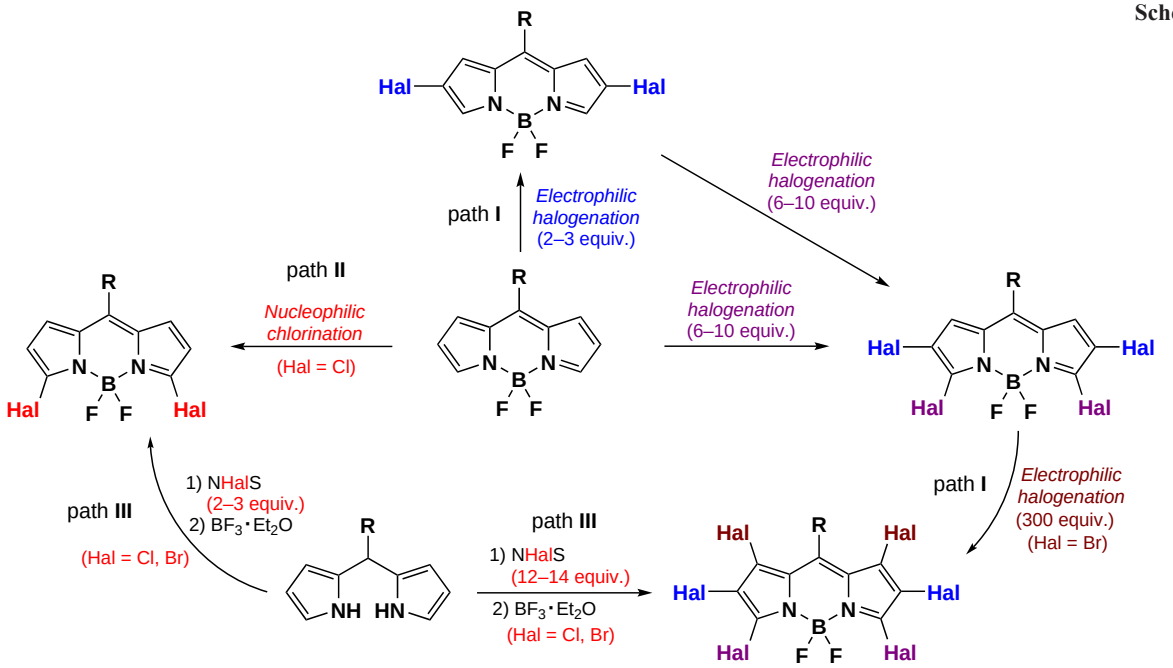

numerous synthetic methods based on nucleophilic substitution reactions (path II) or pre-functionalization of initial pyrroles and dipyrromethanes (path III) have been observed.

The regioselective synthesis of 3,5-dihalogen-BODIPY *via* electrophilic substitution reactions is not feasible. These derivatives can be obtained either through the pre-modification of the initial pyrrole or dipyrromethane or *via* nucleophilic substitution (Scheme 25; the amount of halogenating reagent is given in brackets).

This section reviews electrophilic substitution reactions in BODIPY core, and different methods for synthesis of halogenated BODIPYs, such as nucleophilic halogenation and the pre-functionalization of the parent pyrroles and dipyrromethenes. The photophysical properties of halogen-substituted BODIPYs and their potential applications as photosensitizers in photodynamic therapy (PDT) are also discussed.

3.2.1. Photophysical properties of halogen-substituted BODIPYs

Modification of the BODIPY core with heavy halogen atoms has a great impact on their photophysical properties. Fluorescence is a spin-resolved radiation-induced deactivation of the S_1 state to S_0, which competes with non-radiation-induced deactivation of the S_1 state to S_0 (internal conversion, IC) or to T_1 (ISC) (Fig. 4). The heavy atom enhances the probability of a spin-forbidden $S_1 \rightarrow T_1$ transition and intercombination conversion, which is known as 'heavy atom effect'.[102,103] The relaxation of the selection rule is due to the SOC effect, namely due to the interaction of the electron spin with the orbital magnetic moment. Thus, the modification of BODIPY with heavy atoms leads to an increase in SOC and hence ISC.[104]

The 'heavy atom' effect can be observed in BODIPYs directly bounded to the halogen atom, thus allowing the highest occupied molecular orbital (HOMO) and/or the lowest unoccupied molecular orbital (LUMO) of the molecule to extend to the electrons of the halogen atom. However, this effect is not observed in BODIPYs with halogen atoms in the *para*-position of the *meso*-phenyl group, and the photophysical properties of

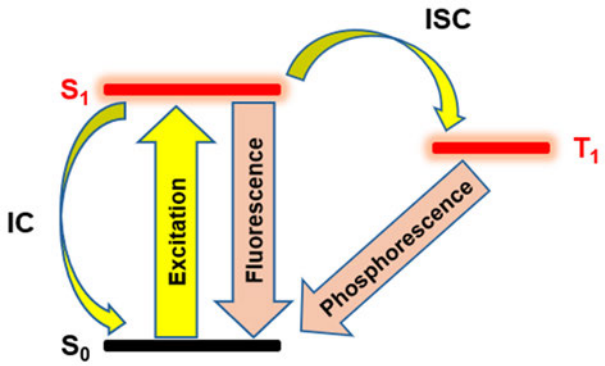

Figure 4. Jablonski diagram: upon excitation, the molecule turns to a singlet excited state (S_1) from which radiative relaxation (fluorescence), irradiation-free relaxation (IC), and spin-forbidden intercombination conversion (ISC) to the triplet excited state T_1 are possible.

these BODIPYs are similar to those of non-halogenated BODIPYs.[105]

Therefore, the photophysical properties of non-halogenated (*e.g.*, compound **31**) and halogen-substituted BODIPYs **32**–**42** differ significantly (Fig. 5). The dihalogenation of BODIPY results in a bathochromic shift of the absorption maximum by 28–50 nm. For *meso*-aryl-BODIPY **31** this shift occurs from 500 nm to 538–551 nm for 2,6-dihalogen-BODIPY **32**, **36** and **40**. As the atomic number of the halogen increases (I > Br > Cl), both the absorption and emission maxima shift to the red region of the spectrum.[99,106–109] The modification of the BODIPY core with four bromine atoms into the BODIPY core results in a shift of λ_{abs} of approximately 16 nm (to 554 nm) in the 2,3,5,6-tetrabromo derivative **38** in comparison to the 2,6-dibrom BODIPY **36**. Moreover, further bromination of BODIPY **36** results in hexabromo-BODIPY **39**, which exhibits a slight hypochromic shift due to steric hindrance to the rotation of the *meso*-aryl substituent.[103]

The 2,3,5,6-tetraiodo-BODIPY **42** exhibits a substantial bathochromic shift in the absorption maximum in comparison with the 2,6-diiodo BODIPY **40** (λ_{abs} = 581 and 548 nm,

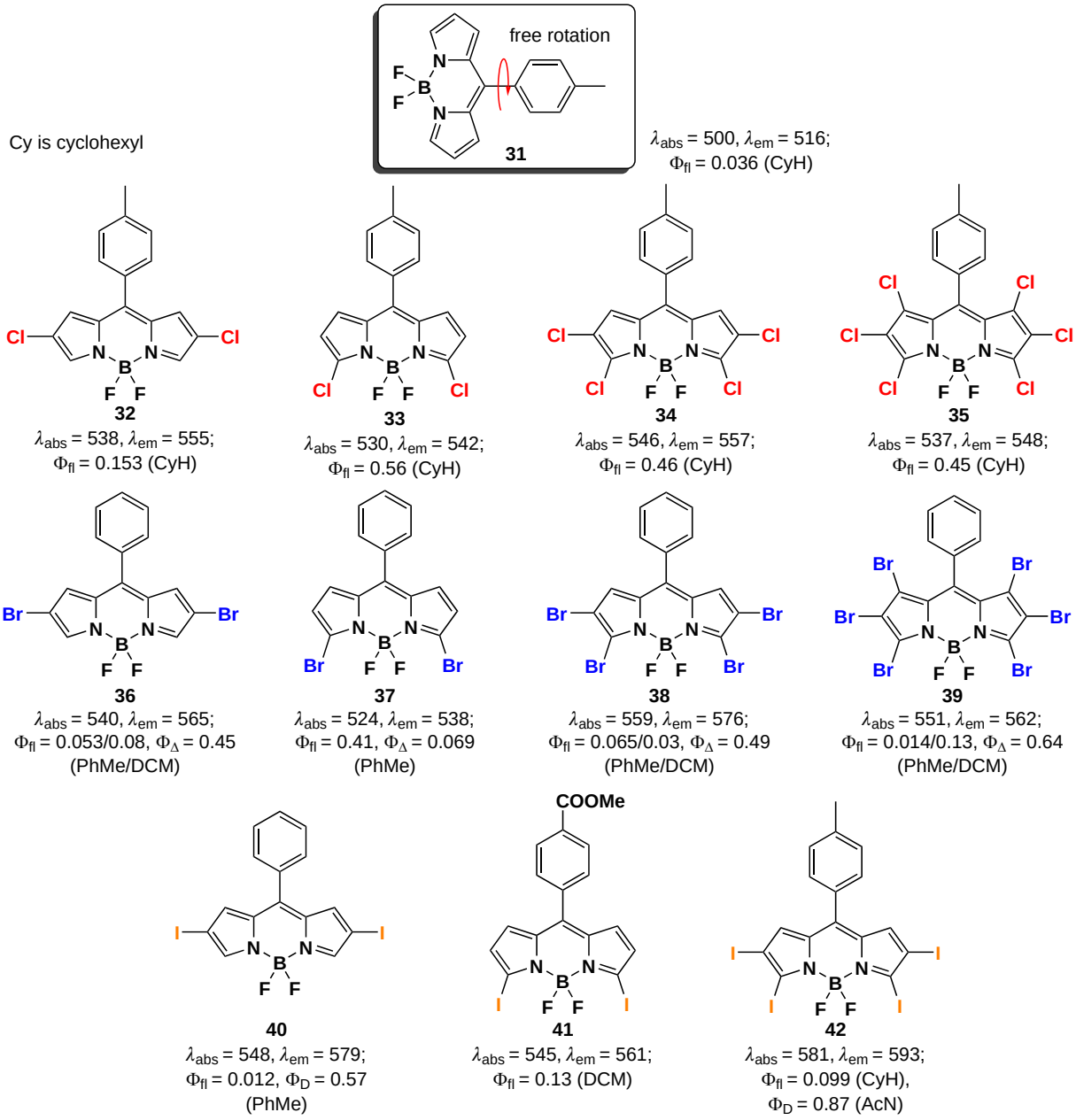

Figure 5. Structures and photophysical properties of BODIPY **31** and halogen derivatives **32**–**42**.[99,100,103,106–113]

respectively). The 2,6-dihalogen-BODIPYs exhibit a Stokes shift of 16–27 nm, which is similar to that observed for unsubstituted BODIPYs. In contrast, the Stokes shift decreases to 11 nm for 1,2,3,5,6,7-hexahalogen-BODIPYs.[100,107] Meanwhile, the halogen-free *meso*-aryl-BODIPY **31** is characterized by low fluorescence quantum yield due to radiation-free relaxation, which is generally <0.1, as a result of the rotation of the *meso*-aryl substituent.

3.2.2. Electrophilic halogenation

N-Halogensuccinimides are the most common electrophilic agents for BODIPY halogenation and can be used under mild conditions (Scheme 26).[114–116] Halogenation of 1,2,3,3,5,6,7-unsubstituted BODIPY by the excess of NCS or N-bromosuccinimide (NBS) gives 2,3,5,6-tetrahalogenated derivatives.[117,118] Similarly, polychloro-substituted BODIPYs (2,6-di- to 2,3,5,6-tetrachloro) can be synthesized by reaction with trichloroisocyanuric acid in acetic acid.[119,120] The sequential synthesis of mono-, di-, tetra-, and hexabromo-BODIPY can be carried out with 2, 3, 6, and 300 equiv. of molecular bromine, respectively.[100,121] The quantities of iodine chloride (5 equiv.), iodine (3.5 equiv.) and iodine trioxide (8 equiv.) or the iodine-iodine(III) oxide system in the ratio of 1 : 0.8, 2.5 : 2, 3.5 : 3 and 4.5 : 4, respectively, were employed (see Scheme 26).[99,122–125]

Hexachloro- and hexabromo-BODIPYs can also be synthesized by exhaustive halogenation of the initial dipyrromethane, followed by oxidation and complexation. In this case, the halogenation reaction of dipyrromethane requires the use of a modest excess of the halogenating agent, which facilitates the formation of hexachlorodipyrromethane in the presence of 14 equivalents of NCS,[107] and hexabromodipyrromethane in the presence of 10 equivalents of NBS[126] (Scheme 27).

Scheme 26

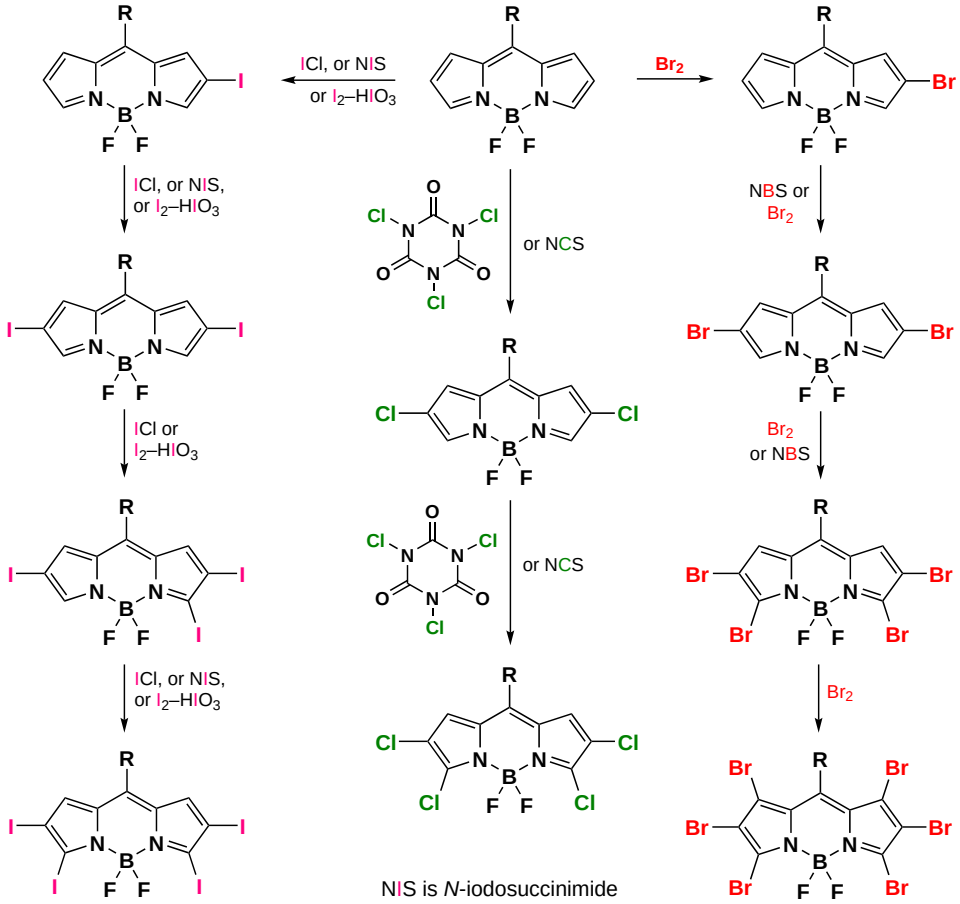

Scheme 27

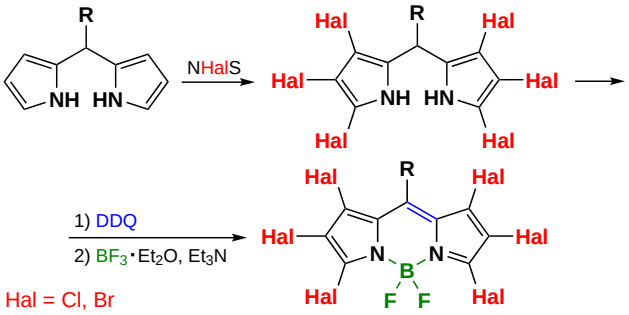

In 2012, Li *et al.*[127] reported an unusual regioselectivity of BODIPY bromination in the reaction of benzyltriethylammonium tribromide with 1,3-dimethyl-BODIPY. Monobromo-BODIPY **43** was synthesized by the electrophilic substitution at position 2, and following nucleophilic attack of the bromide anion at position 5 led to the formation of the 2,5-dibromo-BODIPY **44**. This compound was also capable of further electrophilic bromination yielded in BODIPY **45** (Scheme 28).

The relative reactivity of the BODIPY's carbon atoms is maintained during electrophilic substitution, provided that the C(2) and C(6) carbon atoms are not accessible to electrophilic attack. Consequently, bromination of 2,6-disubstituted BODIPY with molecular bromine occurs at positions 3 and 5, yielding BODIPY **46**. Conversely, bromination of 2,3,5,6-tetrasubstituted BODIPY leads to the substitution at positions 1 and 7, yielding BODIPY **47**.[74,128] Furthermore, iodination of 2,6-dibromo-BODIPY by the I_2–HIO_3 system selectively yields 3,5-diiodo-BODIPY **48** (Scheme 29).[129]

3.2.3. 2,6-Dihalogenated BODIPY as PDT agents

Increasing the population of the T_1-level of BODIPY by introducing halogen atoms into the molecule is a widely used strategy in the development of drugs for photodynamic therapy (PDT) and photothermal therapy (PTT).[114,130–132] In the triplet excited state, the photosensitiser is capable of reacting with biomolecules with radical anion formation, which subsequently reacts with water or oxygen to generate a superoxide anion or hydroxyl radical (type I PDT agent). An alternative process

Scheme 28

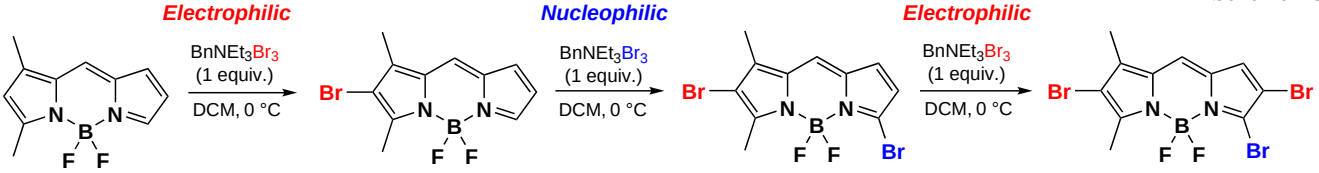

Scheme 29

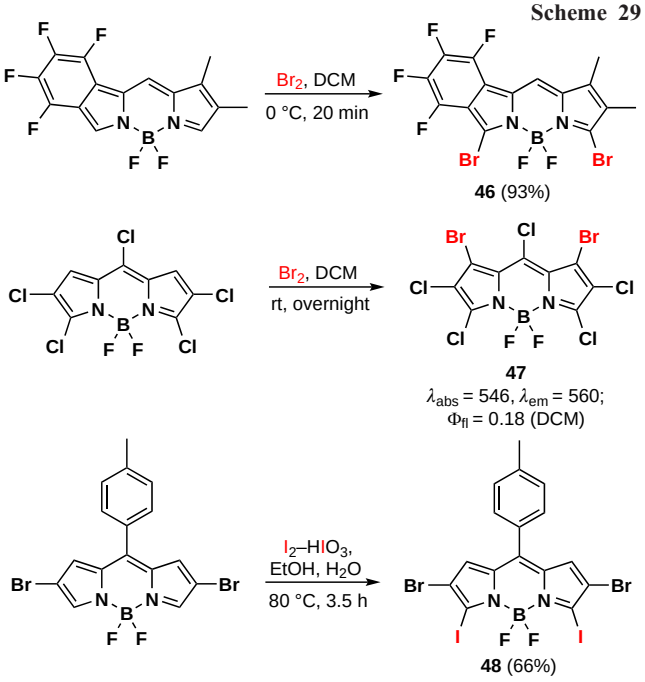

involves the reaction of BODIPY in the triplet excited state with oxygen, resulting in the formation of singlet oxygen (PDT agent type II). [133]

Iodinated BODIPYs are most often considered as photosensitising agents which typically exhibit high quantum yields of singlet oxygen ($\Phi_\Delta = 0.5-0.8$). Furthermore, the photosensitising properties of such compounds are almost independent of the number of halogen atoms or their position in the BODIPY core.[99,134] Bromo-substituted BODIPYs are also capable of acting as photosensitisers, but their singlet oxygen quantum yields are generally lower than those of their iodinated analogues, with values ranging from 0.1 to 0.6.[22,135,136] The fluorescence of 1,3,5,7-tetramethyl-BODIPYs is markedly diminished by the incorporation of halogen atoms, with the effect increasing in accordance with the halogen order number (see structures **49**–**52** in Fig. 6).

In 2021 Won *et al.*[132] synthesised a NIR-absorbing PDT agent based on 2,6-dibromo-3,5-distyryl-BODIPY **53** and an ethacrynic acid-based glutathione-S-transferase inhibitor (Fig. 7).

BODIPY **54** was capable of generating both singlet oxygen (type II) and NO* and ROO* (type I) species, which were detedted using of different traps. Conjugate **54** was also capable of reduction the survival of the GST-pi-expressing cell line MDA-MB-231 in the absence of light at a concentration of 5 μM, with a subsequent decrease to 30% upon irradiation with a 660 nm laser (specific power 100 mW cm^{-2}, 10 min). In an *in vivo* antitumour efficacy study in mice bearing MDA-MB-231 tumour, a statistically significant reduction in tumour growth was observed after four injections of compound **54**, followed by laser irradiation ($\lambda = 660$ nm, 2 W cm^{-2}, 10 min) at week 9 of therapy.

In 2021, Tian *et al.*[137] obtained 2,6-diiodo-BODIPY **55** and **56** and prepared nanoparticles (NPs) based on **56** by encapsulation in poly(oligoethylene glycol methacrylate)-polyaspartic acid (POEGMA23-PAsp20), with photodynamic therapy (PDT) activity (Fig. 8). Both BODIPYs **55** and **56** exhibited absorption in the near-infrared (NIR) range, with a hypochromatic shift of the absorption and emission maxima and quenching of fluorescence due to intersystem crossing (ICT) being observed with increasing solvent polarity. Furthermore, both fluorophores demonstrated high quantum yields of singlet oxygen.

The study of antiproliferative activity on 4T1 breast carcinoma and HeLa cervical cancer cell lines revealed that the half-maximal inhibition concentration (IC_{50}) of compound **56**-based NPs was 0.1 μM under 660 nm laser irradiation (10 mW cm^{-2}, 5 min) with no dark toxicity up to 0.3 μM. *In vivo* therapuitic efficacy study on mice with 4T1 tumours revealed complete tumour disappearance on the 20th day of therapy after three injections of NPs and irradiation with a 660 nm laser (40 mW cm^{-2}, 15 min).

In 2023, Spingler *et al.*[78] synthesised a series of isoindole-based 6-iodo derivatives of BODIPY **57** (Scheme 30). BODIPYs **57a** and **57b** were able to form triplet states and generate singlet oxygen upon irradiation. BODIPYs **57** were non-toxic in the absence of light on HeLa cells, but when irradiated with 630 nm light (5 J cm^{-2}), they exhibited IC_{50} values in the nanomolar concentration range. For instance, compound **57a** demonstrated an IC_{50} value of 6 nm. The activity of BODIPY **57a** and BODIPY **57b** was not reduced under hypoxic conditions on HeLa cells, indicating an oxygen-independent mechanism of action. In particular, BODIPY **57a** exhibited a hypoxia phototoxicity index exceeding 360 000. Intracellular localisation of BODIPY **57a** revealed the intracellular formation of aggregates of varying sizes, which presumably exerted a photothermal effect upon irradiation.

A series of PDT agents based on cationic 2,6-dibromo-BODIPY (**58a**) and 2,6-diiodo-BODIPY (**58b**) were synthesised by Badon *et al.*[136] (Scheme 31). The calculation of the energy gap between the first singlet excited level (S_1) and various triplet excited levels (T_1-T_3) for BODIPY **58a,b**

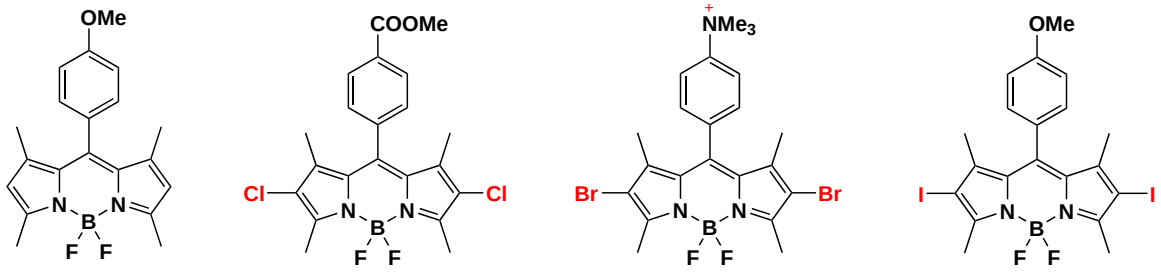

49
λ_{abs} = 505, λ_{em} = 513;
Φ_{fl} = 0.64 (DCM)

50
λ_{abs}= 528, λ_{em} = 543;
Φ_{fl} = 0.285 (DMF)

51
λ_{abs} = 524, λ_{em} = 546;
Φ_{fl} = 0.06, Φ_Δ = 0.13 (MeOH)

52
λ_{abs} = 537, λ_{em} = 552;
Φ_{fl} = 0.02, Φ_Δ = 0.79 (DCM)

Figure 6. Structures and photophysical properties of 1,3,5,7-tetramethyl-BODIPY **49** and 2,6-dihalogenated derivatives **50**–**52**.[106,134,136]

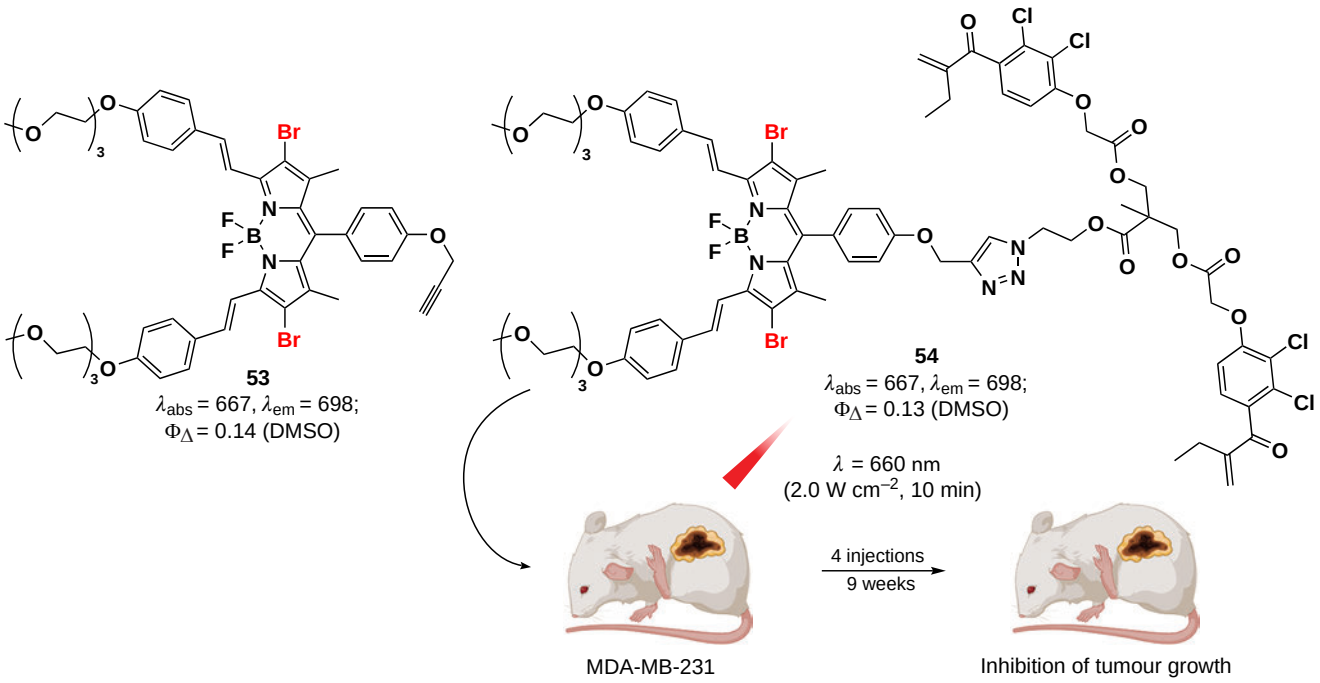

Figure 7. Structure of a PDT agent based on 2,6-dibromo-3,5-distyryl-BODIPY **53** and schematic representation of its *in vivo* action. The figure created by the authors based on the data of the publication [132].

demonstrated that intercombination conversion occurs *via* the $S_1 \rightarrow T_2$ pathway.

BODIPYs **58a**,**b** were non-toxic to MCF-7 and HeLa cells in the dark, but under 520 nm laser irradiation (7 mW cm^{-2}, 10 min) IC_{50} values were in the 48–60 nm range. Compounds **58a**,**b** accumulated in mitochondria due to the presence of a charged quaternary ammonium group in the *meso*-aryl substituent.

In 2023, Jung *et al.*[138] reported an NIR-absorbing 2,6-dibromo-BODIPY conjugate **59** and an ROS-generating copper **59-Cu^{II}** complex. This compound proved to be a promising agent for chemodynamic therapy (CDT) due to the presence of a vector fragment that targeted cancer stem cells by binding to CAIX9.[138] In the conjugate **59**, the 2,6-dibromo-3,5-distyryl-BODIPY motif and the vector to CSC (cancer stem cell) acetazolamide were linked *via* a triazole linker (Fig. 9).

The fluorescence of the **59-Cu** complex was almost completely absent, and the rate of $^1O_2$ formation was found to be 2.5 times lower under 660 nm laser irradiation (2 W cm^{-2}, 10 min) compared to ligand **59**. The **59-Cu** complex

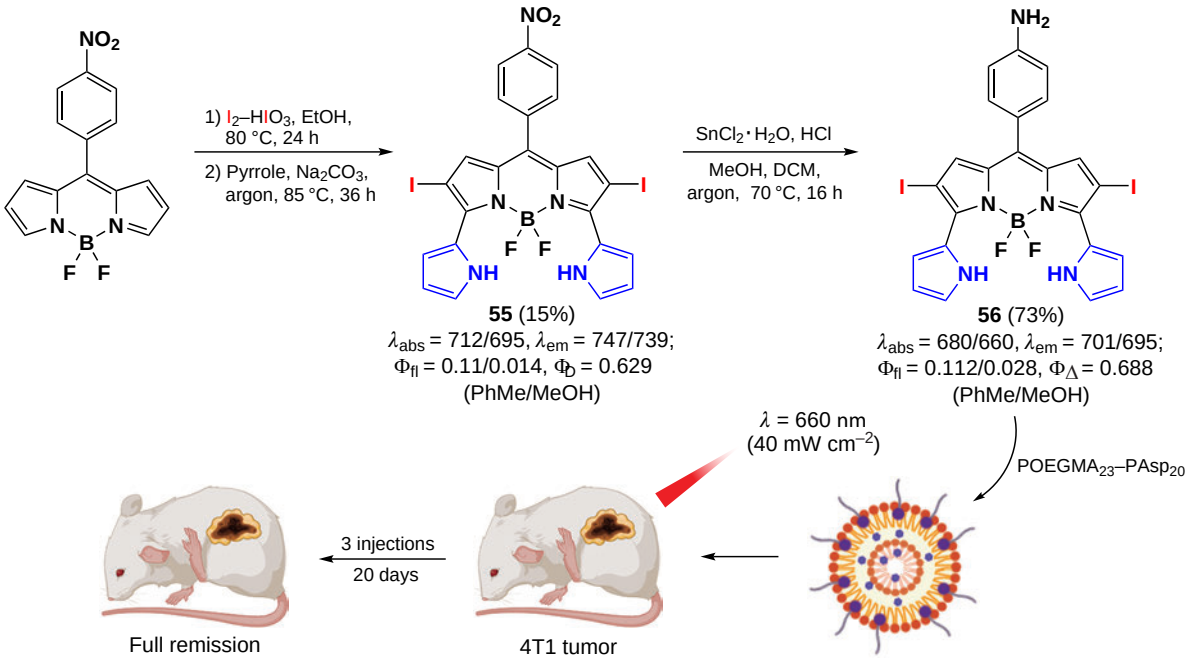

Figure 8. Synthesis and structure of NIR-absorbing 2,6-diiodo-BODIPY **56** with PDT activity, and a schematic representation of the *in vivo* action of NPs based on it. The figure created by the authors based on the data of the publication [137].

Scheme 30

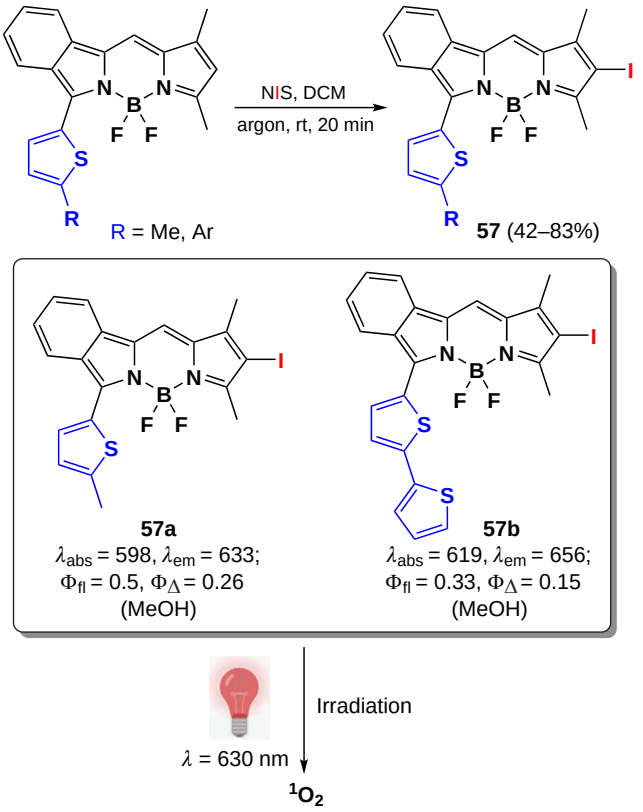

Scheme 31

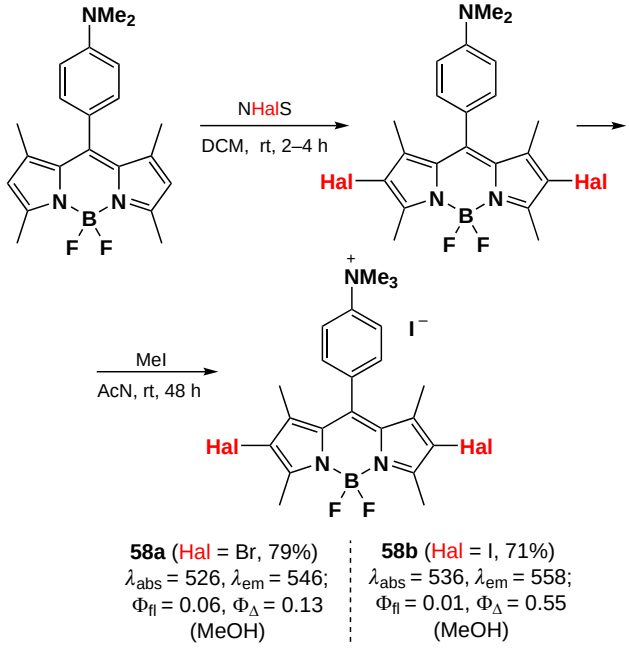

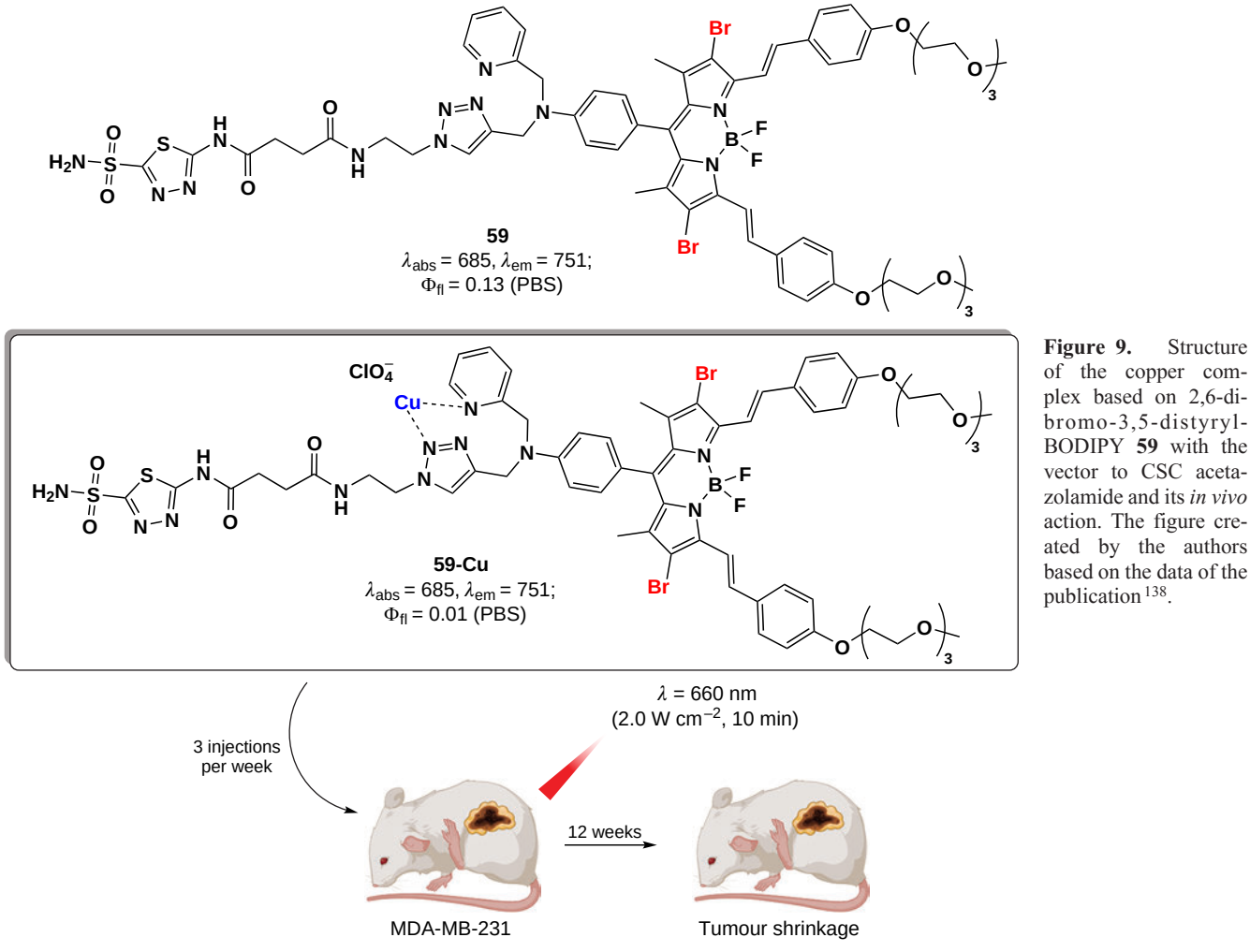

Figure 9. Structure of the copper complex based on 2,6-dibromo-3,5-distyryl-BODIPY **59** with the vector to CSC acetazolamide and its *in vivo* action. The figure created by the authors based on the data of the publication [138].

demonstrated moderate activity against the MDA-MB-231 cell line in the absence of light, and high activity under 660 nm laser irradiation (100 mW cm^{-2}, 5 min) in both normoxic and hypoxic conditions. *In vivo* experiments were conducted on mice bearing MDA-MB-231 tumors, which were administered three injections of the **59**-Cu conjugate once a week and irradiated with a 660 nm laser (2 W cm^{-2}, 10 min) for 12 weeks. A statistically significant reduction in tumor size was observed in the group of animals that received the complex compared to the group that received free ligand **59** and the control groups.

3.2.4. Nucleophilic halogenation of BODIPY at positions 3 and 5

In 2015, Zhou *et al.*[139] described a convenient approach for chlorinating BODIPY at positions 3 and 5 by using $CuCl_2$. This method is a one-electron oxidation of BODIPY **60** with copper(II) chloride taken in 50% excess, followed by nucleophilic addition of the chloride anion. This resulted in the formation of the monochloro-derivative **61** in 2 hours (Scheme 32). Increasing the amount of reagent to 3 equiv. and the process time to 8 hours gave 3,5-dichloro-BODIPY **62** in moderate yield.

In 2020, Frank *et al.*[140] developed a method for the synthesis of 3,5-dichlorosubstituted BODIPY **63** *via* nucleophilic substitution reaction by using the $Cu(OTf)_2$ — TBACl system (Tf — trifluoromethanesulfonyl (triflyl), TBA — tetra-*n*-butylammonium). The presence of an acceptor nitro group in the *meso*-aryl substituent contributed to the increase in product yields up to quantitative yields (Scheme 33).

3.2.5. Synthesis of 3-mono- and 3,5-dihalogenated derivatives *via* pre-functionalization path

In a pre-functionalization procedure, a halogen atom can be introduced into the α-position of dipyrromethane in a regioselective manner to form α-halogen-BODIPY after oxidation and complexation reactions.[141] Using α-chloro-substituted pyrroles **64** as starting compounds, BODIPY **65** substituted at positions 3 and 5 were obtained in yields of up to 90% (Scheme 34).[142]

Pre-functionalisation of dipyrromomethane is also employed to obtain 3,5-dibromo-BODIPY **66**. The most commonly used brominating agent for dipyrromomethane is NBS (Scheme 35).[143]

3,5-Dibromo-BODIPY can be synthesized from the corresponding bromo-substituted pyrroles. In 2014, Jiao *et al.*[76,144] obtained 3,5-dibromosubstituted BODIPY **67** through the self-condensation of 5-bromo-3-methoxypyrrole-2-carbaldehyde (Scheme 36).

In 2021, Frank *et al.*[111] proposed to use the Filkinstein reaction to obtain 3,5-diiodo substituted BODIPY **68** from the corresponding dichloro- or dibromo-BODIPY. This reaction is typically employed in the synthesis of substituted BODIPYs. In the aromatic series, the Filkinstein reaction requires the use of a photo- or metal catalyst. However, due to the propensity of 3,5-dihalogenated BODIPY to undergo nucleophilic substitution,

Scheme 32

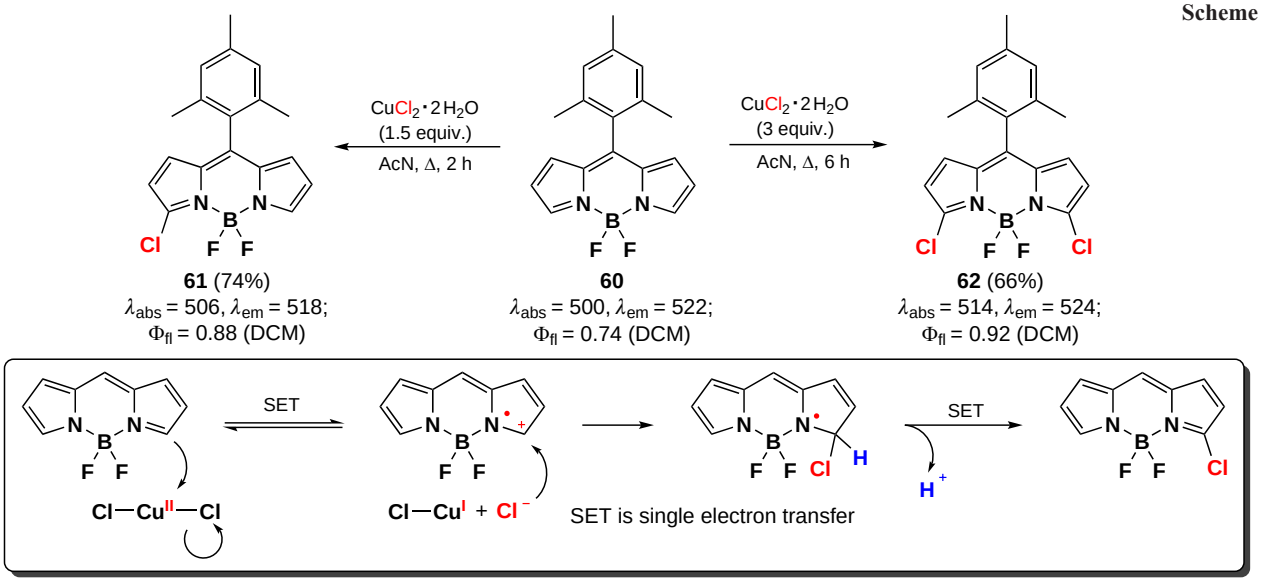

Scheme 33

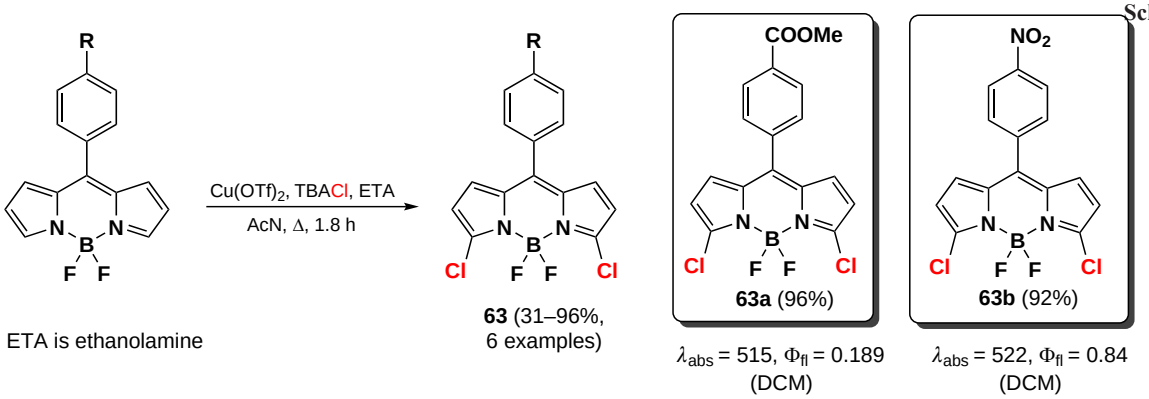

Scheme 34

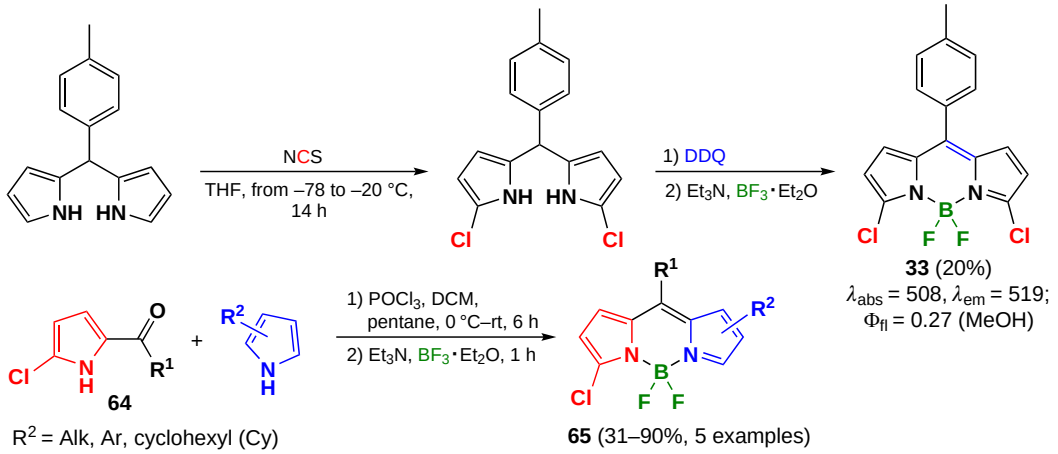

Scheme 35

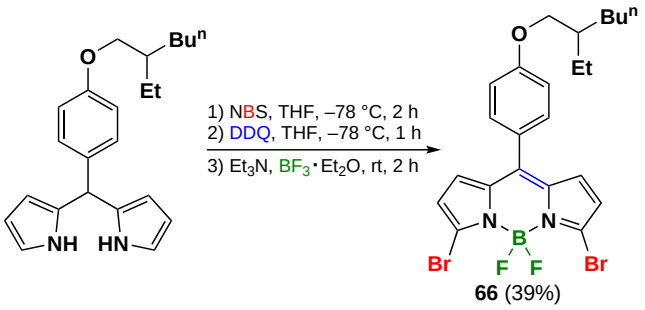

Scheme 36

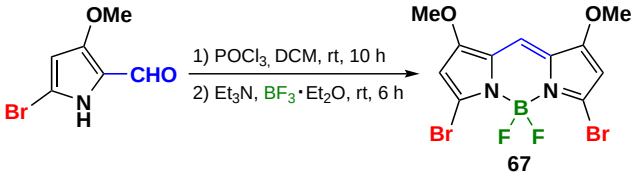

Scheme 37

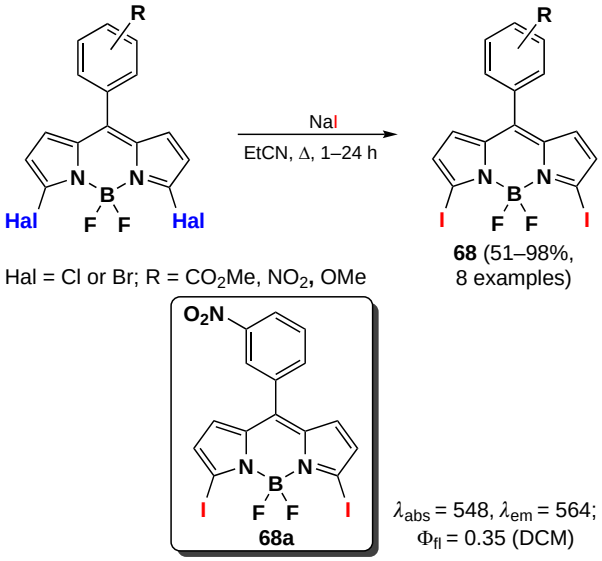

it was possible to carry out the Filkinstein reaction without a catalyst (Scheme 37).

3.2.6. Fluorination of the BODIPY core

Direct electrophilic fluorination of the BODIPY core is feasible through the use of electrophilic fluorinating agents, including N-fluorobenzenesulfonimide and bis(tetrafluoroborate) 4-fluoro-1-chloromethyldiazoniabicyclo[2,2,2,2]octane (commercially named Selecfluor). Therefore, in 2016, Huynh *et al.*,[145] reported the fluorination of BODIPY *via* using the Selecfluor reagent. In the case of blocked positions 3 and 5, the electrophilic fluorination reaction proceeded at position 2 of BODIPY. Conversely, when α-unsubstituted 1,3-dimethyl-BODIPY was subjected to the same reaction, nucleophilic fluorination occurred at position 5.[139] BODIPY **69** and **70** exhibited bright fluorescence with a fluorescence lifetime of 0.8 to 1.0 nanoseconds. Given the low yields of the products in this process, an alternative indirect route for their synthesis was proposed.[146] This involved sequential reactions of halogenation, preparation of pinacol esters of boronic acid, and palladium-catalyzed fluorination, as previously described for aromatic substrates. However, the total yield of these transformations was only 1–2% (Scheme 38).

In 2024, Larkovich *et al.*[24] presented the synthesis of 1,7-fluorinated BODIPY **71** from fluorinated pyrroles obtained *via* the Barton-Zard method, which refers to the reaction of β-fluoro-β-nitrostyrenes with 2-ethylisocyanoacetate. The presence of an electron-accepting carboxyethyl group at positions 3 and 5 resulted in low fluorescence quantum yields ($\Phi_{fl} < 0.02$) for these fluorophores. The introduction of a fluorine atom into the molecule had no significant impact on the absorption maximum in the spectrum, but led to an increase in the Stokes shift from 20–60 to 60–80 nm (Scheme 39).

3.3. Other reactions of electrophilic substitution in the BODIPY core

3.3.1. Sulfonation

Electrophilic sulfonation reactions proceed with the formation of 2,6-substituted BODIPY under the action of such reagents as chlorosulfonic acid or SO_3-pyridine complex. In 2015, an amphiphilic sensor for the detection of Al^{3+} cations based on BODIPY was synthesized through sulfonation of 1,3,5,7-tetramethyl-BODIPY at positions 2 and 6.[147] The presence of sulfo-groups in BODIPY **72** resulted in bright fluorescence and good solubility in water. The long aliphatic substituent at the *meso*-position facilitated micelle formation in aqueous solution. The fluorescence of this compound was quenched in the presence of Al^{3+}ions due to the formation of micelles. Conversely, the addition of citric acid led to the

Scheme 38

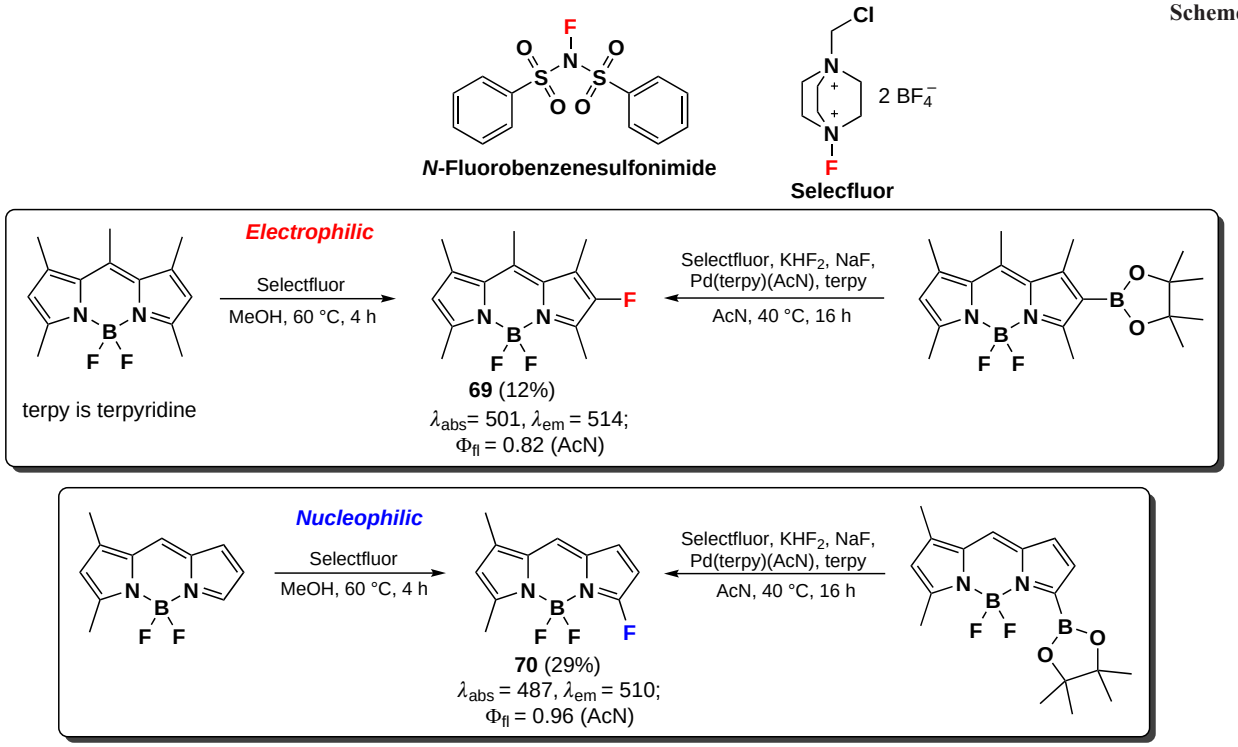

Scheme 39

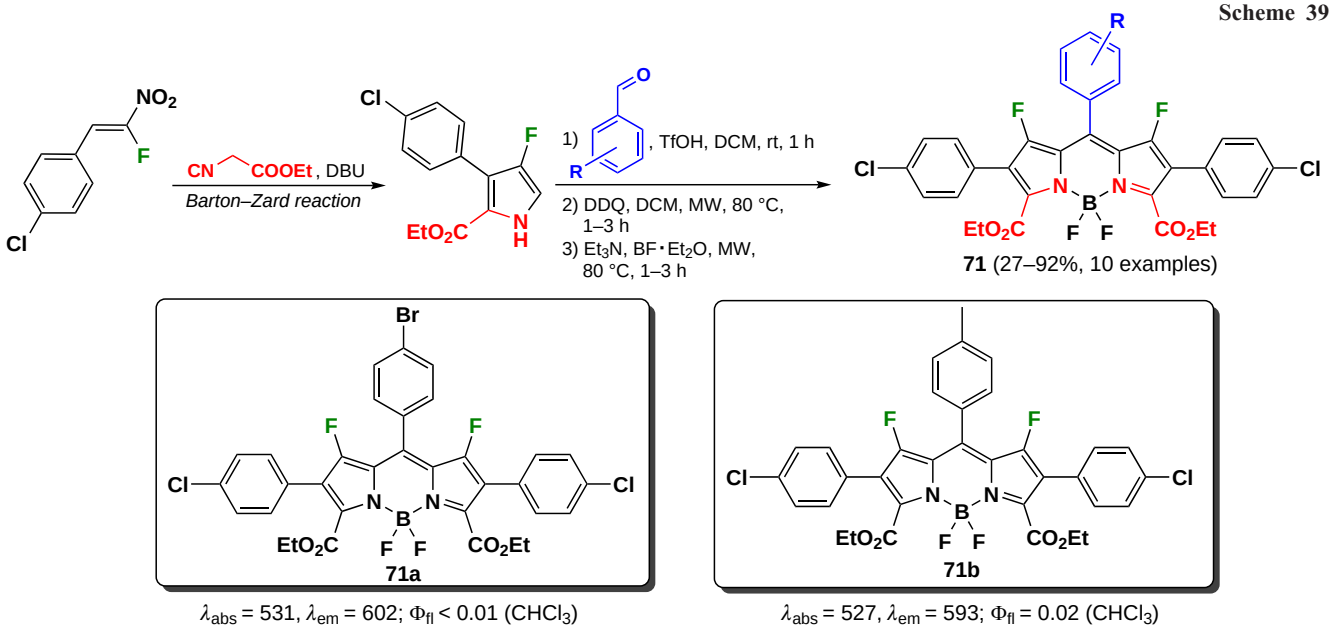

λ_{abs} = 531, λ_{em} = 602; Φ_{fl} < 0.01 ($CHCl_3$)

λ_{abs} = 527, λ_{em} = 593; Φ_{fl} = 0.02 ($CHCl_3$)

destruction of micelles and an increase in fluorescence, with a detection limit of 5 μM (Scheme 40).

The introduction of sulfonate groups at positions 2 and 6 of benzylated 1,3,5,7-tetramethyl-8-pyrocatechin-BODIPY to form compound **73** was carried out in 2014 by Kim *et al.*[148] After removing the protecting groups, a water-soluble fluorescent probe for HClO detection was obtained (Scheme 41). The fluorescence of compound **74** was observed to be low due to the occurrence of resonance energy transfer (RET) from the donor fragment of pyrocatechin to the BODIPY core. In the presence of HClO or ClO^-, pyrocatechin was oxidized to benzoquinone, which suppressed the RET and caused the fluorescence enhancement. BODIPY **74** demonstrated high selectivity for hypochlorite and did not exhibit fluorescence ignition in the presence of other oxidants, such as H_2O_2 and *tert*-butyl peroxide.

As part of the development of BODIPY-based photoremovable protecting groups, in 2020 Kand *et al.*[149] synthesized 2-sulfo- and 2,6-disulfo-BODIPYs **75a**,**b** *via* using an SO_3-pyridine complex (Scheme 42). The introduction of strong electron-acceptor sulfonate groups at positions 2 and 6 of BODIPY **75** led to a notable increase in the photolysis barrier of the C–O bond at the *meso*-position. This resulted in the inability of such compounds to release leaving groups upon irradiation.

3.3.2. Nitration

The nitration of BODIPY at positions 2 and/or 6 can be carried out with nitric acid solutions of different concentrations,

Scheme 40

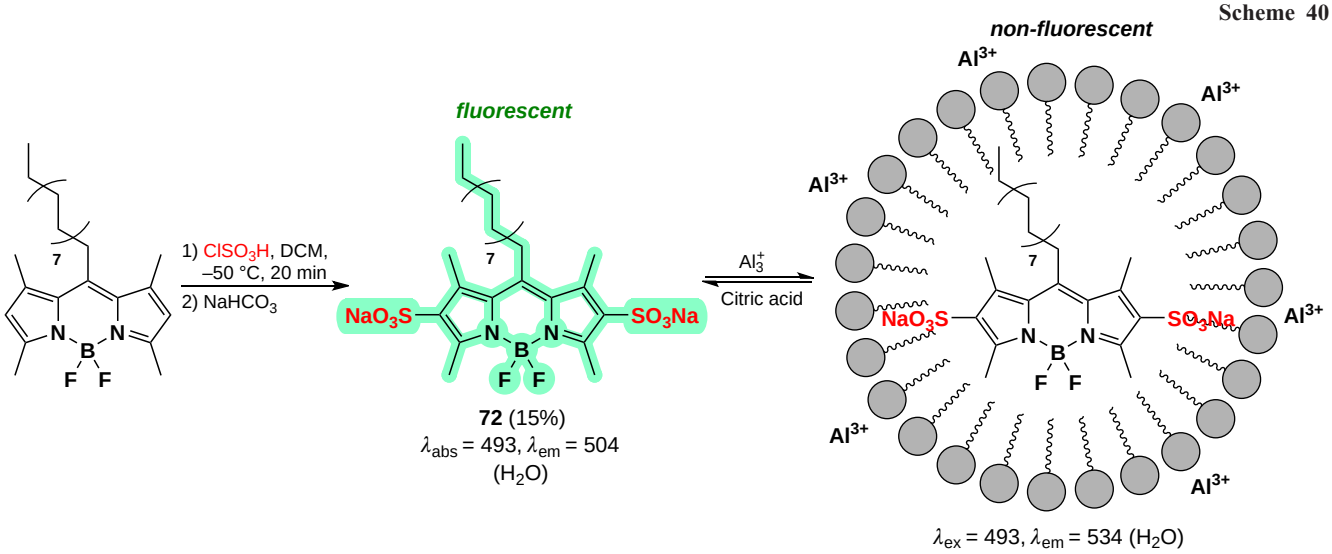

Scheme 41

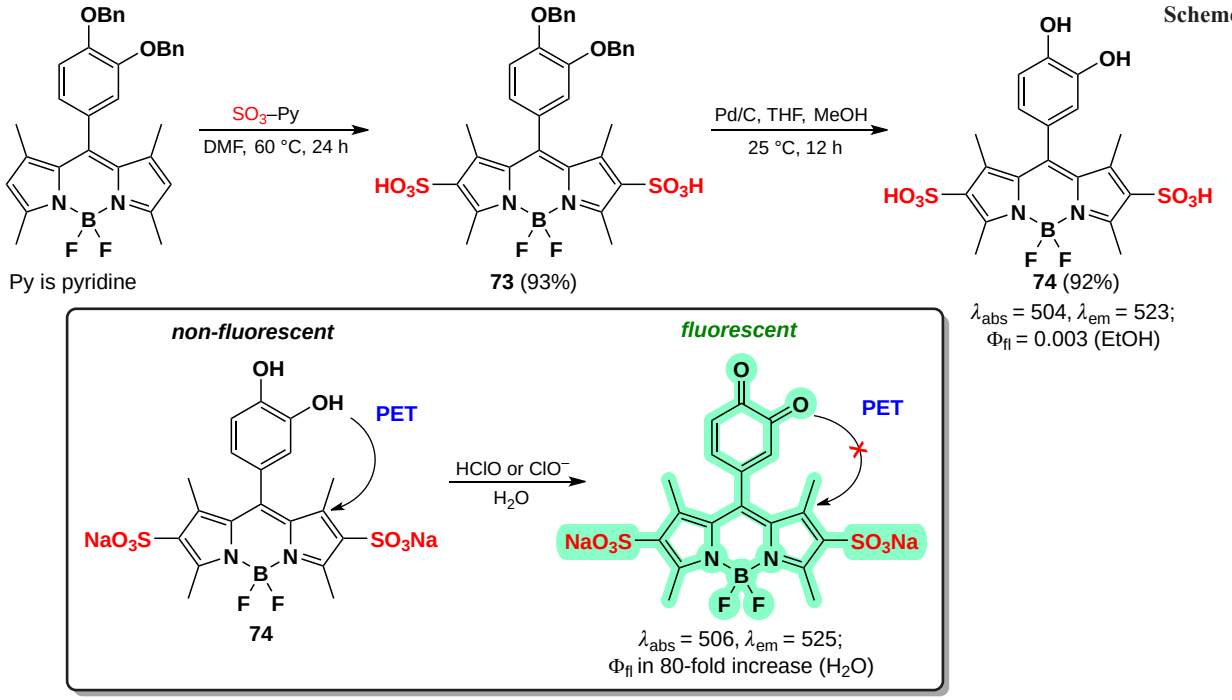

Scheme 42

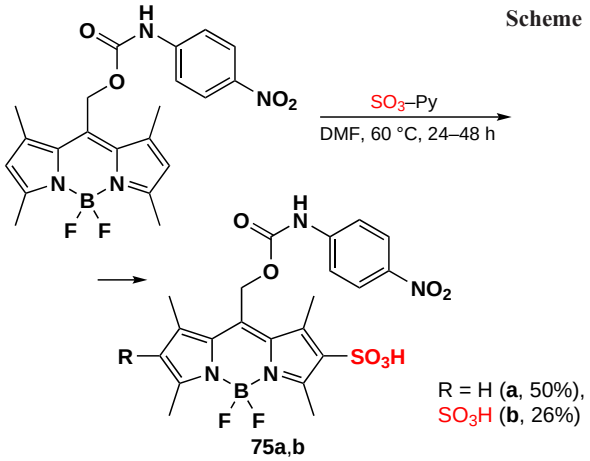

resulting in the formation of mono- or disubstituted products. The use of concentrated (70%) acid leads to the formation of the disubstituted product **76**, whereas the use of dilute (40%) acid gives the mono-substituted 2-nitro-BODIPY **77**.[150,151] Nitration of 1,2,3,8-tetraalkyl-BODIPY with nitric acid in the presence of acetic anhydride leads to a mixture of products **78** and **79** with a nitro group at positions 5 and 6.[152] In 2023, Ndung'U *et al.*[153] demonstrated that it is possible to introduce a nitro group into BODIPY at position 2, leading to the formation of product **80**, using NO_2BF_4. Nitro-BODIPYs are characterized by a hypsochromic shift of the absorption maximum and quenching of fluorescence compared to the parent BODIPY due to ICT (Scheme 43).

3.3.3. Nitrosation

The nitrosation of fluorescent molecules represents a promising avenue in the design of sensors for the sulfide anion, which is able to reduce nitroso compounds to the corresponding amines.[154] In 2020, Gil de Melo *et al.*[155] presented a novel method for the nitrosation of BODIPY under mild conditions in

Scheme 43

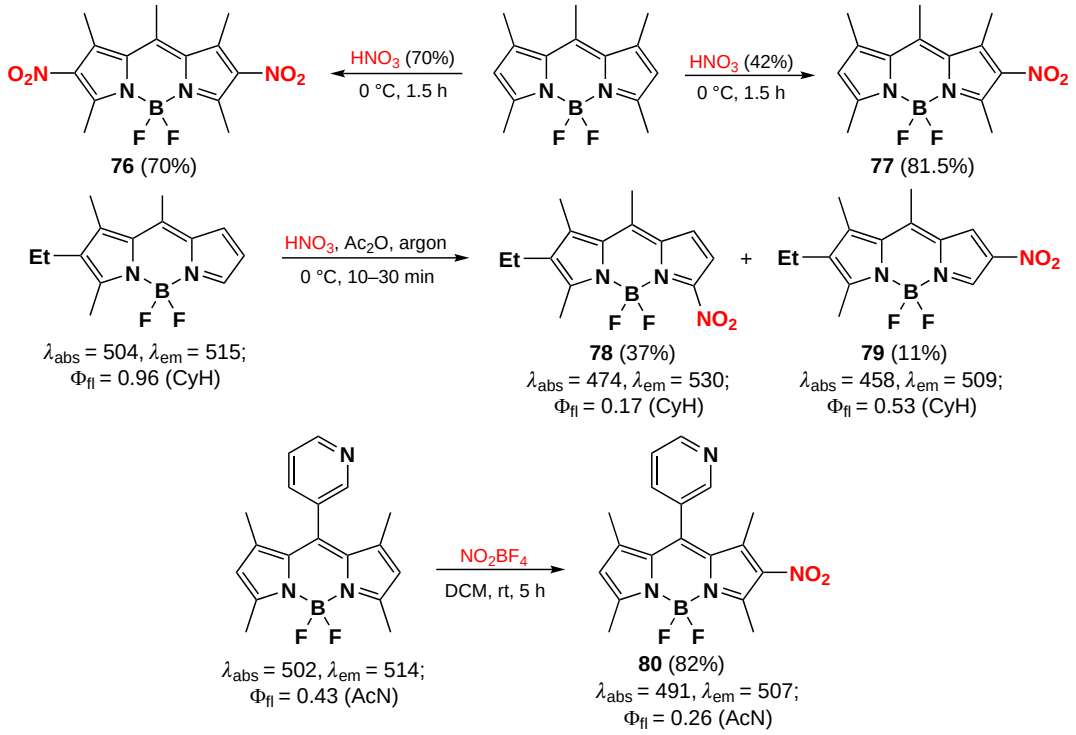

the presence of $NOBF_4$, leading to the formation of compounds **81a–c** and **82a–e**. Reactions with 1,3,5,7-tetramethyl-BODIPY yielded 2-substitution products **82a–d**; nitrosation of 3-phenyl-BODIPY led only to compound **82e**, an electrophilic substitution product at position 3. The regioselectivity of the nitrosation at position 2 can be explained by the preferential formation of a six-membered σ-complex intermediate stabilized by the tetrafluoroborate anion (Scheme 44).

2-Nitroso-substituted BODIPYs exhibit a significant hypsochromic shift of absorption maxima, accompanied by a reduction in fluorescence intensity in polar solvents, probably due to ICT.

3.3.4. Formylation

The formylation of BODIPY at positions 2 and 6 is usually conducted *via* the classical Wilsmeyer–Haack reaction.[105,156,157]

Scheme 44

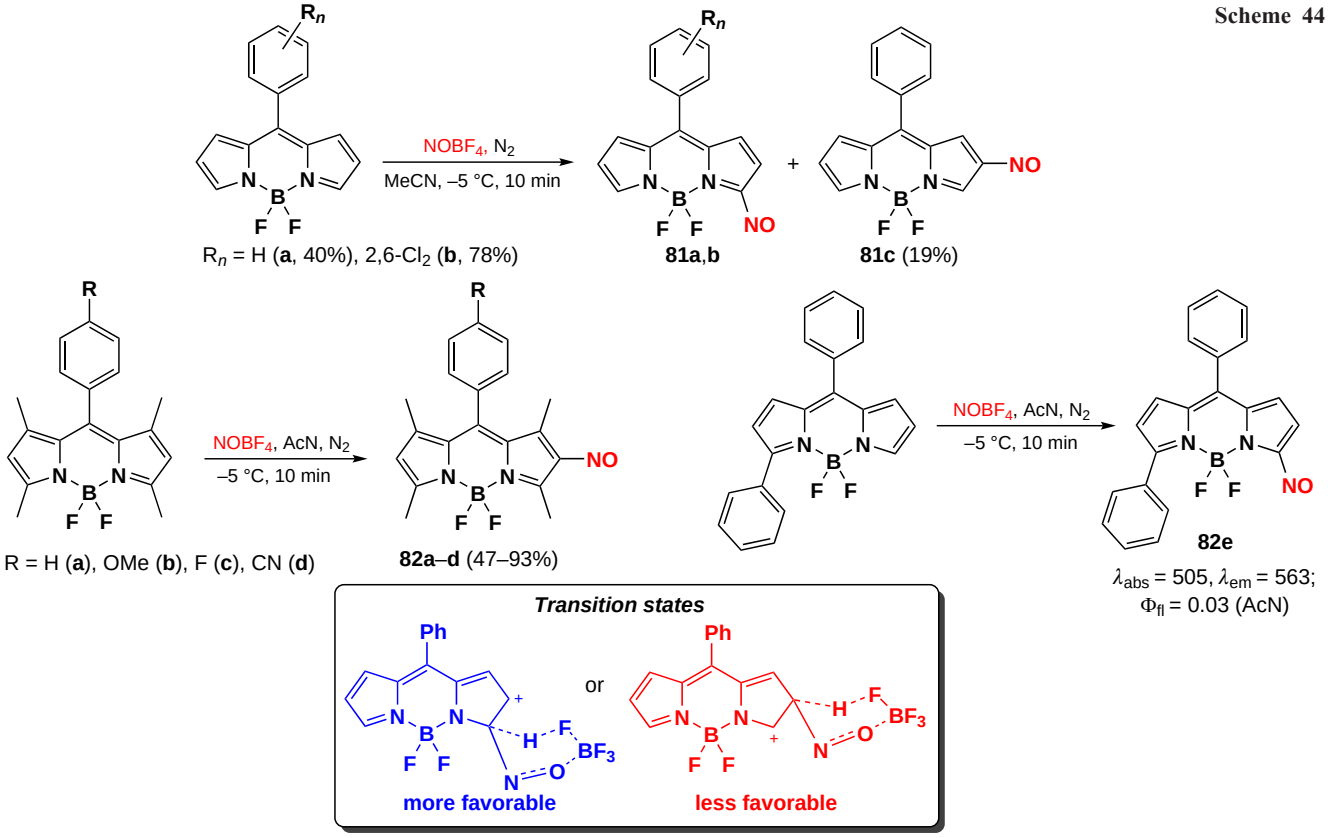

The process is initiated with the formation of a monoformylation product, typically using 1,2-dichloroethane as a solvent.[158] However, the synthesis can also be conducted in DMF.[159] The photophysical properties of 2-formyl-BODIPYs are nearly identical to those of the unmodified parent BODIPYs.[105] To obtain BODIPY **83** diformylated at positions 2 and 6, the reaction is carried out in two successive steps. The introduction of a second formyl group requires an excess of electrophilic agent, long reaction times and high temperatures.[160,161] In contrast to the formylation product of 2-formyl-BODIPY **84**, 2,6-diformyl-BODIPY **85** exhibits a minor bathochromic shift in absorption (Scheme 45).[160]

The synthesis of 3,5-diformyl-BODIPY **86** involves the pre-functionalization of the parent dipyrromethane by the Vilsmeyer reaction, followed by oxidation and complexation.[162] The resulting compound exhibits a bathochromic shift of 40 nm. In an alkaline solution, the aldehyde group of BODIPY **86** is a PET-quencher of the excited state of the nucleus, but in an acidic medium, PET is suppressed due to protonation of the aldehyde group, resulting in an up to 17-fold increase in fluorescence at pH 4 compared to the intensity at pH 7 (Scheme 46).

In 2018, Yeung *et al.*[163] proposed the radical reaction of electron-deficient heterocycles using trioxolane as an equivalent of formyl group (Scheme 47).

A year later, Fan *et al.*[164] described the formylation of BODIPY **60** at positions 3 and 5 by radical reaction with an unsubstituted 1,3-dioxolane. The transformation involved radical addition steps to generate the intermediate **87** and removal of the protecting group, resulting in the product **88** (Scheme 48). A full discussion of the radical reactions of BODIPY can be found in Section 3.6.

Scheme 45

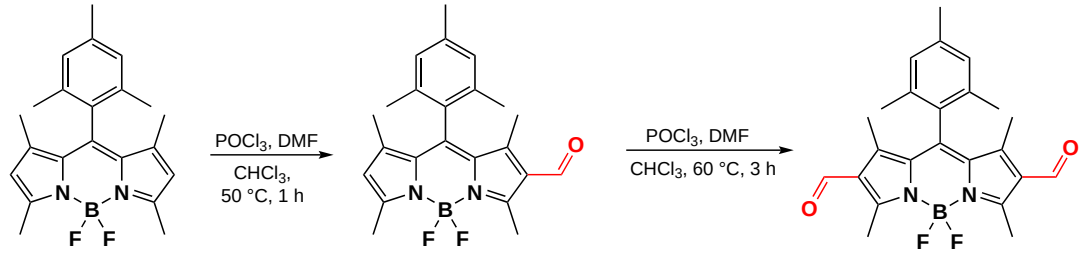

83
λ_{abs} = 504, λ_{em} = 512;
Φ_{fl} = 0.95 (PhMe)

84 (80%)
λ_{abs} = 502, λ_{em} = 512;
Φ_{fl} = 1.0 (PhMe)

85 (76%)
λ_{abs} = 510, λ_{em} = 519;
Φ_{fl} = 0.96 (PhMe)

Scheme 46

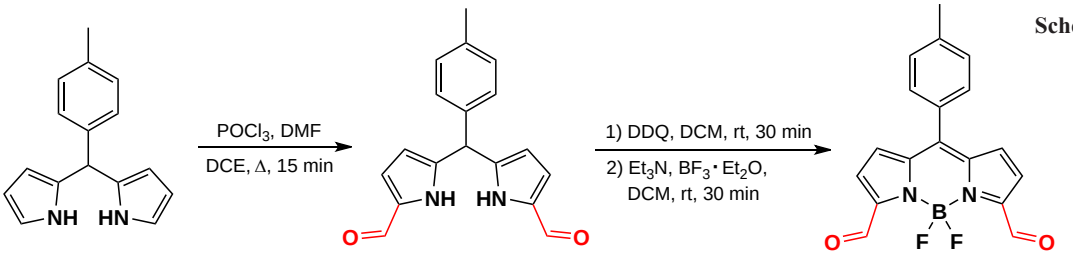

DCE is 1,2-dichloroethane

86 (14%)
λ_{abs} = 546, λ_{em} = 556;
Φ_{fl} = 0.31 ($CHCl_3$)

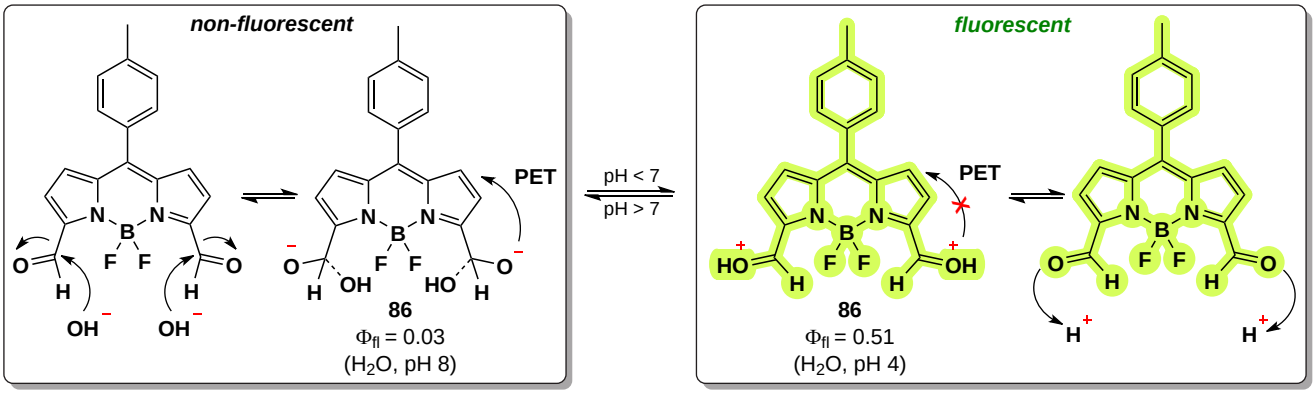

86
Φ_{fl} = 0.03
(H_2O, pH 8)

86
Φ_{fl} = 0.51
(H_2O, pH 4)

Scheme 47

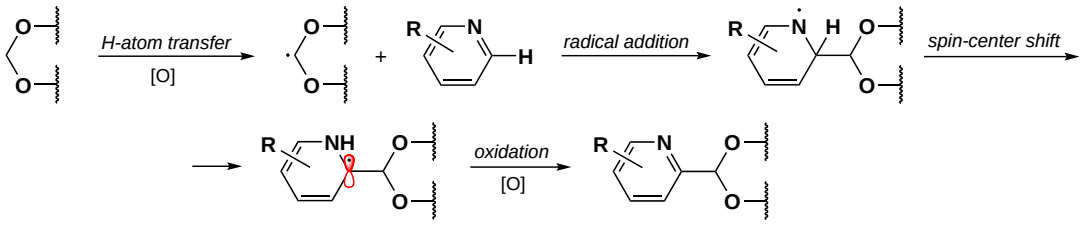

Scheme 48

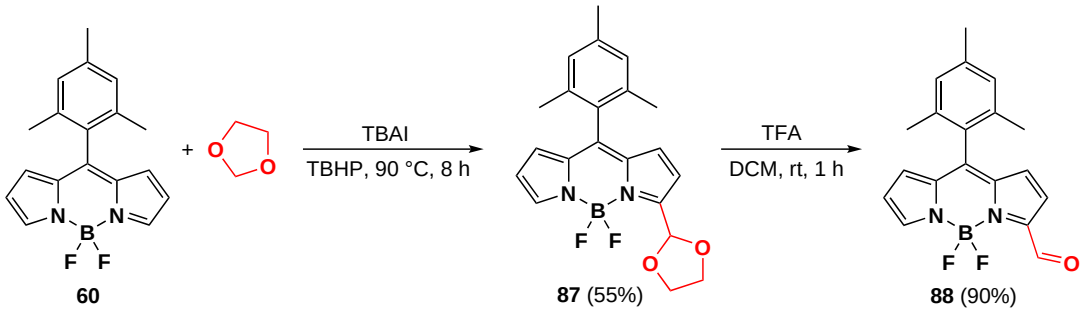

60
λ_{abs} = 500, λ_{em} = 522;
Φ_{fl} = 0.74 (DCM)

87 (55%)
λ_{abs} = 505, λ_{em} = 522;
Φ_{fl} = 0.81 (DCM)

88 (90%)
λ_{abs} = 519, λ_{em} = 536;
Φ_{fl} = 0.68 (DCM)

TBHP is *tert*-butylhydroperoxide

3.3.5. Acylation

The classical Lewis acids-catalysed Friedel–Crafts acylation is not applicable to the functionalisation of BODIPY, as the presence of protonic Brønsted acids facilitates the removal of the BF_2 group.[165] Conversely, the Lewis acid $AlCl_3$, which is commonly employed in electrophilic aromatic substitution reactions, facilitates nucleophilic substitution reactions at the boron atom (see section 3.7).[166,167]

In 2016, Mirri *et al.*[168] proposed the acylation of BODIPY under the action of BF_3–Et_2O as a Lewis acid. BODIPY **20** was demonstrated to undergo Friedel–Crafts acylation at position 2 in the presence of acyl chlorides. BODIPY **89** (Scheme 49) exhibited a notable decrease in fluorescence quantum yield, from 0.95 to 0.6–0.8.

This approach was applied in 2020 by de Jong *et al.*[169] in the synthesis of fluorescent dyes **90** and **91**, which are specific to the endoplasmic reticulum (ER). The highest co-localization ratio in the ER was observed for compound **90** (0.91), which can be attributed to the optimal ratio of lipophilic to amphiphilic parts in the molecule (Scheme 50).

The modification of the molecule by an acyl group at positions 3 and 5 can also be accomplished by radical reaction with 1,3-dioxalanes, in a manner similar to the radical formylation described in Section 3.3.4. By varying the reaction time, mono- (**92**) and diacylation products (**93**) were obtained.[164] (Scheme 51).

Both approaches to the acylation of BODIPY, radical and Lewis acid catalyzed, were used by Gonzalez-Vera *et al.*[170] in the synthesis of the fluorescent solvatochrome Prodan derivatives **94** and **95** (Scheme 52). The structure of solvatochrome dyes typically comprises an electron-donor and an electron-acceptor group. Upon photoexcitation, intermolecular charge transfer (ICT) from the donor to the acceptor occurs, resulting in an increased dipole moment in the excited state relative to the ground state. This makes the probe sensitive to environmental conditions, particularly solvent polarity. The emission in polar solvents was quenched by ICT for both BODIPY derivatives, **94** and **95**. However, the former exhibited a higher degree of emission in non-polar solvents, while the latter demonstrated a comparatively reduced emission in polar solvents.

In 2023, Fan *et al.*[18] proposed a copper-catalysed method for the direct acylation of BODIPY at the α-position by aliphatic and aromatic aldehydes, yielding BODIPY **96** (Scheme 53).

The authors demonstrated that the reaction involves radical particles. The presence of 2,2,6,6-tetramethylpiperidin-1-yl)-oxyl (TEMPO) or 2,6-di-tert-butyl-4-methylphenol (BHT) was found to inhibit the reaction. The authors proposed a mechanism whereby the acyl radical attacks position 3 of BODIPY,

Scheme 49

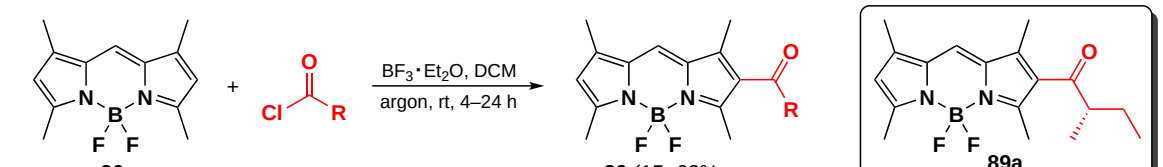

20
λ_{abs} = 506, λ_{em} = 512;
Φ_{fl} = 0.95 (DCM)

R = Alk, Ar

89 (15–62%,
5 examples)

89a
λ_{abs} = 506, λ_{em} = 516;
Φ_{fl} = 0.62 (DCM)

Scheme 50

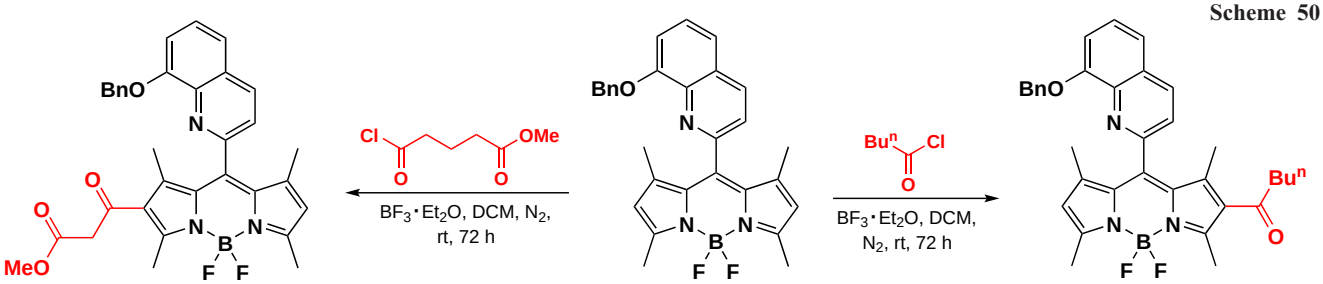

90 (45%)
λ_{abs} = 503, λ_{em} = 520;
Φ_{fl} = 0.12 (MeOH)

91 (70%)
λ_{abs} = 503, λ_{em} = 524;
Φ_{fl} = 0.12 (MeOH)

Scheme 51

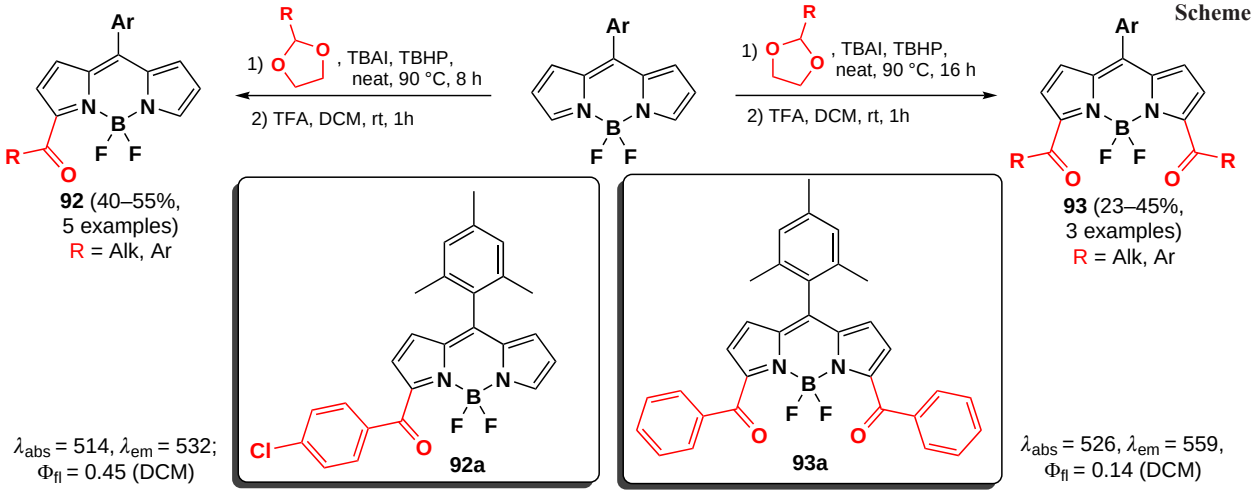

Scheme 52

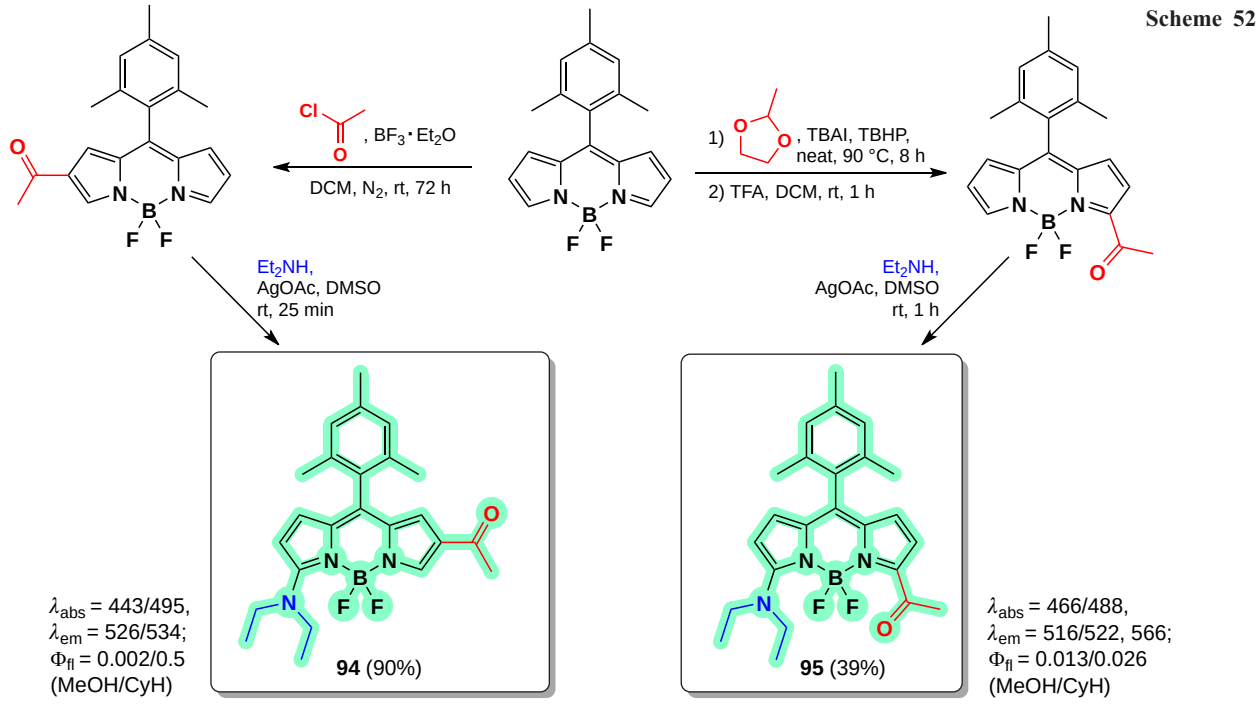

subsequently undergoing oxidation to the cation by interaction with copper(II) ion. The resulting 3,5-diacylated BODIPY exhibited a slight bathochromic shift in the absorption maxima, accompanied by a reduction in fluorescence quantum yields.

3.3.6. Alkylation

In 2021, Yanai *et al.*[171] synthesized carbanionic derivatives of BODIPY with high water solubility and good emission properties. The 2,6-dialkylation products **97** were obtained by alkylation with 2-fluoropyridinium ethanide to form in situ 1,1-bis[(trifluoromethyl)sulfonyl]ethene. The carbanionic BODIPYs **97** exhibited a minor bathochromic shift in their absorption and emission spectra. The relatively weak impact of the carbanionic substituent on the photophysical properties can be primarily attributed to the presence of a benzylic CH_2 group between the carbanion and the BODIPY core. BODIPY **97** exhibited bright fluorescence in both organic and aqueous solutions, with BODIPY **97a** demonstrating an exceptionally high solubility of > 10 000 mg L^{-1} (Scheme 54).

3.3.7. β-Alkenylation

In 2024, Mertinez *et al.*[25] reported a Lewis acid-catalized electrophilic β-alkenylation of BODIPY. The substitution occurred at positions 2 and 6, resulting in the formation of the Markovnikov adduct **98** (Scheme 55).

The highest yields in electrophilic substitution reactions with electron-deficient alkynes with an ester group were achieved using indium iodide as a Lewis acid, which was explained by its high oxophilicity. As a possible mechanism, the authors proposed that InI_3 could coordinate with the alkyne triple bond, followed by BODIPY anti-attachment, further aromatization and protodemetallation. An intermediate alkenyl cation is also likely to form.

For electron deficient alkynes with an ester group, the authors considered σ-coordination of InI_3 with the carbonyl moiety and subsequent β-addition of BODIPY to form a zwitterionic allenyl enolate. This yielded trisubstituted (*Z*)-alkenes **99**, which could be further alkenylated to give products **100**. Most of the alkenylated BODIPYs had high fluorescence quantum yields,

Scheme 53

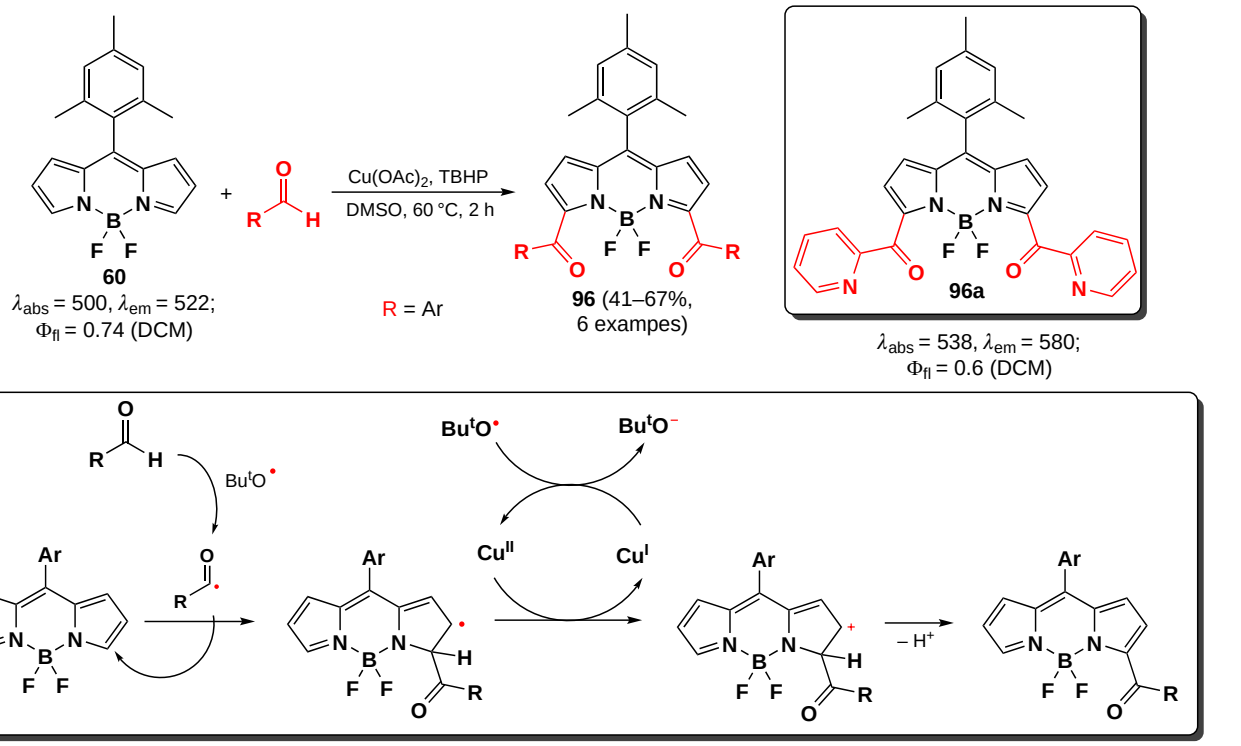

Scheme 54

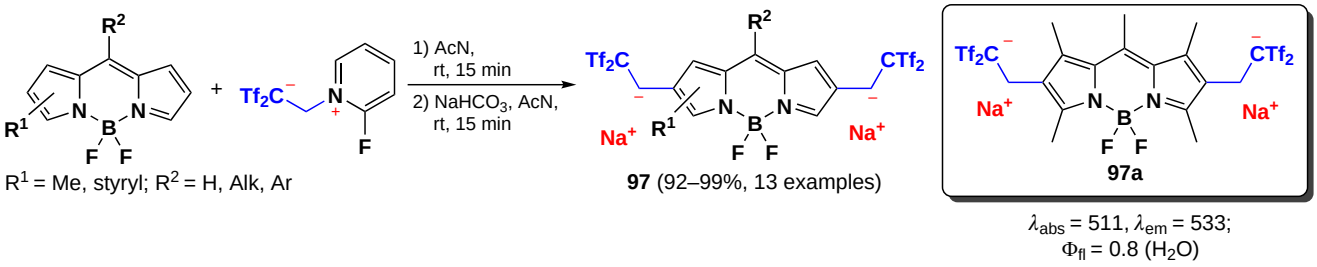

Scheme 55

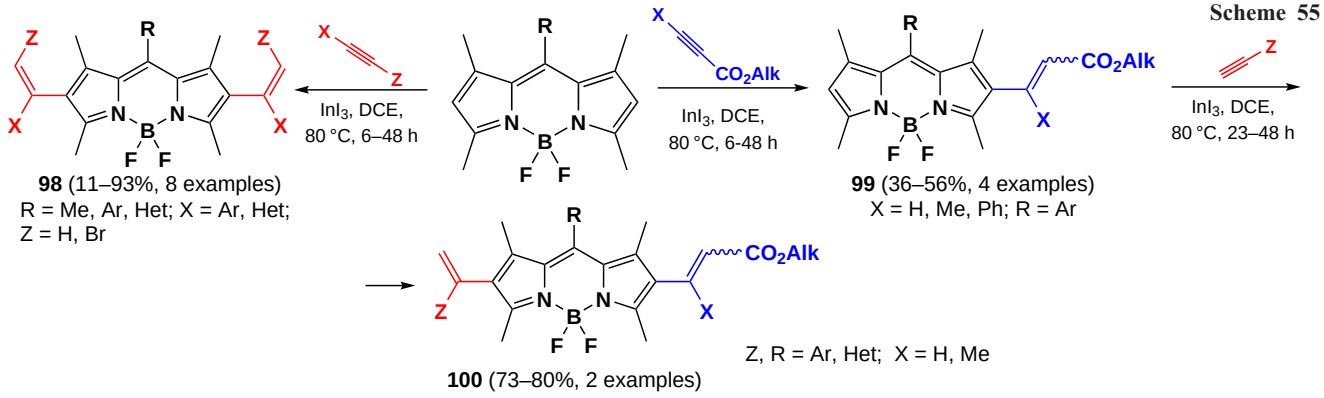

which depended on both the nature of the alkenyl and the nature of the *meso*-aryl substituents.

3.3.8. Nicholas reaction

In 2021, Uriel *et al.*[172] showed that 1,3,5,7-tetramethyl-BODIPY is able to react with an electrophilic propargyl cation stabilized by a cobalt complex (Nicholas reaction) at positions 2 and 6. The interaction of 1,3,5,7-tetramethyl-BODIPY with different *meso*-substituents with the propargyl-cobalt complex in the presence of BF_3–Et_2O at –15 °C led to the formation of 2,6-disubstituted BODIPYs **101**. 2,6-dipropargyl BODIPY derivatives **102** were obtained by the demetallation reaction with iodine or ethylenediamine. The use of a slight excess (1.1 equiv.) of the initial cobalt complex leads to monosubstitution products in position 2 — complexes **103**. BODIPYs **104** can be synthesized from corresponding complexes **103** *via* demetallization (Scheme 56).

In 2023, Ventura *et al.*[173] compared the reactivity of the $B(CN)_2$ substituted BODIPYs with BF_2-BODIPYs in the

Scheme 56

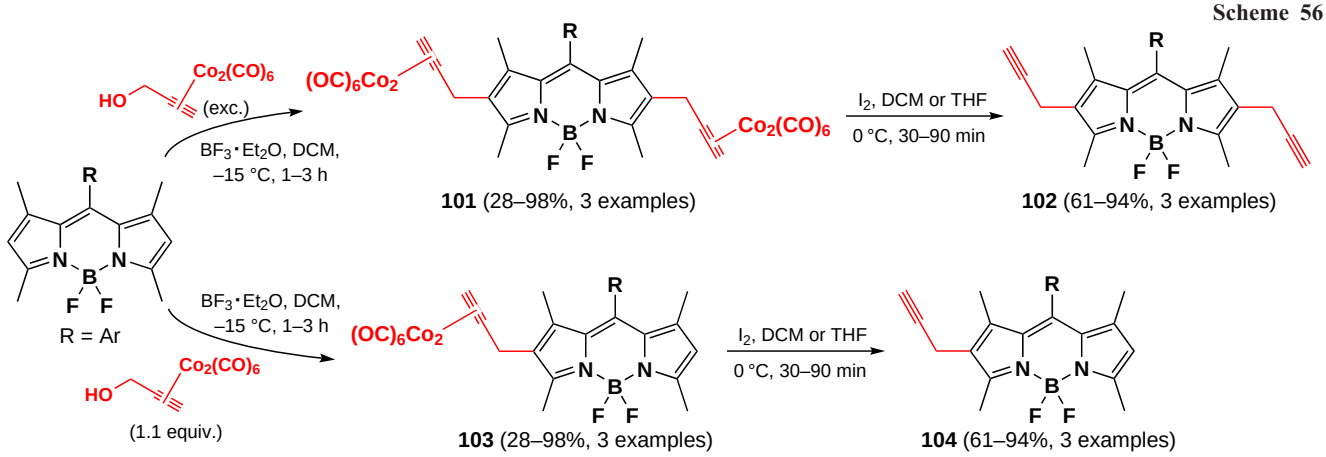

Scheme 57

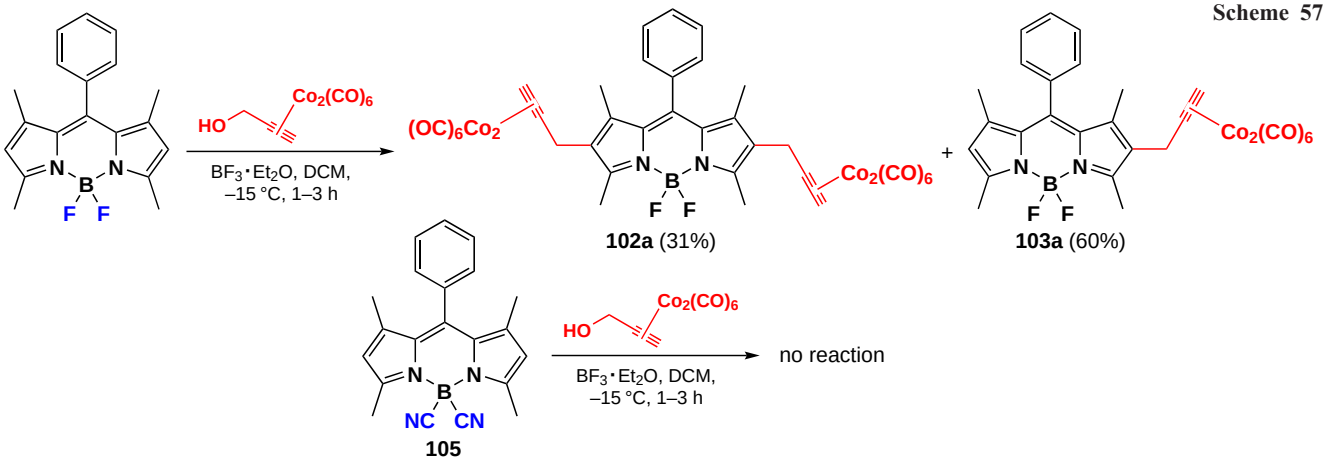

Nicholas reaction. It was shown that $B(CN)_2$-BODIPYs barely participate in electrophilic halogenation or formylation reactions, and do not participate at all in the Nicholas reaction due to the increased electron acceptability of the CN-groups. Under Nicholas reaction conditions, the mixture of $B(CN)_2$-BODIPY and BF_2-BODIPY gave only substitution products **105a**,**b** (Scheme 57).

3.4. Nucleophilic substitution reactions

3.4.1. Nucleophilic substitution reaction at positions 1, 3, 5 and 7

The reactivity of 3-chloro- and 3,5-dichloro-BODIPYs in nucleophilic substitution reactions with oxygen-, sulfur-, and nitrogen-based nucleophiles was initially examined by Rohand *et al.* in 2006.[141] Nucleophilic substitution at positions 3 and 5 resulted in a bathochromic shift of absorbtion. BODIPY **106**, **107** exhibited high fluorescence quantum yields, and fluorescence quenching for compounds **106a** and **107a** was observed due to the ICT effect. In 2009, Vosch *et al.*[174] synthesized a series of 3,5-chalcogen-substituted BODIPY **108a**–**e** from 3,5-dichloro BODIPYs. An increase in the atomic mass of chalcogen and a decrease in electronegativity from oxygen to tellurium resulted in a bathochromic shift of maxima in the absorption and emission spectra. α-Te-BODIPY **108e** showed the ability to form triplet states due to the 'heavy atom' effect (Scheme 58).

In 2011, Jiao *et al.*[100] investigated the reactivity of polybromo-BODIPY in reactions with O-, N-, and S-nucleophiles. The reaction of tetrabromo-BODIPY with aliphatic or aromatic amines resulted in the formation of 3-monosubstitution products **109** and **110**. In the case of S-nucleophiles, the reaction gave 1,3,5-tri- (**111**) and 1,3,5,7-tetrasubstitution products (**112**). Leen *et al.*[101] demonstrated that nucleophilic substitution also occurs with 1,7-dihalogen-BODIPY, resulting in the formation of compound **113**, which exhibits bright fluorescence, bathochromically shifted absorption and emission, and pronounced solvatochromism (Scheme 59).

Nucleophilic substitution at the α-position of BODIPY also occurs with C-nucleophiles, foe example, pyrroles. The 3- and 3,5-dipyrrolyl-BODIPY **114** and **115** compounds display bathochromically shifted absorption and emission bands, accompanied by a notable suppression of fluorescence in polar solvents due to ICT (Scheme 60).[144]

In 2019, Belmonte-Vázquez *et al.*[118] reported the synthesis of a condensed benzofuran-BODIPY **116** *via* sequential nucleophilic substitution reactions at positions 3 and 5 of BODIPY, and intramolecular Pd^0-catalysed arylation. Due to high planarity, BODIPYs **116** exhibited bathochromic shifts up to 110 nm, as well as small Stokes shifts. Except for BODIPY **116a** with a formyl group, compounds **116** demonstrated high laser efficiency‡ ($\Phi_{laser} > 40\%$) and laser emission within the $\lambda = 642–647$ nm range. BODIPY **116b** exhibited the highest laser efficiency (Scheme 61).

In 2022, Ribagorda *et al.*[17] synthesized 3-azoconjugated BODIPYs **118** that were able to act as hypoxia-sensitive

‡ This characteristic demonstrates the ratio of the energy received by the laser to the energy of the generated laser radiation.

Scheme 58

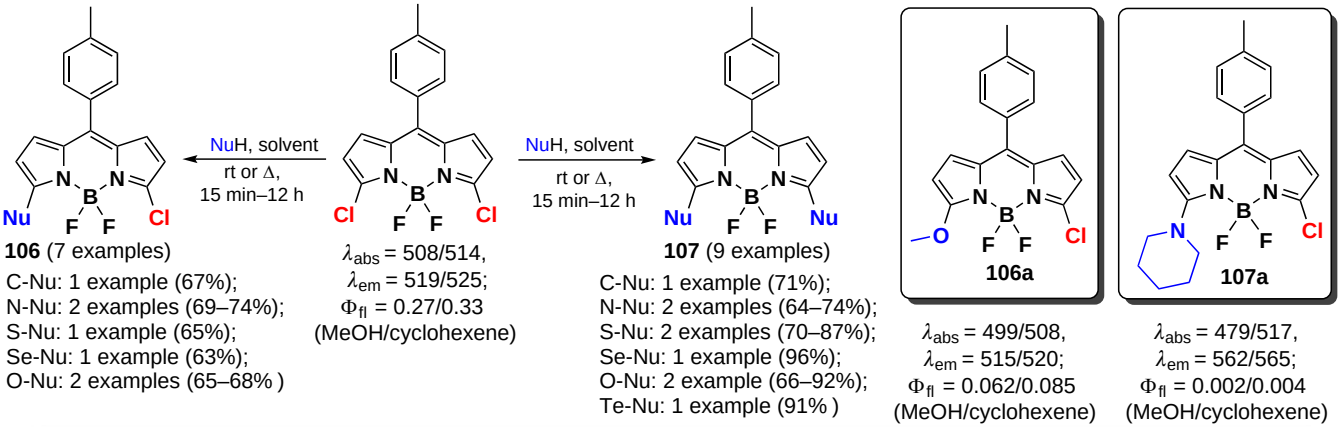

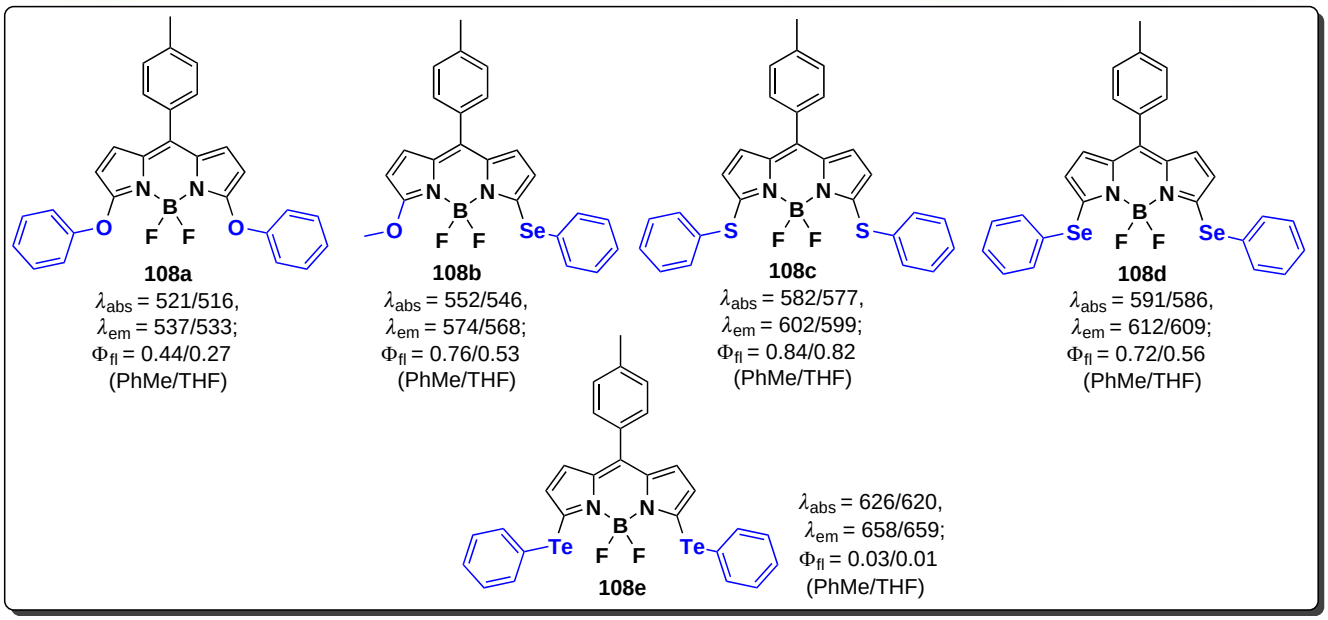

Scheme 59

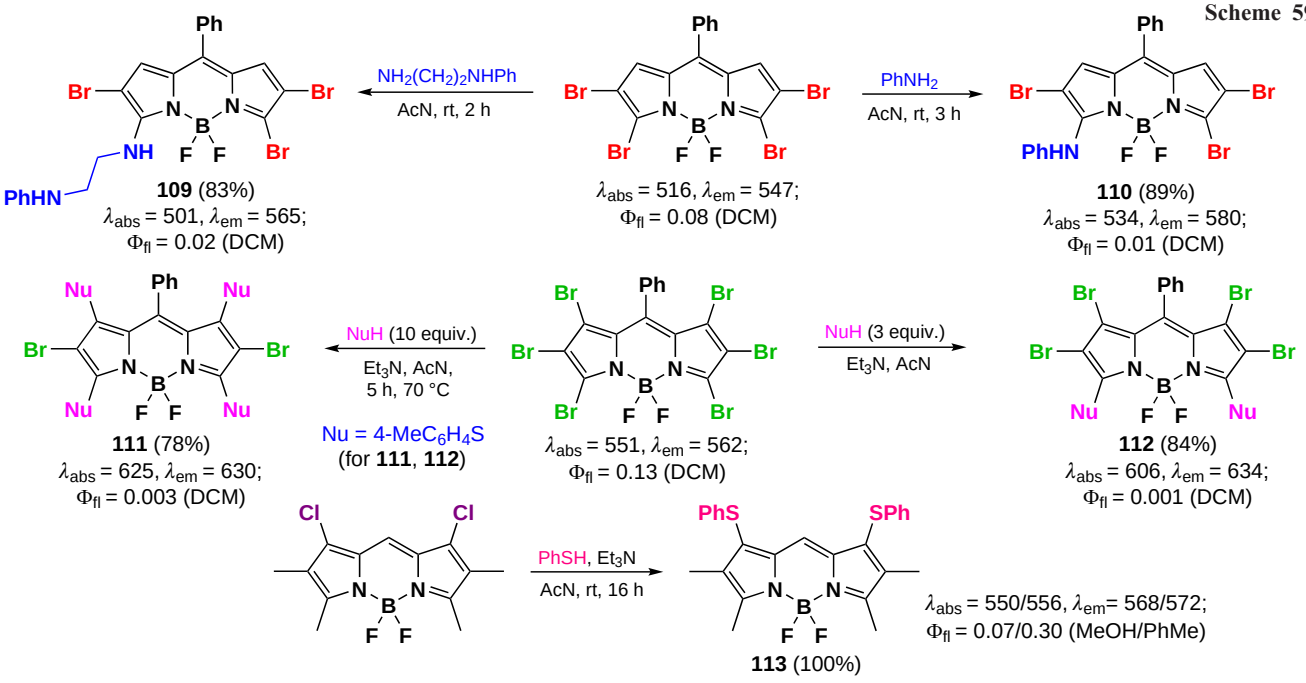

Scheme 60

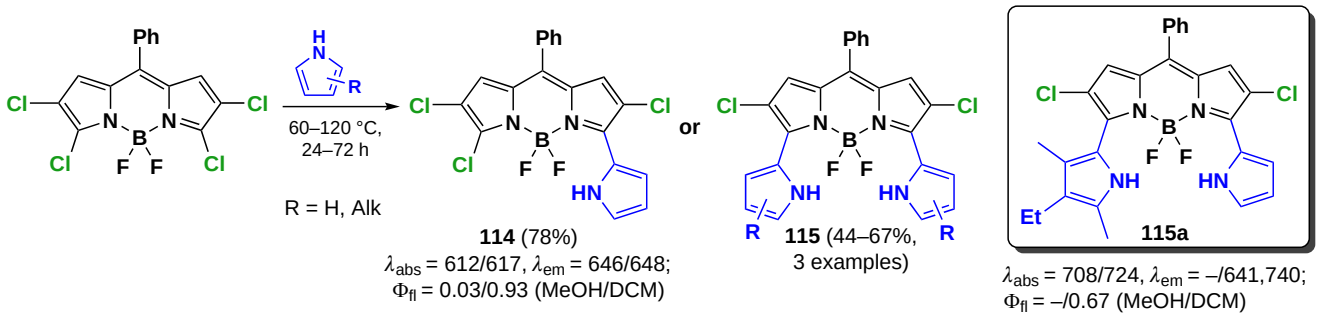

Scheme 61

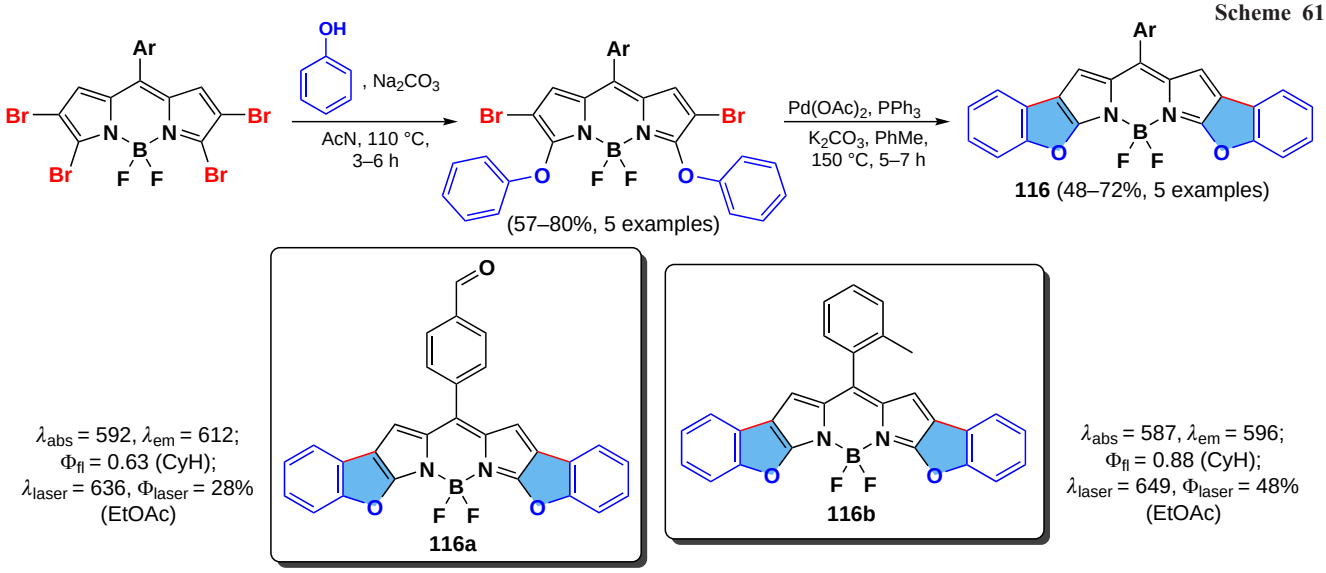

fluorescent sensors. The products were obtained by nucleophilic substitution of α-halogen atoms by hydrazine, condensation with bis-(dimethylacetal) *p*-benzoquinone (DMA-BQ), and arylation with boronic acids in the presence of a Pd-catalyst. Under the action of bacterial (i-AzoRBC) and human (human NQO1) reductases as a result of azo-bond cleavage of probes **118**, a hypsochromic shift in the absorption spectrum at 140 nm and fluorescence broadening to a value of $\Phi_{fl} = 0.95$ were observed, including in hypoxic HeLa cells (Scheme 62).

Han *et al.* [35, 175] developed HClO-sensitive fluorescent probes based on isoindole-BODIPYs. BODIPYs **119** and **120** were synthesized through nucleophilic substitution reactions of α-chloro-BODIPY with diphenylphosphine and selenamorpholine (Schemes 63, 64). In the presence of HClO, both probes exhibited an emission flare-up due to the oxidation of the phosphorus or selenium atom, which suppressed PET. The probes showed low detection limit (10–20 nm) and the ability to detect HClO *in vitro* and *in vivo* in Danio fish.

In 2023, Song *et al.*[176] syntesized a hydrogen peroxide/medium viscosity sensitive BODIPY **121** through a series of nucleophilic substitution reactions of a chlorine atom at the α-position and aldol condensation of the intermediate 3-formyl-BODIPY with a 2-methylindole derivative (**A**) (Fig. 10). In a viscous medium the rotation of the hemicyanine moiety is

Scheme 62

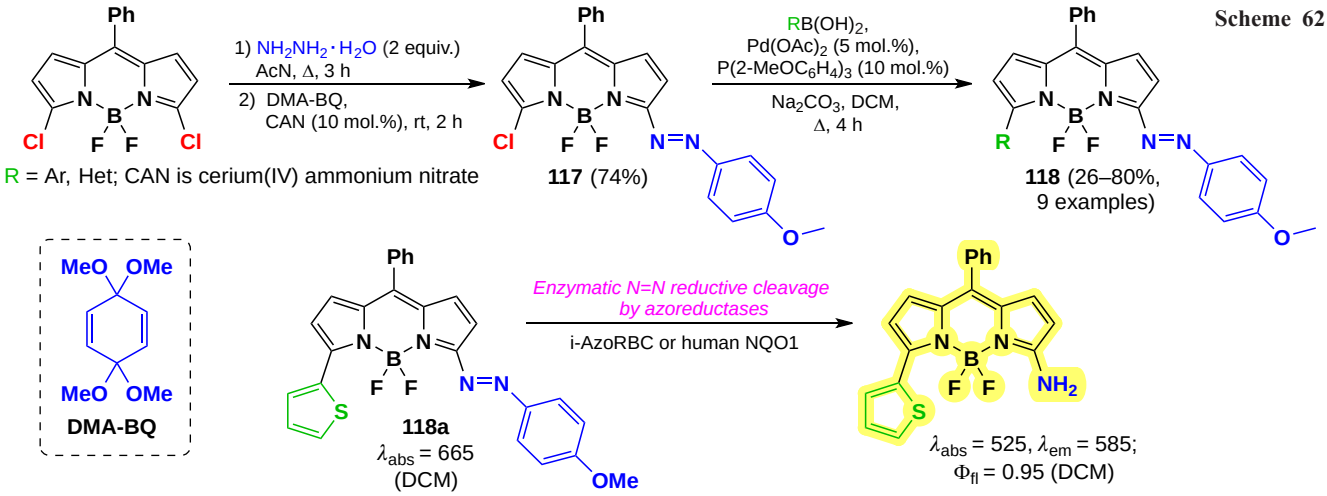

Scheme 63

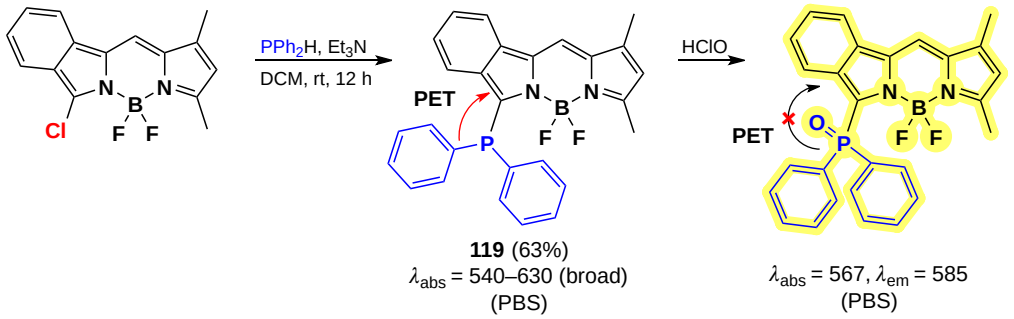

Scheme 64

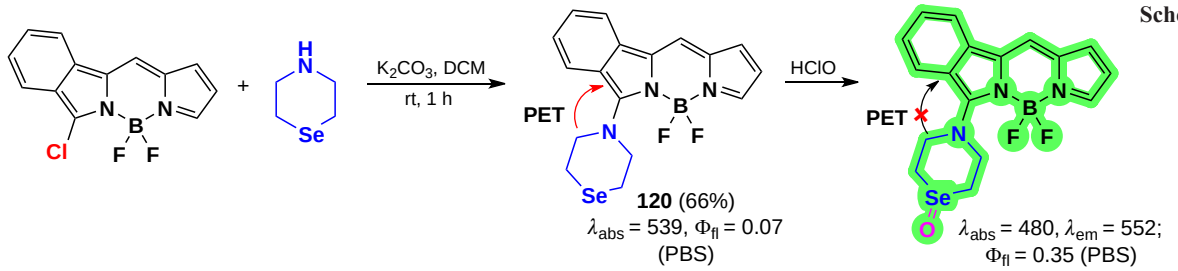

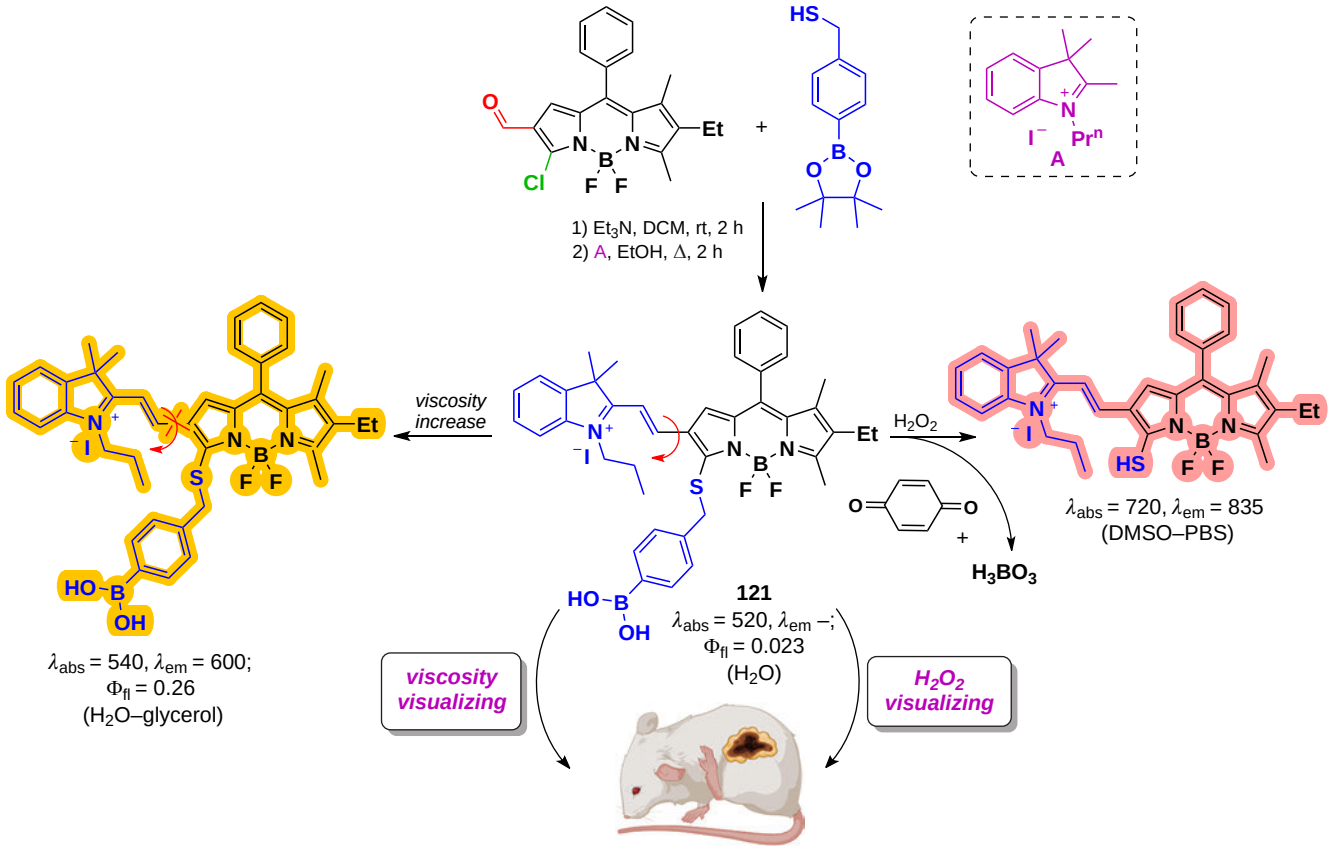

Figure 10. Synthesis scheme and principle of hydrogen peroxide and medium viscosity detection by probe **121**. The figure created by the authors based on the publication [176].

inhibited, followed by an increase in the emission of BODIPY **121** at λ = 600 nm. Additionally, in the presence of H_2O_2 an increase in both absorption (λ_{abs} = 720 nm) and emission (λ_{em} = 835 nm) were observed due to the cleavage of the α-sulfide moiety. An ability of **BODIPY 121** to visualize the viscosity gradient and detect exo- or endogenous hydrogen peroxide in HepG2 cells as well as in mouse organs was confirmed.

3.4.1.1. Application of nucleophilic substitution reactions in BODIPY in biosensorics

Nucleophilic substitution reactions in BODIPY are commonly used in the design of fluorescent probes capable of biomolecule detection, such as biothiols cysteine (Cys), homocysteine (Hcy) and glutathione (GSH). This approach was first reported in 2012 by Yang *et al.*[177] 3-Chloro-BODIPY **122** was used as a selective fluorescent probe for GSH detection. Nucleophilic substitution

of the α- chlorine atom in BODIPY **122** with GSH resulted in a shift of the fluorescence maximum from 556 to 588 nm. At the same time, a similar nucleophilic substitution of the α-chlorine in BODIPY **122** with Cys or Hcy resulted in an intramolecular rearrangement of α-sulfur-substituted BODIPY to α-amino-substituted BODIPY, resulting in a shift of an emission maximum to564 nm. Probe **122** demonstrated the capability of ratiometric (I_{588}/I_{556}) selective detection of GSH with a detection limit of 86 nm.

Further, a Cys-selective probe **123** was obtained by replacing the α-chlorine atom in probe **122** with *p*-nitrophenol.[178] In this case, a double nucleophilic substitution reaction took place with the product fluorescence flaring up at 564 nm due to a decrease of PET. Upon the reaction of probe **123** with GSH (Hcy), a second nucleophilic substitution reaction (α-sulfur-substituted BODIPY into α-amino-substituted BODIPY) was slower due to the less favourable transition state, resulting in a main product with emission at 588 nm. The modification of probe **122** at the second α-position with quaternised imidazole moiety yielded probe **124**, capable of simultaneous detection of GSH or Cys(Hcy) (Scheme 65).[179] In the presence of GSH, the nucleophilic substitution of both thiophenol and imidazolinium resulted in a bright emission at 588 nm at an excitation wavelength (λ_{ex}) of 568 nm. Nucleophilic substitution with Cys(Hcy) resulted in bright emission at 530 nm (λ_{ex} = 443 nm).

For BODIPY **125** with a disulfide moiety that cleaves in the presence of biothiols, fluorescence emission was observed at different wavelengths in the presence of GSH or Hcy/Cys.[180] Nucleophilic substitution of a similar probe **126** with Cys, Hcy and GSH gave products of different polarity, allowing the simultaneous detection of all three biothiols.[181] BODIPY **127** with hydrophilic polyethylene glycol (PEG) chains and fluorescein was capable to form non-fluorescent NPs, which undergone disaggregation and release of fluorescent BODIPY (λ_{em} = 595 nm) and dye (λ_{em} = 512 nm) upon reaction with GSH.[182] Probes **128** and **129** demonstrated the ability to detect Cys, Hcy and GSH based on differences in the fluorescence of the resulting products.[183] 3-Chloro-5-(*m*-nitrophenoxy)-BODIPY **129** was found to be an appropriate fluorophore for two-step ratiometric fluorescence detection of GSH across three concentration ranges, in the absence of a fluorescence response to Cys(Hcy).[184] The use of probe **130** with a vector to mitochondria and a triphenylphosphine moieties enables the detection of GSH in mitochondria.[185]

In 2017, Guo *et al.*[186] reported a hydrogen sulfide-sensitive fluorescent probe **131** based on 3,5- phenylselenide BODIPY. Replacement of the PhSe leaving group with a sulfonyl (SH) resulted in a 49-fold fluorescence attenuation and a hypsochromic shift of the absorption bands. The detection limit of probe **131** was 2.5 nm, and its ability to visualize GSH in living cells was also demonstrated (Scheme 66).

3.4.1.2. Oxidative nucleophilic substitution of hydrogen at 3,5-positions

In 2010, Leen *et al.*[187] investigated oxidative nucleophilic substitution in the BODIPY core. Positions 3 and 5 of the

Scheme 65

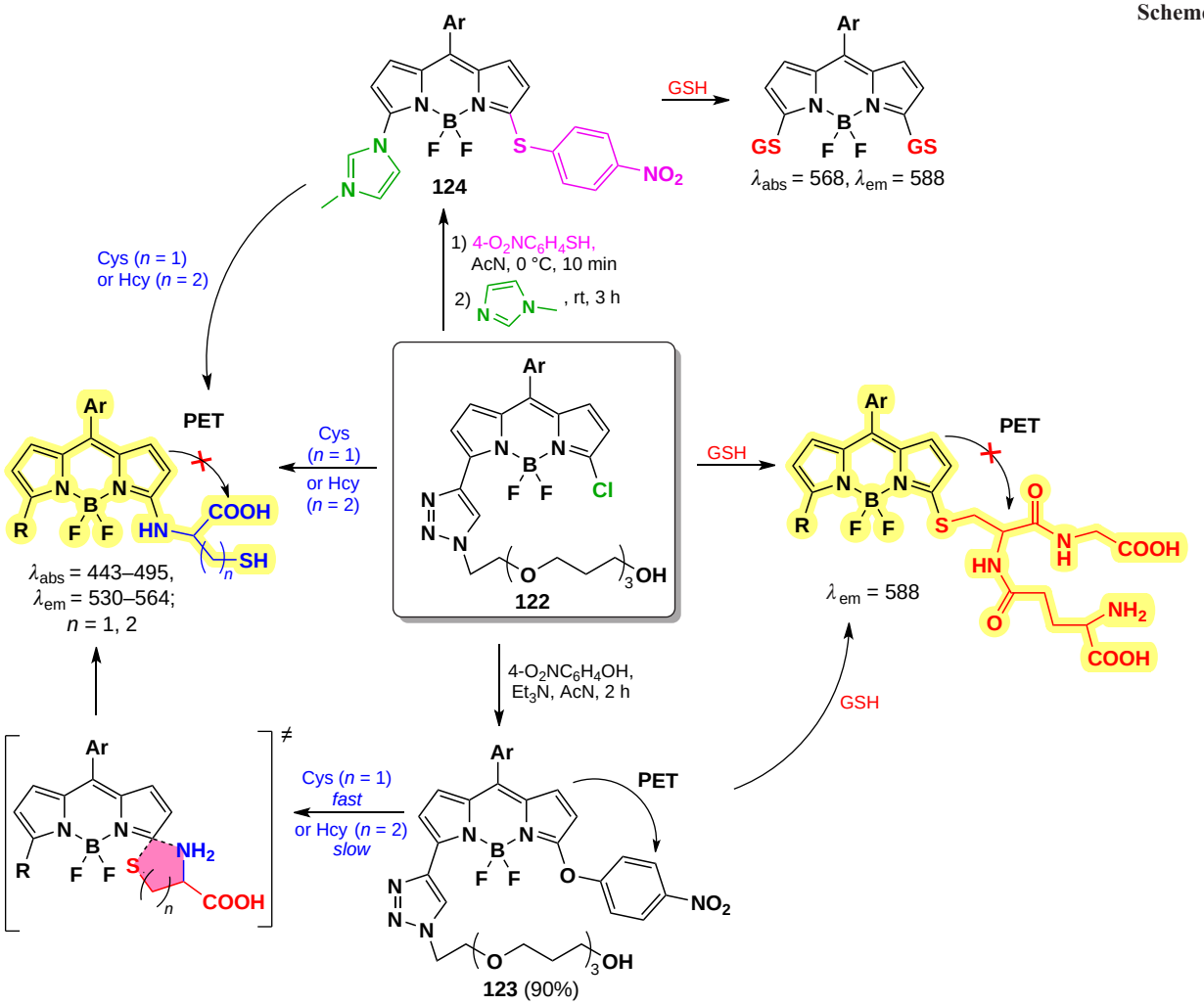

Structures 125–130

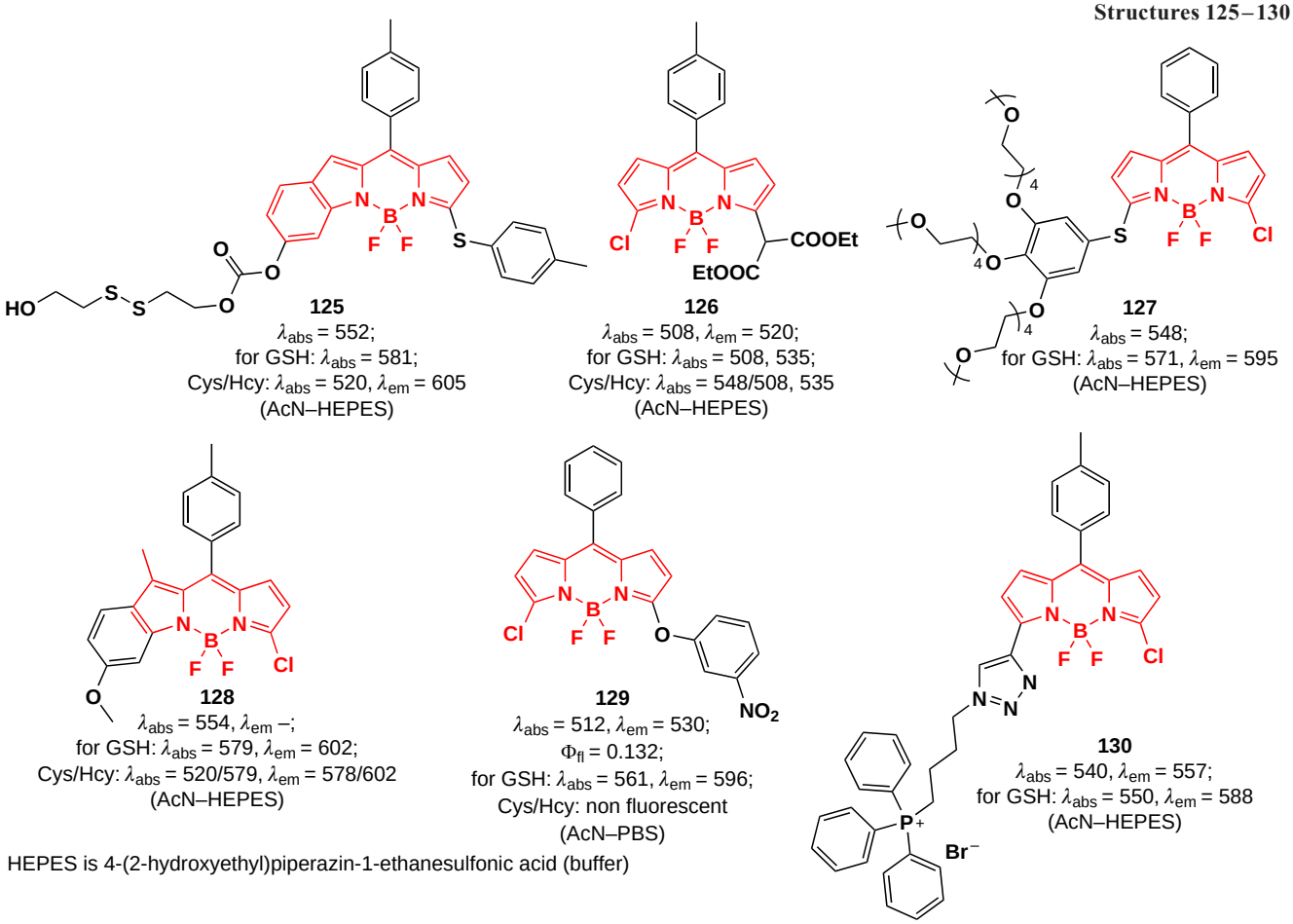

125
λ_{abs} = 552;
for GSH: λ_{abs} = 581;
Cys/Hcy: λ_{abs} = 520, λ_{em} = 605
(AcN–HEPES)

126
λ_{abs} = 508, λ_{em} = 520;
for GSH: λ_{abs} = 508, 535;
Cys/Hcy: λ_{abs} = 548/508, 535
(AcN–HEPES)

127
λ_{abs} = 548;
for GSH: λ_{abs} = 571, λ_{em} = 595
(AcN–HEPES)

128
λ_{abs} = 554, λ_{em} –;
for GSH: λ_{abs} = 579, λ_{em} = 602;
Cys/Hcy: λ_{abs} = 520/579, λ_{em} = 578/602
(AcN–HEPES)

129
λ_{abs} = 512, λ_{em} = 530;
Φ_{fl} = 0.132;
for GSH: λ_{abs} = 561, λ_{em} = 596;
Cys/Hcy: non fluorescent
(AcN–PBS)

130
λ_{abs} = 540, λ_{em} = 557;
for GSH: λ_{abs} = 550, λ_{em} = 588
(AcN–HEPES)

HEPES is 4-(2-hydroxyethyl)piperazin-1-ethanesulfonic acid (buffer)

Scheme 66

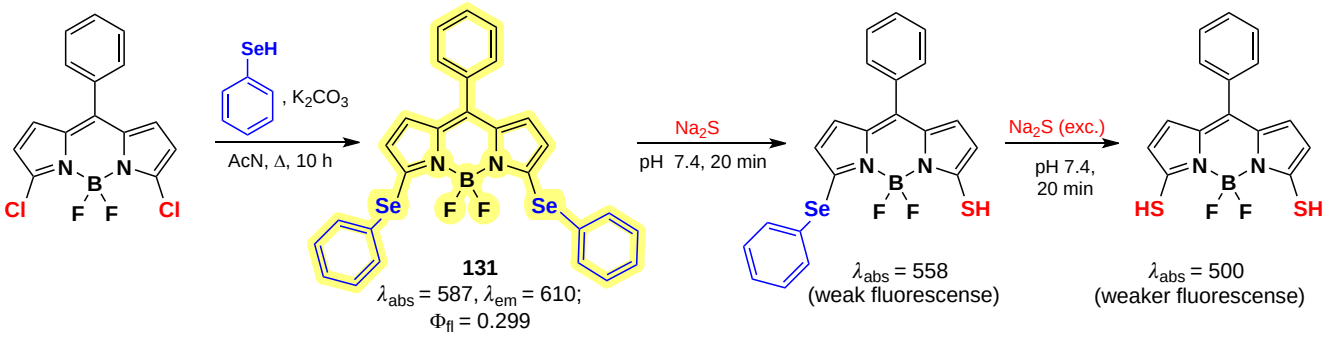

131
λ_{abs} = 587, λ_{em} = 610;
Φ_{fl} = 0.299

λ_{abs} = 558
(weak fluorescense)

λ_{abs} = 500
(weaker fluorescense)

BODIPY molecule are electron-depleted and undergo nucleophilic attack to form a negatively charged δ(H)-complex, which is stabilized by a boron atom. Subsequent oxidation leads to the formation of substitution products. Reactions with N- and C-nucleophiles at the α-position of BODIPY can proceed in the presence of oxygen, leading to the formation of products **132** and **133** (Scheme 67).

Primary and secondary aliphatic amines demonstrated the ability to act as nucleophiles in the reaction of oxidative nucleophilic substitution with BODIPY, resulting in the deactivation at the second α-position. A similar result was observed in the oxidative nucleophilic substitution reaction with pyrroles; BODIPY **134** was formed and exhibited bright fluorescence [188] (Scheme 68).

In 2021, Santos *et al.*[189] demonstrated the possibility of oxidative nucleophilic substitution reactions at 3,5-positions of BODIPY, even in the presence of halogen atoms at C(2) and C(6). This was achieved by reacting a 2,6-dibromo-substituted BODIPY with an *in situ* generated selenophenol, forming mono- and disubstituted products (**135** and **136**) (Scheme 69).

In 2023, Zuo *et al.*[19] proposed a new method for introducing a cyano group at 3,5-positions of BODIPY. The proposed approach involved oxidative nucleophilic substitution reactions with $Pb(OAc)_4$ as an oxidant, resulting in the formation of BODIPYs **137** and **138** (Scheme 70). When the *meso*-position of BODIPY was free, the formation of 8-CN-substituted BODIPY **139** was observed. The introduction of cyano groups into the BODIPY core resulted in a bathochromic shift of the absorption and emission bands, as well as an increase in the reduction potentials ($E_{(1/2)red}$). The values of $E_{(1/2)red}$ were –0.76, –0.45 and –0.04 V for the unsubstituted BODIPY and BODIPYs **137a** and **b**, respectively. Also, a reduction in the LUMO energy from –3.88 eV for the unsubstituted BODIPY to –4.43 eV for the cyano derivative **138a** was observed. Moreover, in the

Scheme 67

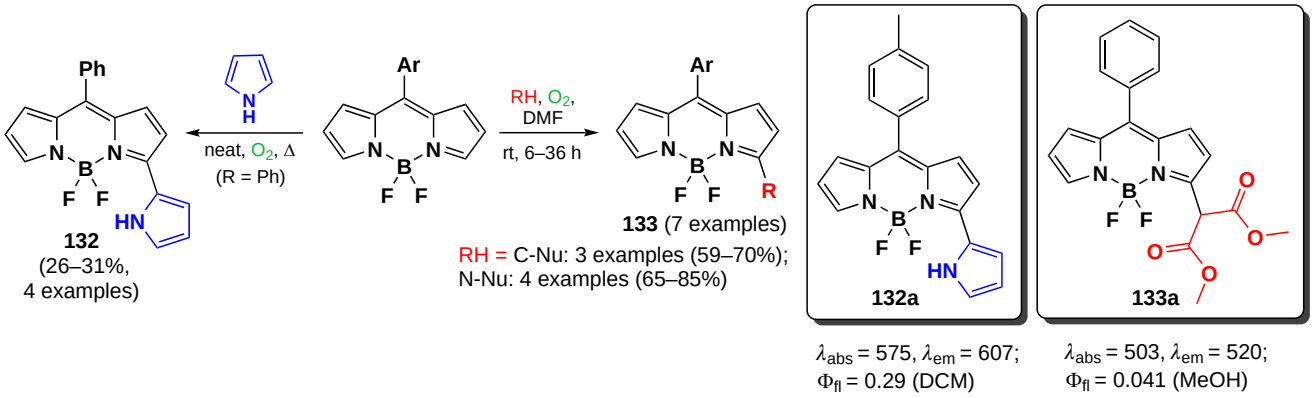

Scheme 68

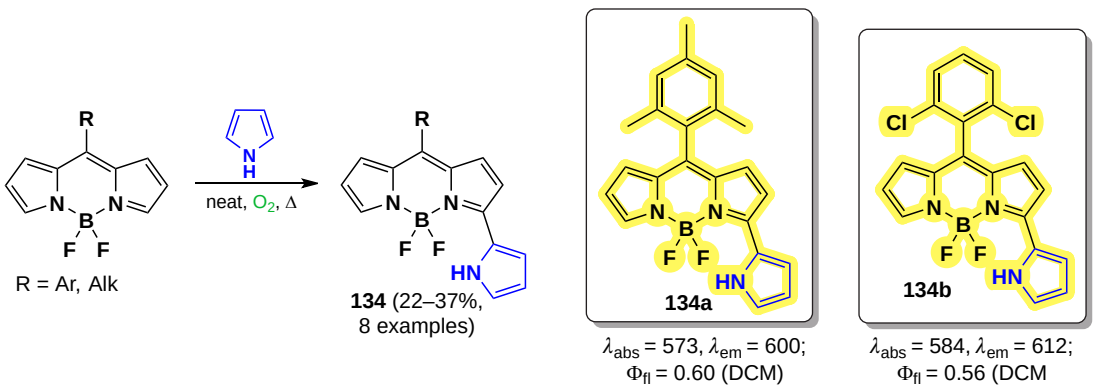

Scheme 69

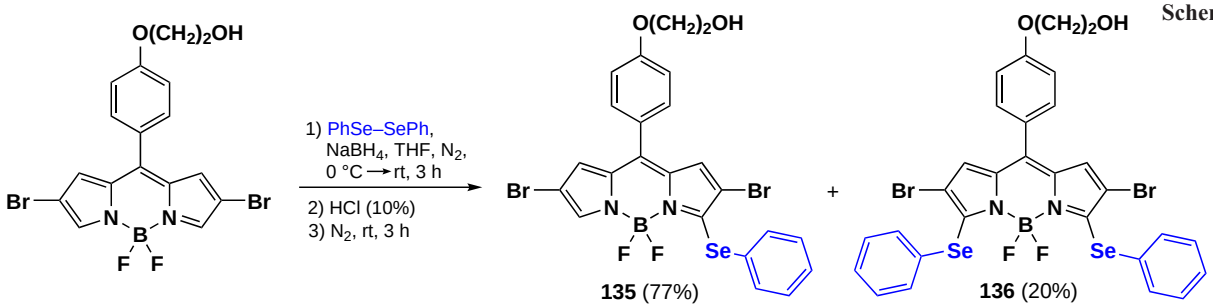

Scheme 70

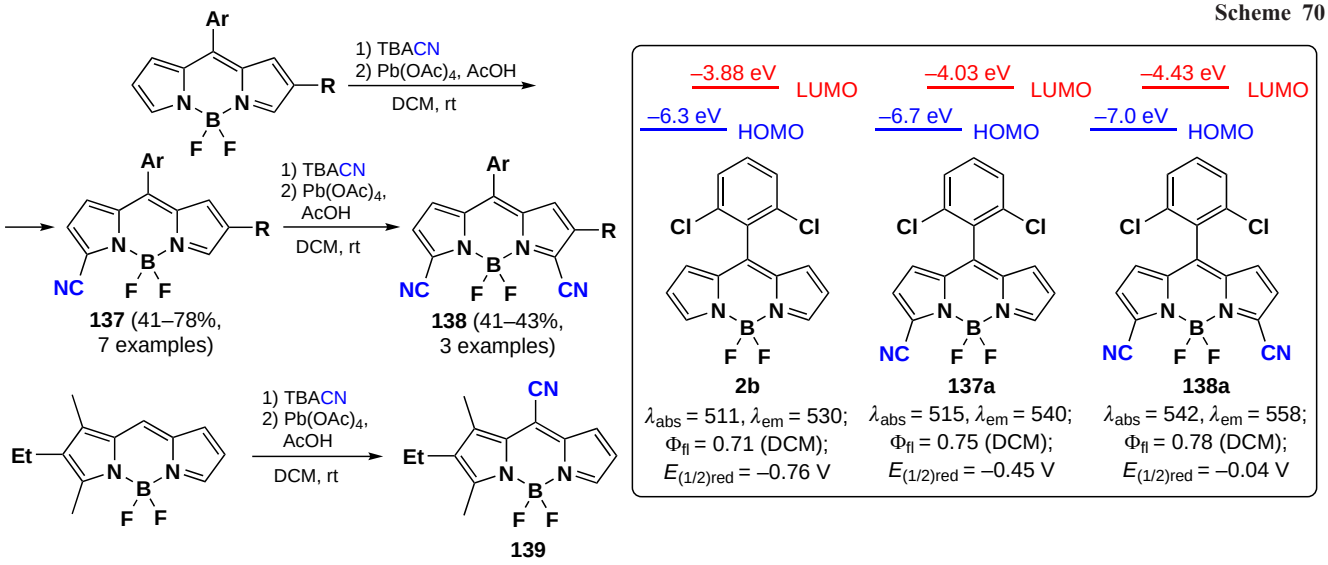

Scheme 71

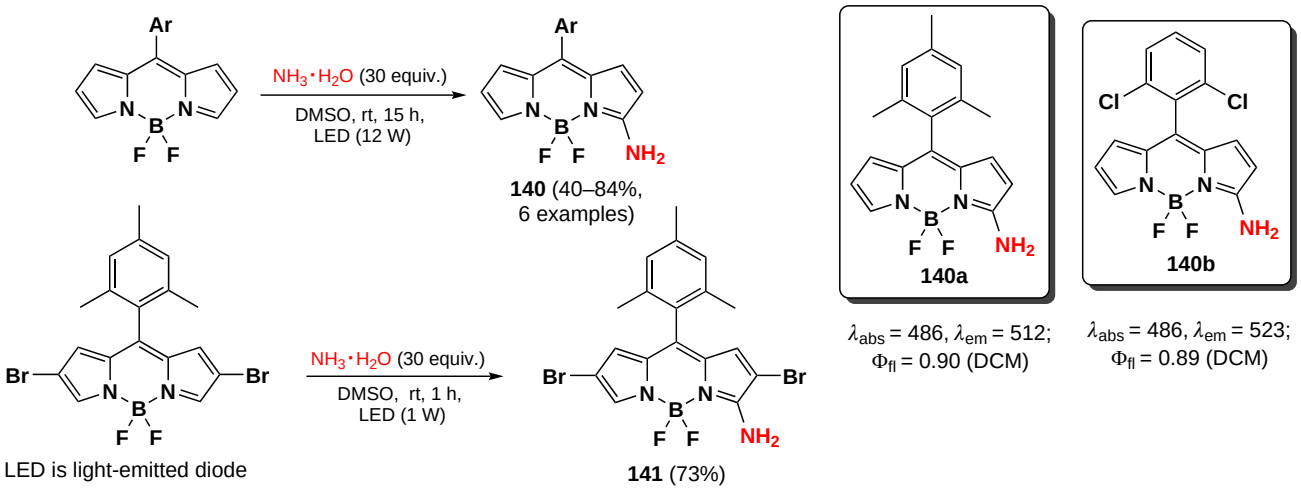

presence of triethylamine and cobaltocene, BODIPY **138a** formed an anion radical, which was detected by EPR spectroscopy.

In 2023, Wang *et al.*[20] demonstrated that oxidative nucleophilic substitution in BODIPY with weak nucleophiles can occur under light irradiation. Light-induced oxidative nucleophilic substitution with ammonia yielded BODIPYs **140** and **141** (Scheme 71). The reaction exhibited a faster rate with the 2,6-dibromo BODIPY, suggesting that the electronegativity of BODIPY is increased in its excited state. The aminated BODIPY **140** showed bright fluorescence up to $\Phi_{fl} = 0.9$ and a hypsochromic shift in the absorption spectra.

3.4.1.3. Vicarious nucleophilic substitution at 3,5-position of BODIPY

In 2011, Leen *et al.*[190] investigated vicarious nucleophilic substitution at the α-position of *meso*-substituted BODIPY in reactions with 2-substituted acetic acid esters. The products **142** were obtained in the presence of the bases, DBU (1,8-diazabicyclo[5.4.0]undec-7-ene), K_2CO_3 and Bu^tOK (Scheme 72).

In addition, a tandem Michael addition/vicarious substitution reaction with nitroalkenes has been reported, yielding 3-styryl-substituted BODIPY **143**, which was previously available for synthesis *via* the Knoevenagel condensation (Scheme 73).

In 2015, Knight *et al.*[191] developed a method for amination of BODIPY *via* copper-catalysed vicarious nucleophilic substitution with primary and secondary amines (Scheme 74). The resulting α-amino-BODIPY **144** showed low fluorescence quantum yields due to the free rotation of *meso*-aryl. A reaction mechanism was proposed involving the nucleophilic attack of copper amide at position 3 of the BODIPY; followed by anion formation, protonation and HI elimination under the action of base to give the desired product.

3.4.2. Nucleophilic substitution at the *meso*-position of BODIPY

The *meso*-position of BODIPY is highly sensitive to the nature of the substituent, due to the significant increase in electron density on the C(8) atom that occurs during the transition from the HOMO to the LUMO.[192,193] Consequently, when the heteroatom is at the *meso*-position, the formation of a hemicyanine nucleus and a rearrangement of the electron density

Scheme 72

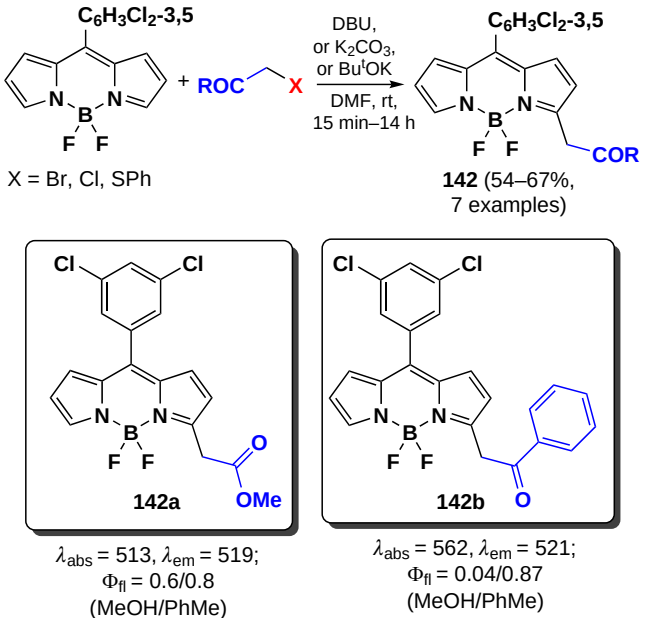

of BODIPY can take place.[97] In the absence of steric hindrance, the conjugation of the unshared electron pair of the nitrogen atom to BODIPY results in the formation of a new π-system, non-equivalence of pyrrole cycles, an increased LUMO energy, an increased energy gap between the HOMO and the LUMO, a hypsochromic shift, bright fluorescence in non-polar media and high laser efficiency (Fig. 11).[194]

3.4.2.1. Nucleophilic substitution of the 8-SMe group

In 2006, Goud *et al.*[80] investigated the reactivity of the SMe group at the *meso*-position of BODIPY in nucleophilic substitution reactions. The methylsulfanyl group was readily substituted with anilines yielding 8-NHPh derivatives (**145a**,**b**), for which the hemicyanine structure was proposed based on spectral characteristics. Consequently, these derivatives did not exhibit emission properties (Scheme 75).

In 2020, Gomez-Duran *et al.*[194] synthesised 8-aminopropargyl-BODIPY **146** by a nucleophilic substitution reaction of a *meso*-thiomethyl group (Scheme 76). BODIPY **146** existed in two rotameric forms (**146a** and **146b**), with the unshared electron

Scheme 73

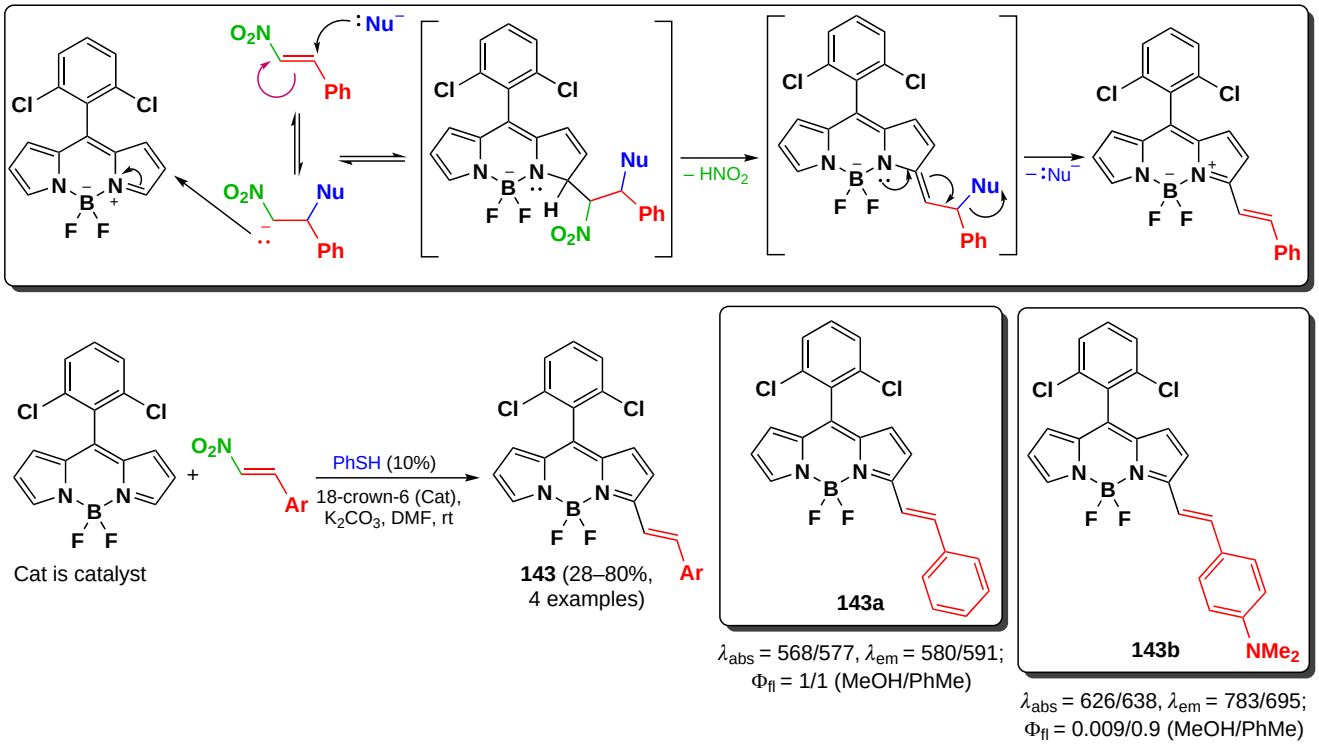

Scheme 74

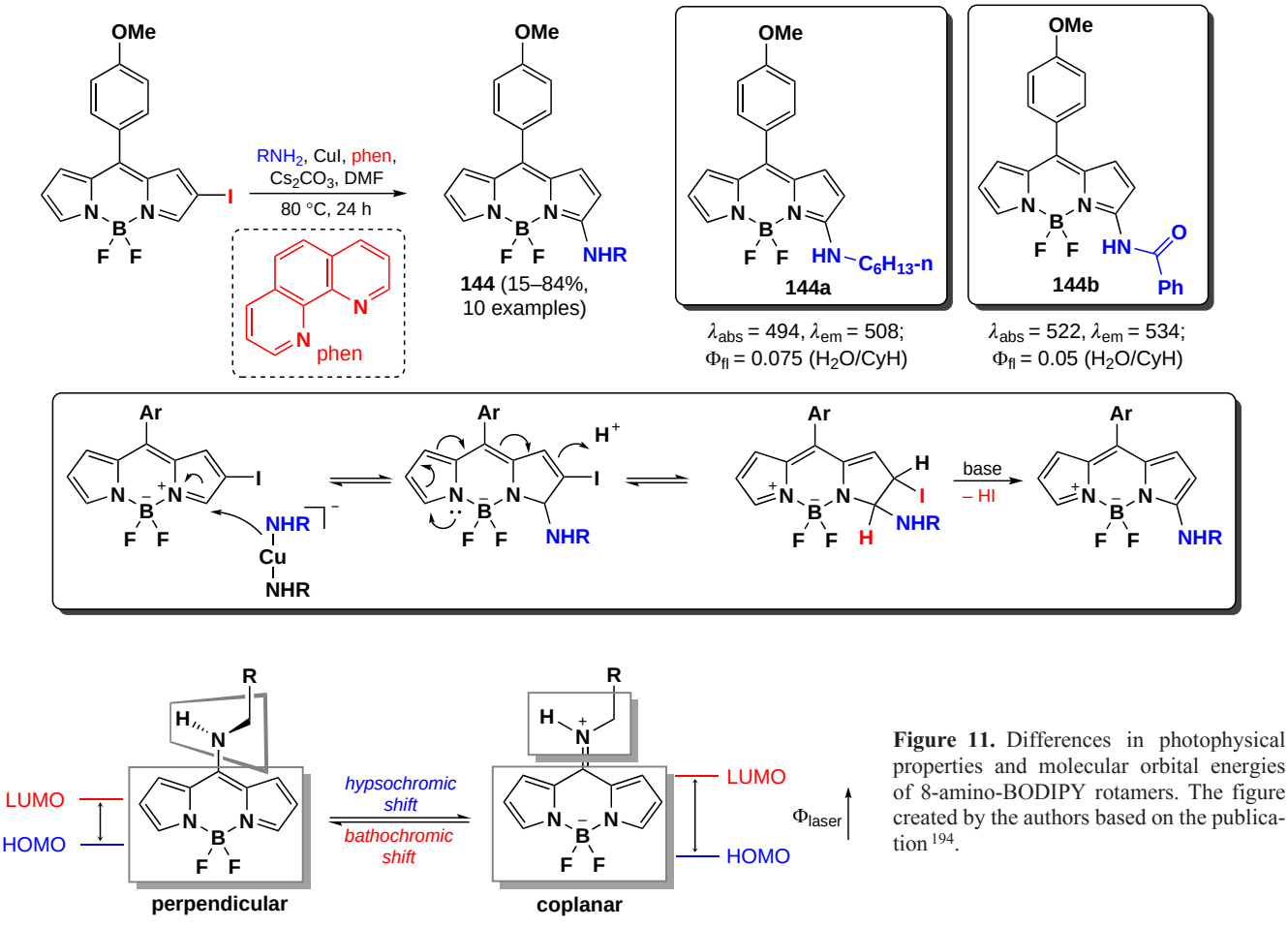

Figure 11. Differences in photophysical properties and molecular orbital energies of 8-amino-BODIPY rotamers. The figure created by the authors based on the publication [194].

Scheme 75

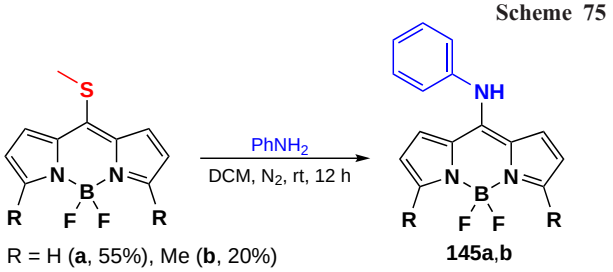

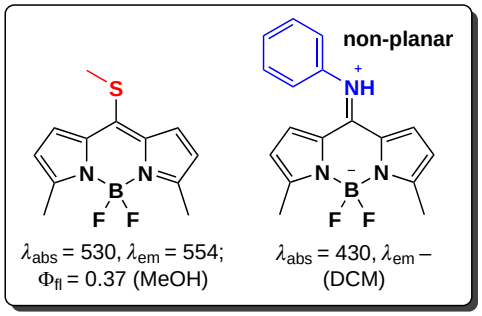

Scheme 76

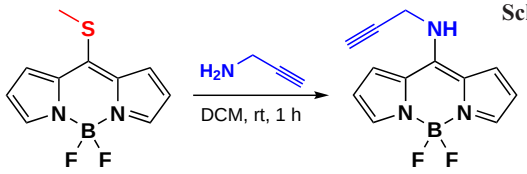

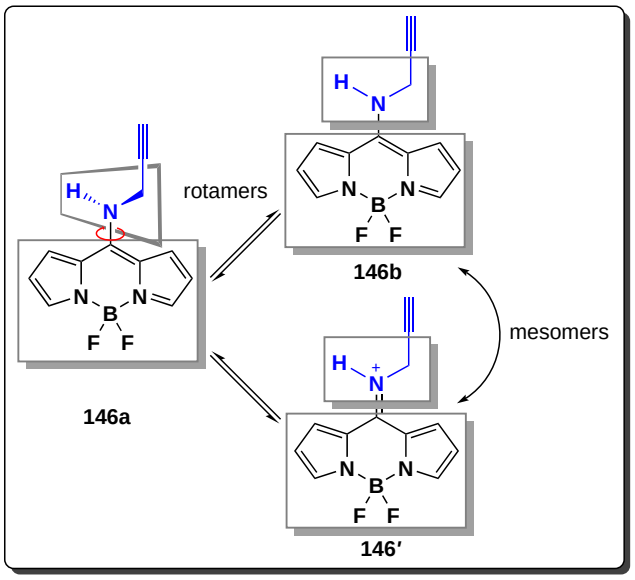

pair of the nitrogen atom conjugated to the BODIPY in rotamer **146b**. The results of quantum mechanical calculations confirmed that the HOMO is localised on the pyrrole moieties, while the LUMO is localised on the nitrogen atom, which is in good agreement with the hypsochromic shift of the absorption band and the large Stokes shift observed. The reduction in the dipole moment by 2 D in the excited state is also in accordance with the redistribution of electron density resulting from the excitation. Compound **146** demonstrated a high level of laser efficiency (35%).

In 2011, Arbeloa *et al.*[195] demonstrated that an increase in the electron-donating ability of the amine in a series of 8-amino-substituted BODIPYs **147** results in a hypsochromic shift and a decrease in fluorescence quantum yields due to ICT. Some of the synthesized BODIPYs, for example, BODIPY **147a**, exhibited high fluorescence quantum yields and high laser efficiency (Scheme 77).

In 2012, Peña–Cabrera *et al.* proved that the observed hypochromic shift and increase in Stokes shift for 8-amino-BODIPY rotamers with tert-butyl (**148**) and propargyl (**149**) were due to the destabilisation of the LUMO in the absence of *meso*-substituent effects on the HOMO.[196] In sterically hindered amines, the coplanar arrangement of the amine and the BODIPY core was disrupted, thereby preventing the formation of a hemicyanine. The 'twisted' arrangement of the amino group was also found to contribute to ICT, resulting in a lower fluorescence quantum yield. In 2013, Roacho *et al.*[197] demonstrated significant solvatochromism of 8-amino-BODIPYs **150a**,**b**, and for BODIPY with the 8-NEt_2 substituent **150b**, a disruption of planarity of the pyrrole cycles was also observed, resulting in a complete lack of emission (Scheme 78).

In 2013, Esnal *et al.*[81] reported a synthesis of BODIPYs **151** *via* substitution of the 8-SMe group with P,O-nucleophiles. The 8-NHMe- and 8-SMe-derivatives **151a**,**b** exhibited a hypochromic shift, which can be explained by the conjugation of an unshared electron pair of the heteroatom with the BODIPY core. An increase in the electron-donating ability of the

Scheme 77

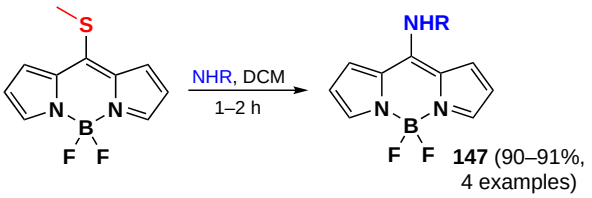

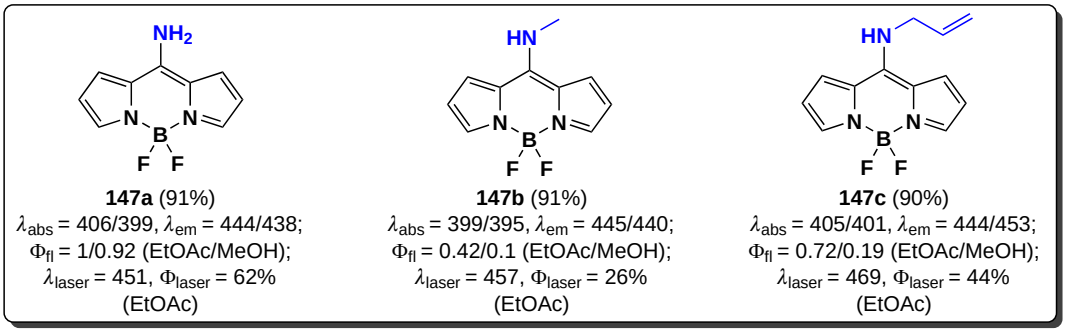

Scheme 78

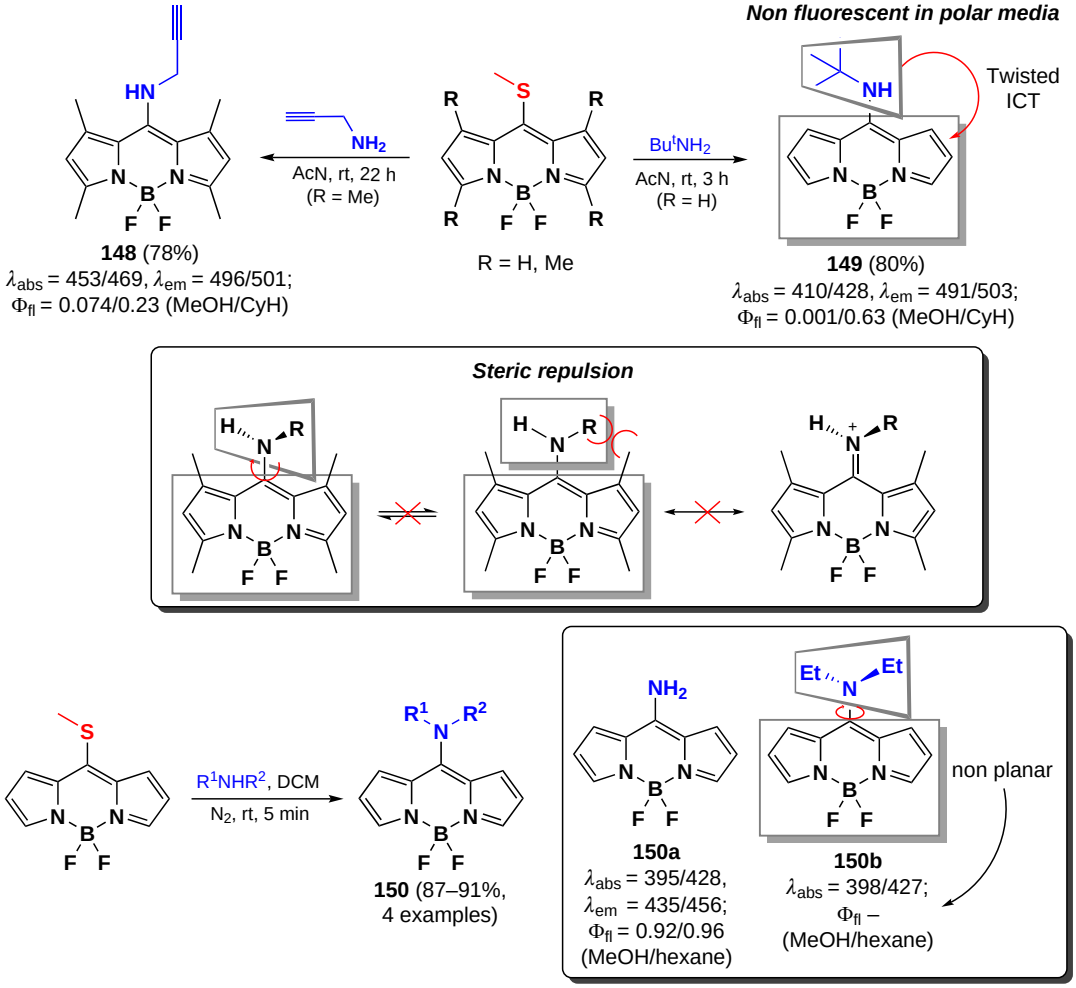

heteroatom results in a negative shift in the reduction potentials of the BODIPY, due to an increase in the LUMO energy, an increase in the LUMO–HOMO energy gap and a hypsochromic shift in the electronic spectra. In contrast, the 8-PPh_2 substituted BODIPY **151c** demonstrated a bathochromic shift in the absorption spectrum and exhibited no emission due to the free rotation of the PPh_2 group. BODIPY **151** exhibited bright emission, which was enhanced by the presence of methyl groups

Scheme 79

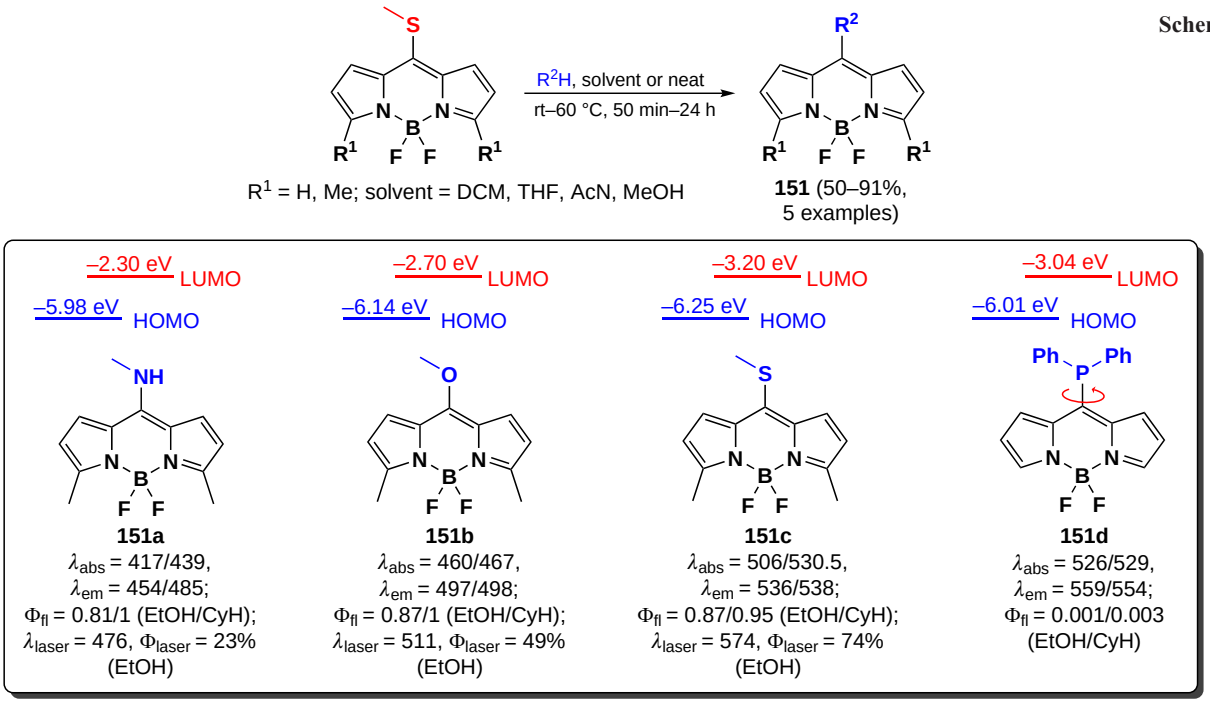

Scheme 80

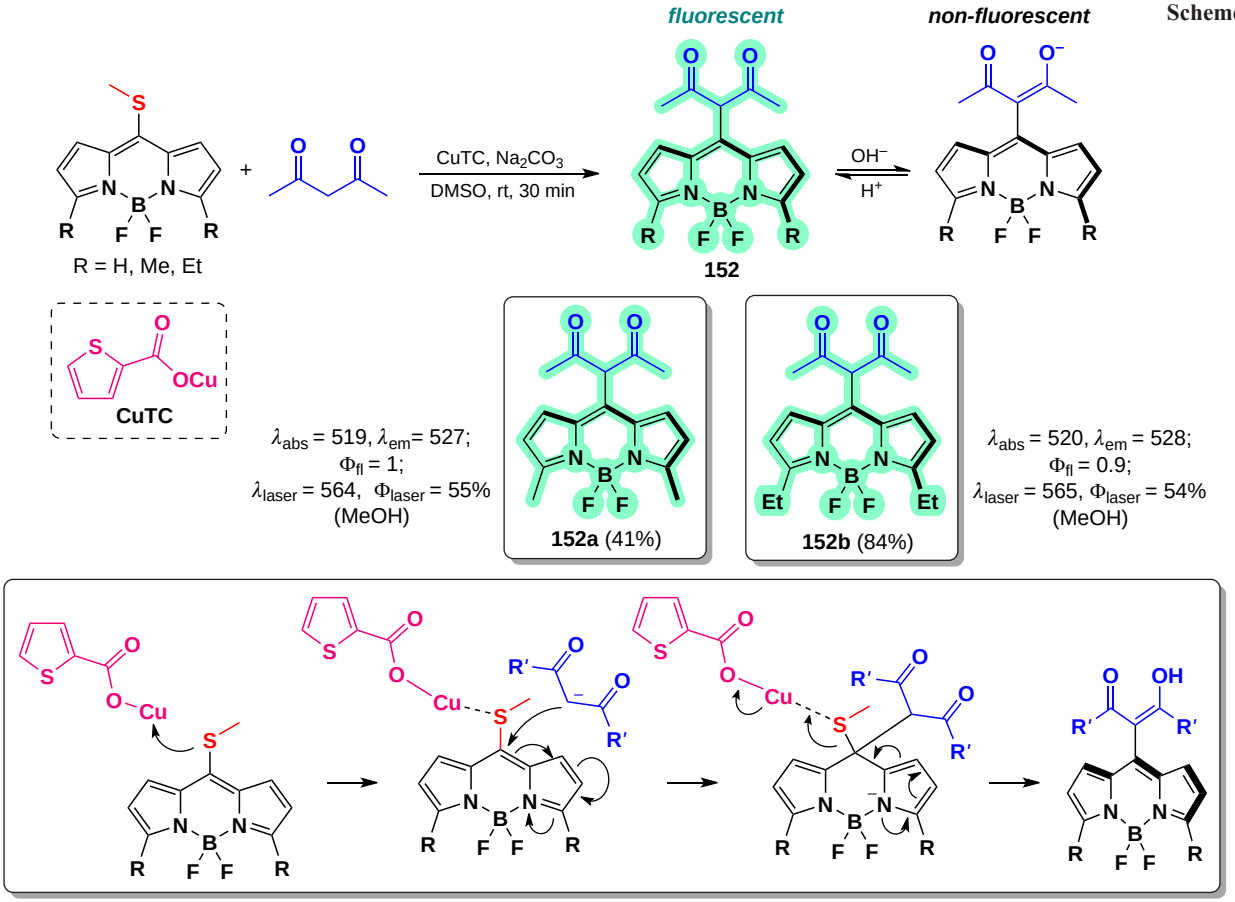

at 3,5-positions. Additionally, high laser efficiency of BODIPYs was observed, with the exception of compound **151d**. (Scheme 79).

In 2015, Gutiérrez-Ramos *et al.*[198] reported a nucleophilic substitution of thiomethyl group under the action of sodium enolates of 1,3-dicarbonyl compounds in the presence of copper(I) thiophene-2-carboxylate (TC). The proposed mechanism involves the coordination of Cu^{I}-carboxylate on the sulfur atom, which is then attacked by soft nucleophiles (Scheme 80). BODIPYs **152a**,**b** exhibited pH-dependent fluorescence, which was suppressed in basic medium. This suppression was attributed to the conjugation of the enol group to the BODIPY core and the enhancement of radiation-free relaxation pathways. Furthermore, these compounds exhibited high laser efficiency.

In 2015, Roacho *et al.*[199] reported a regioselective nucleophilic substitution of the thiophenol group at the *meso*-position in unsubstituted 8-SMe-BODIPY, yielding BODIPY **153**. In addition, nucleophilic attack at 3,5-positions took place when THF was used as a solvent, yielding BODIPYs **154** and **155**. BODIPYs **156** were obtained by nucleophilic substitution with secondary amines using dichloromethane as a solvent[200] (Scheme 81).

In 2021, Yagishita *et al.*[201] synthesised fluorescent probes for imaging aldehyde dehydrogenase 1 (ALDH1) stem cells. *Meso*-amino-BODIPYs **157** and **158** were obtained *via* a nucleophilic substitution of a thiomethyl group with benzylamine in the

Scheme 81

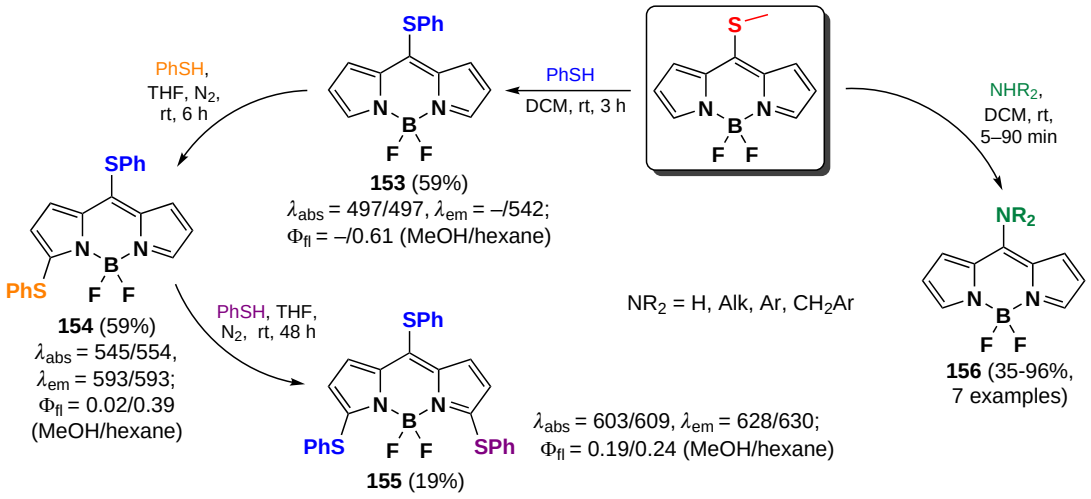

Scheme 82

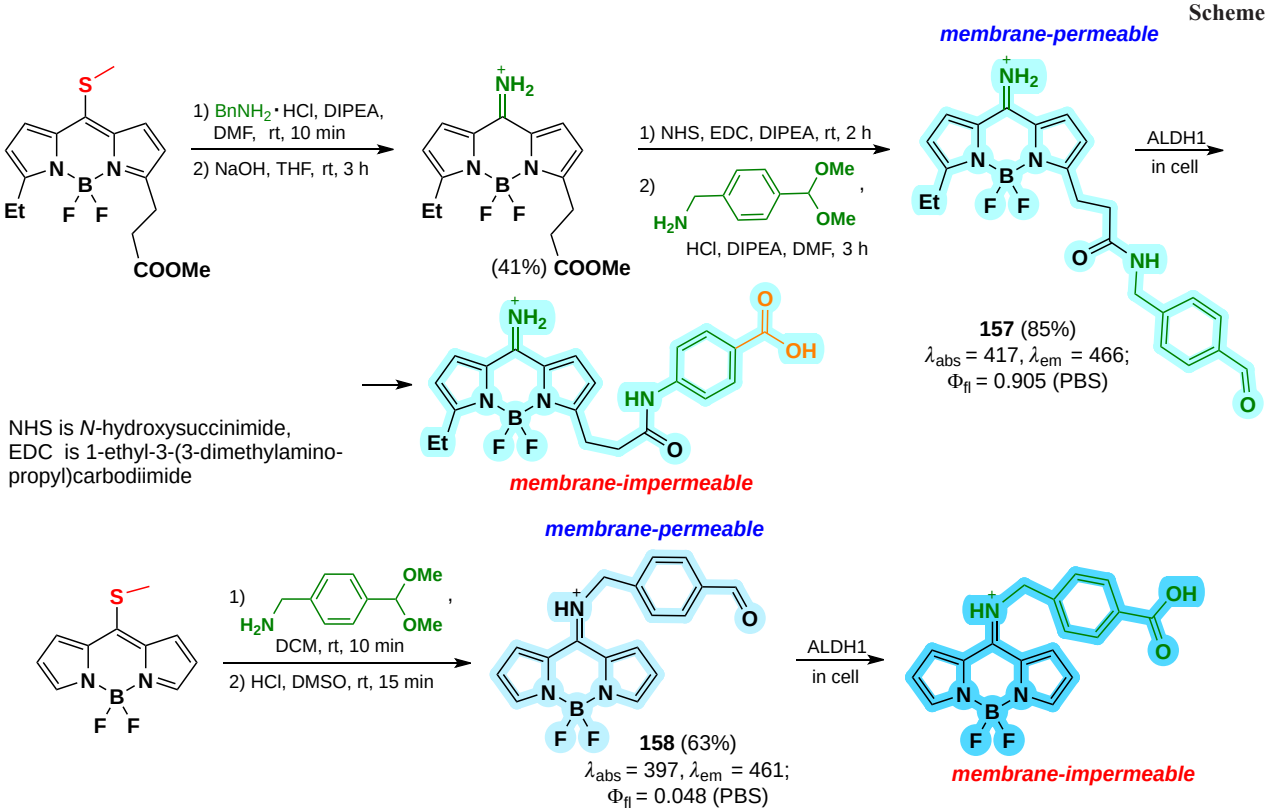

meso-position of BODIPY. The mechanism of ALDH1 detection was based on the permeability of the cell membrane for aldehyde-bearing BODIPYs **157** and **158**, while the carboxylic acids oxidised by dehydrogenase were unable to leave the cell. Both probes demonstrated the ability to detect ALDH1 in human embryonic stem cells SBC5 (Scheme 82).

Since the presence of an amino group at the *meso*-position of BODIPY results in a hypsochromic shift, *meso*-amino BODIPYs have limited application as bioimaging probes. In 2022, Wu *et al.*[202] proposed a strategy to reduce the LUMO energy of *meso*-amino BODIPYs and to reduce the HOMO–LUMO energy gap by introducing an electron acceptor group at the *meso*-nitrogen atom. The resulting 8-(*N*-acyl)-BODIPY **159** showed a bathochromic shift in the absorption spectrum up to 770 nm and a bright emission up to $\Phi_{fl} = 0.99$. The potential of these fluorophores for bioimaging was demonstrated in reverse-

Scheme 83

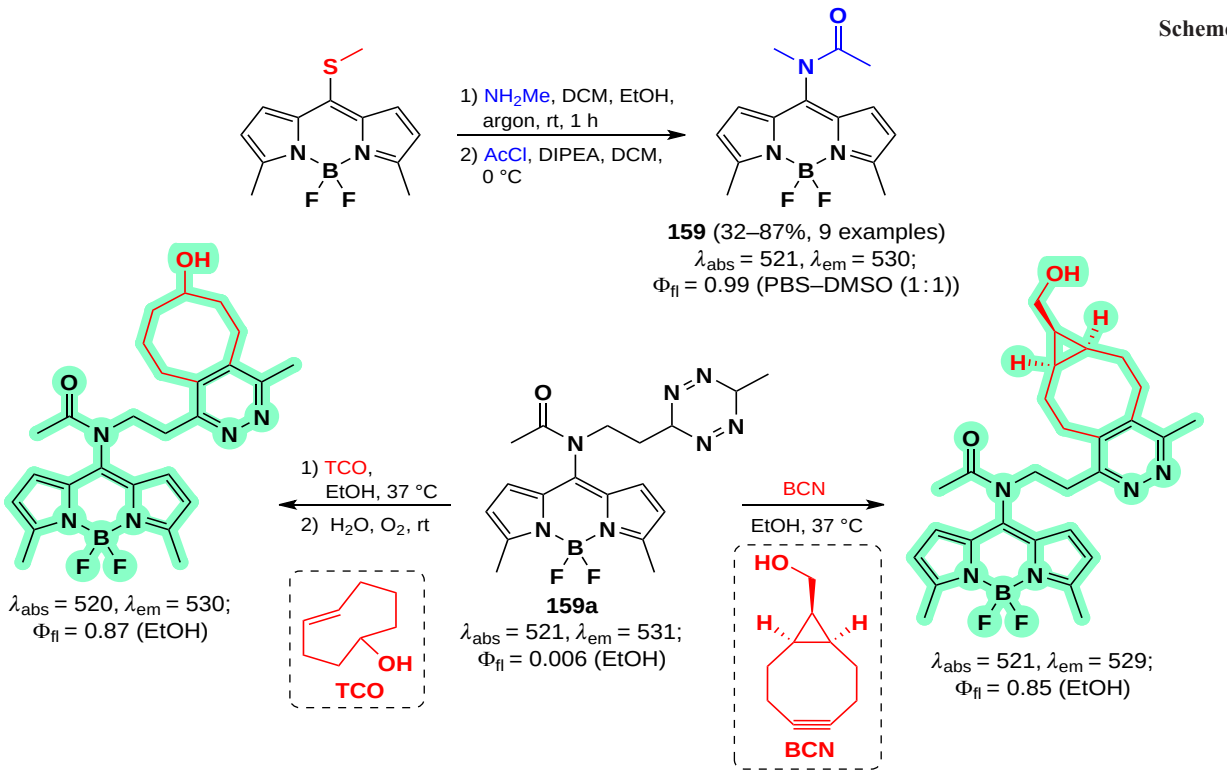

Scheme 84

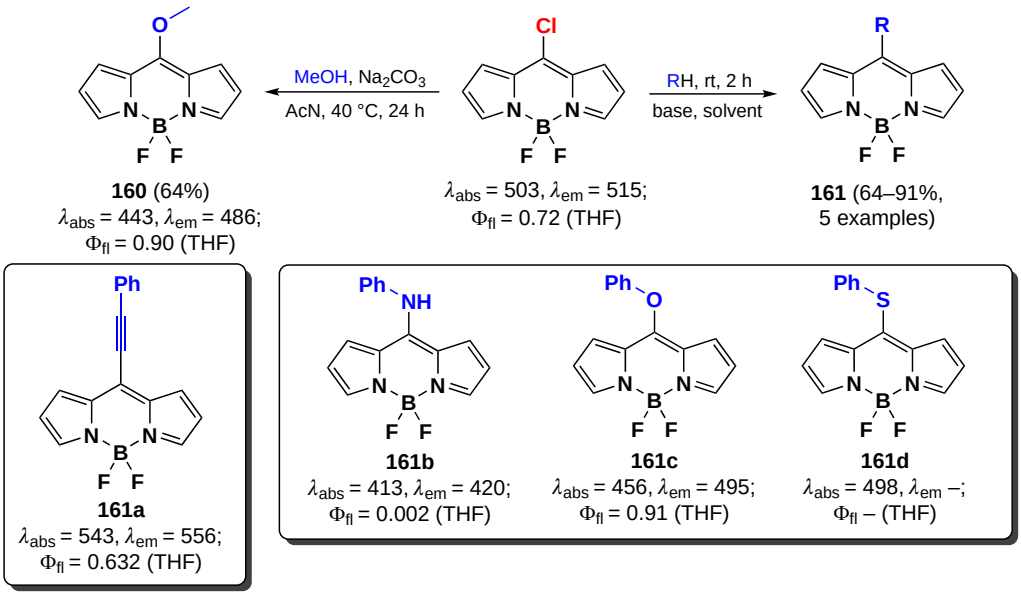

electron Diels-Alder reaction of 8-(*N*-acyl)-BODIPY **159a** with a tetrazine cycle with *trans*-cyclooctene (TCO) or spiro[2.3]-hex-1-ene (BCN), which was accompanied by a 128-fold increase in fluorescence. It seems reasonable to assume that fluorescence enhancement was facilitated by the presence of a flexible alkyl linker in compound **159a** (Scheme 83).

3.4.2.2. Nucleophilic substitution of meso-halogen atom

In 2012, Leen *et al.*[82] investigated the reactivity of 8-chloro-BODIPYs with different nucleophiles, such as anilines, aromatic and aliphatic thiols, phenols and alcohols, yielding BODIPYs **160**. *Meso*-substituted BODIPYs **160a,c** exhibited remarkably high fluorescence quantum yields, whereas no emission was detected for *meso*-anilino-BODIPYs **161b,d**. Subsequently, Boens *et al.*[203] investigated the photophysical and spectral properties of BODIPYs substituted with C-, N-, O-, and S-nucleophiles. Their findings demonstrated that the introduction of a heteroatom at the meso-position of BODIPY resulted in a hypsochromic shift of the maximum in the absorption spectrum for BODIPY **161b**–**d**. The alkynyl-BODIPY (**161a**) exhibited a bathochromic shift due to the conjugation between the BODIPY core and the *meso*-substituent (Scheme 84).

In 2014, Misra *et al.*[204] synthesized a series of *O*- and *N*-substituted dimers of BODIPY **162** and **163**, conjugated *via* phenyldiol and phenylenediamine-based linkers. The resulting dimers exhibited a hypsochromic shift in their absorption spectra. Notably, the *N*-dimers displayed no fluorescence, while the O-dimers exhibited green fluorescence, which was attributed to the conjugation of an unshared electron pair to the BODIPY. Electrochemical studies demonstrated that the extensive delocalization of the unshared electron pair of the *meso*-substituent on the BODIPY nucleus facilitates the oxidation of dimers and the generation of cationic radicals (Scheme 85).

Jiang *et al.*[144] reported a synthesis of 8-pyrrolyl BODIPYs **164** *via* nucleophilic substitution of cholorine in meso-chloro-BODIPY with pyrroles. A similar BODIPY **165** was synthesized by Popov and Plenio in 2022[205] *via* nucleophilic substitution of *meso*-chloroine in BODIPY with imidazole during the synthesis of a series of BODIPY-based photosensitisers (Scheme 86).

3.4.2.3. Nucleophilic substitution reactions at the *meso*-position of BODIPY in biosensorics

Since the meso-position of the BODIPY is sensitive to the electron-donating ability of the substituent, the ability of amino-

Scheme 85

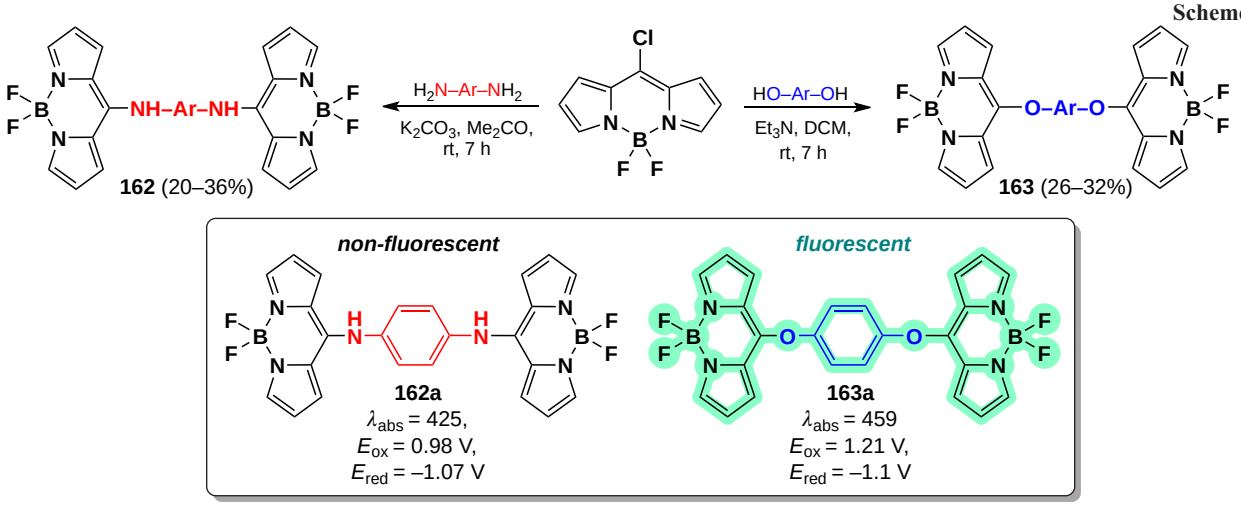

Scheme 86

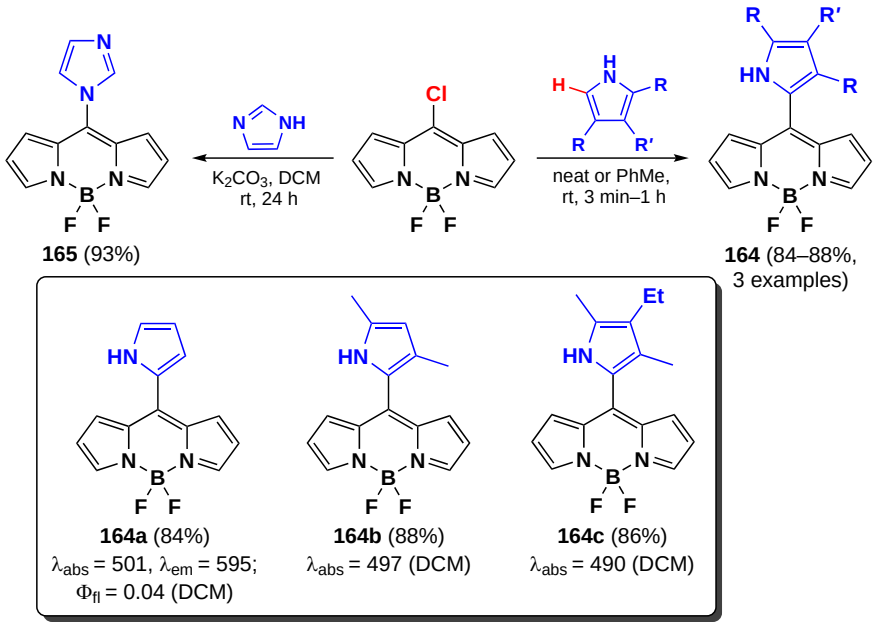

BODIPYs to form a hemicyanine provides the potential for the use of 8-heteroatom-substituted BODIPY as fluorescent probes. Their mechanism of action is based on the disruption of the conjugation between a heteroatom and a BODIPY core, which results in a significant change in the spectral properties due to the blocking of ICT or PET processes and the rearrangement of the π-system.

3.4.2.3.1. Phosgene detection

In 2019, Wei *et al.*[16] synthesized a phosgene-sensitive sensor **166** based on an 8-hydrazido-BODIPY, obtained from meso-chloro-BODIPY *via* nucleophilic substitution. PET from the nitrogen atom to BODIPY resulted in the complete suppression of emission from the sensor. In the presence of phosgene, the oxadiazolone cycle formation took place, thereby preventing the PET process and enhancing fluorescence. BODIPY **166** exhibited a fast response time (1.5 seconds) with a low detection limit for phosgene (0.15 nanomolars), and high selectivity. In the context of the test strips, sensor **166** demonstrated the ability to detect phosgene in the gas phase at a concentration of 20 ppm (Scheme 87).

In 2022, Zeng *et al.*[206] presented a series of *trans*- and *cis*-8-diaminocyclohexano-BODIPY-based probes designed to detect phosgene, diethylchlorophosphate, and other acyl chlorides with a similar mechanism of toxic action. The interaction of *trans*-isomer **167** with phosgene and its analogues resulted in a decrease of PET, a bathochromic shift, a rapid change in fluorescence (from weak blue to bright green). BODIPY **167** showed a low limit of detection (0.52 nm). The enhanced sensitivity of the *trans*-isomer compared to the *cis*-isomer is explained by the presence of intramolecular hydrogen bonding. In the presence of acyl chlorides, the sensor showed increased blue fluorescence, with a detection limit of 0.77 nm. (Scheme 88).

3.4.2.3.2. HClO and ClO^- detection

In 2019, Xu *et al.*[207] synthesized 8-seleno-BODIPYs **168a–c**, as an effective fluorescent probe for the detection of HClO and ClO^-. The mechanism of action of these probes is based on the oxidation of non-fluorescent (*via* PET) selenides **168** to fluorescent selenoxides (no PET). The sensitivity of the sensors was found to be dependent on the electron-donating ability of the substituent present at the meso-position. BODIPY **168a** demonstrated the highest sensitivity and fastest response, while BODIPY **168b** exhibited the highest selectivity towards various ROS. Furthermore, the latter was also able to visualize exo- and endogenous HClO in living cells, with the majority of the latter localized in mitochondria. (Scheme 89).

Scheme 87

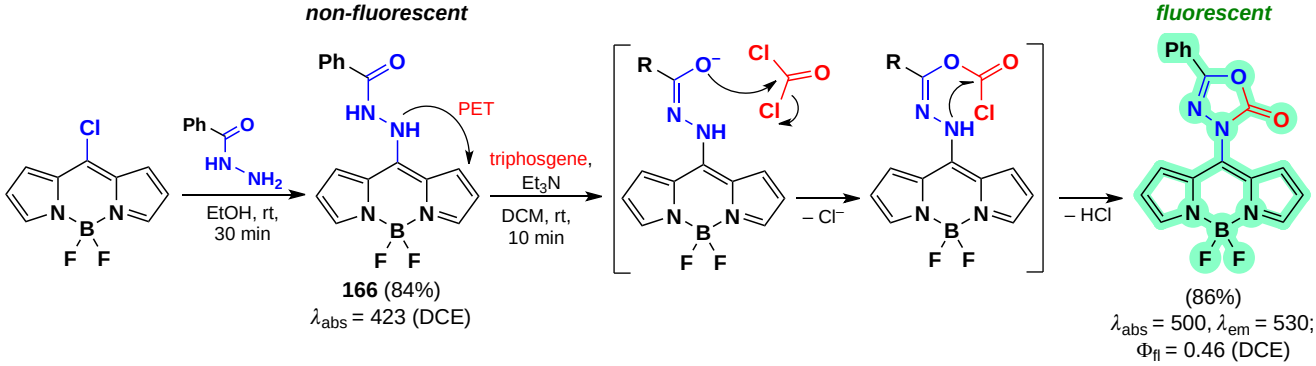

Scheme 88

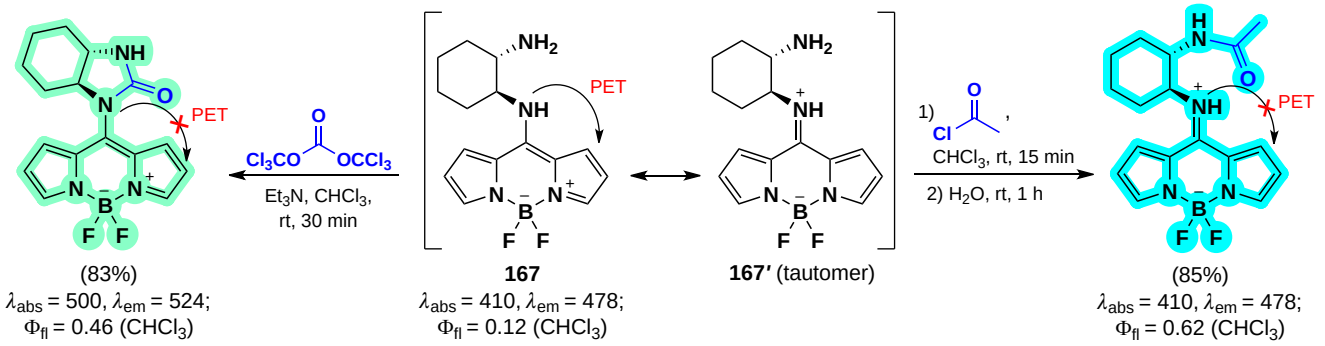

(83%)
λ_{abs} = 500, λ_{em} = 524;
Φ_{fl} = 0.46 ($CHCl_3$)

167
λ_{abs} = 410, λ_{em} = 478;
Φ_{fl} = 0.12 ($CHCl_3$)

167′ (tautomer)

(85%)
λ_{abs} = 410, λ_{em} = 478;
Φ_{fl} = 0.62 ($CHCl_3$)

Scheme 89

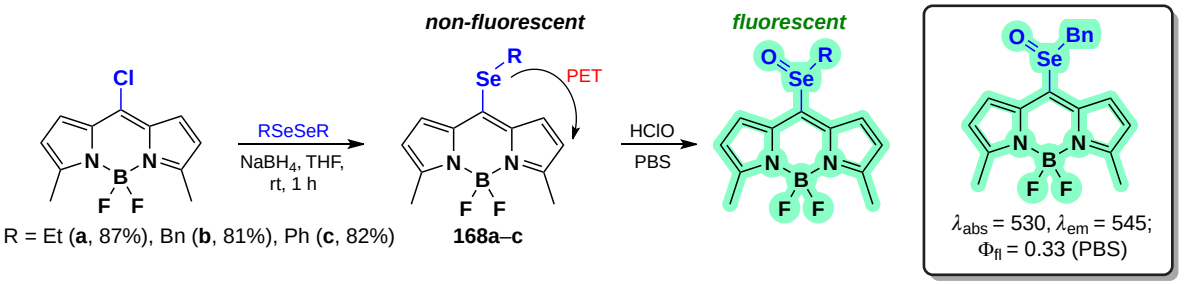

R = Et (**a**, 87%), Bn (**b**, 81%), Ph (**c**, 82%)

168a–c

λ_{abs} = 530, λ_{em} = 545;
Φ_{fl} = 0.33 (PBS)

3.4.2.3.3. Biothiol detection

The detection of biothiols by fluorescent sensors is based on two distinct nucleophilic substitution reactions: the first nucleophilic attack of the sulfur atom, and subsequent an intramolecular rearrangement involving a nucleophilic attack of the nitrogen atom. BODIPY-based probes for the detection of biothiols undergoing nucleophilic substitution reactions at positions 3 and 5 are discussed in detail in section 3.4.1.1. The ability of 8-SMe-BODIPY **169** to detect Cys and Hcy by a similar mechanism has been also demonstrated.[208] Nucleophilic substitution of the methylsulfanyl group for Cys and Hcy residues, followed by intramolecular rearrangement and substitution of the sulfur atom with an amino group, resulted in a hypochromic shift not observed in the presence of other biothiols (Scheme 90).

In 2021, Ji *et al.*[209] synthesized a series of 8-pyridyloxy-(thioxy)-BODIPY **170a–c** *via* a nucleophilic substitution of the *meso*-chlorine atom, and then proceeded to quaternise the nitrogen atom in the pyridine cycle with the formation of salts **171a–c**. When in cells, BODIPY **171a** underwent a reaction with Cys in accordance with the aforementioned mechanism, resulting in the formation of an 8-(N-Cys) derivative with pronounced fluorescence at 620 nm (Scheme 91).

In 2023, Zhang *et al.*[210] reported 8-(*p*-methoxyphenyl)-sulfanyl-BODIPY **172** as a cysteine-sensitive fluorescent probe, which was synthesized *via* a nucleophilic substitution reaction between *meso*-chloro-BODIPY and p-methoxythiophenol. The reaction of the sensor with Cys was accompanied by a change in the solution colour from blue to pink, together with a fluorescence enhancement. BODIPY **172** demonstrated a rapid reaction time (10 minutes), a high signal-to-noise ratio (3150), and an low detection limit for cysteine (11.2 nm) (Scheme 92).

In 2024, Zeng *et al.*[36] developed a nitrite-anion sensor based on 8-(*o*-phenylenediamino)-BODIPY **173**. At pH 1, the nitrite anion formed the electrophilic nitrosyl cation **174**, which then reacted with the NH_2-group at the meso-position of BODIPY to form a diazonium cation. Subsequently, the diazonium cation was subjected to nucleophilic attack by an amine, resulting in the formation of a triazole ring and the emission of fluorescence due to the PET disruption (Scheme 93).

3.4.2.3.4. Hg^{2+} detection

In 2012, Ahn *et al.*[211] proposed to use the metal-catalysed nucleophilic substitution reaction of the 8-thiomethyl group of BODIPY **169** with water for the selective fluorescence detection of mercury cations in the presence of other metals. The replacement of the thiomethyl group with a hydroxyl group resulted in a hypsochromic shift of both the absorption and fluorescence maximum. Quantum mechanical calculations for BODIPY **169** and its hydrolysis product predicted a larger HOMO–LUMO energy gap for the product (3.48 eV) compared

Scheme 90

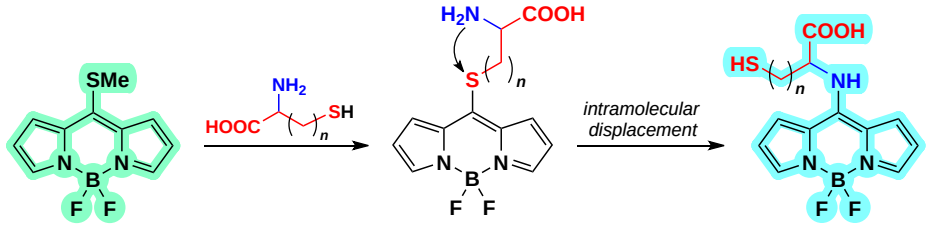

169
λ_{abs} = 483, λ_{em} = 524
(AcN–HEPES)

n = 1 (cysteine), 2 (homocysteine)

λ_{abs} = 400, λ_{em} = 467
(AcN–HEPES)

Scheme 91

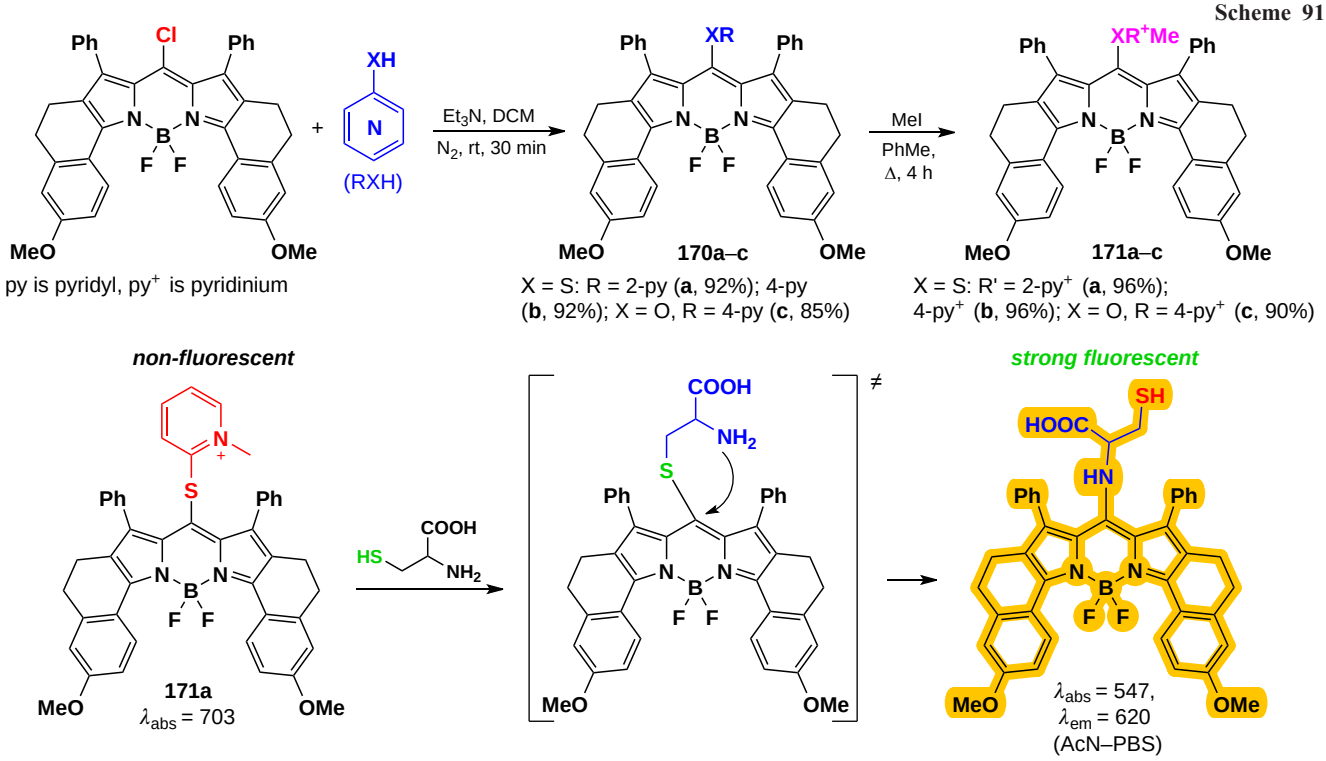

Scheme 92

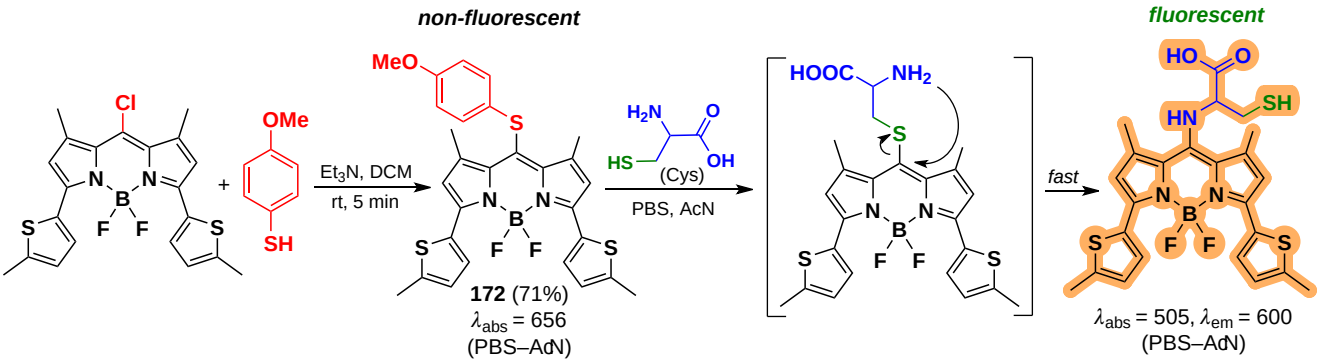

Scheme 93

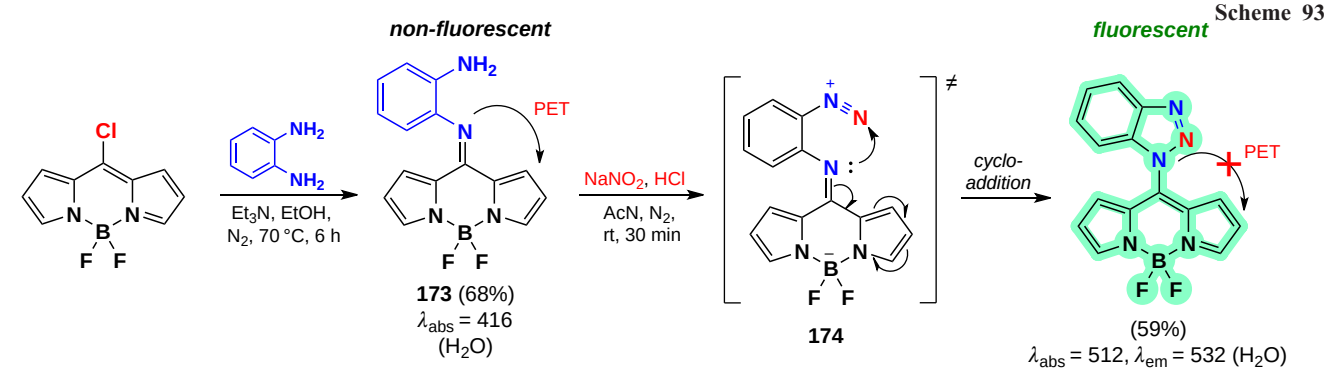

to the original sensor (3.03 eV), which is consistent with the shift of the absorption spectrum to the blue region (Scheme 94).

3.5. Reactions involving methyl groups

A significant number of both commercially used and described in the literature BODIPYs contain methyl groups as substituents in various positions. The presence of 1,7-methyl groups inhibits the free rotation of the *meso*-substituent and enhances the emission of the fluorophores.[212] In some cases, the methyl groups at C(3) and C(5) positions also contribute to the increased emission.[81]

Methyl groups at positions 3, 5, and 8 are able to form stabilized benzylic anions, cations, or radicals.[6,213,214] The delocalization of the positive charge at positions 1, 3, 5, 7, and 8 increases the CH-acidity of the methyl groups, opening up

Scheme 94

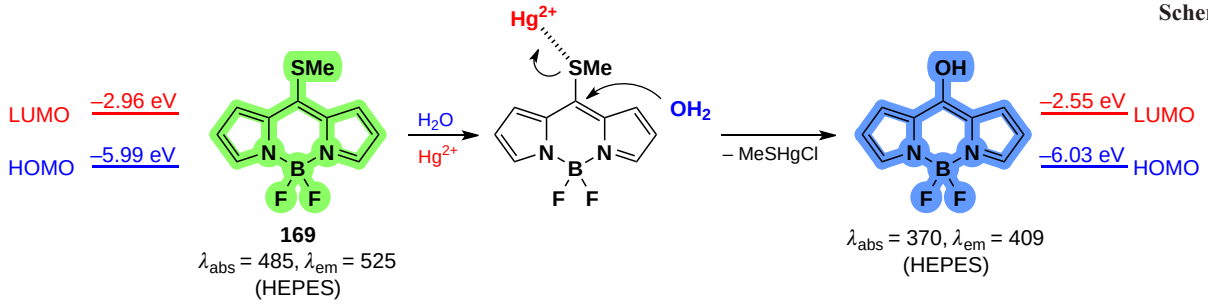

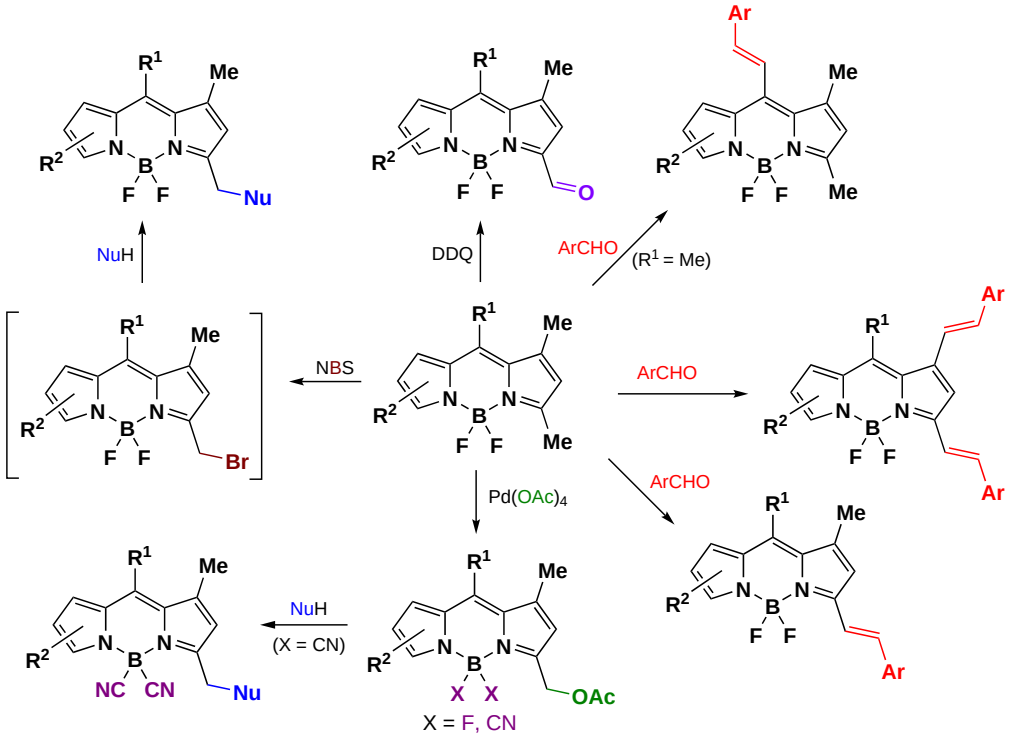

Figure 12. Reactions involving the methyl groups of BODIPY discussed in Section 3.

possibilities for modifications of the BODIPY core, leading to changes in the physicochemical, photophysical, and biological properties (Fig. 12).[10,215] This section discusses postmodification reactions of BODIPY *via* modification of methyl groups, including the Knoevenagel condensation, oxidation, and electrophilic substitution reactions.

3.5.1. Knoevenagel condensation

One of the most widely used reactions involving methyl groups in BODIPY is the Knoevenagel condensation. The methyl groups at positions 3, 5, and 8 are the most active in this condensation, while those at positions 1 and 7 are less active. This activity pattern is consistent with the calculated electron density distribution in the BODIPY core, which decreases in the order 2 and 6 > 1 and 7 > 3 and 5 > 8. The chemical shifts of the protons of the methyl groups in the nmR spectra agree with these data (Fig. 13).[216]

Products of the Knoevenagel condensation are styryl-substituted BODIPYs, that exhibit a bathochromic shift in their absorption and emission spectra. Condensation of methyl groups at positions 3 and 5 results in a larger bathochromic shift compared to similar modification at positions 1 and 7.[38,216,217] Molecular orbital energy calculations show that the HOMO–LUMO energy gap in 3,5-distyryl-BODIPY is significantly larger than that observed for 1,7-distyryl-

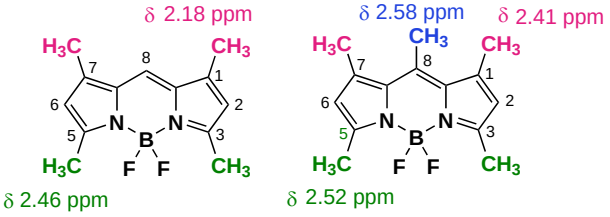

Figure 13. Chemical shifts of the protons of the methyl groups of BODIPY in ^{1}H nmR spectra.

BODIPY.[192] The reaction conditions allow for the use of multiple aldehydes with different stereoelectronic characteristics. The introduction of donor substituents into the BODIPY molecule promotes charge transfer within the resulting mono- and distyryl derivatives, which is utilized in the design of chemosensors and molecular switches.[216]

The use of the Knoevenagel condensation to modify BODIPY and to tune the photophysical properties of the resulting products has been the subject of several reviews (see, *e.g.*, Refs[38,218,219]). Styryl derivatives of BODIPY are of interest in the development of solar panels,[220] bioimaging agents[66,221,222] and PDT drugs.[223,224] Due to the incredibly large variety of techniques for the synthesis of styryl-BODIPY using the Knoevenagel

condensation, only the most interesting examples are discussed below.

3.5.1.1. Knoevenagel condensations at position 3

The first monostyryl BODIPY **175** was obtained by the Knoevenagel condensation by Rurack *et al.*[215] in 2001 (Scheme 95). The introduction of a styryl moiety with an electron-donating substituent at position 3 of the BODIPY core resulted in a bathochromic shift of the absorption and emission maxima in the electronic spectra and imparted considerable solvatochromism to the resulting fluorophore. Protonation of BODIPY **175** caused a hypsochromic shift in the absorption and emission spectra and disappearance of solvatochromism due to the disruption of charge transfer from the dimethylamine fragment to the BODIPY core. Compound **175** also showed the ability to oxidize with the formation of a cation-radical at a lower potential than BODIPY with other donor groups, indicating a high degree of charge delocalization within the molecule.

In 2021, Kaya *et al.*[225] synthesized styryl-BODIPY **176** as a 'trap' for singlet oxygen (Scheme 96). In the presence of singlet oxygen generated from the photosensitizer *meso*-tetraphenylporphyrin (TPP) under red light (630 nm), the opening of the furan cycle occurred, accompanied by a decrease in absorbance in the spectrum at 600 nm and the appearance of new maxima at 510 and 560 nm.

In 2020, Yang *et al.*[226] synthesized 2-styryl-BODIPY **177** by condensation of BODIPY with carbazole-3-carbaldehyde for use as an electron-donating material in organic photovoltaic cells (Scheme 97). The HOMO–LUMO energy gap calculated from cyclic voltammetry (CV) data for compound **177** was 1.99 eV, which is lower than that of the parent BODIPY (2.33 eV).[227] The ability to act as a solar cell component was investigated in a glass/ITO/PEDOT:PSS/active layer/PFN/Al configuration (PEDOT: PSS — poly(3,4-ethylenedioxythiophene)polystyrene sulfonate, PFN — conducting polymer), where BODIPY **177** was the electron donor in the active layer composition and the fullerene derivative $PC_{71}BM$ (methyl-[(6,6)-phenyl-C_{71}]-butyrate) acted as the electron acceptor. The highest energy conversion efficiency achieved using BODIPY **177** as part of solar cells of this configuration was 6.41%.

In 2012, Huang *et al.*[224] reported the synthesis of fullerene-conjugated distyryl-BODIPY by the Knoevenagel condensation

Scheme 95

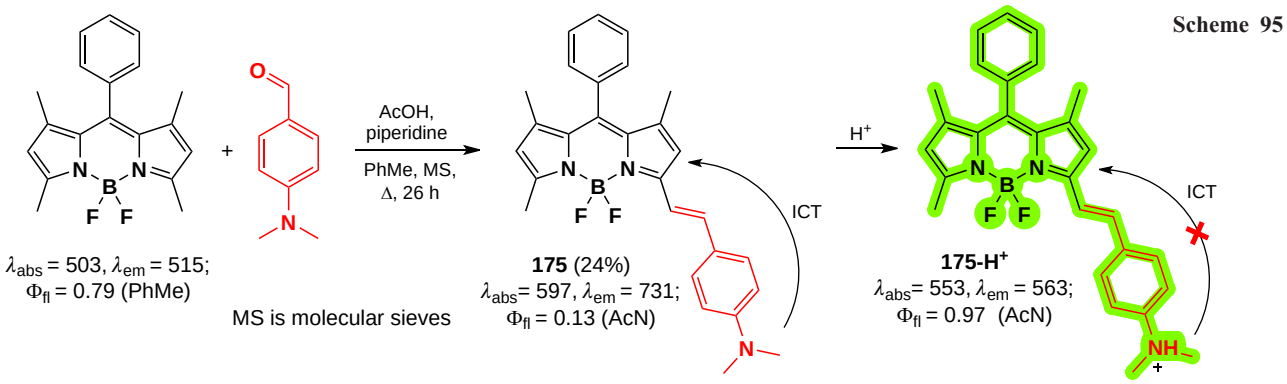

Scheme 96

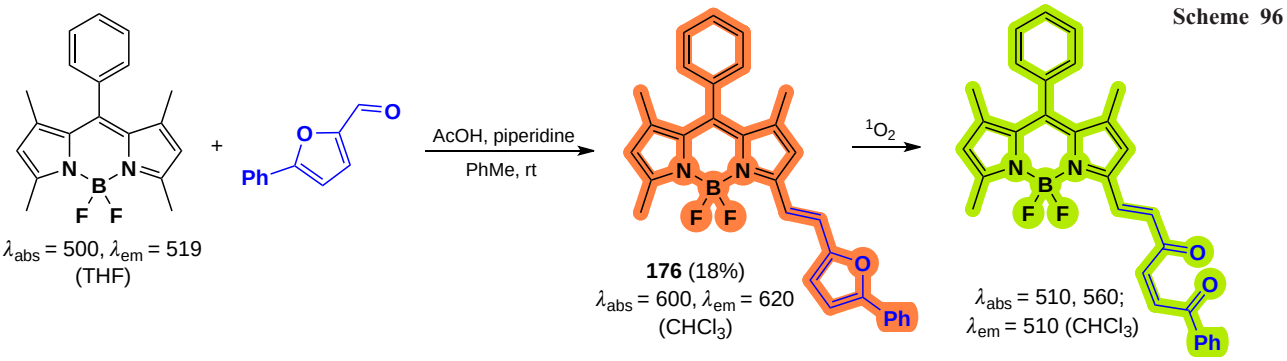

Scheme 97

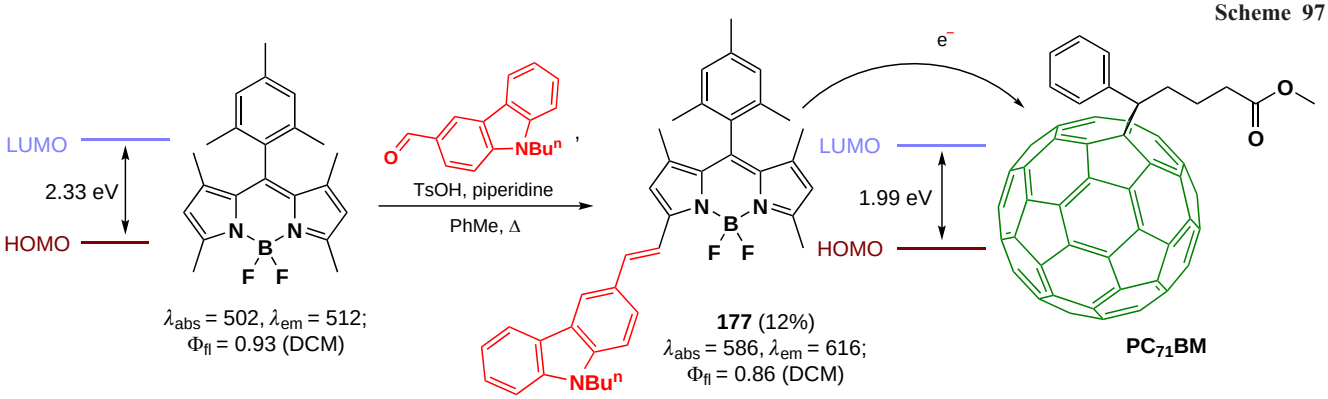

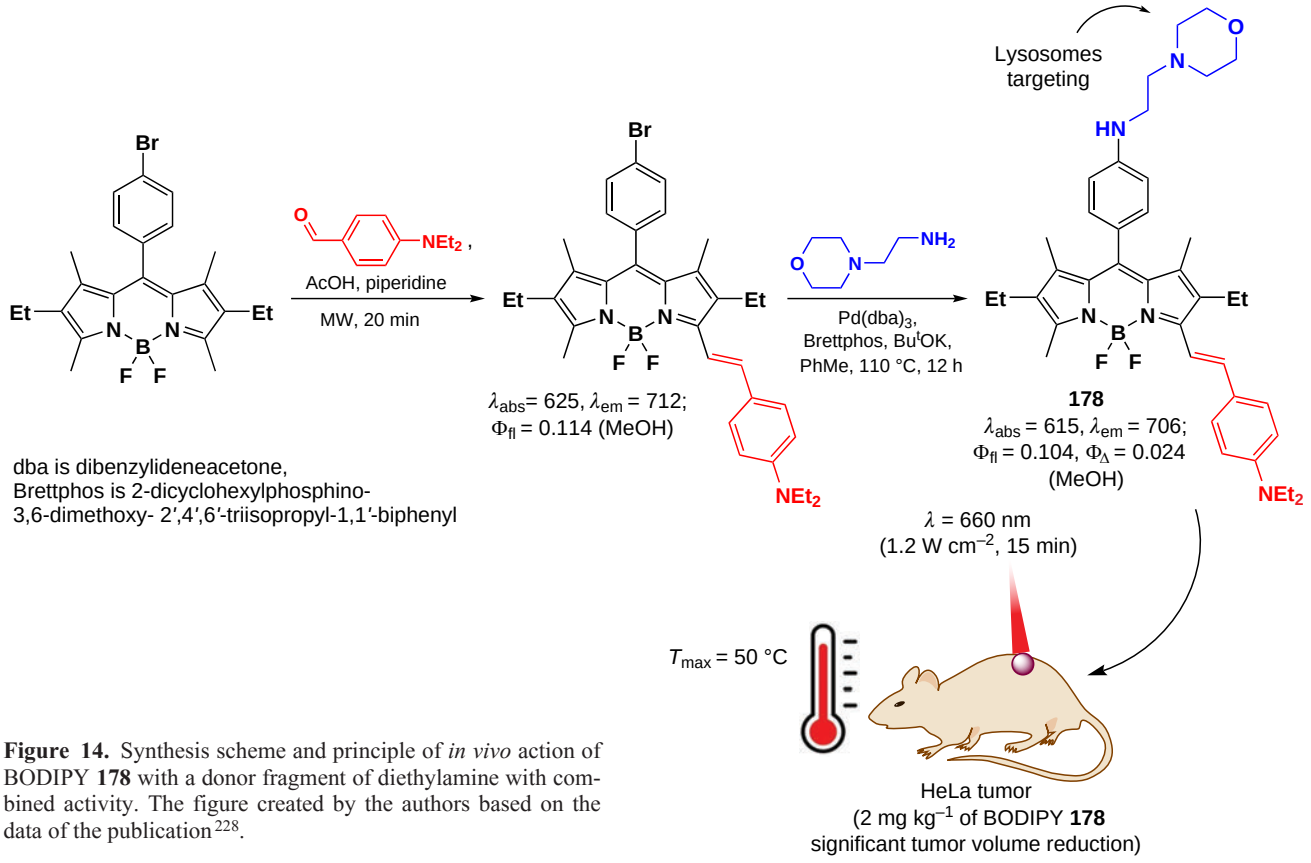

Figure 14. Synthesis scheme and principle of *in vivo* action of BODIPY **178** with a donor fragment of diethylamine with combined activity. The figure created by the authors based on the data of the publication[228].

under microwave irradiation. Eleven years later, Liu *et al.*[228] also used microwave irradiation to synthesize lysosome-targeted BODIPY **178** with combined activity (PDT and PTT) (Fig. 14). Compound **178** showed a fluorescence quantum yield of 0.1, indicating the predominance of nonradiative decay pathways, with a photothermal conversion efficiency (PCE) of 23%. Due to the presence of a morpholine fragment, BODIPY **178** accumulated in the lysosomes of HeLa cells and exhibited phototoxicity under 660 nm red light (1.2 W cm^{-2}, 5 min). *In vivo* experiments showed that, after a single injection of this compound into mice and irradiation with a diode at λ = 660 nm (1.2 W cm^{-2}, 1080 J cm^{-2}, 15 min,) a significant reduction in tumor volume was observed on the 14th day of therapy.

3.5.1.2. Knoevenagel condensations at positions 3 and 5

The Knoevenagel condensation of the methyl groups at C(3) and C(5) positions of BODIPY to give distyryl derivatives leads to a significant bathochromic shift of the absorption and emission maxima. Therefore, this method of BODIPY modification is widely used in the development of PDT and PTT agents, fluorescent probes, and optical materials.[219,223,229–237]

An expansion of the BODIPY π-system with styryl moieties at positions 3 and 5 promotes π–π-stacking and aggregation of fluorophores with the formation of J- or H-aggregates. According to the Kasha's exciton theory, the nature of the aggregates formed depends on the slip angle between the direction of the transition dipole moment and the longitudinal axis of the centers of mass of the molecules.[90] When the slip angle exceeds 54.7°, the molecules are in a face-to-face orientation and form H-aggregates, which are characterized by a hypsochromic shift, a high degree of charge transfer, and fluorescence quenching.[238] When the slip angle is <54.7°, J-aggregates are formed, in which the molecules are in a head-to-tail orientation. J-aggregates are characterized by a bathochromic shift of the absorption and

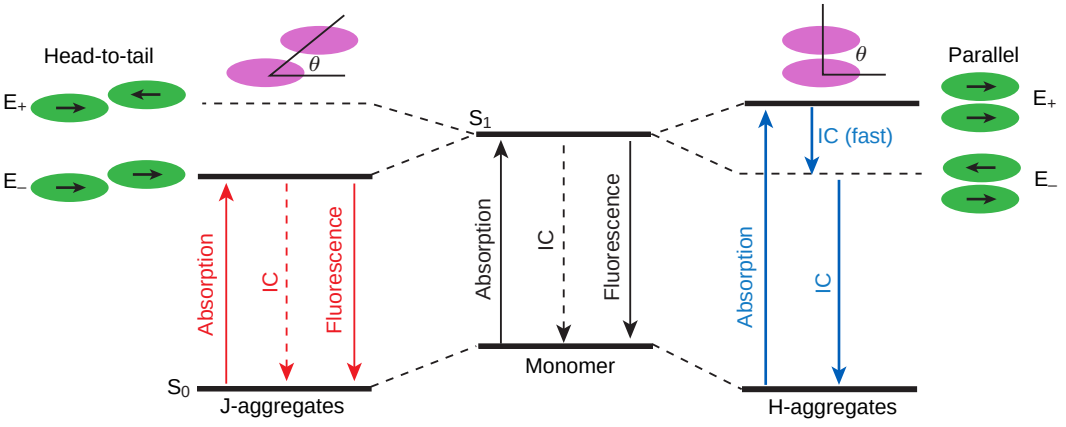

Figure 15. HOMO–LUMO energy gap as a function of slip angle (θ) in J- and H-aggregates.[243]

emission maxima and an increase in fluorescence quantum yields.[239] However, J-aggregates can also suppress fluorescence and the ISC process in favor of nonradiative decay pathways,[240] or, conversely, activate ISC by reducing the energy gap between singlet and triplet states.[241] The bathochromic shift can be enhanced by a donor-acceptor-donor (D–A–D) fluorophore configuration in which the magnitude of the HOMO–LUMO gap is determined by the electronic properties of the donor and acceptor moieties,[242] thus shifting the absorption and emission bands into the NIR-II band (Fig. 15).[243]

J-Aggregation is promoted by the presence of sterically hindered groups in the structure, which strengthen the head-to-tail orientation by formation of hydrogen bonds. External and intramolecular exciton interaction, *i.e.* delocalization of excitation energy in the π-system of the molecule and between molecules in the aggregate, also promotes J-aggregation.[238,244,245] As a result of aggregation, the fluorescence of the molecule can be quenched, leaving energy dissipation *via* internal conversion and vibrational relaxation as the only way for the molecule to relaxa from the excited state.[246] The process of converting absorbed light into thermal energy is fundamental to PTT, whereby tumor tissues are heated by light, resulting in the induction of cell apoptosis.[247]

In 2017, Han *et al.*[248] presented a dyad in which a resonance energy transfer (RET) from the donor distyryl BODIPY (**179a**) to the acceptor (**179b**) was observed. The latter contains heavy iodine atoms at positions 2 and 6, promoting internal conversion and the ability of the molecule to form singlet oxygen (Fig. 16). Dyad **180** exhibited better singlet oxygen generation efficiency compared to that of diiodo-BODIPY **179b**. BODIPY **180**-based NPs obtained after encapsulation with folic acid and pluronic F-127 exhibited PDT activity on HeLa cell line in *in vitro* experiments (IC_{50} = 14.8 μg mL^{-1}). In an *in vivo* study under the action of low-power NIR radiation (10 mW cm^{-2}) a significant inhibition of 4T1 tumor growth was observed in comparison to the control groups.

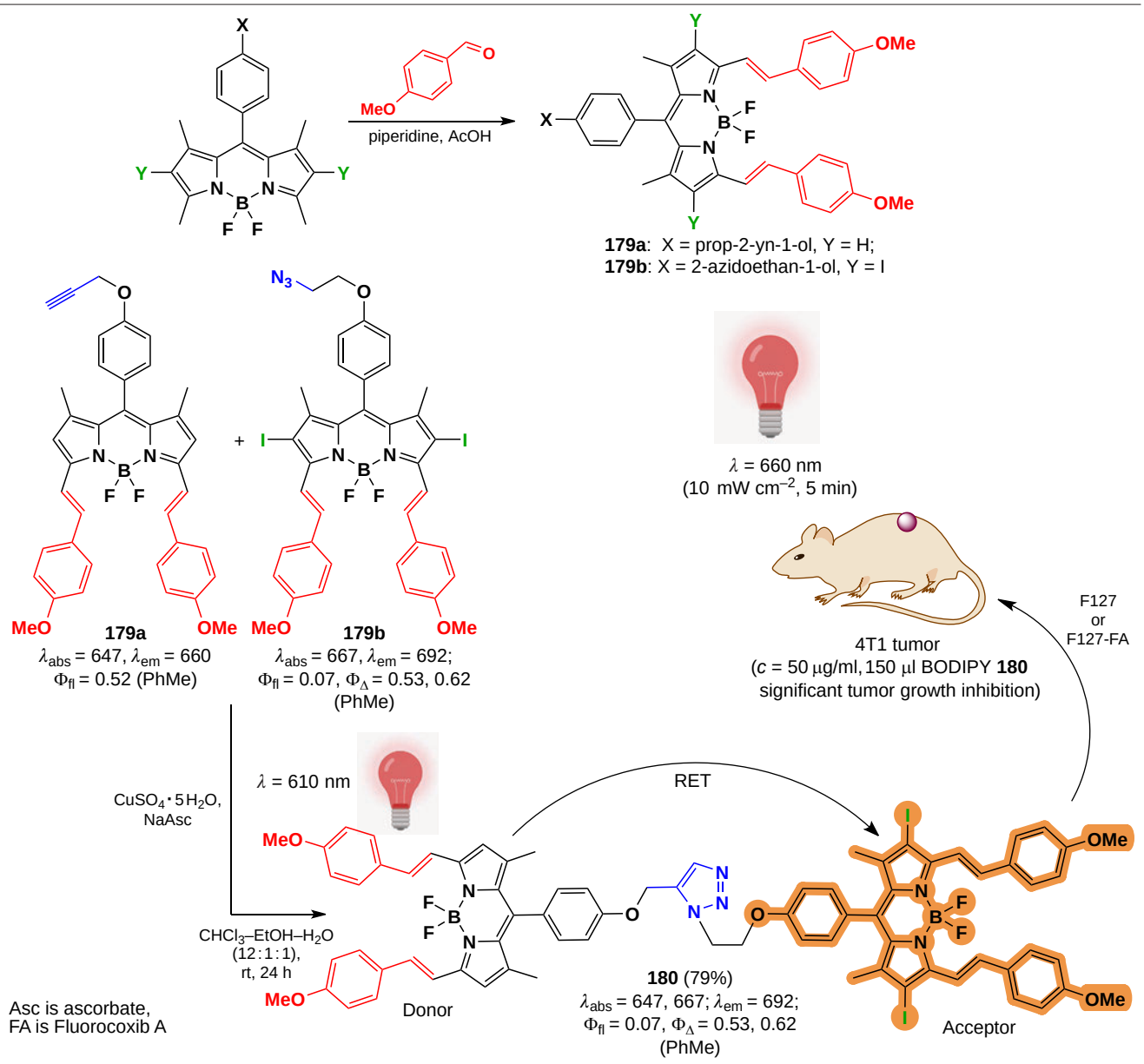

Figure 16. Synthesis scheme of dyad **180**, its principle of action and therapeutic effect *in vivo*. The figure created by the authors based on the data of the publication[248].

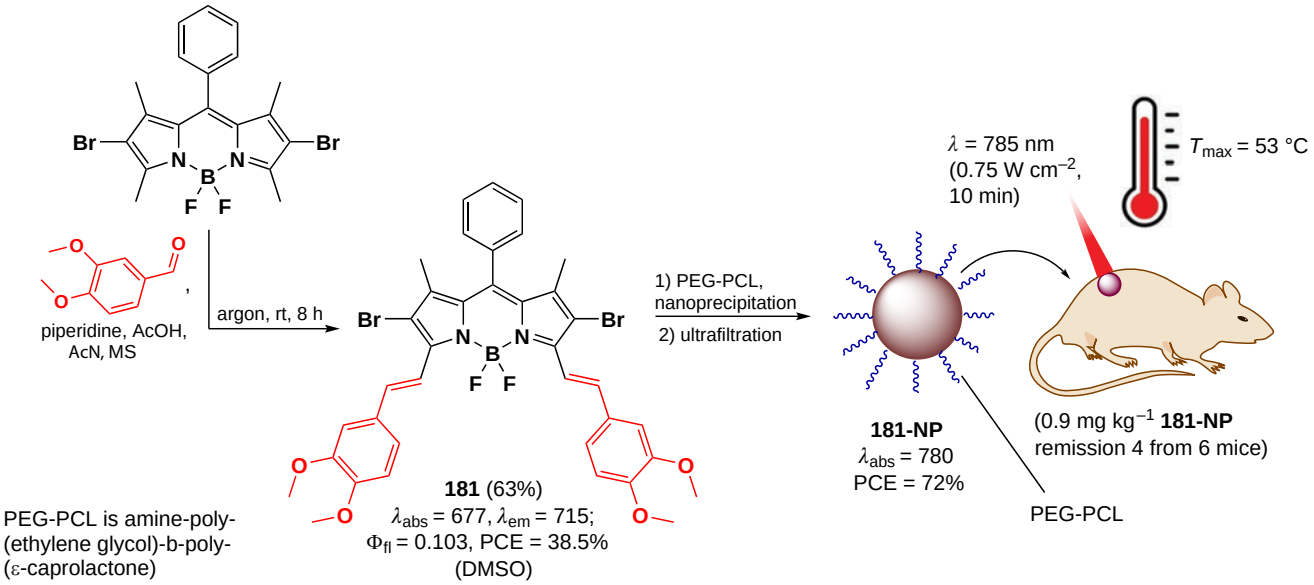

Figure 17. Schematic of the synthesis of **181-NP** nanoparticles with PTT activity and their therapeutic effects in vivo. The figure created by the authors based on the data of the publication[240].

In 2021, Su *et al.*[240] synthesized distyryl NIR-absorbing BODIPY **181**, which was capable of J-aggregation in order to design NPs with PTT activity (Fig. 17). The presence of an electronegative bromine atom at positions 2 and 6 and the electron-deficient core of BODIPY **181** promoted the formation of van der Waals Hal–π bonds and the aggregation of this BODIPY as two-dimensional sheets composed of antiparallel J-dimers (see Fig. 17).[249] Spherical NPs of **181-NP** showed a PCE of 72% and high phototoxicity on 4T1 cells *in vitro* at a concentration of 10 μM under 785 nm laser irradiation (0.75 W cm^{-2}, 10 min). When the therapeutic efficacy was examined *in vivo*, it was found that after administration of 0.9 mg kg^{-1} **181-NP** into 4T1 tumors and 785 nm laser irradiation (0.5 W cm^{-2}, 10 min), 4 out of 6 tumors disappeared on the 21st day.

In 2023, Jiang *et al.*[32] synthesized four distyryl derivatives of BODIPY **182** with different aromatic substituents (Fig. 18). The D–A–D configuration of BODIPY derivatives favored a shift of absorption to the NIR region,[250] and in aqueous media, all such compounds spontaneously formed J-aggregates. BODIPY **182**-based nanoparticles proved to be effective PDT and PTT agents. The optimal ratio of Φ_Δ and PCE values for the **182a-NP** was found to be 40.76 and 54.9%, respectively. In *in vitro* experiments on the 4T1 cell line, **182a** and **182b** NPs showed the highest activity with IC_{50} values = 0.4 and 2.23 μg mL^{-1}, respectively. In an *in vivo* study, **182a-NP** and **182b-NP** induced complete remission in BALB/C mice with 4T1 tumor line after irradiation with laser at λ = 808 nm (1 W cm^{-2}, 3 min).

In 2021, Ansteatt *et al.*[251] synthesized a series of 3,5-diarylethynyl-BODIPY **183a–f** *via* the Knoevenagel condensation (Scheme 98). Water-soluble BODIPYs **183g,h** were obtained using a 'click' reaction with tetraethylene glycol azide (TEG). A significant bathochromic shift in the electronic spectra was observed for the donor distyryl-BODIPY compounds **183c–e** compared to the parent BODIPYs. BODIPY **183g** modified with TEG moieties exhibited moderate fluorescence intensity in the 730–740 nm region in polar solvents, including water, while being in micelles with Pluronic F127, Tween 20, and Triton X100.

In 2020, Xi *et al.*[34] reported a highly efficient PTT agent based on styryl-substituted BODIPY **184** with a meso-CF_3 group (Fig. 19). The PCE of **184-NP** nanoparticles was 88.3%. This large PCE value was shown to be a consequence of the low transition energy between the HOMO and LUMO, which increased the fraction of nonradiative decay pathways, as well as the free rotation of the *meso*-CF_3-group. **184-NP** nanoparticles showed significant phototoxicity under low doses of red light (λ = 808 nm, 0.3 W cm^{-2}) on HeLa, MCF-7 and 4T1 cell lines. *In vivo* photoacoustic (PA) imaging of **184-NP** nanoparticles in BALB/C mice showed a high-contrast signal in a tumor region. The *in vivo* therapeutic efficacy study showed complete disappearance of 4T1 tumors after a single injection of **184-NP** nanoparticles (at a dose of 300 μM in 100 μL) and light irradiation (λ = 808 nm, 0.3 W cm^{-2}, 8 min) on the 16th day after administration.

In 2023, Chen *et al.*[31] designed NIR-absorbing 3,5-diene-BODIPY with PTT activity (Fig. 20). Due to the presence of a freely rotating *meso*-CF_3 group, the fluorescence of BODIPY **185** was negligible. Upon acidification of BODIPY **185**, sequential protonation of the nme_2 groups occurred, resulting in a shift of an absorption maximum from 836 to 774 and 710 nm due to suppression of ICT. However, no fluorescence enhancement was observed upon acidification, indicating that the rotation of the CF_3 group is the primary nonradiative decay pathway. Despite the inability of compound **185** to generate $^1O_2$ upon irradiation, nanoparticles based on it (**185-NP**) exhibited photothermal activity with a PCE of 44.4%. In an *in vitro* study, **185-NP** nanoparticles at a concentration of 30 μM significantly reduced the survival of MGC-803 cells upon irradiation with an 808 nm laser (0.3 W cm^{-2}, 30 min).

In 2023, Gao *et al.*[30] utilized two sequential Knoevenagel condensations to synthesize BODIPY **186** with PDT and PTT activity. BODIPY **186** was designed with a lysosome-targeting morpholino moiety within its styryl substituents, and the second styryl moiety was nitrogen mustard, bis(2-chloroethyl)aniline (Fig. 21). BODIPY **186** demonstrated high PTT activity (PCE = 40%) and accumulated effectively in lysosomes. The IC_{50} values for the HeLa cell line irradiated with a 760 nm laser (0.5 W cm^{-2}) were 8.75 μM under normoxic conditions and

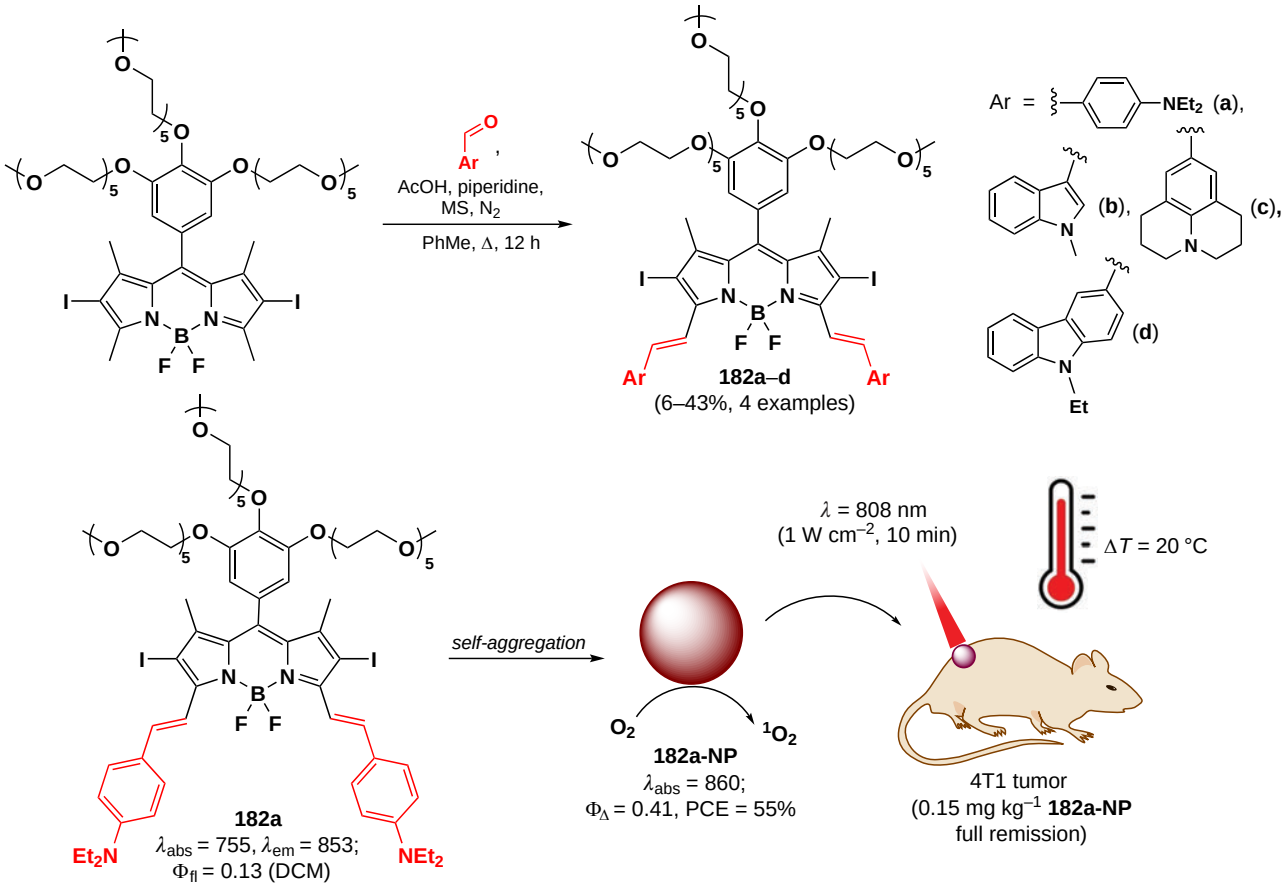

Figure 18. Schematic of the synthesis of BODIPY **182** and the therapeutic effects of **182a-NP** nanoparticles *in vivo*. The figure created by the authors based on the data of the publication[250].

Scheme 98

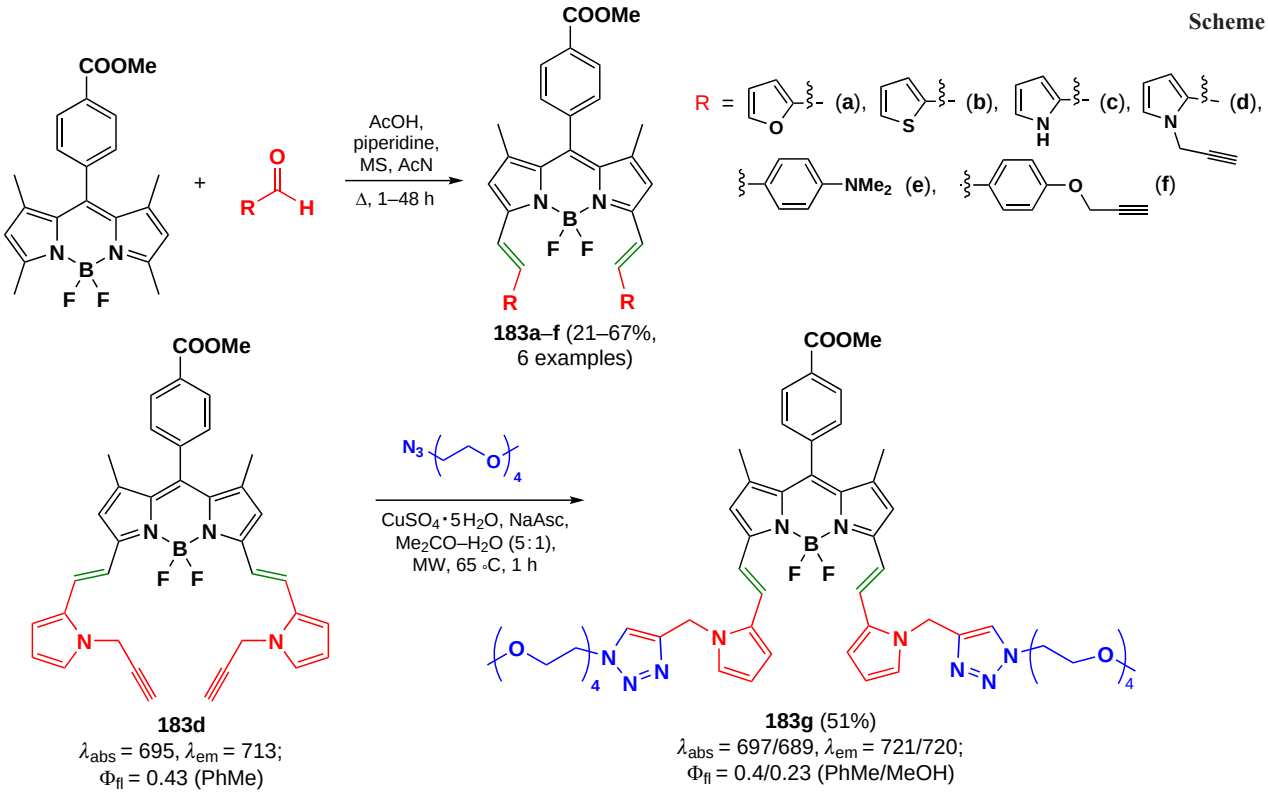

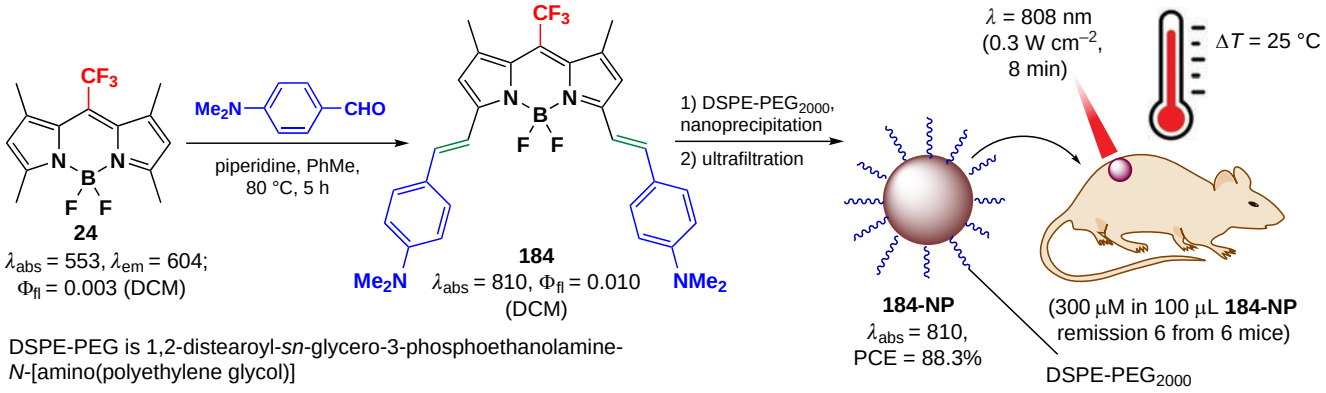

Figure 19. Schematic of BODIPY **184** synthesis and in vivo action of **184-NP** nanoparticles. The figure created by the authors based on the data of the publication[34].

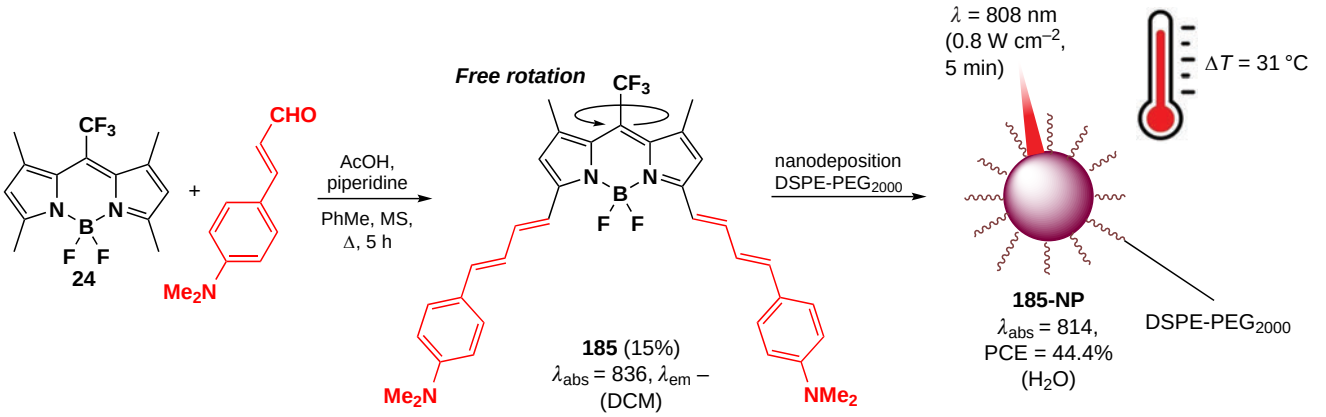

Figure 20. Scheme of the synthesis of BODIPY **185** and the in vitro action of the NPs based on it. The figure created by the authors based on the data of the publication[34]. A dash indicates no emission.

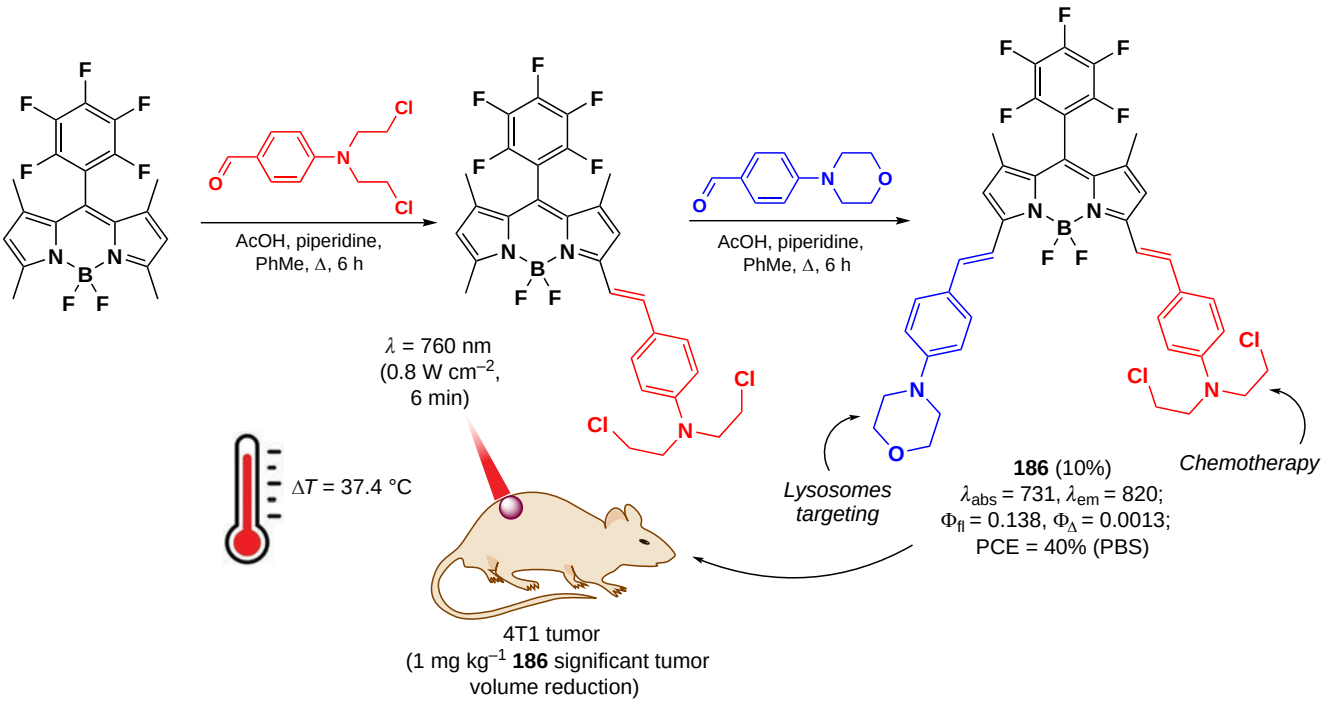

Figure 21. Synthesis scheme of BODIPY **186**, its principle of action and therapeutic effect *in vivo*. The figure created by the authors based on the data of the publication[30].

Scheme 99

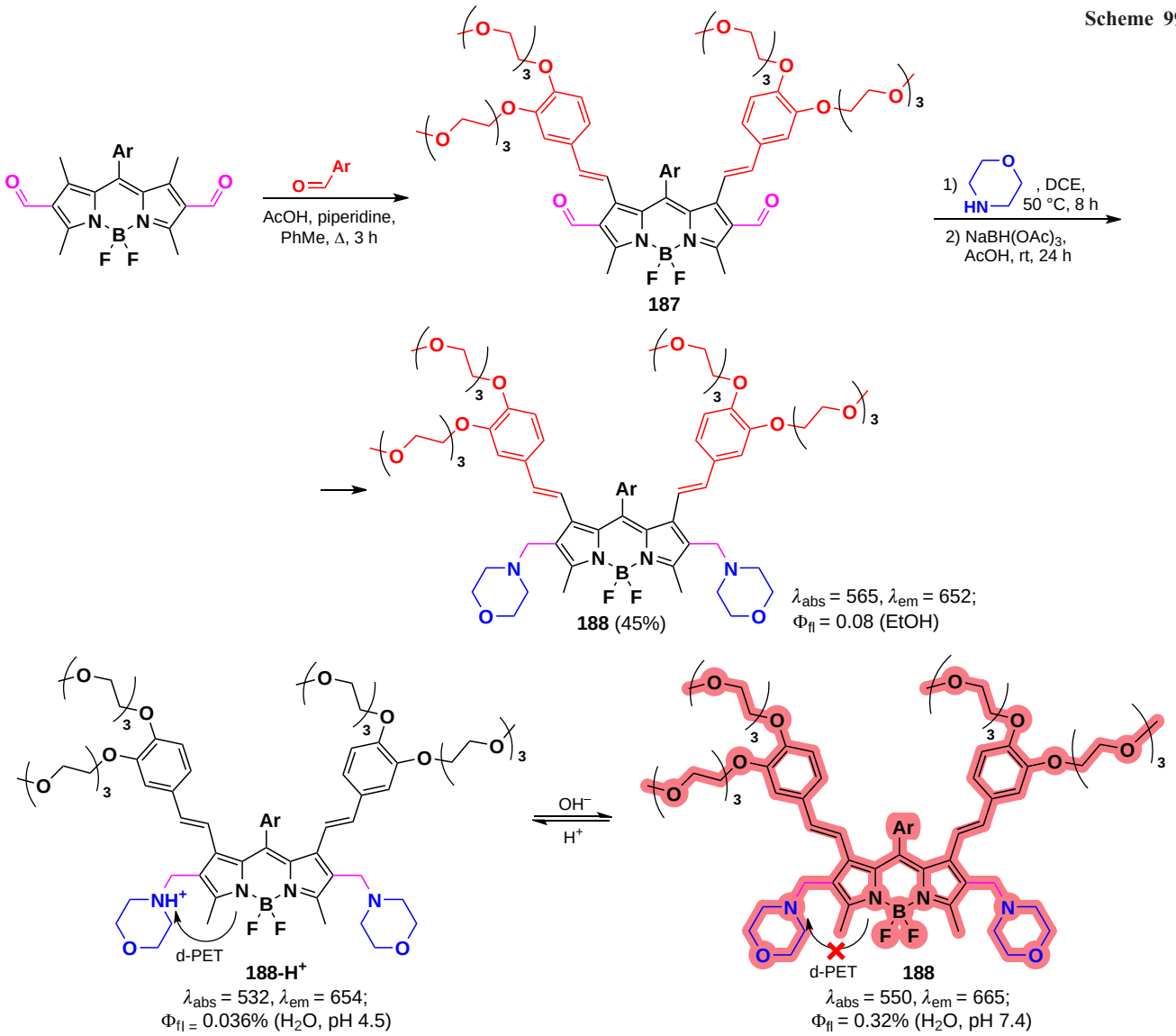

10.5 μM under hypoxic conditions. In an *in vivo* study on 4T1-bearing mice, a significant reduction in tumor volume was observed on day 14 after intravenous injection of BODIPY **186** into mice, followed by irradiation with a 760 nm laser (0.8 W cm^{-2}, 6 min).

Methyl groups at positions 1 and 7 of *meso*-aryl-BODIPY exhibit low reactivity due to steric hindrance.[216] Despite this, Zhang *et al.*[252] demonstrated non-standard 1,7 regioselectivity in the Knoevenagel condensation. The reaction of 2,6-diformyl-1,3,5,7-tetramethyl-BODIPY with substituted benzaldehyde resulted in a disubstitution product at methyl groups at positions 1 and 7, yielding compound **187** (Scheme 99). Further reductive amination gave BODIPY **188**, a pH-sensitive sensor whose fluorescence quantum yield increased more than 14-fold as the pH increased from 4.5 to 7.4. The pH-response mechanism involved the suppression of PET by the deprotonated form of the compound. In acidic conditions, probe **188** exhibited no fluorescence due to the d-PET[§] process from BODIPY to protonated morpholine. When evaluating the ability of sensor **188** to visualize HUVEC-C cells intracellularly, it was found that it selectively accumulates in lysosomes and produces a strong fluorescence response at intracellular alkaline pH.

In 2023, Zhu *et al.*[33] reported highly fluorescent BODIPY **189** with electron-acceptor substituents for NIR-II fluorescence imaging (Scheme 100). Due to the formation of J-aggregates that were encapsulated in the NPs, the absorption and emission of **189-NP** nanoparticles shifted to the NIR band in the spectrum. A high fluorescence quantum yield was also observed in the NIR-II band (Φ_{fl} = 0.005), which was attributed to the full planarity of the BODIPY core and optimal stacking for J-aggregation. In an *in vivo* imaging study, high-contrast real-time imaging of the mouse vascular system was obtained. Due to its ability to emit both in the visible range as monomers and in the NIR-II region in the form of J-aggregates, an anti-counterfeiting ink was developed based on BODIPY **189**.

In 2024, Li *et al.*[15] designed 3,5-distyryl-BODIPY **190** as an agent for sonodynamic therapy (Fig. 22). Due to the «heavy atom» effect and low fluorescence intensity, compound **190** was found to be a good photosensitizer with Φ_{Δ} = 0.95. It showed the ability to be sonosensitized by ultrasound (US) at 1.5 W cm^{-2}, with singlet oxygen being the main product of this process. In the intracellular environment, BODIPY **190** could form ROS upon US exposure. The IC_{50} value on 4T1 cells was 3.81 μM in normoxia and 5.36 μM in hypoxia. In a study of antitumor

[§] The symbol ‘d’ (from «donor») indicates that the electron is transferred from the excited BODIPY.

Scheme 100

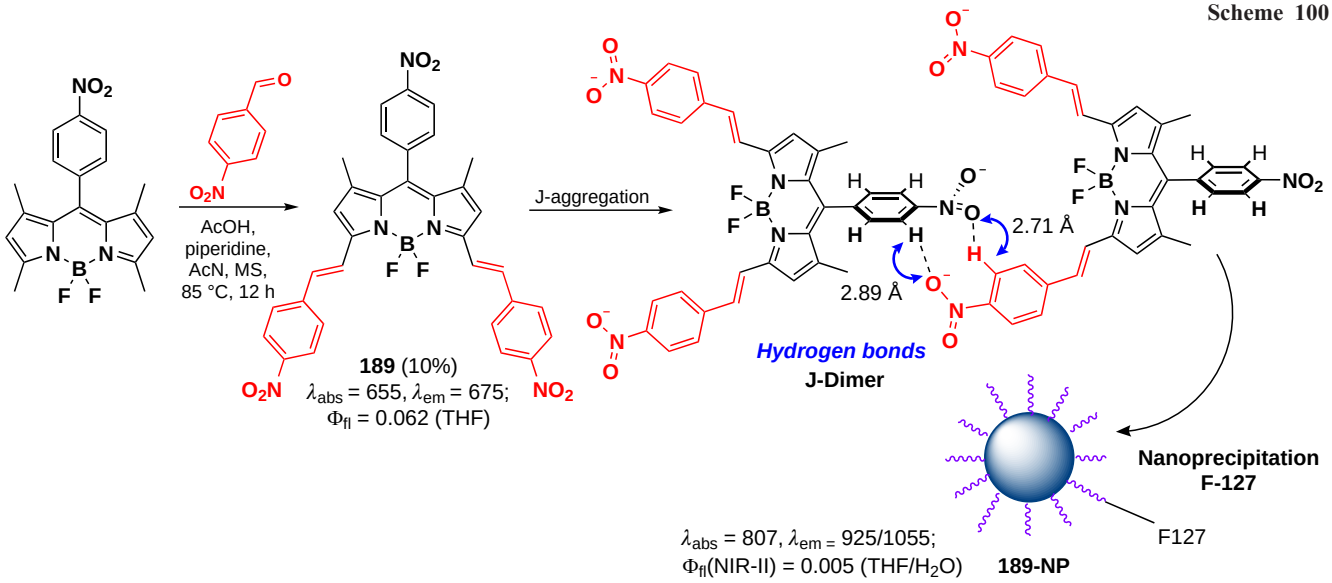

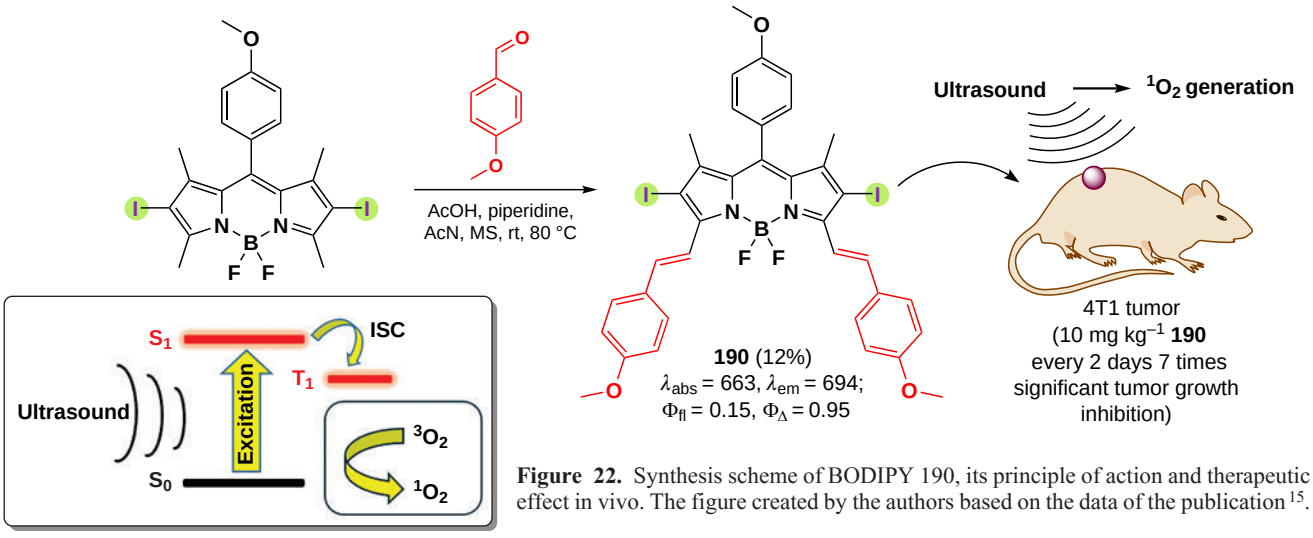

Figure 22. Synthesis scheme of BODIPY 190, its principle of action and therapeutic effect in vivo. The figure created by the authors based on the data of the publication [15].

activity *in vivo*, statistically significant inhibition of tumor growth was observed on the 15th day of therapy after 7 injections of BODIPY **190** every 2 days, followed by US irradiation (1.5 W cm^{-2}, 5 min).

3.5.1.3. Knoevenagel condensation at the Me-groups in positions 1, 3, 5, and 7

In 2009, Buyukcakir *et al.*[216] proposed a method for the synthesis of 1,3,5,7-tetrastyryl-BODIPY **191** from the tetramethyl derivative in the presence of 7 equivalents of anisaldehyde (Scheme 101). Upon the condensation at positions 1 and 7, the bathochromic shift in the spectrum was approximately 20 nm, which was much smaller than the ~70 nm shift upon condensation at positions 3 and 5. The fluorescence quantum yields of tri- and tetrastyryl-BODIPY remained almost unchanged when styryl substituents were introduced at positions 1 and 7, compared to 3,5-distyryl-BODIPY.

In 2014, the same research group [192] synthesized a series of 2,6-ethynylaryl-BODIPYs with two different styryl substituents at positions 3, 5 and 1, 7 (Scheme 102). The resulting BODIPYs exhibited selective response to Hg^{2+} cations; coordination of the Hg^{2+} cation to probe **193** with mercury-chelating moieties at positions 3 and 5 resulted in a shift of the absorption maximum in the spectrum from 800 to 715 nm and a fluorescence enhancement at 736 nm. Meanwhile, coordination of the Hg^{2+} cation to probe **192** with mercury-chelating moieties at positions 1 and 7 did not result in a shift of the absorption bands. The differences in the nature of the response of BODIPY **192** and **193** to Hg^{2+} were explained by the greater sensitivity of the HOMO of 3,5-distyryl-BODIPY to protonation or the binding to the cation than that of the analogous orbitals of 1,7-distyryl-BODIPY, due to the greater destabilization of the HOMO upon introduction of styryl substituents at positions 3 and 5 than at positions 1 and 7.

2,6-Ethynylaryl-1,3,5,7-tetrastyryl-BODIPY are also of interest as PTT agents. In 2019, Hu *et al.*[253] synthesized tetrastyryl-BODIPY **194** as a promising NIR-absorbing PTT agent (Fig. 23). According to density functional theory (DFT) calculations, in the antiparallel J-dimer **194** the electron density of the HOMO is completely delocalized on one of the dimer molecules and the LUMO on the other, indicating an emission-damping intermolecular charge transfer due to excitation. **194-NP** nanoparticles obtained after encapsulation of **194** in DSPE-mPEG5000 showed high PCE (61%) and proved to be good PTT agents in *in vivo* experiments: inhibition of HeLa tumor growth was observed after irradiation of mice with λ = 808 nm laser (0.3 W cm^{-2}, 5 min).

Scheme 101

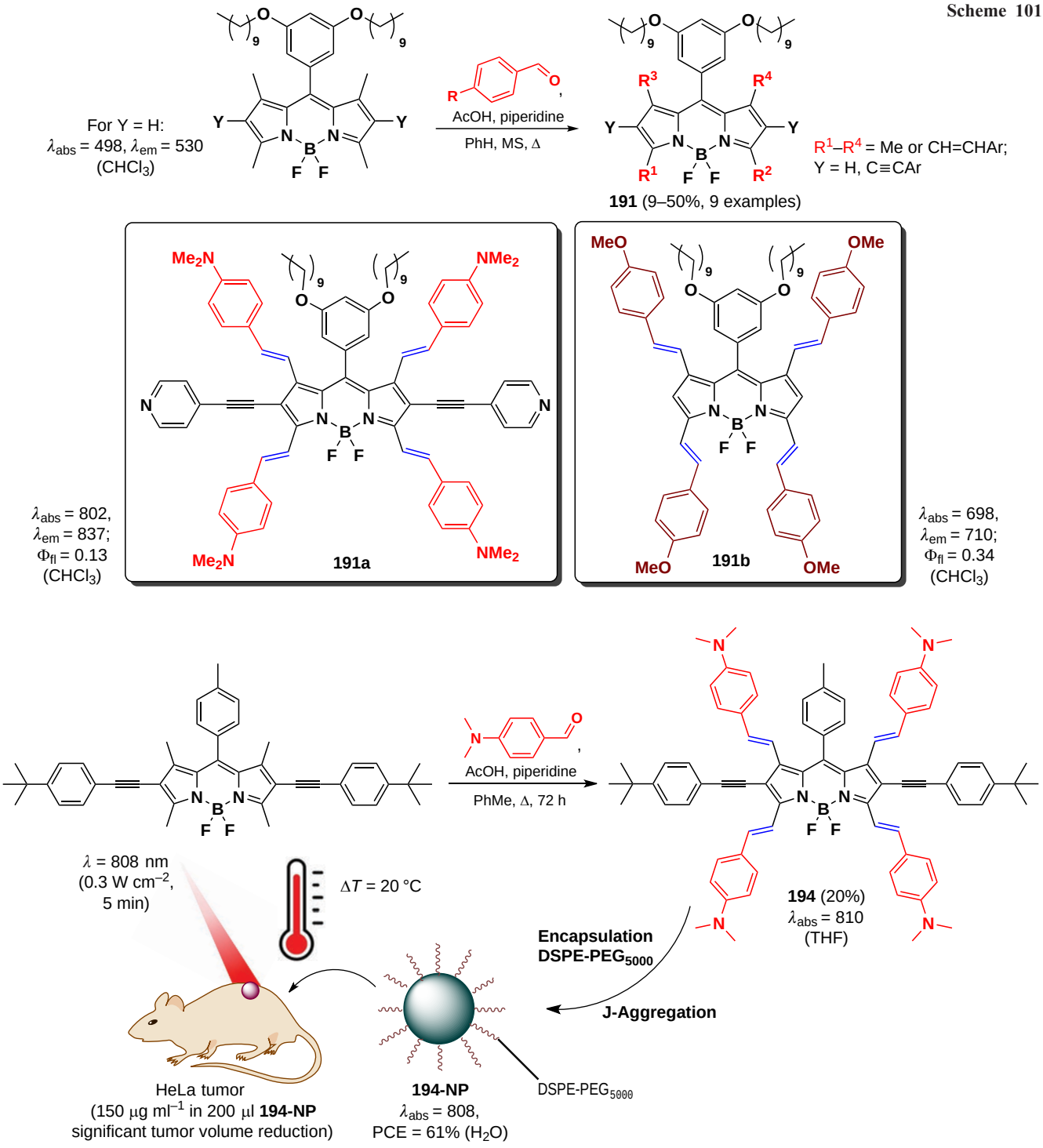

Figure 23. Synthesis scheme of BODIPY 194 and the principle of action of NPs based on it *in vivo*. The figure created by the authors based on the data of the publication [253].

A series of mono-, di-, and tristyryl-BODIPY **195a–c** were synthesized and investigated as agents for combined PDT/PTT therapy in 2019 by Zou *et al.*[217] (Fig. 24). At acidic pH, the absorption of BODIPY NPs shifted to the red region of the spectrum, which was accompanied by an increase in PCE due to the suppression of intramolecular charge transfer (ICT) as a molecule relaxation pathway. In *in vitro* study, **195c-NP** NPs showed IC_{50} values = 4.16 μM, the highest PCE (60.5%), and effectively inhibited HeLa tumor growth after intravenous administration and irradiation with an 808 nm laser (1 W cm^{-2}, 8 min).

3.5.1.4. Knoevenagel condensation with *meso*-methyl group

In 2011, Chattopadhyay *et al.*[98] reported the synthesis of 8-styryl derivatives **196** from commercially available BODIPY PM597 (R^1 = Bu^t, R^2 = Me) and PM567 (R^1 = Et, R^2 = Me) (Scheme 103). The authors attributed the regioselectivity of the condensation to the alle*via*tion of steric hindrance present in alkyl-BODIPY between the protons of the methyl groups at the C(1), C(7) and *meso*-position atoms and to the increased

Scheme 102

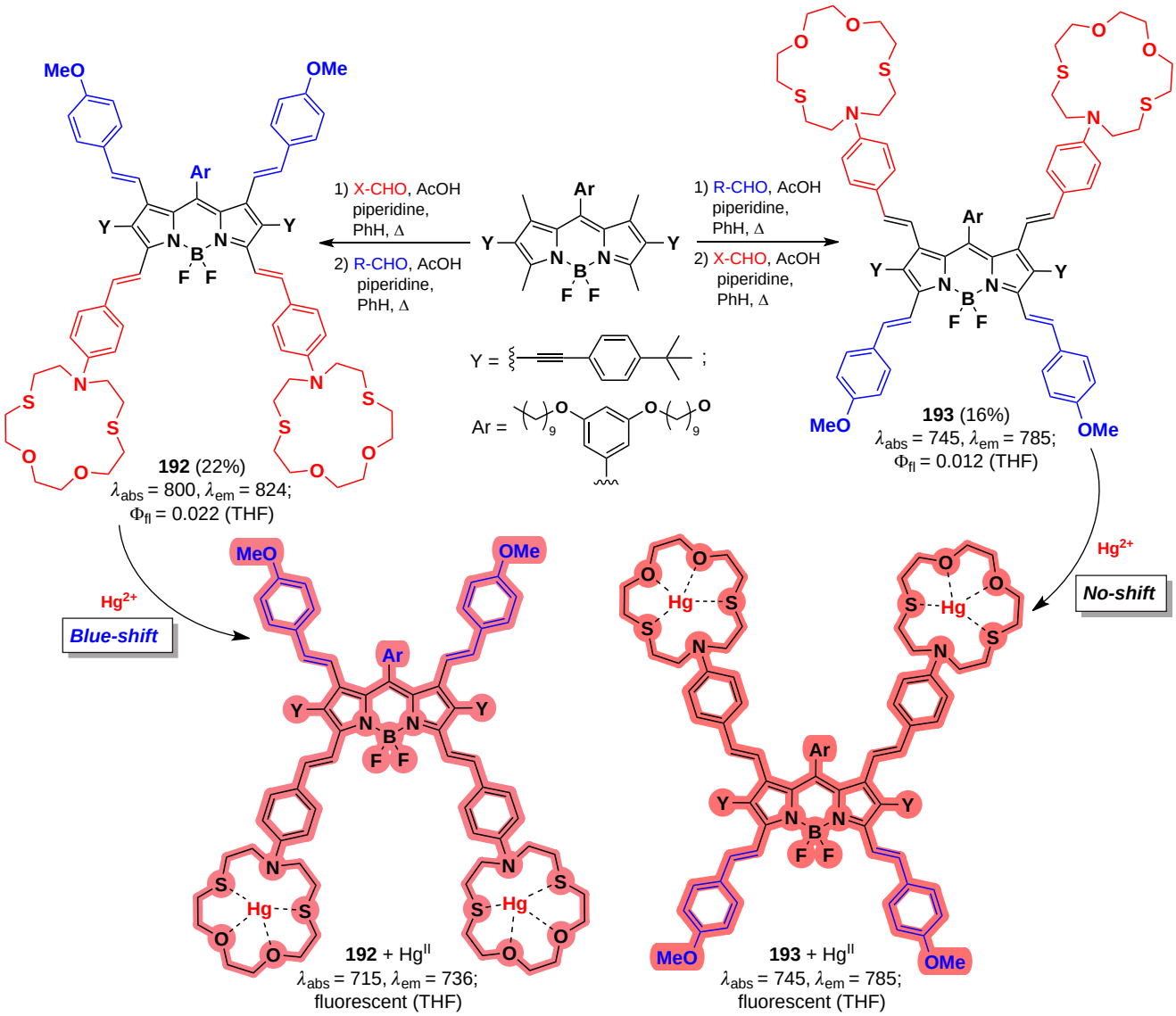

planarity of the molecule resulting from condensation. Nevertheless, Palao *et al.*[254] demonstrated that the Knoevenagel condensation proceeds regioselectively at the *meso*-position even in the absence of methyl groups at positions 1, 7, leading to the formation of BODIPY **197**. This regioselectivity is primarily due to the preferential delocalization of the positive charge of BODIPY at the *meso*-position. The introduction of styryl substituents at the *meso*-position of BODIPY results in a small bathochromic shift (8–30 nm) and complete quenching of fluorescence, which is due to nonradiative relaxation caused by vibrations of the pyrrole cycles outside the plane of the BODIPY core.[255] An additional contribution to the fluorescence quenching is made by the ICT effect, which manifests itself in the case of aldehydes with both donor and acceptor substituents.

In 2012 and 2016, Yu *et al.*[77,256] reported the synthesis of isoindole-based NIR-absorbing 8-styryl-substituted BODIPYs, which also exhibited almost no fluorescence (Scheme 104).

3.5.2. Electrophilic Substitution Reactions in the α-methyl groups of BODIPY

The methyl group at the α-position of BODIPY exhibits significant CH-acidity; the nucleophilic anion formed as a result of deprotonation is capable of reacting with various electrophiles. In 2009, Shandura *et al.*[257] demonstrated that the sequential reaction of 3,5-dimethyl-BODIPY with 1,1-di(methoxy) trimethylamine and TFA produced enamine **199a** and aldehyde **199b**, respectively (Scheme 105). Oxidation of the 3-methyl group caused a bathochromic shift of the absorption maximum for enamine **199a** and complete quenching of the fluorescence due to the PET effect, whereas hydrolysis of enamine to aldehyde **199b** restored the photophysical characteristics to those identical to the parent 3,5-dimethyl-BODIPY.

In 2012, Ulrich *et al.*[258] reported the electrophilic bromination of hexaalkyl-BODIPY with NBS to form unstable 3-bromomethyl- and 3,5-bis(bromomethyl) BODIPYs. These compounds readily react with various O-, N-, S-, and P-nucleophiles in nucleophilic substitution reactions yielding mono- (**200**) and di-substituted BODIPYs (**201**) (Scheme 106). The introduction of nucleophiles at positions 3 and 5 did not significantly affect the absorption and emission properties of BODIPY. However, BODIPY **201a** with a tertiary amino group exhibited an extremely low fluorescence quantum yield (Φ_{fl} = 0.01) due to the PET effect.

In 2020, Kand *et al.*[149] utilized the nucleophilic substitution reaction of the bromine atoms at positions 3 and 5 to conjugate

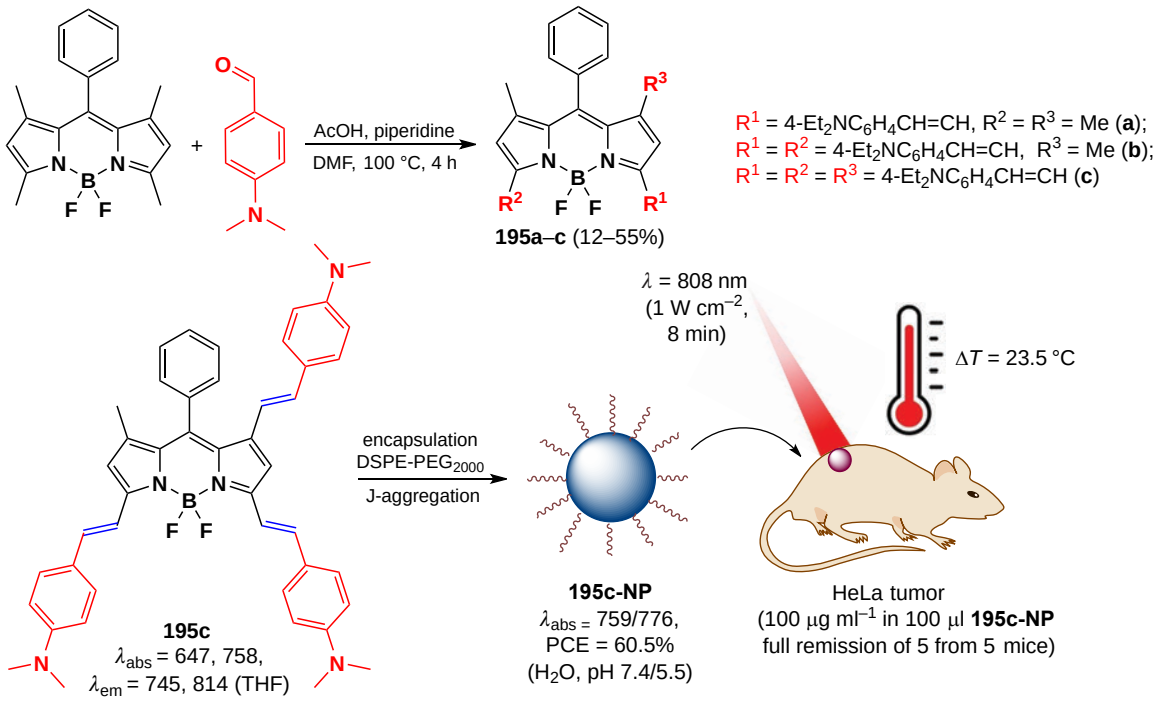

Figure 24. Schematic of the synthesis of BODIPY **195a**–**c** and the principle of action of **195c-NP** nanoparticles *in vivo*. The figure created by the authors based on the data of the publication [217].

Scheme 103

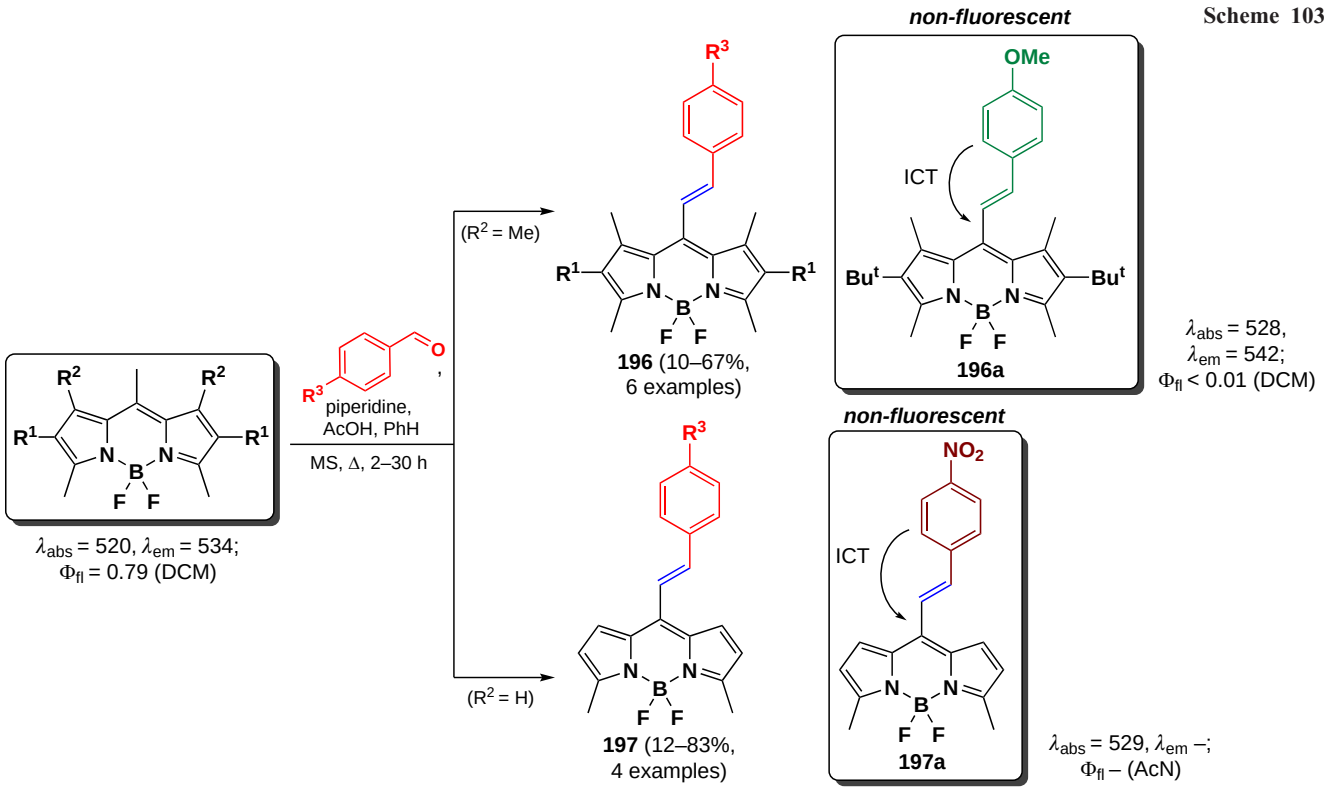

2-mercaptoethanesulfonic acid (MES) with the BODIPY core, yielding water-soluble photo-removable protective groups based on *meso*-substituted BODIPY (Scheme 107). In a study of the ability of MES-BODIPY to accumulate in cells, the mono-substituted BODIPY **202** showed a two-fold higher level of intracellular fluorescence compared to the original BODIPY. In contrast, the disubstituted BODIPY **203** was unable to penetrate HEK293T cells.

3.5.3. Oxidation of α-methyl groups of BODIPY

Due to the possibility of stabilising benzyl-type cations in the α-positions of BODIPY, peralkylated BODIPYs are susceptible to oxidation at these positions *via* DDQ and lead(IV) acetate.[6] In 1994, Sathyamoorthi *et al.*[259] synthesized 3-formyl-BODIPY **204** by oxidation of hexamethyl-BODIPY *via* DDQ and 3,5-bis(acetoxymethyl)-BODIPY **205** by oxidation *via* lead(IV)

Scheme 104

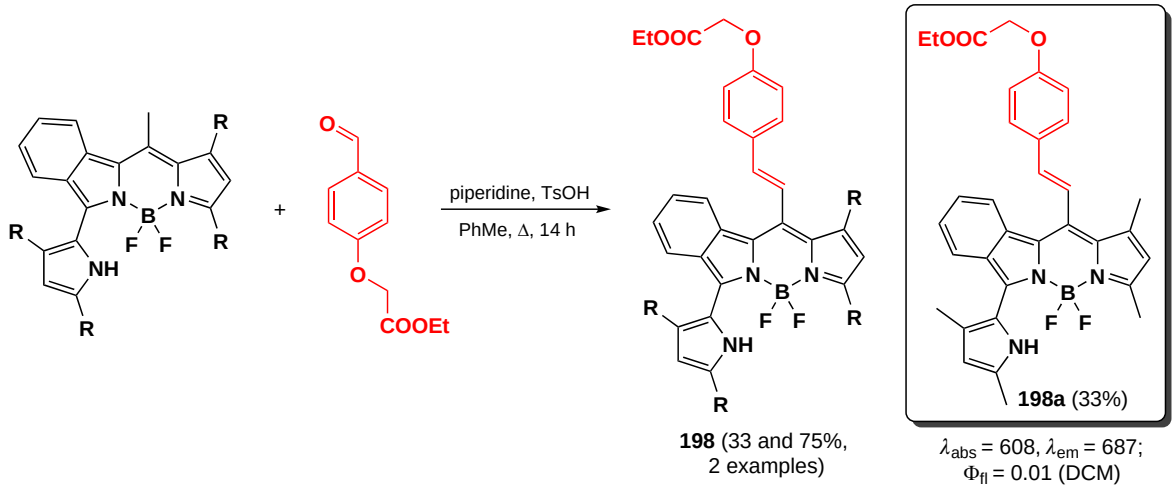

Scheme 105

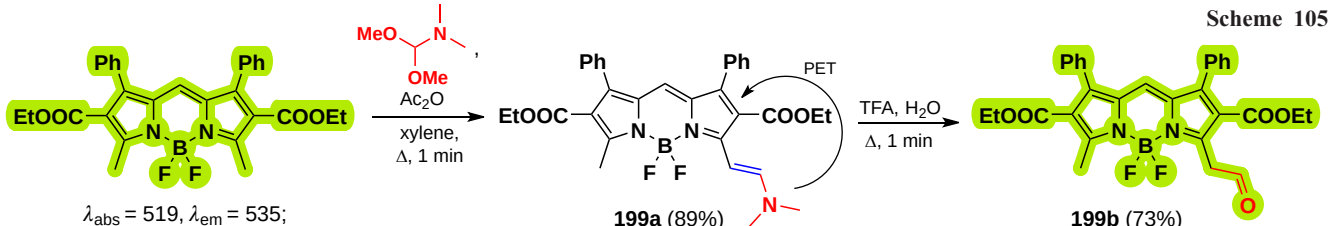

Scheme 106

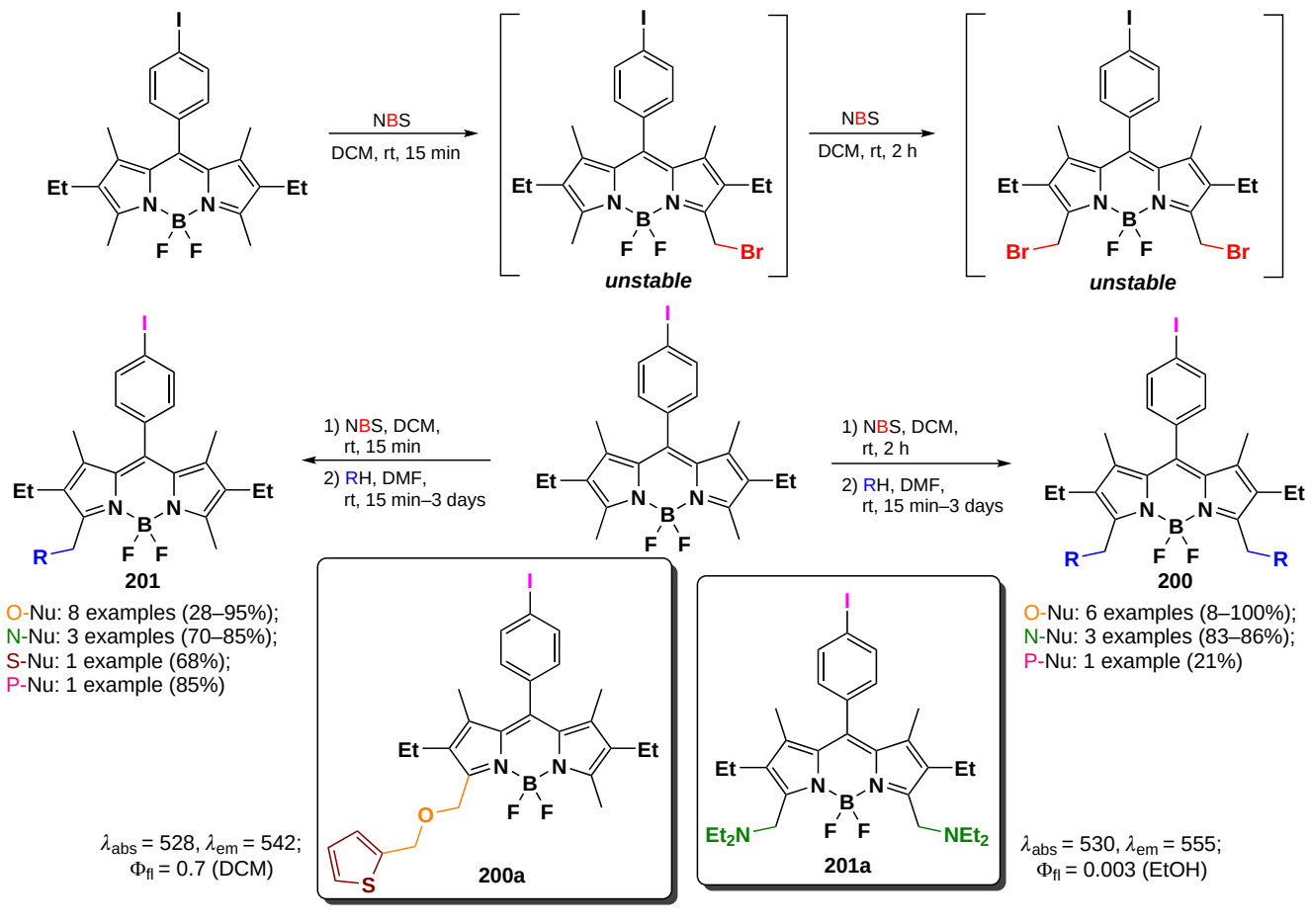

Scheme 107

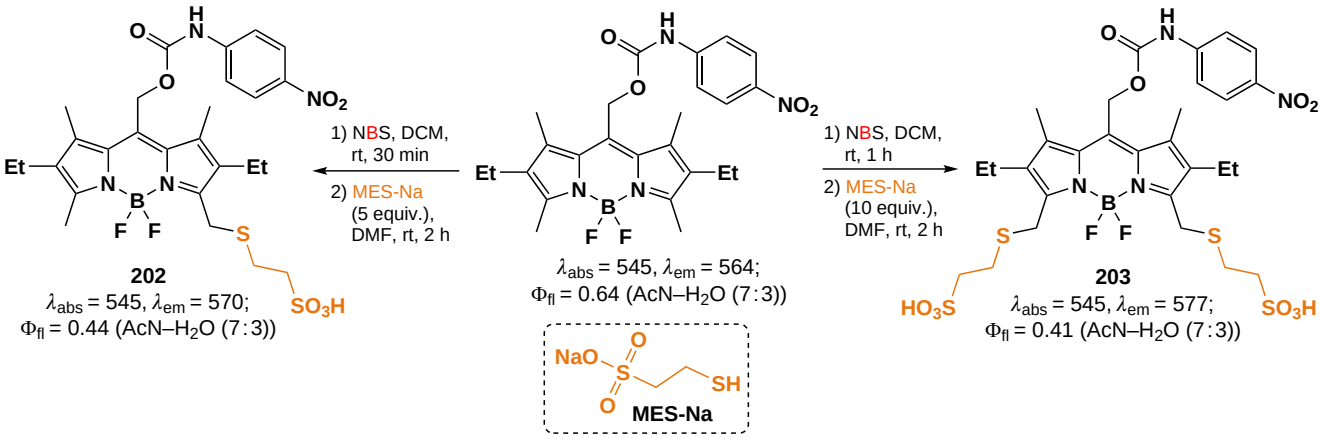

Scheme 108

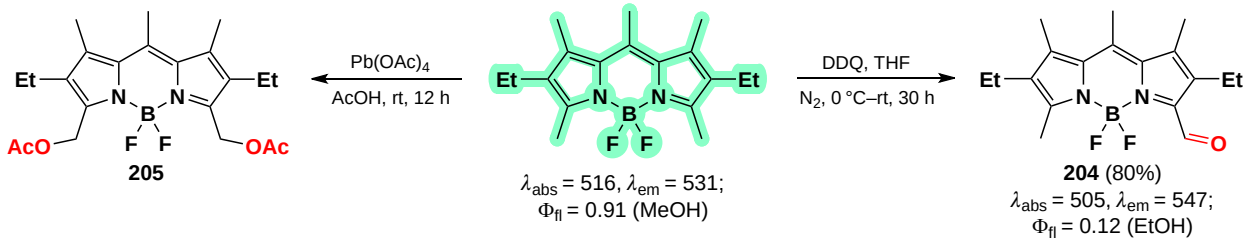

acetate (Scheme 108). Oxidation of the α-methyl group in BODIPY **204** resulted in a quenching of the fluorescence to $\Phi_{fl} = 0.12$.

In 2016, Wu *et al.*[260] designed a Cys-sensitive fluorescent probe based on 1,5,7,8-tetramethyl-3-formyl-2,6-diethyl-BODIPY (**204**) (Scheme 109). Upon reaction with Cys a five-membered ring was closed, resulting in an increase in fluorescence and a bathochromic shift of the absorption maximum due to PET quenching. However, in the presence of other amino acids, including Hcy, no fluorescence response of BODIPY **204** was observed.

In 2022, Blázquez-Moraleja *et al.*[6] proposed the use of 3,5-acetoxymethyl groups as leaving groups for nucleophilic substitution reactions in the B(CN)$_2$-BODIPY (Scheme 110). Substitution of the acetoxy group proceeded *via* the SN_1 mechanism; acid-catalysed hydrolysis led to the formation of a stabilized carbocation, which is readily reactive with various nucleophiles. B(CN)$_2$-BODIPY was used as a starting compound,[261,262] stable in the presence of Lewis acids; then

Scheme 109

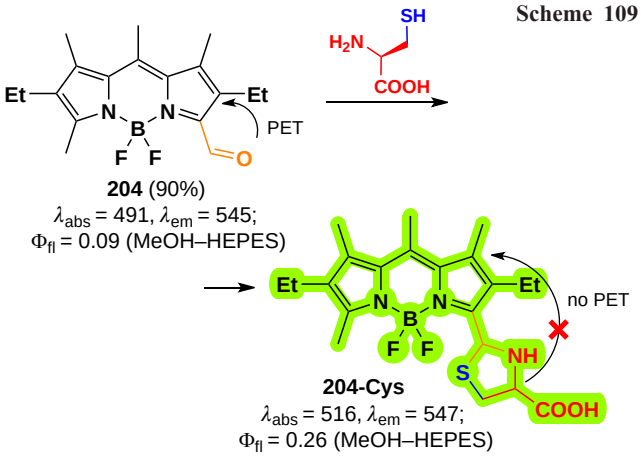

3-acetoxymethyl-BODIPY was obtained through the oxidation *via* lead acetate, followed by the synthesis of BODIPYs **206**–**210** *via* nucleophilic substitution.

Scandium(III) triflate proved to be an optimal catalyst for nucleophilic substitution reactions. The authors investigated the reactivity of 3-methylacetoxy-BODIPY under the action of various O-, N-, S- and C-nucleophiles, yielding >50 BODIPYs as products of nucleophilic substitution. Aliphatic alcohols (BODIPY **206a**) and carboxylic acids were used as O-nucleophiles, while azide and sulfonamide were used as N-nucleophiles yielding BODIPYs **208a**,**b**. C-nucleophiles, including the natural compounds tyrosine and resveratrol, as well as aliphatic and aromatic nucleophiles such as TMSCN (TMS — trimethylsilyl), diethylzinc (**209a**), indole (**209b**), and BODIPY at position 2, were also involved in the reaction. Sequential substitution of the two acetoxy groups in the BODIPY scaffold with different nucleophiles yielded asymmetric nucleophilic substitution products.

3.6. Radical reactions of BODIPY

In 2015, Verbelen *et al.*[263] demonstrated the feasibility of direct radical arylation of the BODIPY core at positions 3 and 5 using diazonium salts and ferrocene as a catalyst, yielding 3-aryl- (**211**) and 3,5-diaryl-BODIPY **212** (Scheme 111). Aryldiazonium salts are well-known sources of aryl radicals formed by homolytic dediazonation. The reactions occurred exclusively at the C(3) and C(5) carbon atoms of BODIPY, since the addition of the radical species at 3-position of one of the pyrrole moiety and subsequent charge delocalization over several double bonds resulted in a stabilized allyl-type radical.

In 2015, the same research group[264] reported the radical alkylation reaction of BODIPY with potassium trifluoroborates and boronic acids, occurring at positions 3, 5, 7, using Mn^{III} acetate as an oxidizing agent. This method allowed to obtain tri- and tetrasubstituted products, as well as unsymmetrical

Scheme 110

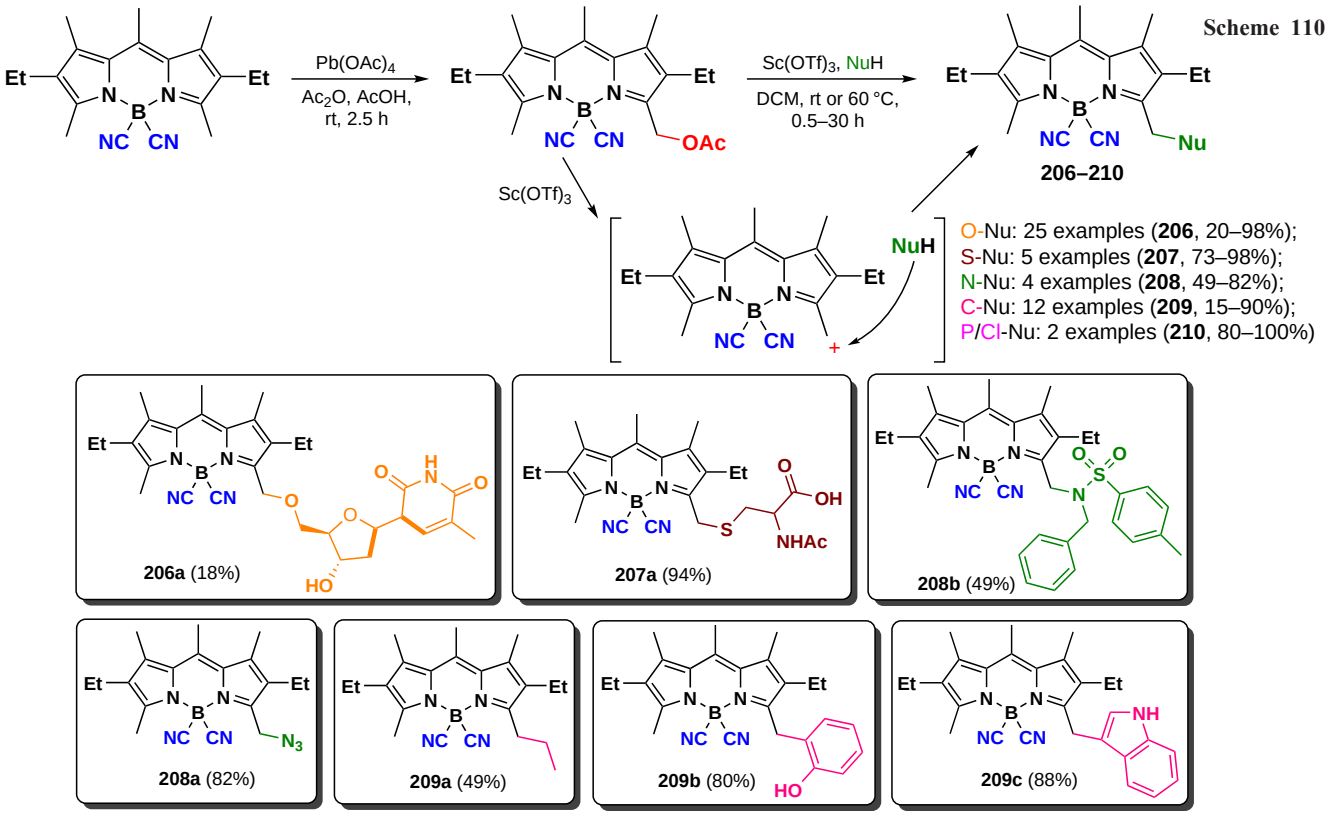

Scheme 111

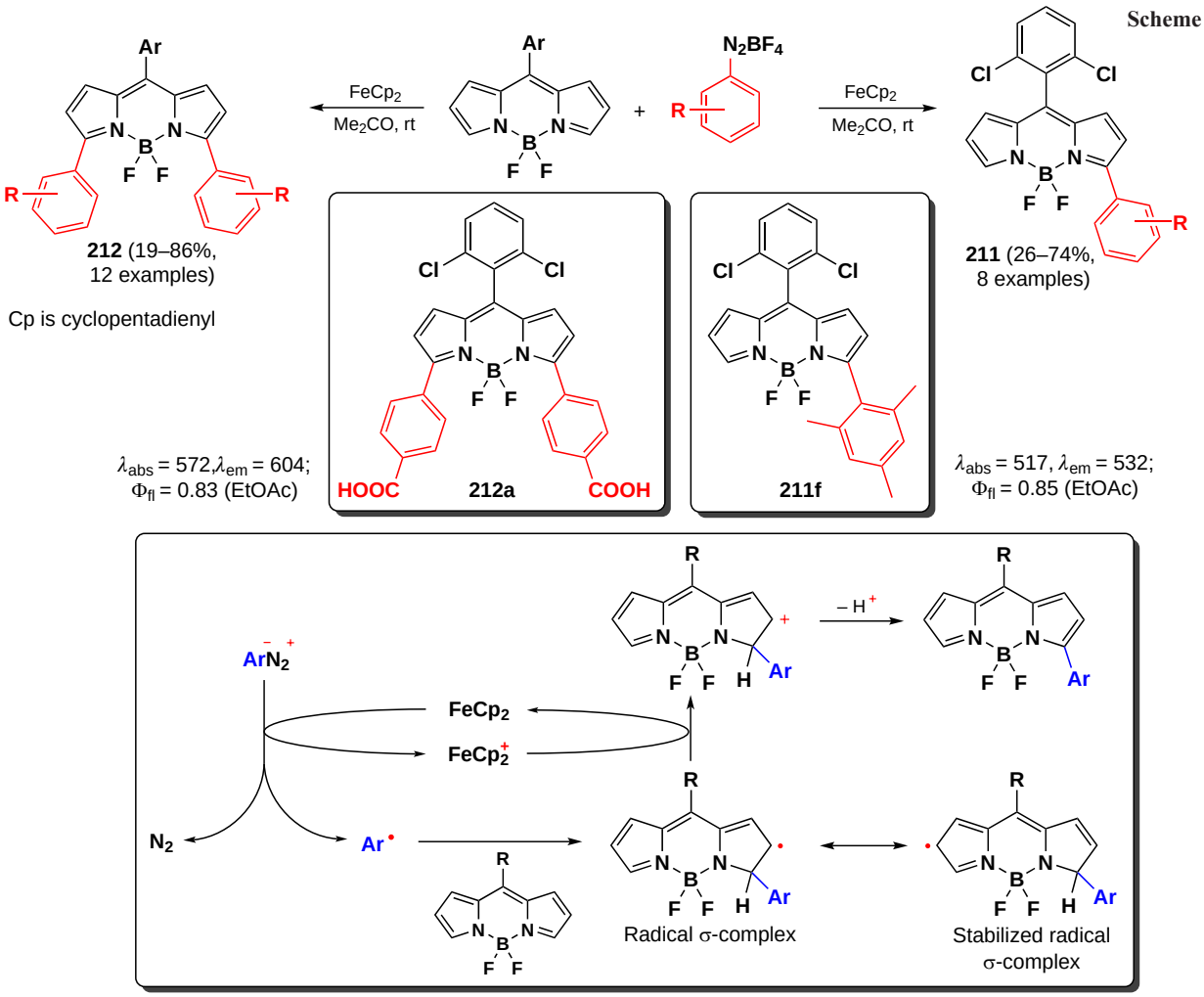

Scheme 112

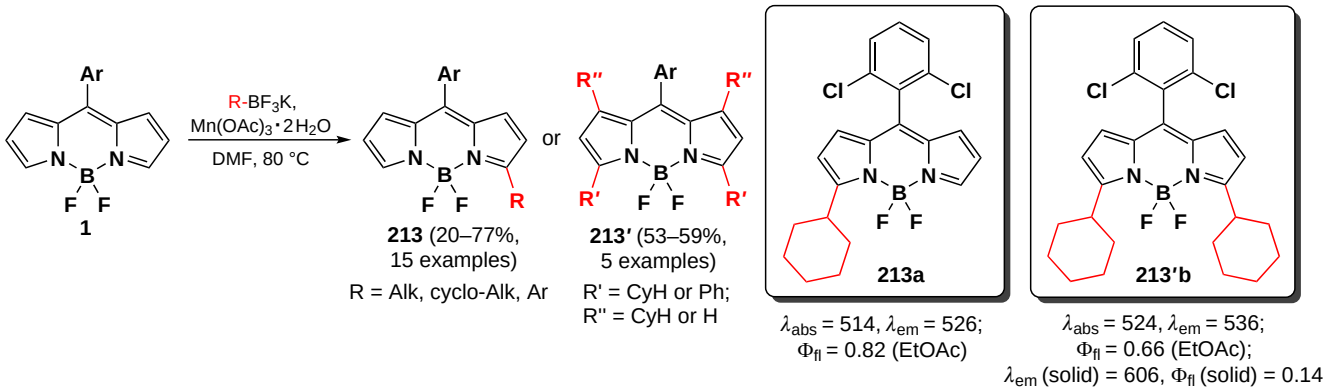

derivatives of BODIPY **213**, by direct CH-alkylation of the BODIPY core (Scheme 112). The introduction of several sterically hindered cycloalkyl groups suppressed the formation of non-fluorescent π–π-aggregates, resulting in solid-state emissive BODIPY with quantum yields up to 0.14 for BODIPY **213b**.

In 2016, Zhou *et al.*[265] proposed a method for radical arylation of BODIPY at positions 3 and 5 using diaryliodonium salts, which provided 3-aryl- (**214**) and 3,5-diaryl derivatives (**215**). The reactions were inhibited in the presence of 2,6-di-*tert*-butyl-4-methylphenol, thereby confirming the presence of free radicals. The proposed mechanism involved the attack of the aryl radical at the α-position to generate radical **A** (Scheme 113), which reacted again with the diaryliodonium salt to form intermediate **B**. An evaluation of the energies of the transition states after the attack of the arynium cation at positions 2 and 3 (routes *a* and *b*) was carried out; the transition state after the attack at position 3 had a lower energy (by 3.3 kcal mol^{-1}), as a result, the product obtained after the attack at position 2, intermediate **C**, was not formed.

In 2017, Boens *et al.*[266] reported the radical alkylation of BODIPY at positions 3 and 5 with allylic alkenes and ethers in the presence of the TBAI–TBHP system. The reactions were inhibited in the presence of BHT and did not proceed at free positions 2 and 6, which excluded the electrophilic nature of the attacking particle. The mechanism proposed by

Scheme 113

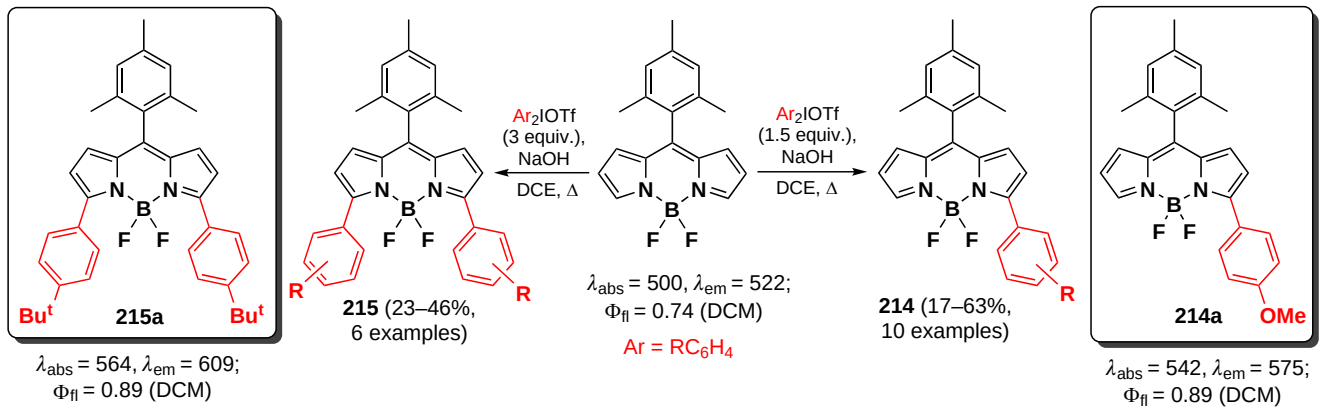

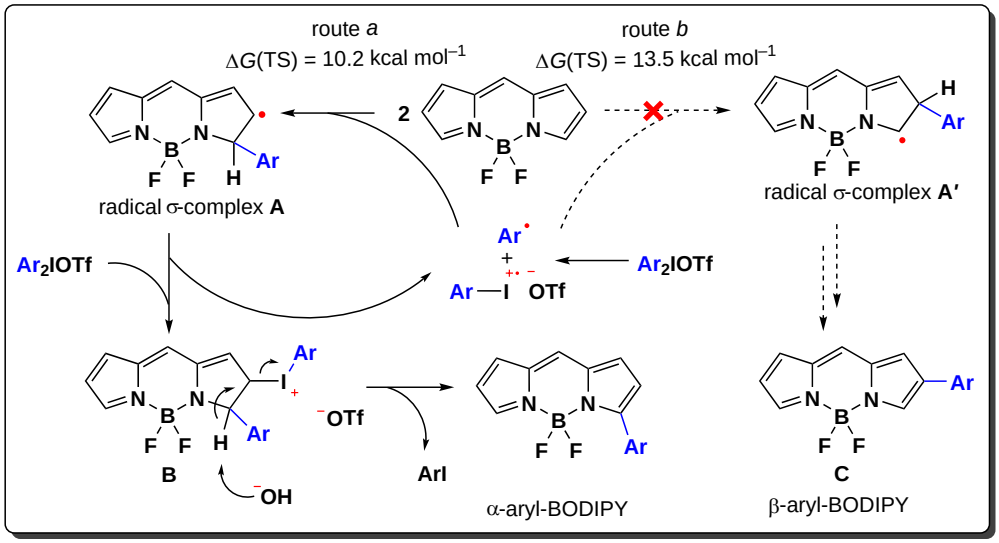

Scheme 114

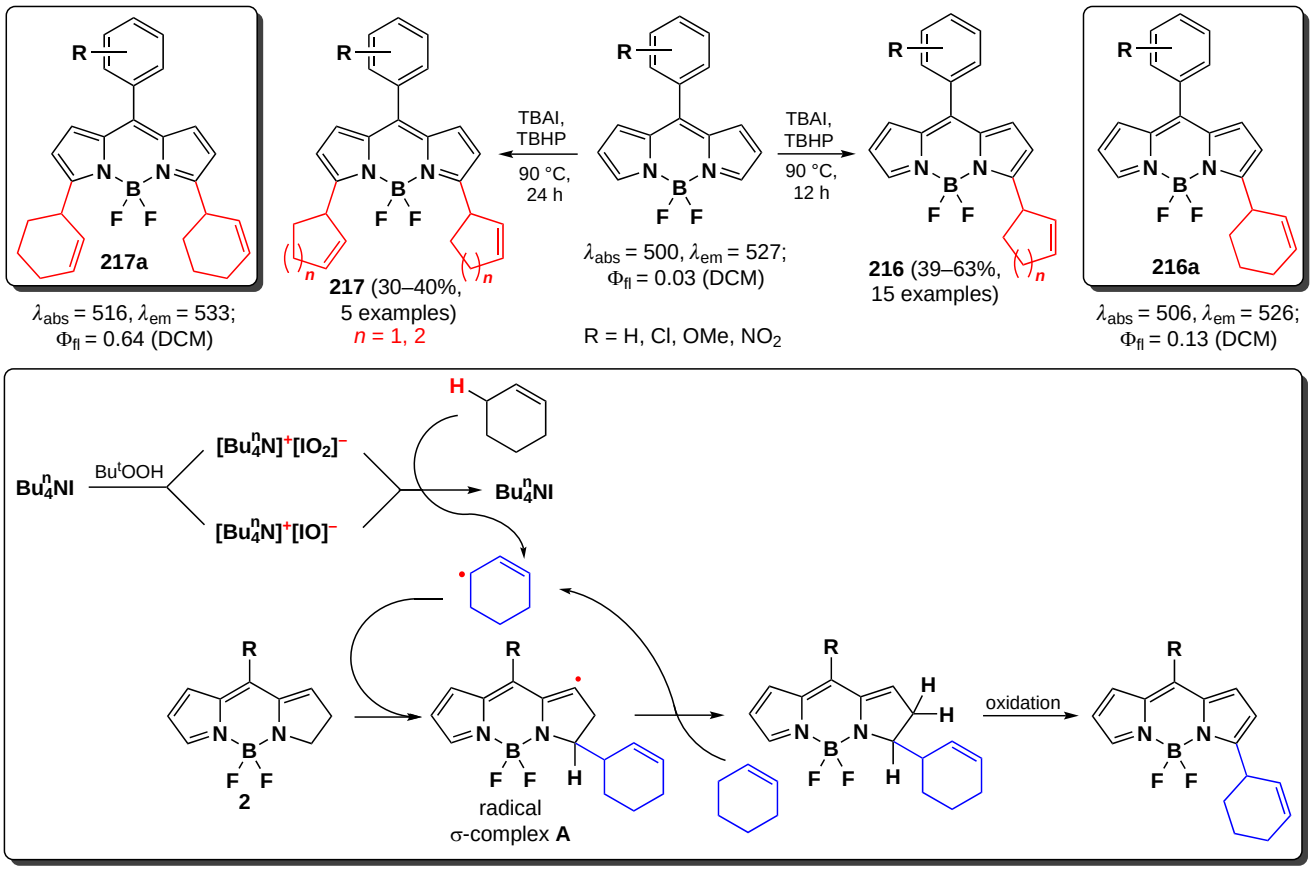

the authors included the formation of an allyl radical as a key intermediate (Scheme 114). For the mono- (**216**) and dialkylated BODIPYs (**217**) obtained, an increase in fluorescence was observed compared to the parent compounds, for example, up to 0.13 and 0.64 for derivatives **216a** and **217a**, respectively.

In 2018, Zhang *et al.*[267] proposed a method for the radical amination of BODIPY at positions 3 and 5 using silver acetate as a catalyst and oxidizer (Scheme 115). The processes were inhibited in the presence of TEMPO and BHT. The mechanism proposed by the authors involved a single electron transfer from Ag^{I} to a secondary amine with generation of an amine radical; this mechanism was confirmed by the formation of a 'silver mirror' during the reaction. A series of synthesized 3,5-diamino-BODIPYs **218**–**220**, in particular **218a**, exhibited high ER specificity together with low cytotoxicity.

In 2019, Lv *et al.*[268] reported radical coupling reactions of BODIPY with thioethers in the presence of *tert*-butylperoxy benzoate (TBPB), which yielded 3- (**221**) and 3,5-dithio-BODIPY (**222**) (Scheme 116). These processes were also inhibited in the presence of TEMPO and BHT, confirming their radical mechanism.

A method for the photocatalyzed coupling of BODIPY with thioethers at positions 3 and 5 was also proposed by Ma *et al.*[269] The authors carried out experiments using thiols with both donor and acceptor substituents, including sterically hindered ones (Scheme 117). For sulfur-containing BODIPYs **223** and **224**, including BODIPYs **223a** and **224a**, a red-shift and fluorescence

Scheme 115

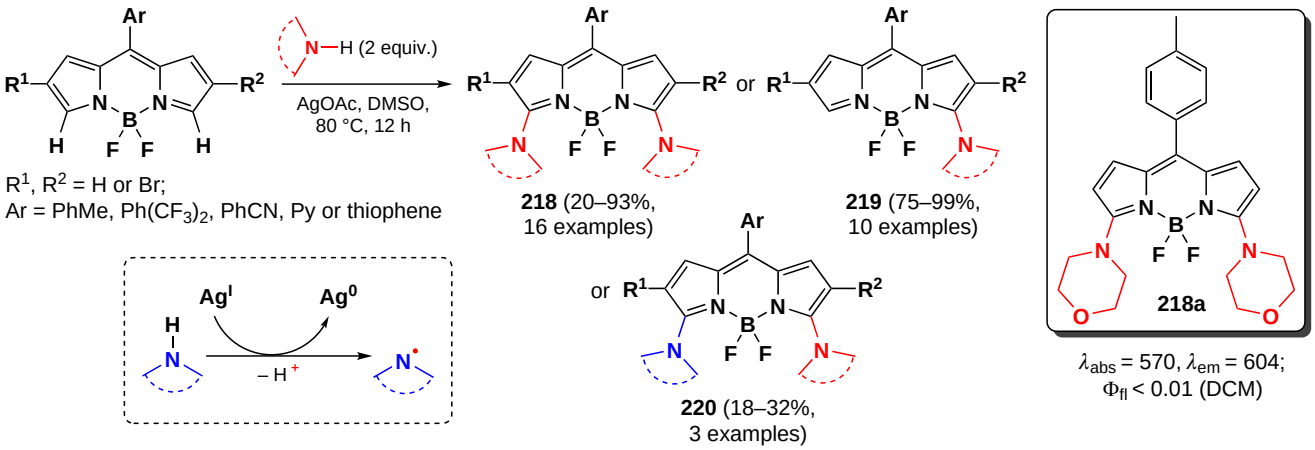

Scheme 116

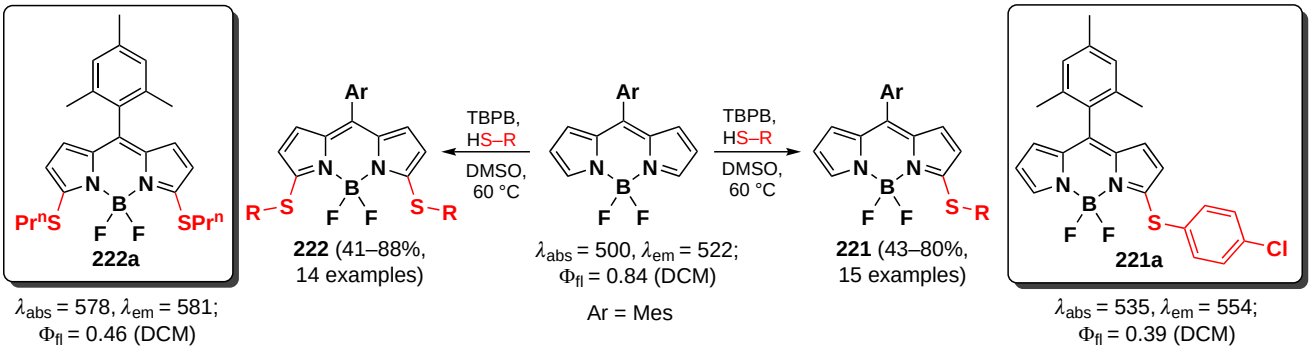

Scheme 117

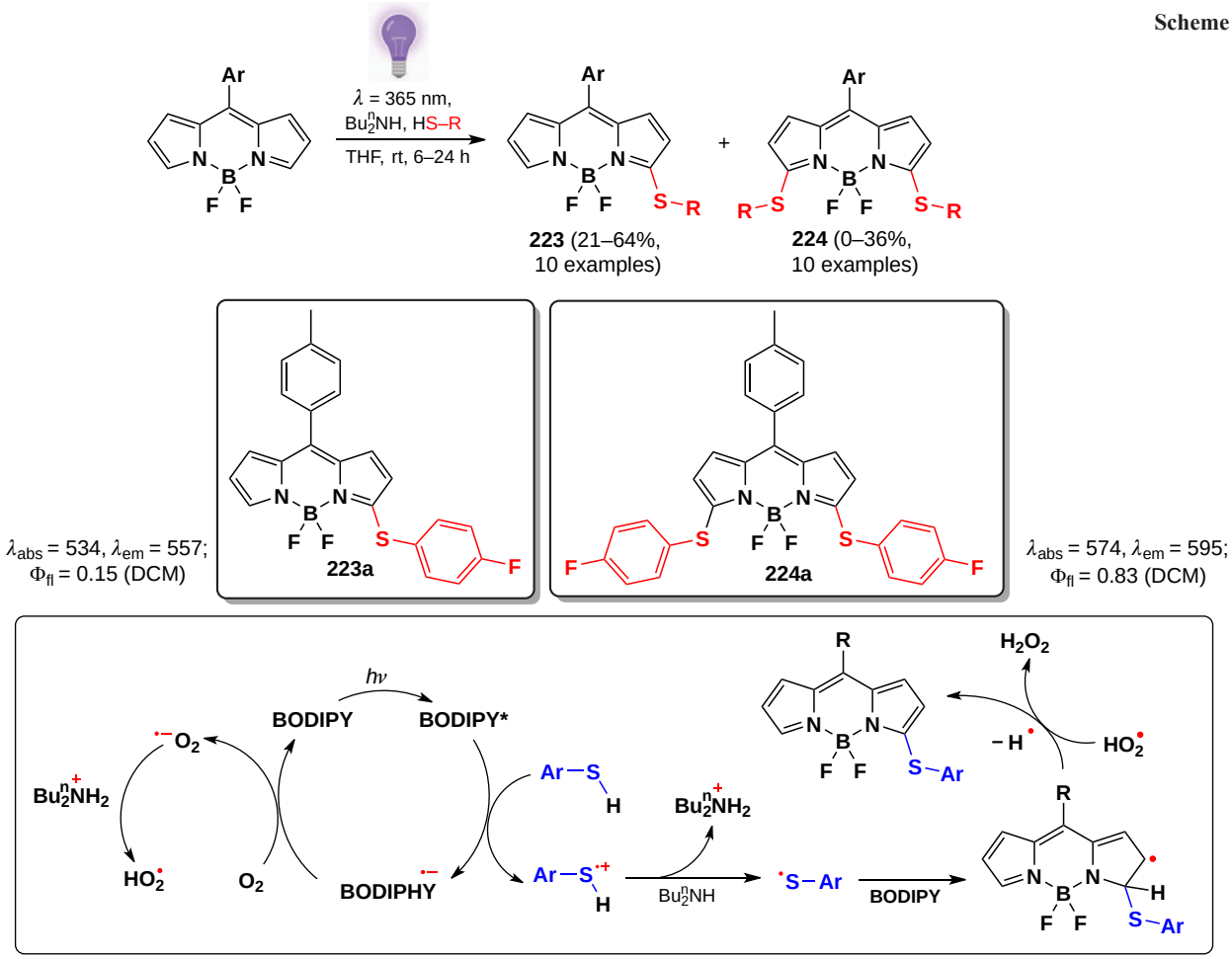

enhancement were observed upon sequential introduction of thiol substituents. The mechanism of the process involved photoexcitation of BODIPY, and then electron transfer from the thiol to the excited BODIPY, which is an oxidizing agent. The radical formed after deprotonation attacked BODIPY at the α-position.

In 2024, Zhang *et al.*[26] developed an electrochemical approach to introduce a tosyl group at the β-position (1,3,5,7) of substituted BODIPY to obtain 2-sulfonyl derivatives **225**. Electrooxidative β-sulfonylation of BODIPY with sulfonylhydrazide did not require the presence of additional oxidizing agents (Scheme 118). Compound **225a** was used for fluorescent staining of the cytoplasm of human hepatocellular carcinoma cells (HepG2).

3.7. Photochemical reactions of BODIPY

3.7.1. BODIPY derivatives as a source of singlet oxygen

In 2011, Jing *et al.*[270] proposed to use BODIPY as photocatalysts for thioanisole oxidation. BODIPYs **226** showed high photocatalytic activity, and the reaction was facilitated by the high polarity of a medium. The mechanism proposed by the authors involved the oxidation of thioanisole by singlet oxygen (Scheme 119).

A year later, the same research group[271] used a heterogeneous catalyst, based on BODIPY, styrene and divinylbenzene, for the photooxidation of sulfides. The catalyst demonstrated high activity, but the reaction proceeded slower compared to the use

Scheme 118

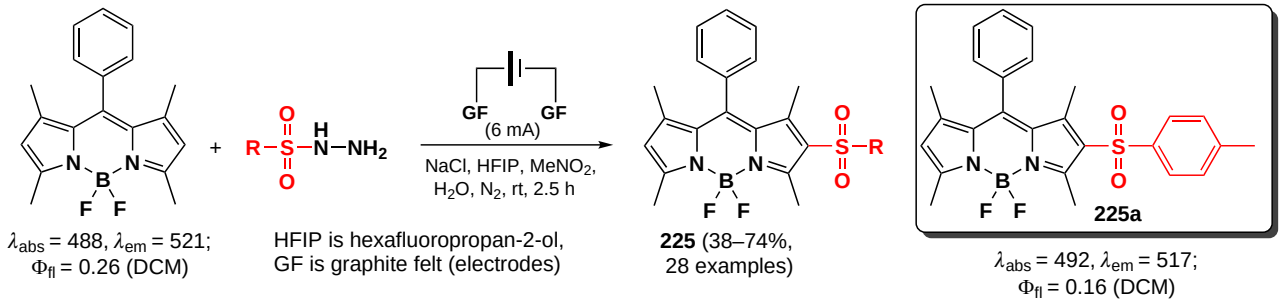

λ_{abs} = 488, λ_{em} = 521; Φ_{fl} = 0.26 (DCM)

HFIP is hexafluoropropan-2-ol, GF is graphite felt (electrodes)

225 (38–74%, 28 examples)

λ_{abs} = 492, λ_{em} = 517; Φ_{fl} = 0.16 (DCM)

Scheme 119

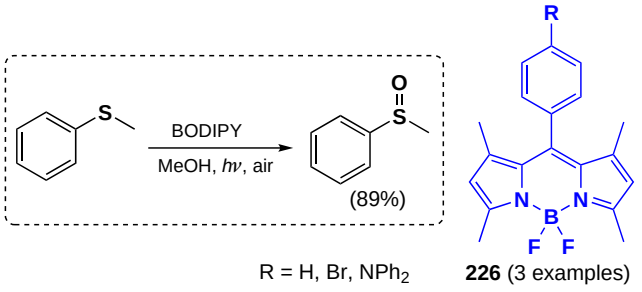

R = H, Br, NPh_2

226 (3 examples)

of a homogeneous catalyst. In 2013, Zhang *et al.*[272] presented dyad PDT agents **227a–c**, capable of resonant energy transfer from the non-iodinated to the iodinated moiety. Spectral studies of the transition state confirmed that the triplet state was shared between the donor and acceptor, since heavy atom-free BODIPYs were not able to populate their triplet states. The authors proposed a 'ping-pong' mechanism of energy transfer, namely, forward singlet energy transfer from the BODIPY-donor to the BODIPY-acceptor (singlet EnT), followed by internal conversion and backward triplet state energy transfer to the BODIPY fragment (triplet EnT). The designed dyads **227a–c** acted as triplet photosensitizers, for example, for the photooxidation of 1,5-dihydronaphthalene.

In 2013, Ma *et al.*[223] used iodinated BODIPY **228a** for the aerobic photocatalysis of two reactions: the oxidative coupling of amines with imine formation, and the photooxidation of dihydroxynaphthalenes followed by one-pot functionalization of 1,4-naphthoquinones to produce *N*-aryl-2-amino-1,4-naphthoquinones (Scheme 120). The transformations occurred for amines containing protons at the α-position. A one-pot reaction of photooxidation of dihydronaphthalenes followed by 1,4-coupling of aromatic amines was also carried out. An EPR study in the presence of 2,2,6,6-tetramethylpiperidine (TEMP) and 5,5-dimethyl-1-pyrroline-*N*-oxide (DMPO), which are 'traps' for singlet oxygen and the oxygen anion radical, revealed the participation of $^1O_2$ in the catalytic cycle. The mechanism of oxidative coupling of amines proposed by the authors was the generation of singlet oxygen by the triplet state of BODIPY **228a**, oxidation of amines to the corresponding imines, and nucleophilic attack of the free amine on the imine carbon atom (see Scheme 120).[223]

3.7.2. Photoexcited BODIPYs as oxidizing or reducing agents

In 2013, Huang and Zhao[273] investigated three redox processes photocatalyzed by BODIPY:

— the Aza-Henry reaction with tetrahydroisoquinoline and the addition of enolate anions;

Structures 227

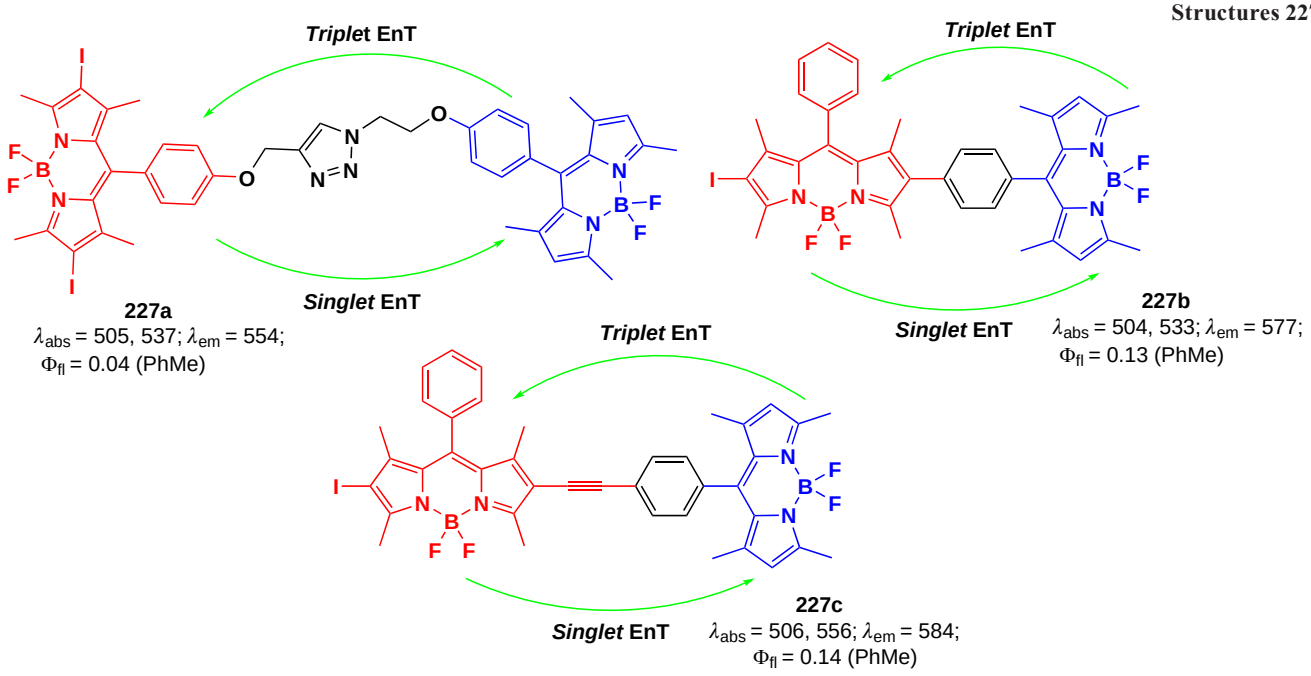

227a
λ_{abs} = 505, 537; λ_{em} = 554; Φ_{fl} = 0.04 (PhMe)

227b
λ_{abs} = 504, 533; λ_{em} = 577; Φ_{fl} = 0.13 (PhMe)

227c
λ_{abs} = 506, 556; λ_{em} = 584; Φ_{fl} = 0.14 (PhMe)

Scheme 120

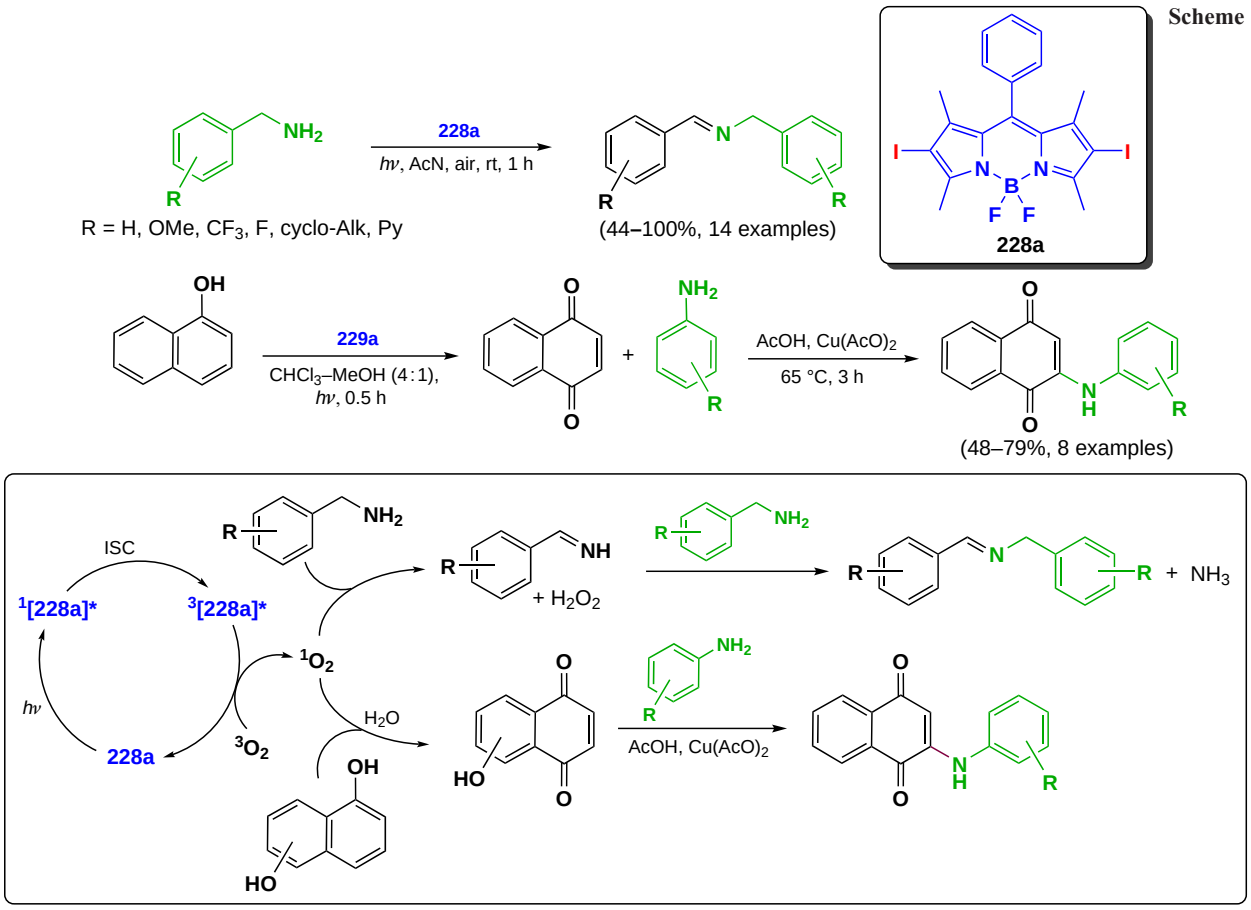

— tandem oxidation/[3+2]-cycloaddition/oxidative aromatization reactions with tetrahydroisoquinolines and maleimides;

— C–H arylation of heteroarenes with diazonium salts.

In all cases, 2,6-diiodo-BODIPY **228a** or **228b** served as photocatalysts (Schemes 121, 122).

The reaction mechanism proposed by the authors involved a single-electron transfer from the amine to BODIPY **228a** or **228b** leading to the formation of an amine radical cation and a BODIPY anion radical, which is an oxidizing agent in its triplet excited state. Oxidation of the amine cation radical resulted in the formation of an iminium cation that reacted with a nucleophile. At the same time, the anion radical of BODIPY **228a** or **228b** reacted with oxygen to form a superoxide radical ($O_2^{-\bullet}$), which was the oxidizing agent in the reaction with the amine cation radical.

The presence of H_2O_2 in the reaction mixture was confirmed by ^{1}H nmR. When BODIPY **228b** was irradiated in the presence of TEMP, the TEMP-$^1O_2$ adduct was detected, which disappeared completely on addition of the amine substrate, confirming the proposed mechanism.

A photocatalytic tandem [3+2]-cycloaddition/oxidation reaction with the *N*-substituted maleimide as a substrate was also carried out to give pyrrolo[2,1-*a*]isoquinolines. The photocatalytic C–H arylation of heterocycles using diazonium salts, in which BODIPY **228a** or **228b** served as a reducing agent, was also studied. Single-electron transfer from the photocatalyst to the diazonium salt led to the formation of an aryl radical; addition of the aryl radical to the heterocycle formed a radical intermediate. As a result of electron transfer from the radical, a carbocation was formed; and deprotonation of the carbocation led to the arylation product of the heterocycle (Scheme 123). Furthermore, the intermediate aryl radical was intercepted by TEMPO, which confirmed the mechanism proposed by the authors.

Similarly, iodinated BODIPY **229** immobilized on molecular sieves was used to obtain pyrrolo[2,1-*a*]isoquinoline *via* tandem oxidation and [3+2]-cycloaddition (Scheme 124).[274]

In 2014, Guo *et al.*[275] reported an alkynylation of tetrahydroisoquinoline in the presence of copper(I), photocatalyzed by triad **230**, based on two BODIPY moieties conjugated with the 2,7-diiodo-BODIPY core *via* a triazole linker (Scheme 125). The triad (**230**) exhibited broadband absorption in the range of 400–750 nm and a high quantum yield of singlet oxygen, thus indicating efficient ISC. Triad **230** was found to be more efficient photocatalyst than the monochromophoric 2,6-diiodo-aza-BODIPY.

In 2015, Wu *et al.*[276] showed that a stable triplet state of BODIPY was not necessary for photocatalysis. Thus, BODIPY **231**, irradiated with white light and free of heavy atoms, catalyzed the formation of C–C and C–P bonds in reactions with *N*-phenyltetrahydroisoquinoline *via* the formation of a reactive iminium cation. The active form of oxygen in the reactions was proven to be the superoxide anion radical ($O_2^{-\bullet}$). The proposed mechanism was based on the fact that BODIPY **231** in the singlet excited state was an oxidizer and promoted the formation of an amine cation radical, the subsequent oxidation led to the formation of an iminium cation, which reacted with the nucleophile. The photocatalytic conditions were used in reactions with nitroalkanes, phosphonium esters, and also with diethyl and dimethyl malonates (Scheme 126).

In 2019, Vairaprakash *et al.*[277] used the 5-hydroxymethylfurfural BODIPY **232**, immobilized on a polymer resin, as a catalyst for the arylation of (het)arenes with aryldiazonium salts (Scheme 127).

Scheme 121

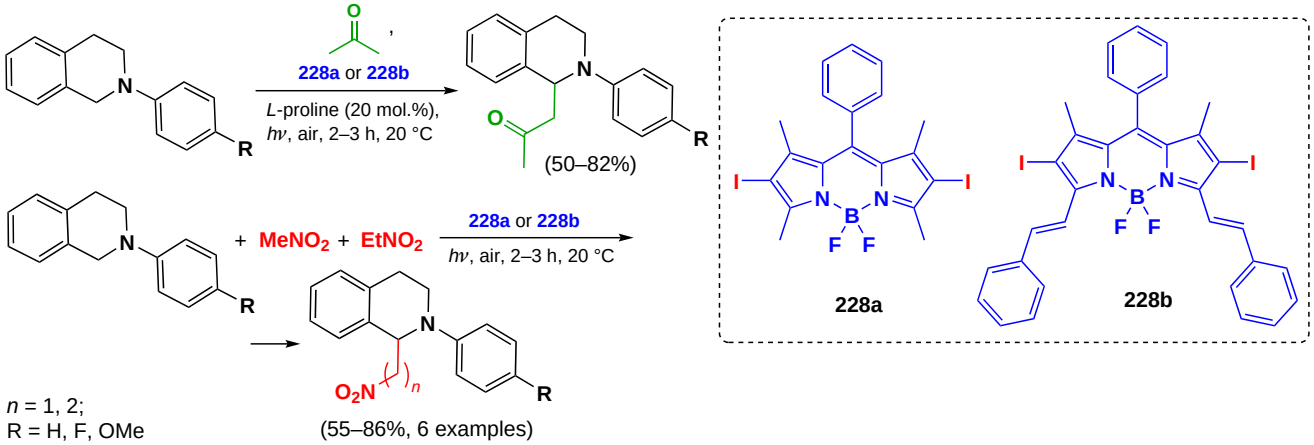

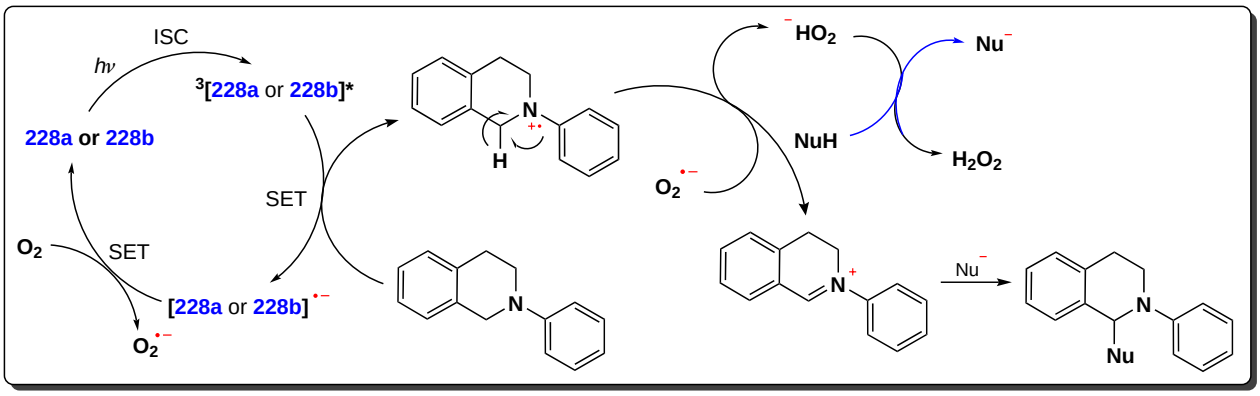

Scheme 122

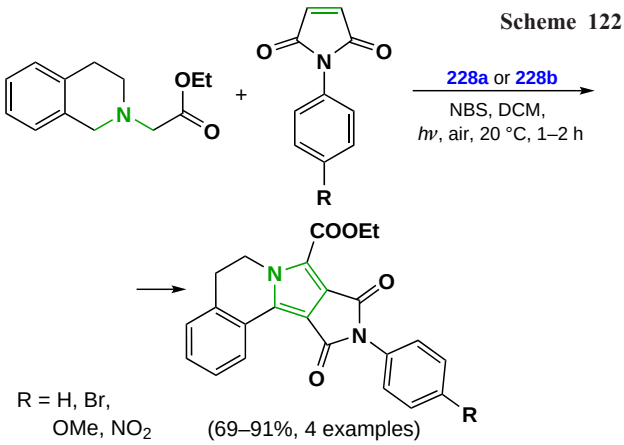

Scheme 123

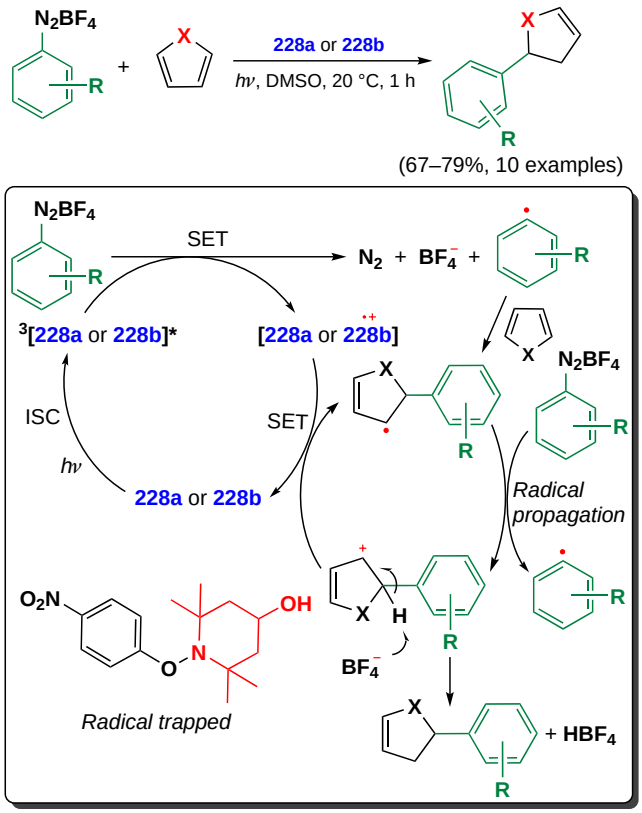

In 2022, Li *et al.*[29] used BODIPY for the photocatalysis of the Beckmann rearrangement. Oximes were readily oxidized to cation radicals by thiomethyl BODIPY **16b** in a triplet excited state, followed by rearrangement into amides. A hydrolysis of oximes with a formation of carbonyl compounds also exhibited high yields under photocatalytic conditions (Scheme 128).

Oxygen anion radical, but not singlet oxygen, was found to be involved in the catalytic cycle, as confirmed by the use of TEMP and DMPO scavengers (Scheme 129). The proposed mechanism involved the formation of an oxime cation radical by reaction with BODIPY **16b** in the triplet excited state; a reaction of the oxime cation with water led to radical formation. The Beckmann rearrangement with the formation of *N*-phenylacetamide took place according to path *A*; an alternative reaction path (*B*) *via* 1,3-transfer of a hydrogen atom ([1,3]-HAT) led to the formation of acetophenone.

Scheme 124

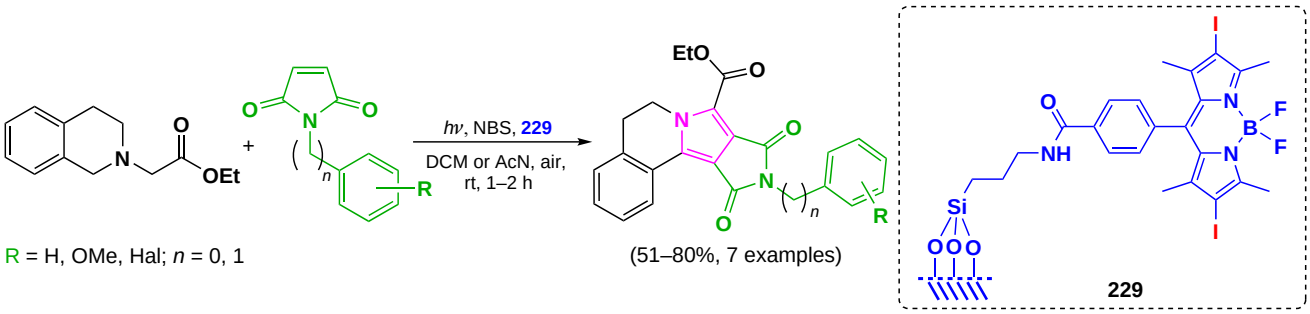

Scheme 125

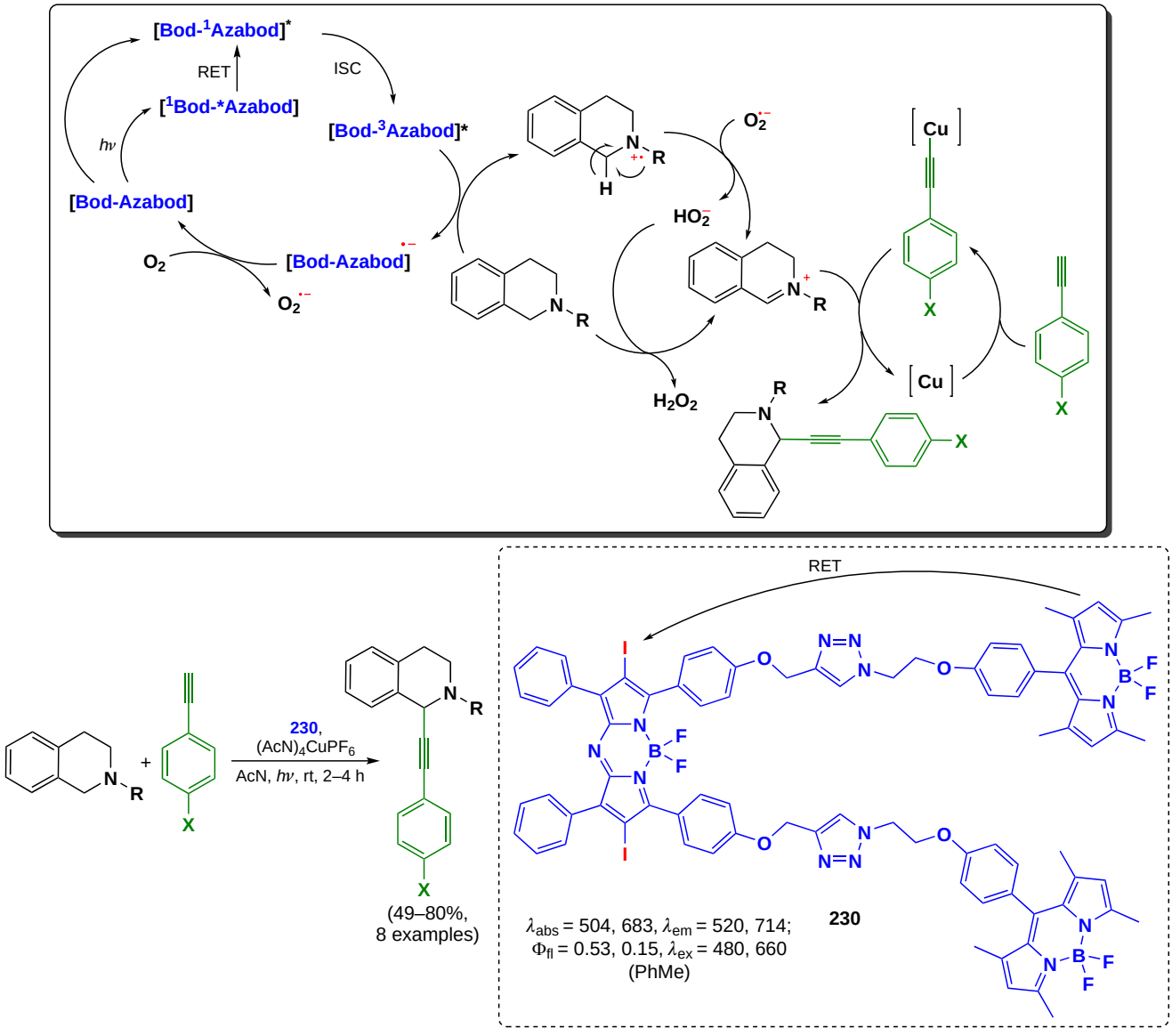

3.7.3. BODIPY catalysis of ion-radical addition to a double bond

The above-described applications of BODIPYs in photocatalytic reactions were limited to singlet oxygen generation or energy transfer. In 2017, Cozzi *et al.*[278] proposed an alternative application of BODIPY as a photocatalysts. Iodosubstituted BODIPY **228a** was found to be an efficient photocatalyst for the radical addition with atom transfer involving bromoalkanes and alkenes. The mechanism of the process involved the formation of the BODIPY anion radical by a triplet state reaction with sodium ascorbate. The anion radical acted as a reducing agent toward haloalkane, leading to the formation of a free radical that was directly involved in the addition (Scheme 130).

In 2021, Cordero-Vargas *et al.*[279] investigated the photocatalyzed ion-radical addition of α-halocarbonyl compounds to vinyl ethers in the presence of 2,6-dibromo-BODIPY **233**. Using this approach, lactones, protected

Scheme 126

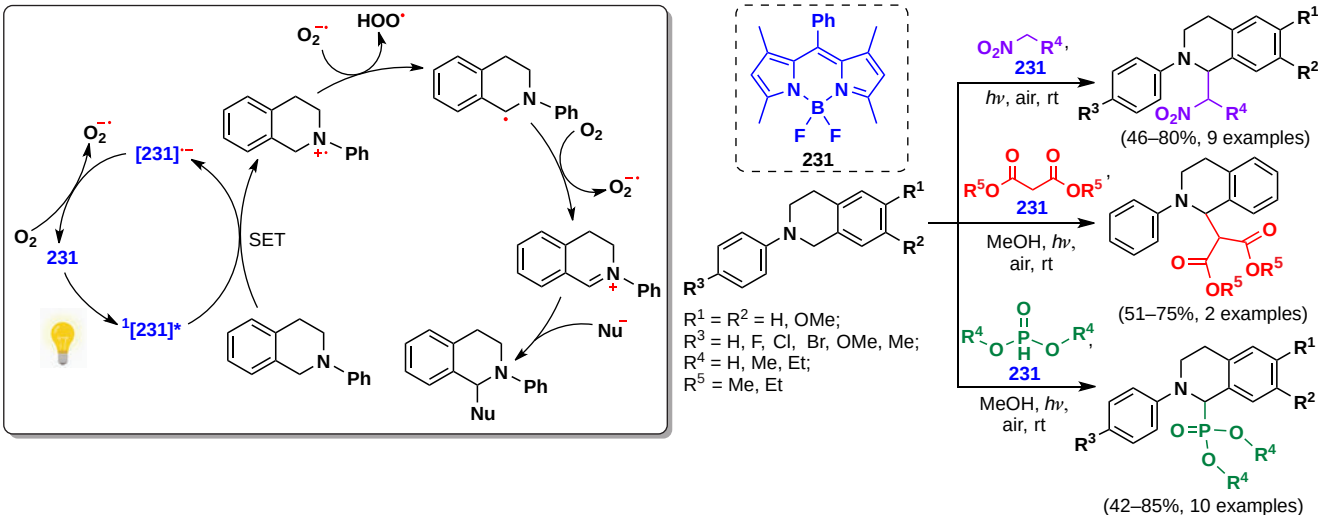

Scheme 127

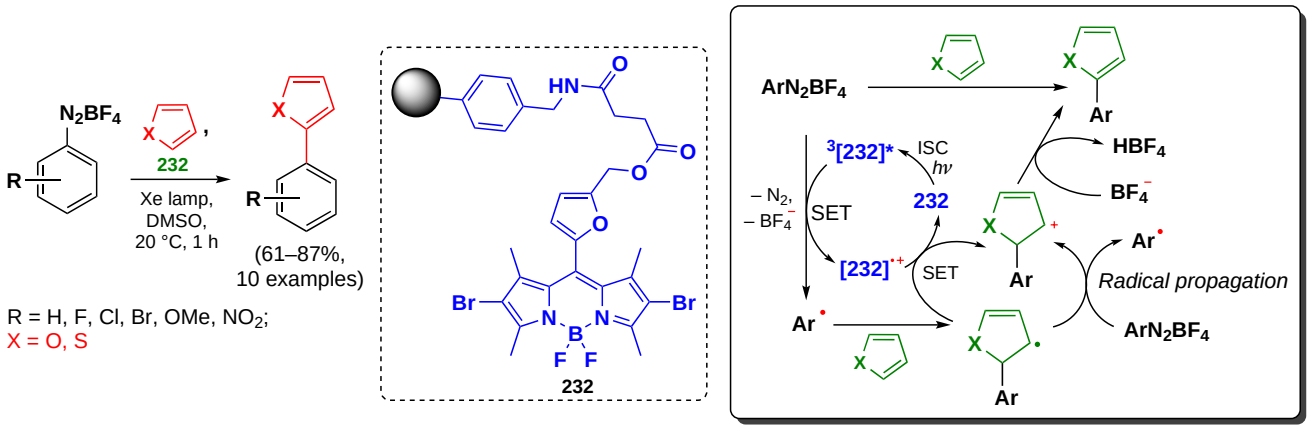

Scheme 128

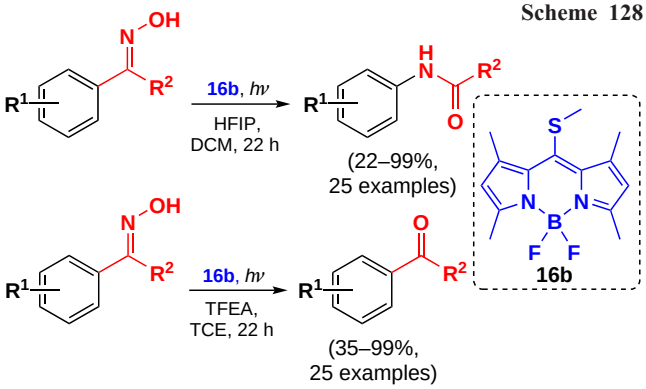

TFEA is 2,2,2-trifluoroethanol, TCE is 1,1,2-trichloroethane

aldehydes, tetrahydroquinolines, dihydrofurans were synthesized (Scheme 131).

According to the proposed mechanism, BODIPY **233** in the excited state was reduced by DIPEA with anion-radical formation, which upon oxidation by the α-haloketone formed radical **B**. The reaction of a radical **B** with an alkene resulted in the formation of a secondary radical **C**, followed by the formation of the radical oxonium cation **E**; the reaction of a nucleophile with **E** lead to the formation of the product (Scheme 132).

In 2021, Esipova *et al.*[28] used meso-anthracene-substituted BODIPY **234a**,**b** dyad as a photocatalyst for the ion-radical addition of bromomalonate to alkenes. The photocatalytic mechanism was based on the excitation of the anthracene fragment (Ant) followed by energy transfer to BODIPY with the formation of a charge-separated state (CS). During spin-orbit charge-transfer intersystem crossing (SOCT-ICT), the photocatalyst transitioned to the triplet excited state, and was then reduced by sodium ascorbate with the formation of an anion radical. Thus, heavy-atom free BODIPY acquires the ability to form triplet states when it is part of a dyad. In the triplet state, BODIPY is an oxidizing agent (Scheme 133).

3.8. Synthesis of BODIPY dimers and oligomers

Various BODIPY dimers and oligomers have attracted the attention of researchers because the interaction between conjugated chromophores significantly affects the photophysical properties of the conjugates, thus allowing the design of materials for various practical applications (Fig. 25). Thus, α,α- and β,β-dimers based on coplanar BODIPY subunits are near-infrared dyes with extended π-conjugation. Orthogonally linked dimers (α,*meso*-, β,*meso*-, β,*meso*-, γ,*meso*- and α,γ-dimers) and oligomers exhibit exciton interactions between BODIPY subunits with effective ISC and are potential ‘heavy atom free’

Scheme 129

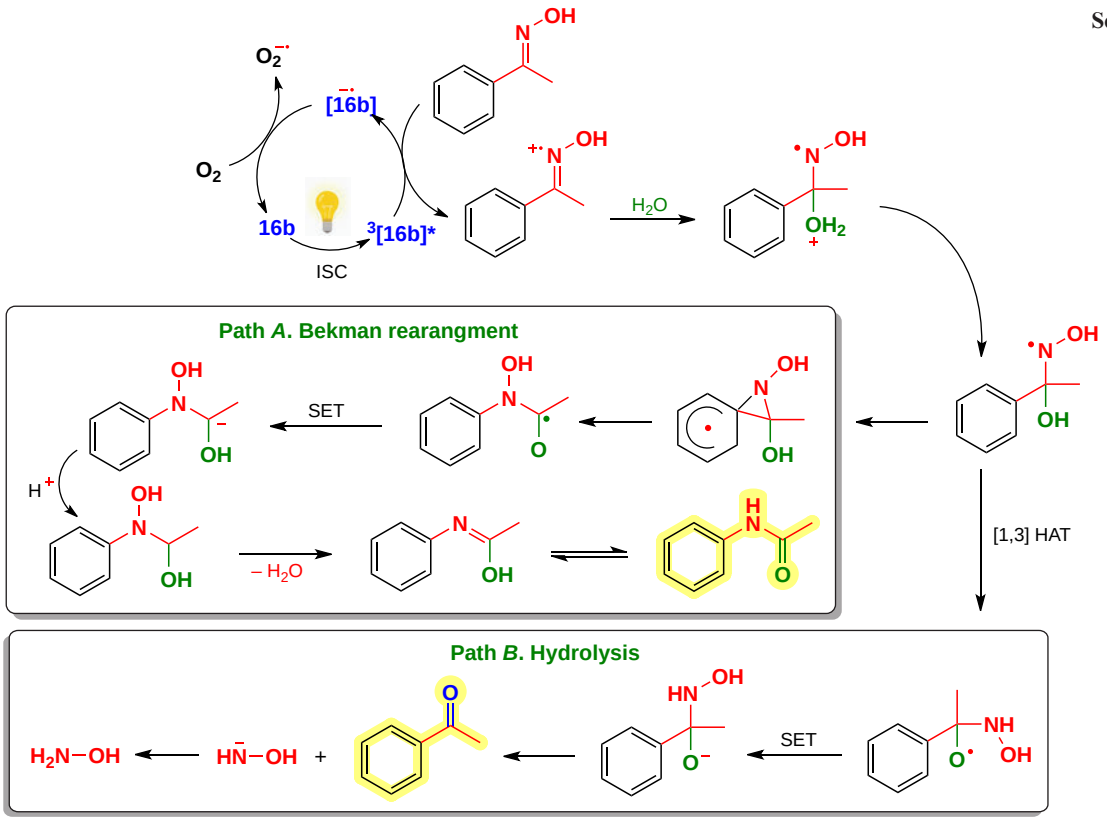

Scheme 130

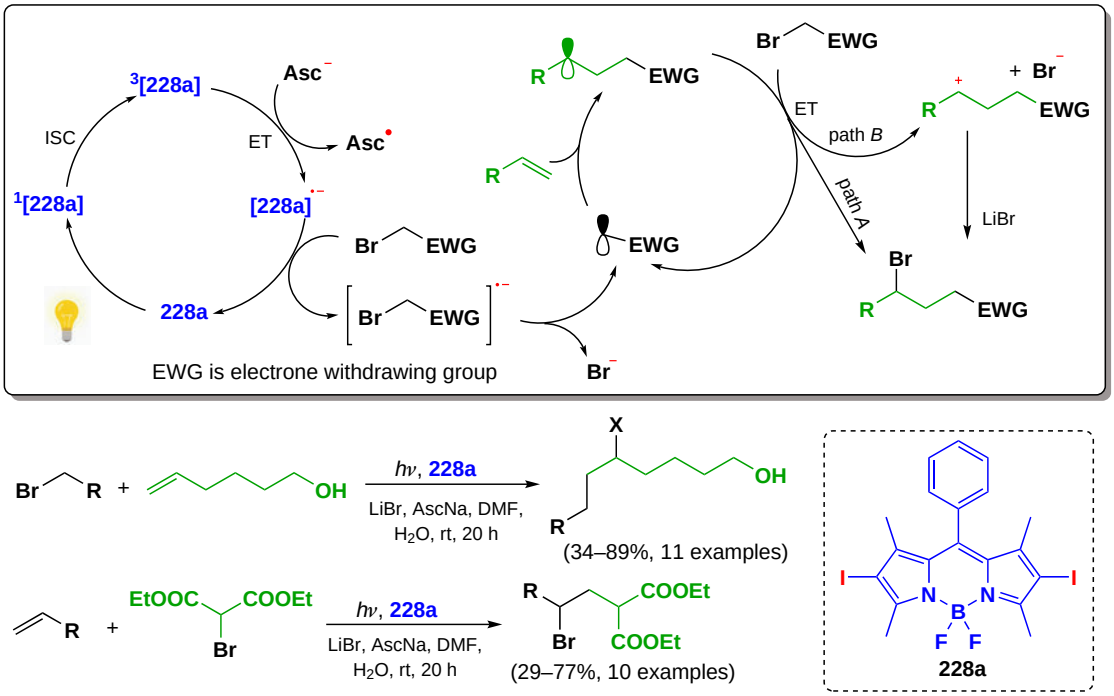

photosensitizers. Exciton interactions between chromophore units lead to the removal of the degeneracy of the S_1 state in α,α-dimers of BODIPY and the occupancy of their triplet state. At the same time, no exciton splitting is observed in orthogonal dimers in which two π-systems of BODIPY are located at an angle of 90°; however, such dimers are able to form stable triplet states, which allows us to consider them as promising PDT agents.

3.8.1. α,α-Dimers and -oligomers

In 2008, Bröring *et al.*[280] synthesized two series of BODIPY α,α-dimers with high fluorescence quantum yields and large Stokes shifts. 8-Unsubstituted α,α-dimers **235a**,**b** were prepared from tetrapyrroles by the reaction with boron trifluoride etherate in the presence of 2,6-lutidine. 8-Aryl dimers **236a**,**b** were synthesized by acylation of dipyrrole followed by condensation with 2,4-dimethylpyrrole

Scheme 131

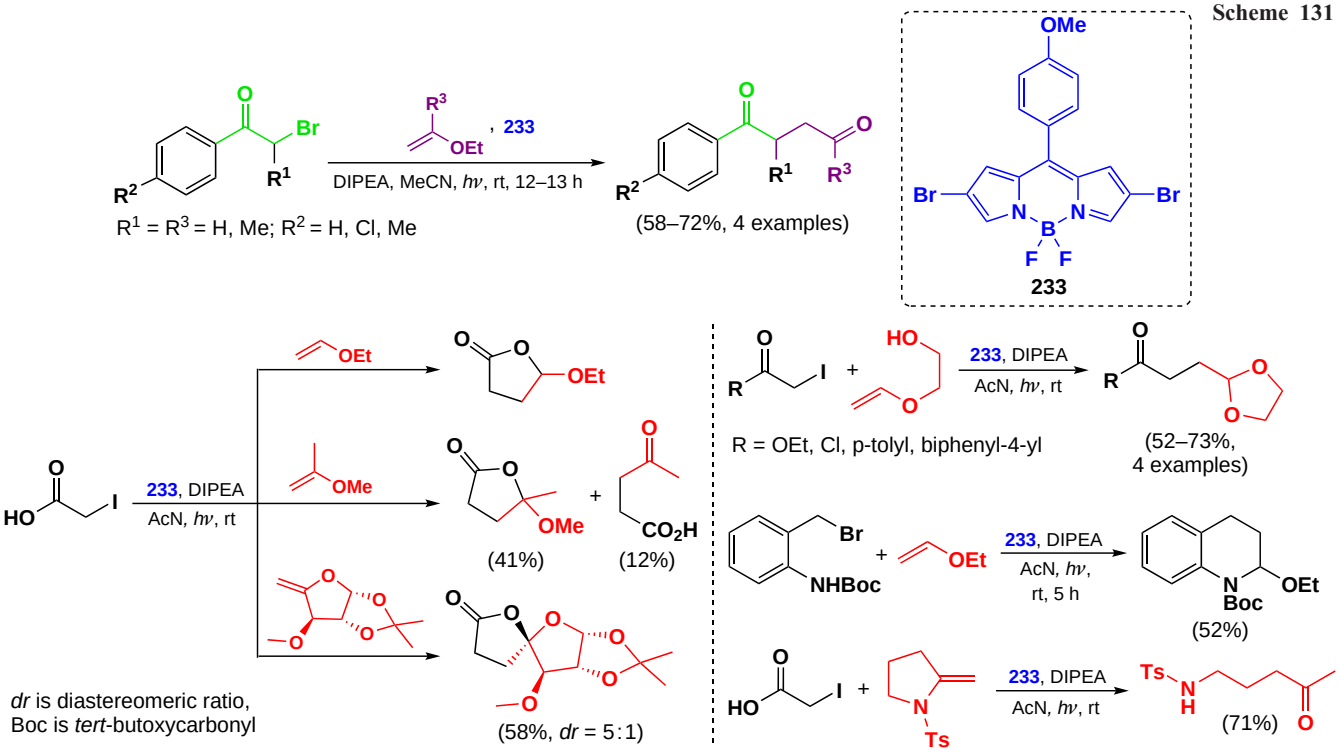

Scheme 132

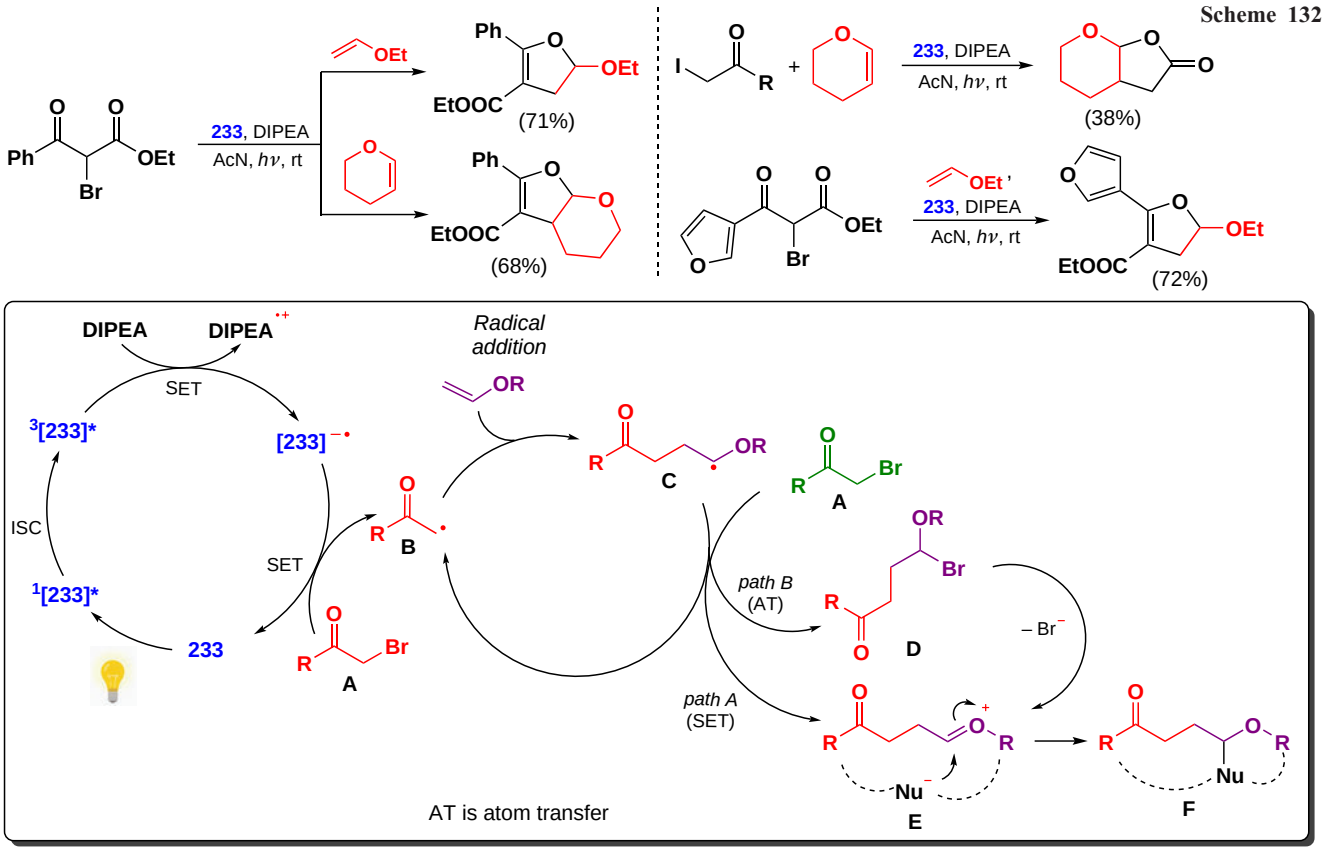

(Scheme 134). X-ray crystallography data of dimer **236b** indicate that the BODIPY subunits are arranged relative at an angle of 96.52° to each other. In addition, each BODIPY fragment contains fluorine atoms, which point «inward» and are 2.968 Å apart. The presence of two pairs of magnetically non-equivalent fluorine atoms observed in the ^{19}F nmR spectrum at –140 and –147 m.d., is consistent with the proposed structure. Dimers **235** and **236** have stable fixed structure and are not prone to aggregation.

Two absorption maxima were observed in the ranges 558–565 nm and 489–494 nm, indicating exciton splitting of excited states. Hypsochromic shifts of the absorption and emission maxima and an increase in Stokes shifts compared to those for the monomers were also detected. The decrease in the

Scheme 133

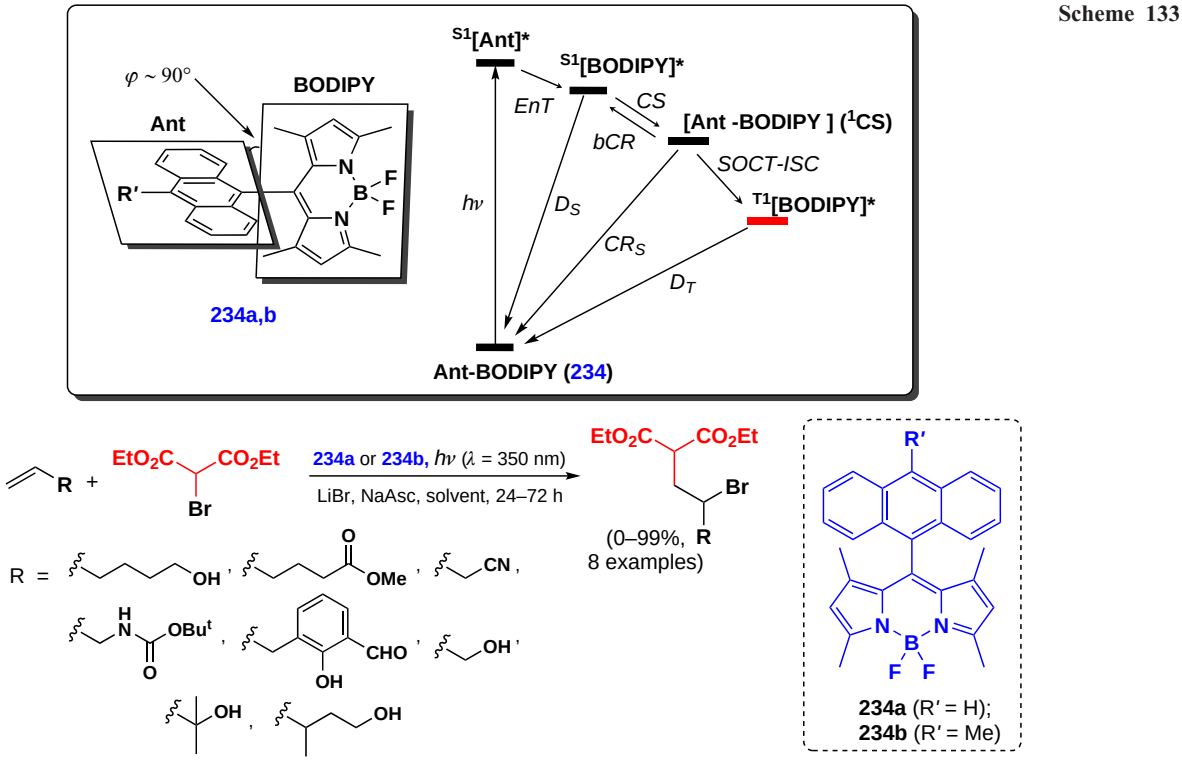

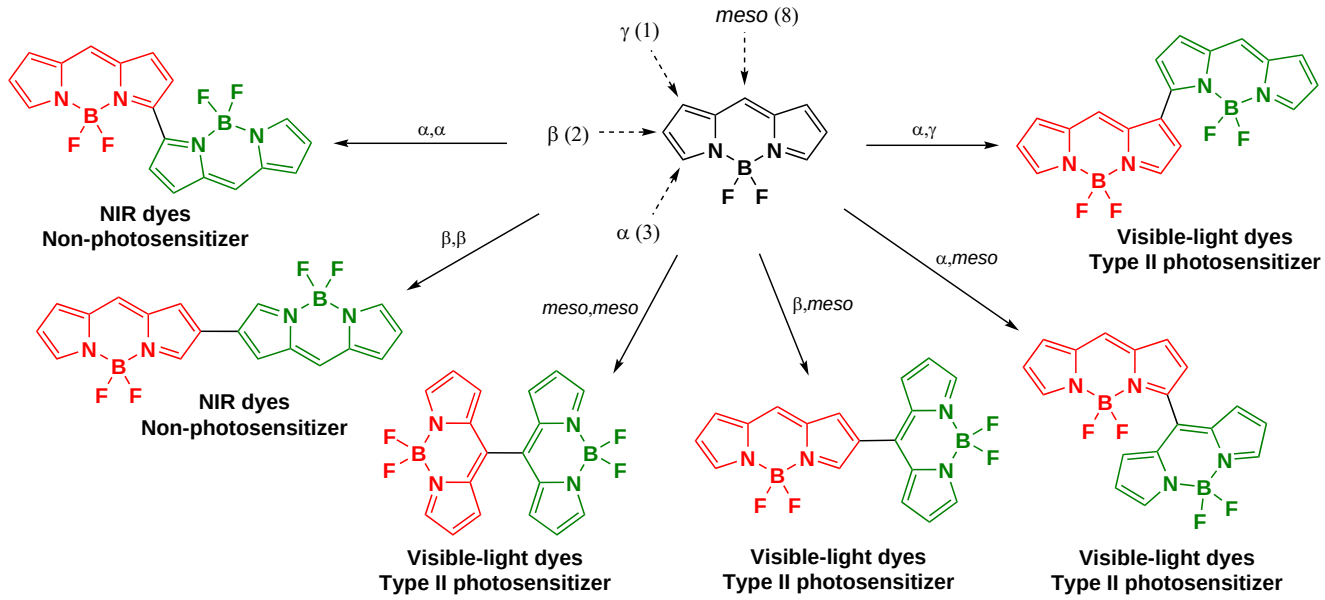

Figure 25. BODIPY dimer types and their photochemical properties.

fluorescence quantum yields of **235**, **236** dimers to 0.67–0.76 when compared to those for monomers indicats an increase in the efficiency of intercombination conversion.

In 2011, Nepomnyashchii *et al.*[214] proposed a method for the synthesis of α,α-dimers from 3,8-unsubstituted BODIPY in oxidative conditions (Scheme 135). For dimer **237**, an exciton coupling with three absorption maxima at 387, 489, and 562 nm was observed. In addition, a higher Stokes shift (88 nm) when compared to parent BODIPY (13 nm) was shown. The decrease in the fluorescence quantum yield of dimer **237** compared to parent BODIPY is due to the increased contribution of intercombination conversion.

In 2014, Bruhn *et al.*[281] reported the synthesis of α,α-dimer of BODIPY **238** *via* oxidative homocombination in the presence of $FeCl_3$, and γ,γ-dimer **239** *via* oxidation of the corresponding 1,2,3,5,6-pentaalkyl derivative under the action of DDQ) (Scheme 136).

The presence of methyl substituents in the β-positions of BODIPY prevented the rotation around the C–C bond; as a result, the obtained dimers **238** and **239** were a racemic mixture of two configurationally stable aptoisomers. For α,α-dimer **238**, the isomer **238-M1** with a negative compartment in the CD spectrum and **238-P1** with a positive compartment were identified by measuring circular dichroism (CD) spectra. The theoretically calculated spectrum using density functional theory (TDCAM-B3LYP) and the exciton chirality method (ECM) agreed with the experimental data. The intensity of the CD spectrum of γ,γ-dimer **239** was 5-fold lower than that of dimer

Scheme 134

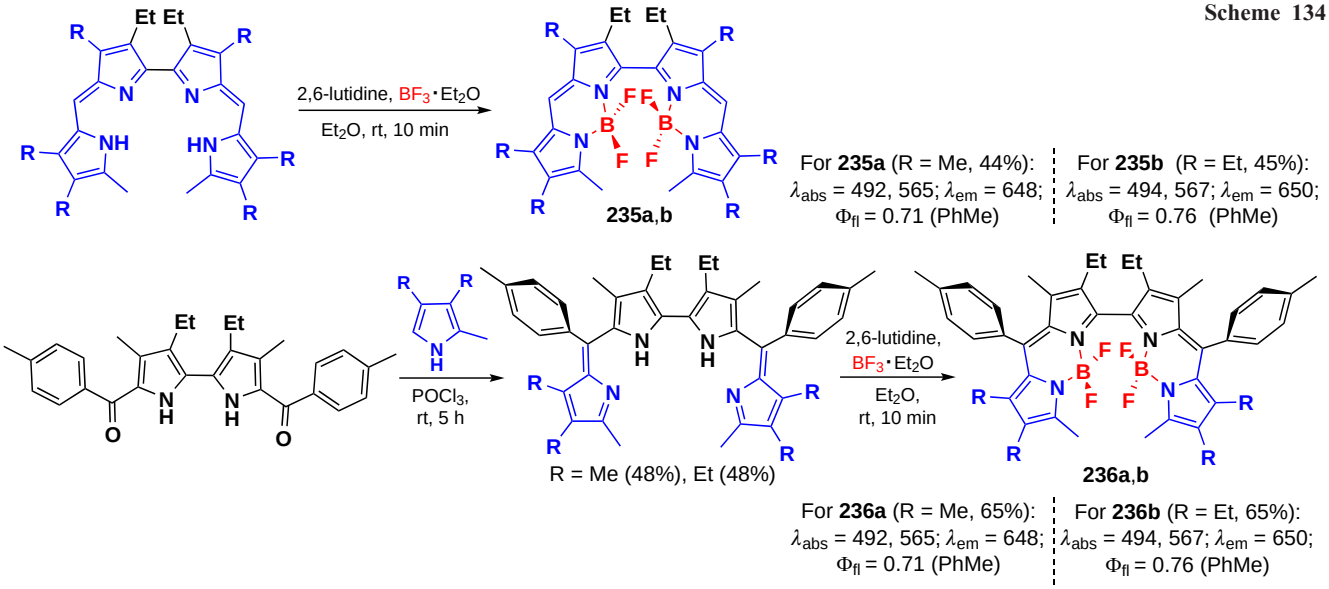

Scheme 135

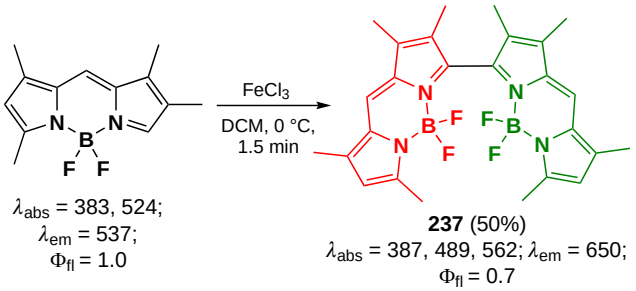

238, and the theoretical calculation (TDCAM-B3LYP) of the CD spectrum for the M-enantiomer predicted a positive couplet, which contradicted the ECM results, which expected a negative couplet for the M-enantiomer. Additional calculations and vibrational circular dichroism measurements confirmed that for γ,γ-dimers of BODIPY the exciton chirality method could not correctly predict their absolute configuration.

In 2020, Wang *et al.*[282] proposed a photochemical method to synthesize α,α- (**240**) and α,γ-dimers of BODIPY (**241**) under mild conditions *via* controlled dimerization in the presence of silver trifluoroacetate. Reduction of the oxidative potential of BODIPY in the excited state promoted the metal-induced formation of BODIPY cation radicals, leading to α,α- and α,γ-dimers. The mechanism of dimer formation proposed by the authors was confirmed by a decrease in the reaction rate in the presence of TEMPO, as well as by the formation of α-adducts when the process was carried out in the presence of BHT (Scheme 137). Dimers **240** and **241** showed a significant bathochromic shift of the absorption and emission maxima. Two absorption maxima were observed in the absorption spectra of α,α-dimers **240**, indicating exciton cleavage, and α,γ-dimers **241** showed the ability to generate singlet oxygen.

In 2021, Kang *et al.*[283] reported a regioselective dimerization of BODIPY yielding α,α-dimers. Theoretical calculations showed that the electron density in the cation radical of unsubstituted BODIPY is distributed between positions 2 and 3, while in the cation radical of 3-aryl-BODIPY, the electron density was at position 5 (Fig. 26). Based on this, the authors hypothesized that the oxidative homoconjugation of 3-aryl-BODIPY would proceed at position 5.

The regioselective oxidative dimerization of 3-substituted BODIPY under the action of iron(III) chloride proceeded at positions 5 and 5′ for both 3-aryl- and 3-chloro-substituted BODIPY (Scheme 138). Two absorption maxima were observed in the absorption spectra of dimer **242**, indicating exciton coupling. DFT calculations showed that dimerization leads to a decrease in the LUMO energy and an increase in the HOMO energy of the α,α-dimers compared to those for monomers, which is in a good agreement with the bathochromic shift in the absorption spectrum. By postfunctionalization, derivatives

Scheme 136

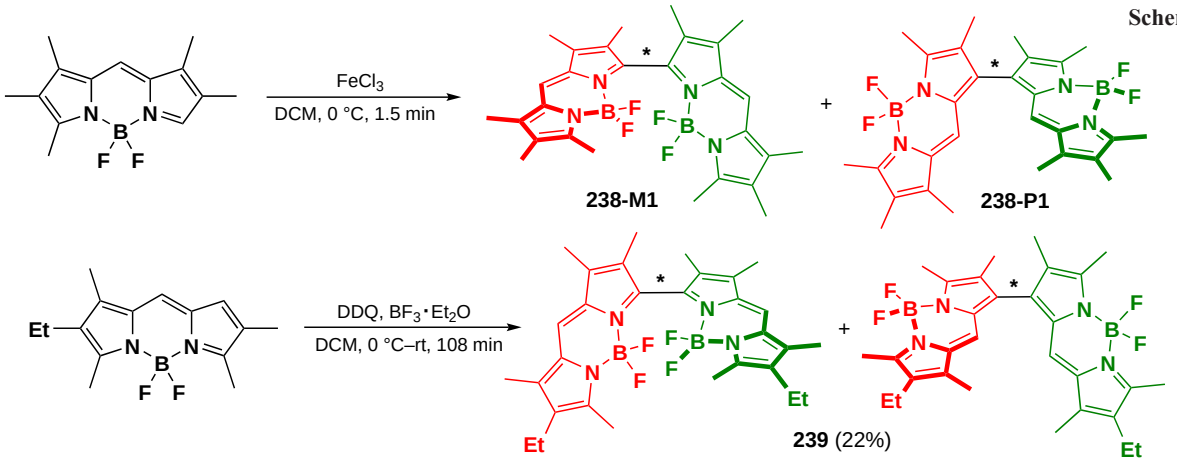

Scheme 137

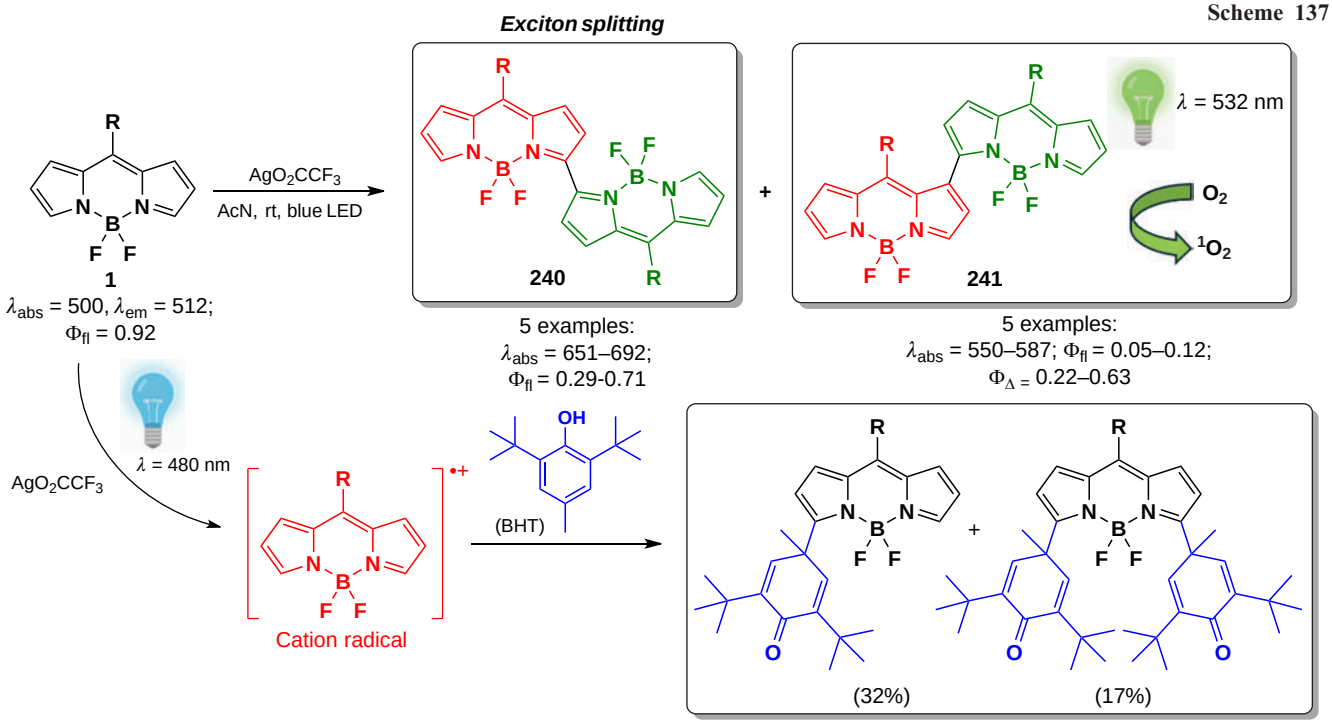

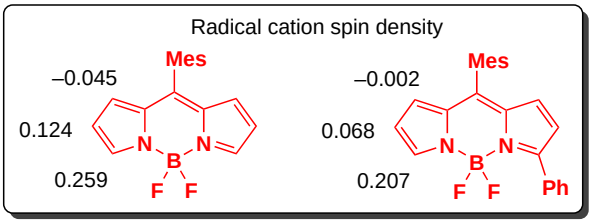

Figure 26. Electron density distribution in the cation radical of unsubstituted and 3-substituted BODIPY.[283]

242f,g were obtained from the dimer **242e** (see scheme 138), among which BODIPY **242g** showed the ability to visualize lysosomes in living HeLa cells.

In 2022, Hao *et al.*[284] reported the synthesis of BODIPY **244** and **246** dimers *via* photochemical extrusion of sulfoxide from BODIPY precursors conjugated with sulfoxide bridges. Photoconversion was found to occur intramolecularly, without the involvement of external radical particles, and the reaction could also proceed without irradiation at high temperature. A biradical concerted process involving the triplet state was proposed as the mechanism. DFT calculations showed that the activation energy of the proposed transition state was 41.3 kcal mol^{-1} (Scheme 139). BODIPY **246** with a lysosome-targeting morpholino fragment showed the ability to visualize lysosomes in living cells.

3.8.2. α,β-Dimers and -oligomers

In 2021, Teng *et al.*[285] described a new class of α,β-dimers of BODIPY as type I NIR-absorbing photosensitizers. Dimer **247** and trimer **248** were synthesized by the Suzuki-Miyaura reaction from 2-Bpin-BODIPY (B2pin2 is bis(pinacolato)diboron) (Scheme 140).

According to X-ray crystallography data, α,β-dimer **247a** has almost planar structure, while in **247b** two BODIPY fragments are located at an angle of 56.42° due to steric repulsion of methyl groups at positions 1, 3, 5 and 7. The planar structure ensures the proximity of the energies of the S_1- and T_2-states of the unsubstituted α,β-dimers of **247**, which contributes to the ISC enhancement. At the same time, according to calculations, the energy of the T_1-state is insufficient for the formation of singlet oxygen, so that the dimers are able to form superoxide radicals. Confirming the calculations, dimers **247** showed reduced fluorescence quantum yields compared to the monomers, as well as the ability to form superoxide radical O_2^-. Flash photolysis experiments showed an extremely long triplet state lifetime of 1514 μs for dimer **247a**.

To shift the absorption of BODIPY to NIR region, α,β-trimer **248** was synthesized, which also formed O_2^{-*} upon irradiation and generated a long-lived (1060 μs) triplet state (Scheme 141). Trimer **248** exhibited high activity upon irradiation with λ = 730 nm (50 mW cm^{-2}, 10 min) in normoxia and hypoxia on HepG2 cell lines with IC_{50} = 0.39 and 0.56 μM. In *in vivo* experiments, therapy of HepG2 tumors-bearing mice with trimer **248**-based nanoparticles, produced using the non-ionogenic detergent pluronic 127 (F127), combined with red-light irradiation (λ = 730 nm, 120 mW cm^{-2}, 10 min) resulted in complete disappearance of tumors on the 6th day.

3.8.3. β,β-Dimers and -oligomers

In 2011, Hayashi *et al.*[286] proposed a method for the synthesis of β,β-dimers of BODIPY using the Suzuki–Miyaura reaction (Scheme 142). β,β-Dimer **249** was prepared by Pd-catalyzed borylation followed by cross-coupling. X-ray crystallography of dimer **249** and trimer **250** showed that in both compounds BODIPY subunits are coplanar due to the absence of alkyl substituents at positions 1, 3, 5, and 7.

In the same year, Nepomnyashchii *et al.*[227] reported an oxidative coupling of BODIPY at positions 2 and 6 to synthesize the corresponding dimers and oligomers (Scheme 143). In the presence of 3.5 equiv. of anhydrous $FeCl_3$, mixtures of dimers **251a**,**b** (10–27%), trimers **252a**,**b** (3–9%), and other oligomers were formed. A bathochromic shift of the absorption maxima was shown for the linear dimers **251** and trimers **252**, and no

Scheme 138

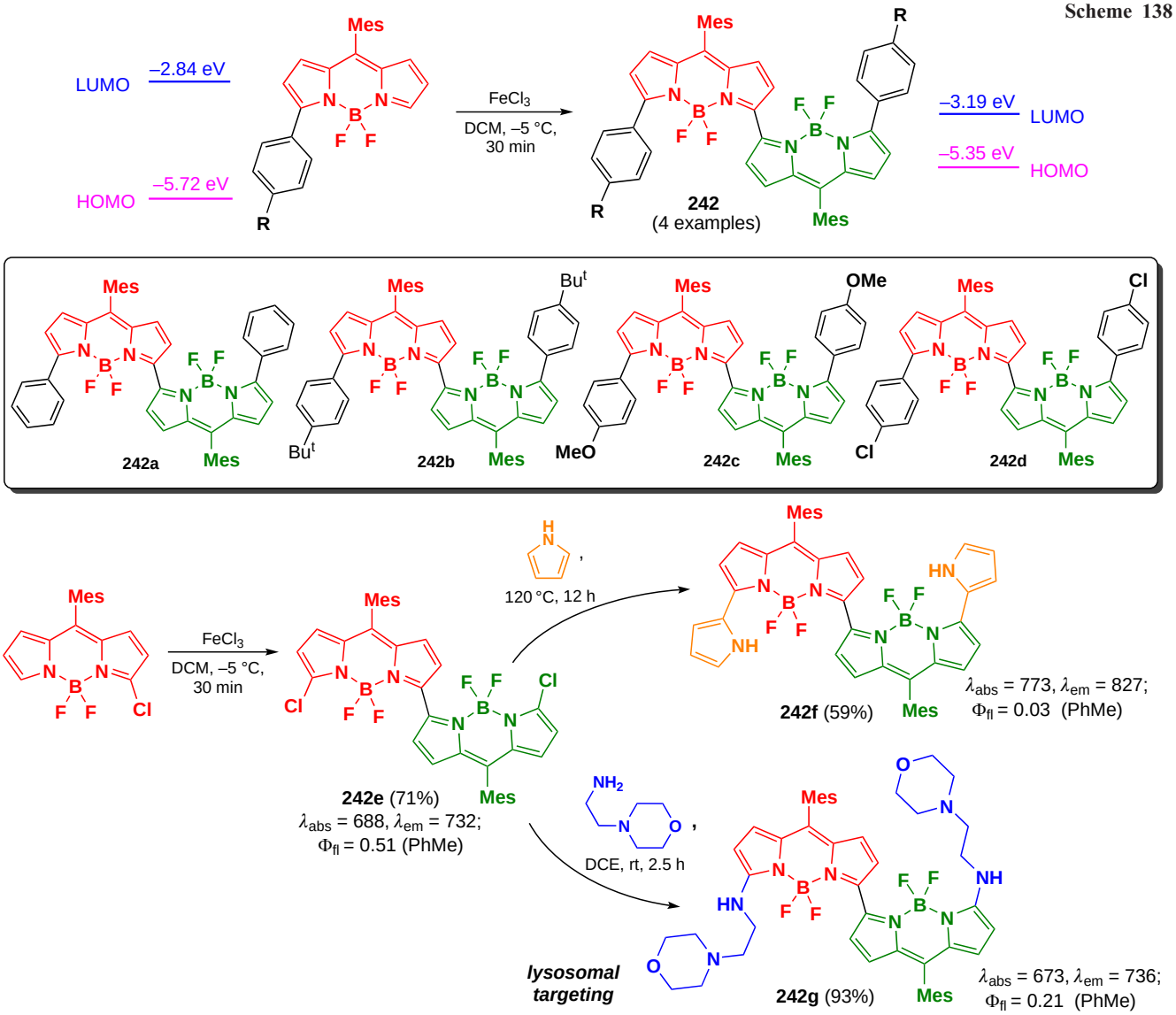

exciton cleavage was observed in the electronic spectra of the β,β-dimers.

In 2011, Rihn *et al.*[287] synthesized symmetric β,β-dimers of BODIPY *via* oxidative coupling reaction with bis(trifluoroacetoxy)iodbenzene (PIFA) as an oxidant (Scheme 144). Bathochromic shifts of 40–70 nm as well as high fluorescence quantum yields were observed for dimer **251a** and trimer **252a**. Based on 2-substituted BODIPY, the corresponding substituted dimers **253** were synthesized in a similar manner. Compound **251a** was modified at the boron atom by reaction with an excess of a Grignard reagent, resulting in BODIPYs **253** with ethynylpyrene moieties in its structure. When the dimer **254** was excited with 285 and 369 nm light, only one emission peak at 562 nm was observed in the emission spectra, indicating a complete exciton energy transfer from the pyrene to the BODIPY dimer.

In 2018, Arroyo-Córdoba *et al.*[288] synthesized the asymmetric β,β-dimer of BODIPY **255** using the Suzuki reaction (Scheme 145). The obtained dimer was interesting as a platform for further functionalization to form derivatives **256**–**258** due to the high reactivity of the *meso*-SMe group in aromatic nucleophilic substitution reactions as well as in the Libeskind–Srogl cross-coupling reaction.

A new method for oxidative coupling of α-amino-BODIPYs was proposed by Wang *et al.* in 2023.[289] Under the action of *m*-CPBA or PIFA as an oxidizing agent, 3-amino-5-aryl-substituted BODIPY formed β,β-dimers **259**. A subsequent reaction of the dimer **259a** (R = 4-MeOC$_6$H$_4$) with PhPCl$_2$ yielded **260** through interaction with reactive amino groups and stabilization of the coplanar orientation of the BODIPY subunits, and chlorination of this substrate upon irradiation gave the derivative **261** (Scheme 146).

The obtained dimers showed a bathochromic shift in the absorption spectrum and a decrease in the fluorescence quantum yield compared to that of the monomers. Dimer **259a** showed a solvatochromic effect as well as the ability to form singlet oxygen and superoxide radical, which is not characteristic of β,β-dimers. Quantum chemical DFT calculations showed charge transfer for the **259a** dimer. Thus, distribution of the HOMO was throughout the whole molecule, whereas the LUMO was localized at the BODIPY core. The authors explain the decrease in fluorescence quantum yields and the ability of dimer **259a** to form ROS as a consequence of the SOCT-ISC process.

Scheme 139

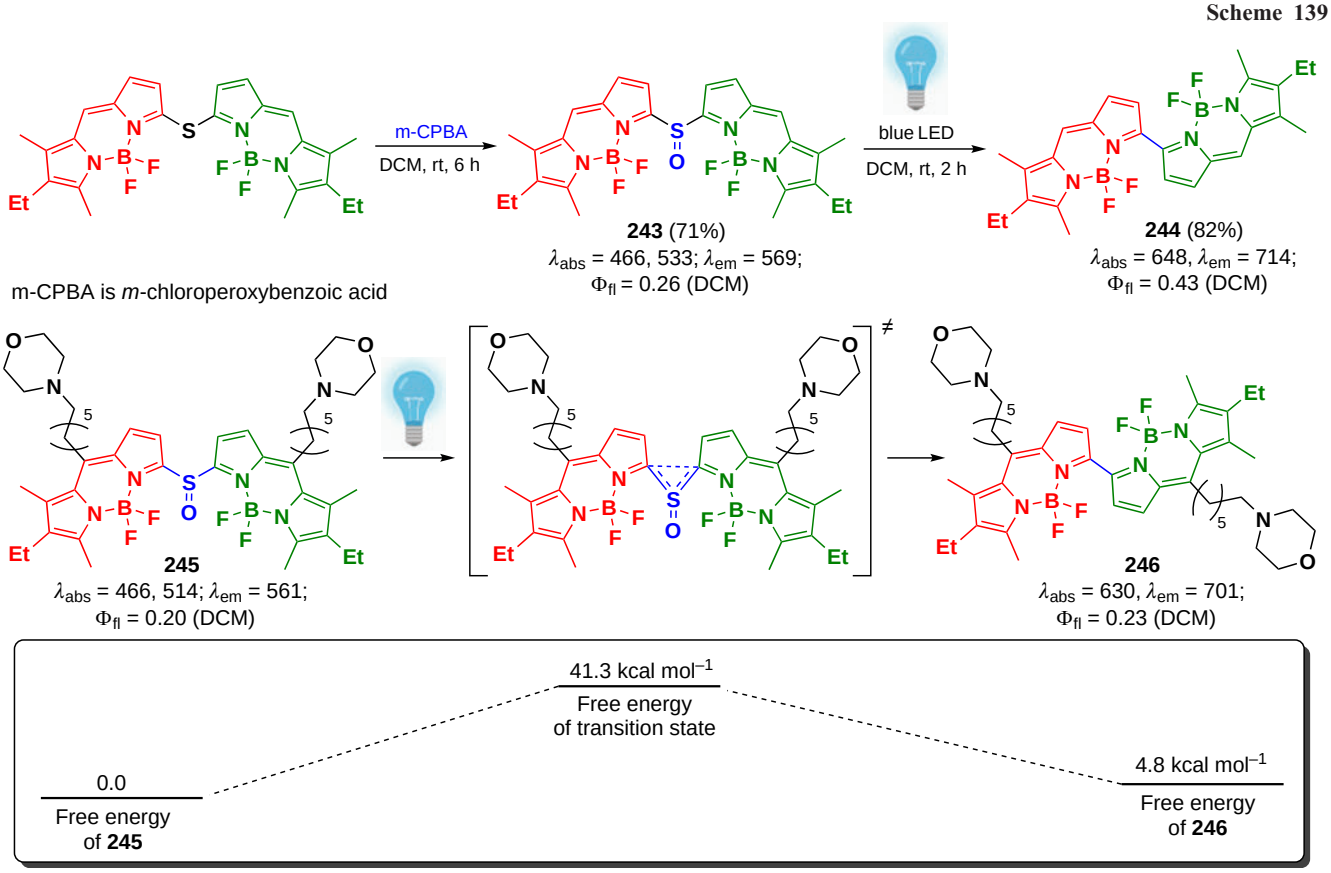

Scheme 140

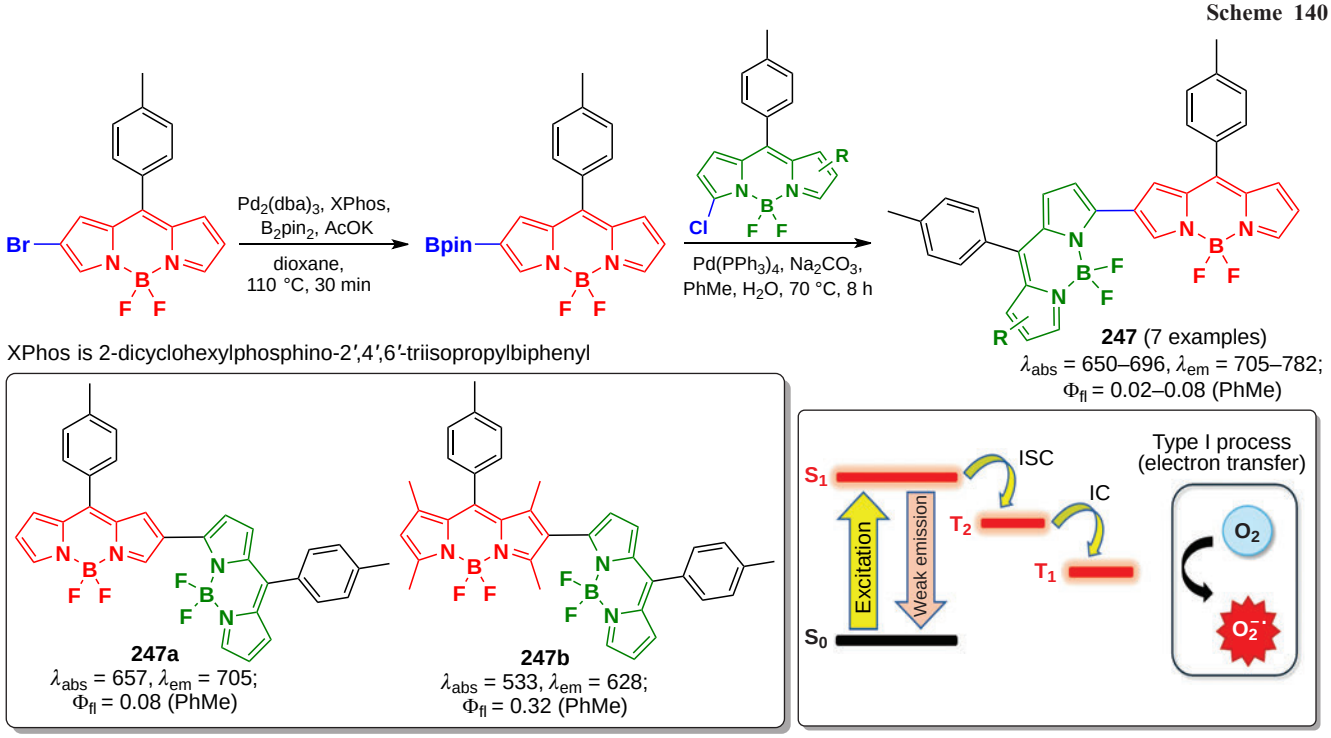

3.8.4. β,γ-Dimers and -oligomers

In 2021, Kang *et al.*[290] synthesized β,γ-dimers of BODIPY **262a–d** by Pd-catalyzed C–H activation; the reaction was carried out in the presence of silver trifluoroacetate as oxidant and $Pd(OAc)_2$ as catalyst (Scheme 147). Trimer **262e**, tetramer **262f**, and pentamer **262g**, also representing β,γ-regioisomers, were obtained with increasing the amount of oxidant.

Oligomers **262a–g** exhibited significant bathochromic absorption shifts in the spectra, exciton splitting, large Stokes shifts (1600–3230 cm^{-1}) and moderate fluorescence quantum yields. Using DFT calculations, it was found that oligomer formation effectively stabilize the LUMO levels (–3.10, –3.22

Scheme 141

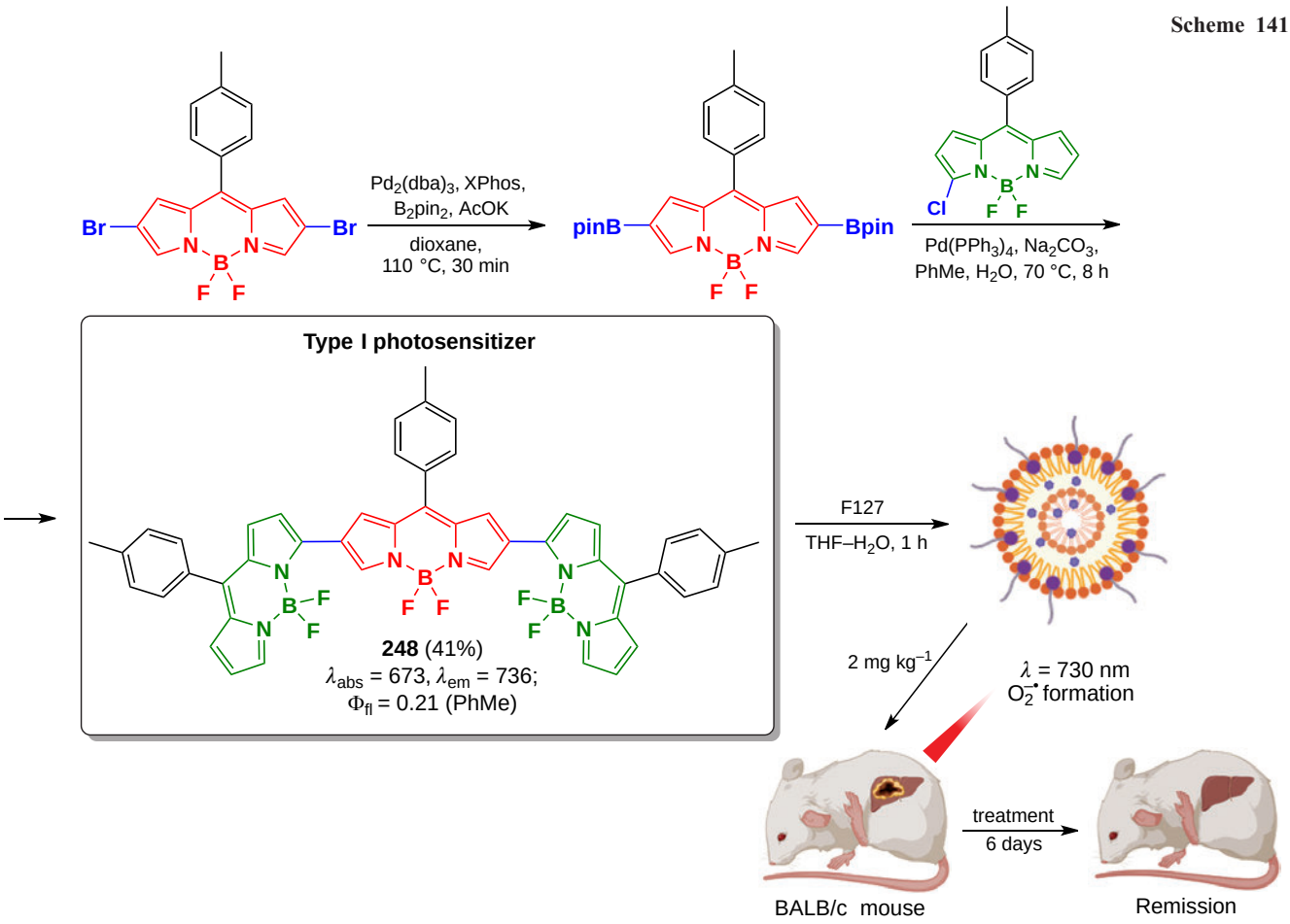

Scheme 142

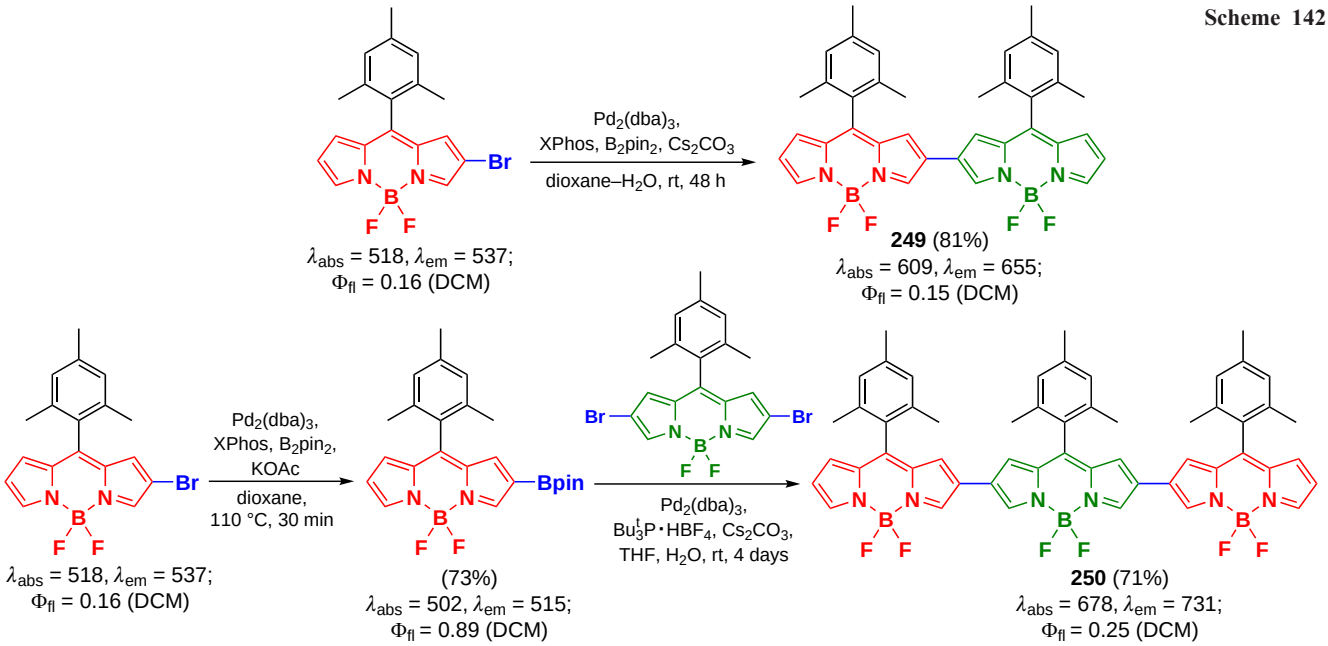

and –3.27 eV for monomer, dimer and trimer, respectively) and destabilize the HOMO levels (–5.79, –5.73 and –5.71 eV). The calculated T_1 energies for compounds **262a**,**e**,**f** were 1.50, 1.47 and 1.46 eV, which is sufficient to generate singlet oxygen. To confirm the calculations, the ability to generate singlet oxygen was experimentally demonstrated for the dimers **262a–d**.

3.8.5. γ,γ-Dimers and -oligomers

In 2012, Poirel *et al.*[291] presented a method for the synthesis of γ,γ-dimers by oxidative homocoupling reaction in the presence of PIFA. γ,γ -Dimer **263a** and α,γ-dimer with a methylene bridge **263b** formed *via* a benzyl-type cation radical were obtained. Dimers **264a–b**, in which BODIPY moieties were linked

Scheme 143

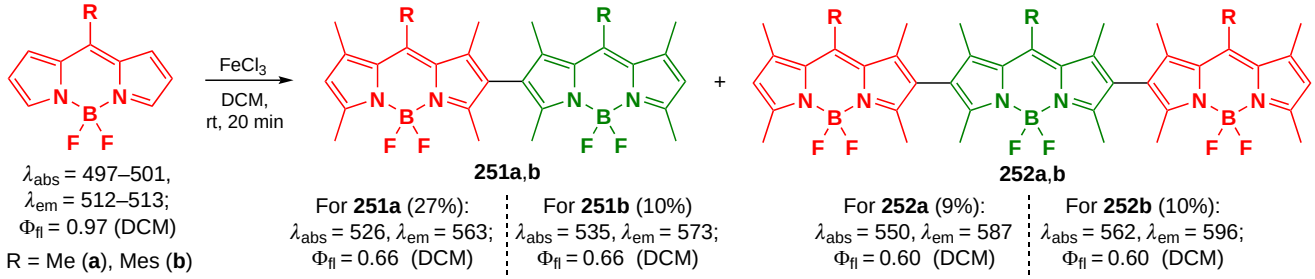

Scheme 144

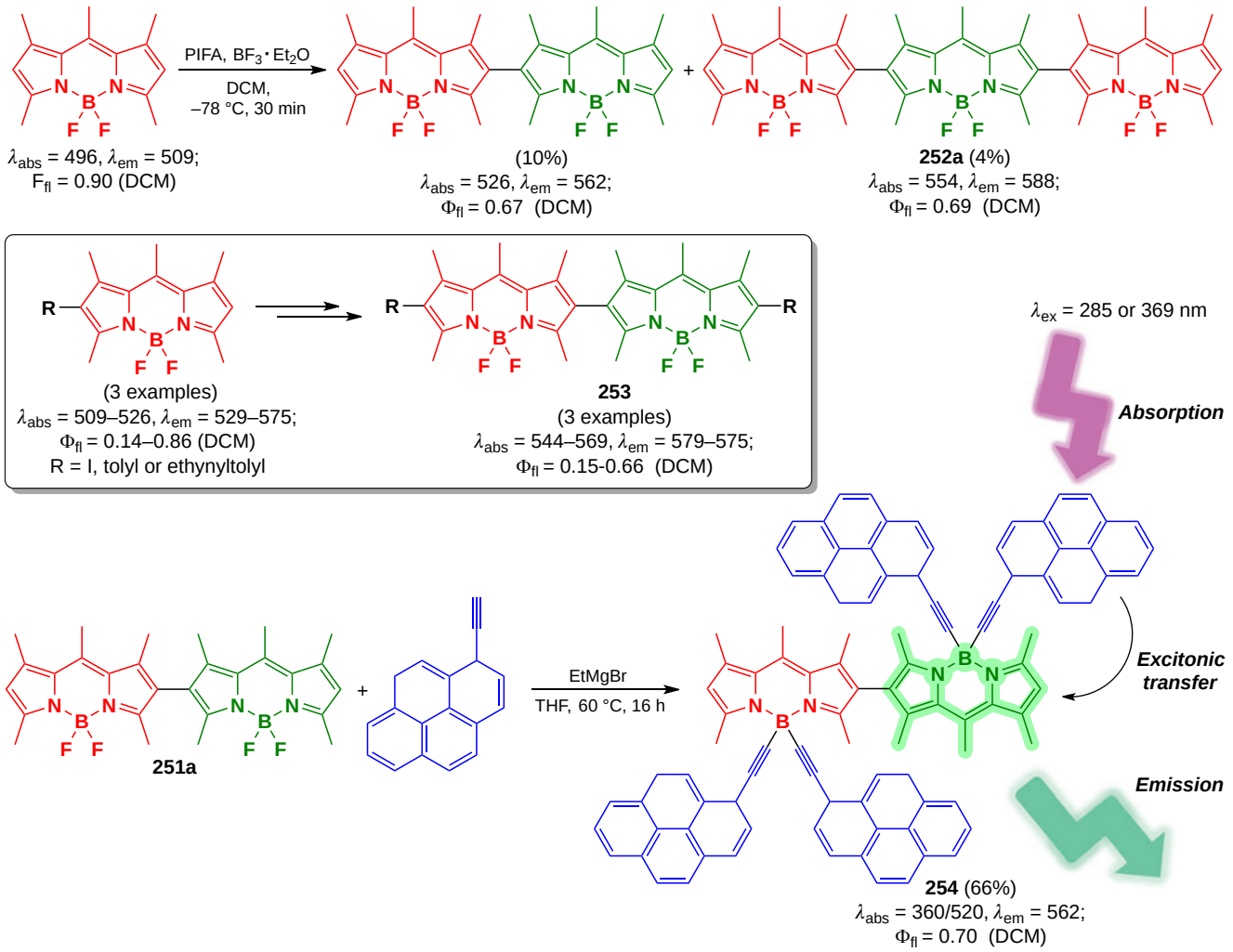

through the α-positions of bithiophene, were synthesized under the same conditions (Scheme 148).

Moderate exciton coupling was observed in the absorption spectra of dimers **263a**,**b**, and the fluorescence quantum yield and excited state lifetimes were significantly lower than those of the monomer. Dimers **264a**,**b** also exhibited exciton coupling, low photoluminescence efficiency and reduced excited state lifetimes. The photoluminescence and fluorescence efficiencies of the dimers appeared to be solvent-dependent, thus indicating the ICT effect.

3.8.6. *Meso*,*meso*-dimers

In 2011, Cakmak *et al.*[158] proposed the use of BODIPY dimers as promising PDT agents. By condensation of β- or *meso*-formyl-substituted 1,3,5,7-tetramethyl-BODIPY with 2,4-dimethylpyrrole, β,*meso*- and *meso*,*meso*-dimers **265a–c** were synthesized (Scheme 149).

Dimers with BODIPY π-systems that are orthogonal to each other can transition to an excited state with equal probability. This doubly substituted excited state promotes the $S_1 \rightarrow T_1$ transition.[292] Theoretical calculations of the molecular orbitals of the β,*meso*-dimer **265a** showed that the transition to the S_1 state represents a linear combination of the HOMO-1 to LUMO and HOMO to LUMO+1 transitions, as well as other doubly substituted transitions, which in turn significantly hinders the $S_1 \rightarrow S_0$ relaxation and promotes the transition to the T_1 state. The ability to form singlet oxygen was demonstrated for the **265a–c** dimer, confirming the

Scheme 145

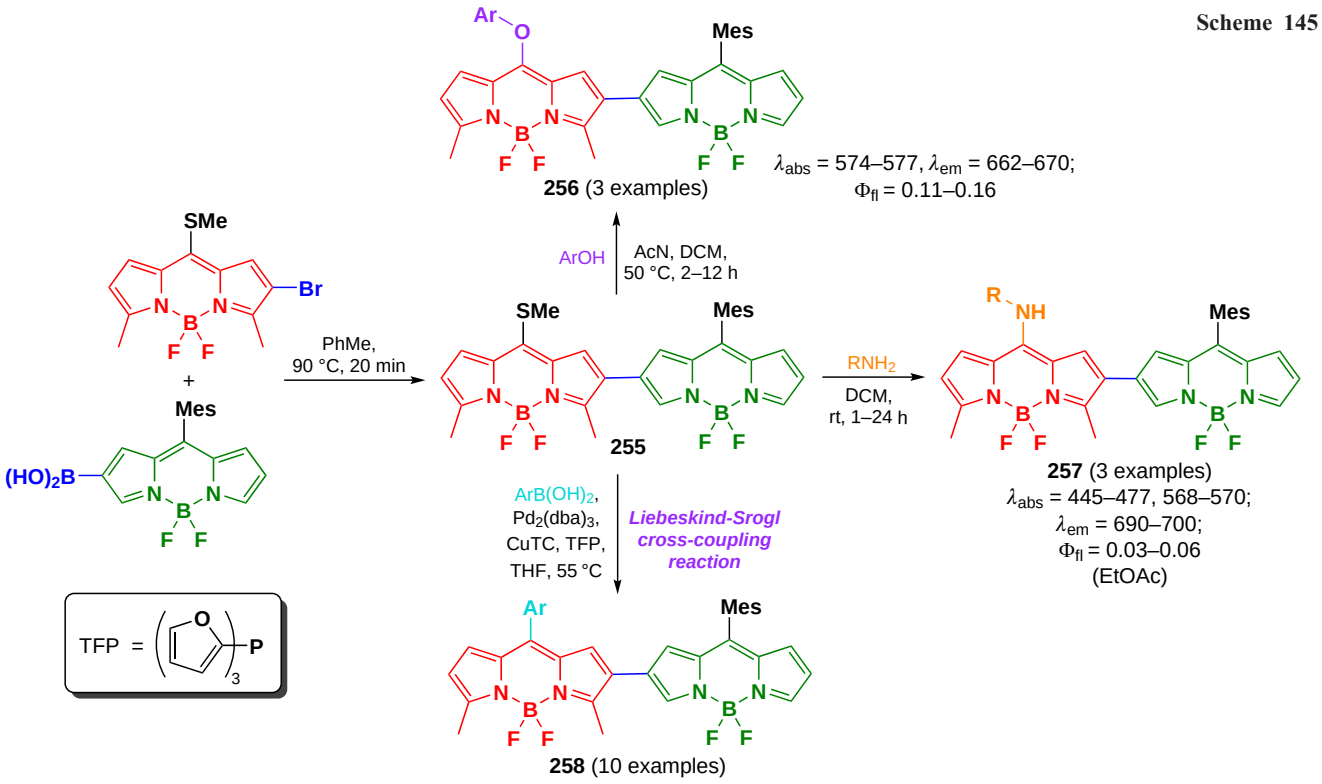

Scheme 146

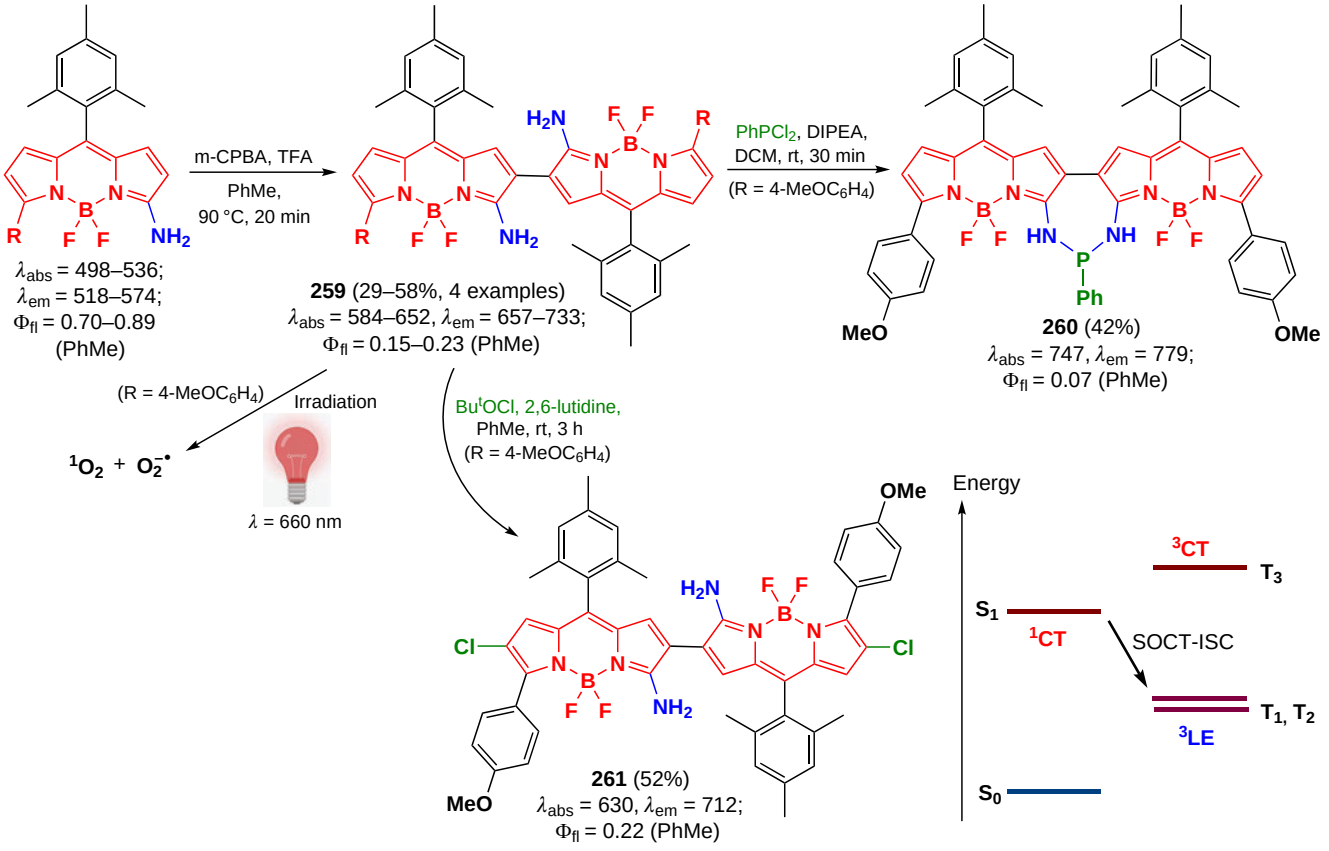

results of theoretical calculations. The β,*meso*-dimer **265a** showed the highest quantum yield ($\Phi_\Delta = 0.51$). In an antiproliferative activity study on K562 erythroleukemia cells under irradiation with $\lambda = 514$ nm light (2.5 mW cm^{-2}, 4 h), the half-maximal effective concentration (EC_{50}) of dimer **265a** was 50 nm.

3.8.7. Condensed dimers

In 2015, Yu *et al.*[293] applied an oxidative dimerization method to synthesize conjugated cyclic BODIPY dimers. Oxidation of the bridging dimer **266** with iron(III) chloride gave the condensed BODIPY dimer **267** was obtained, which was further introduced

Scheme 147

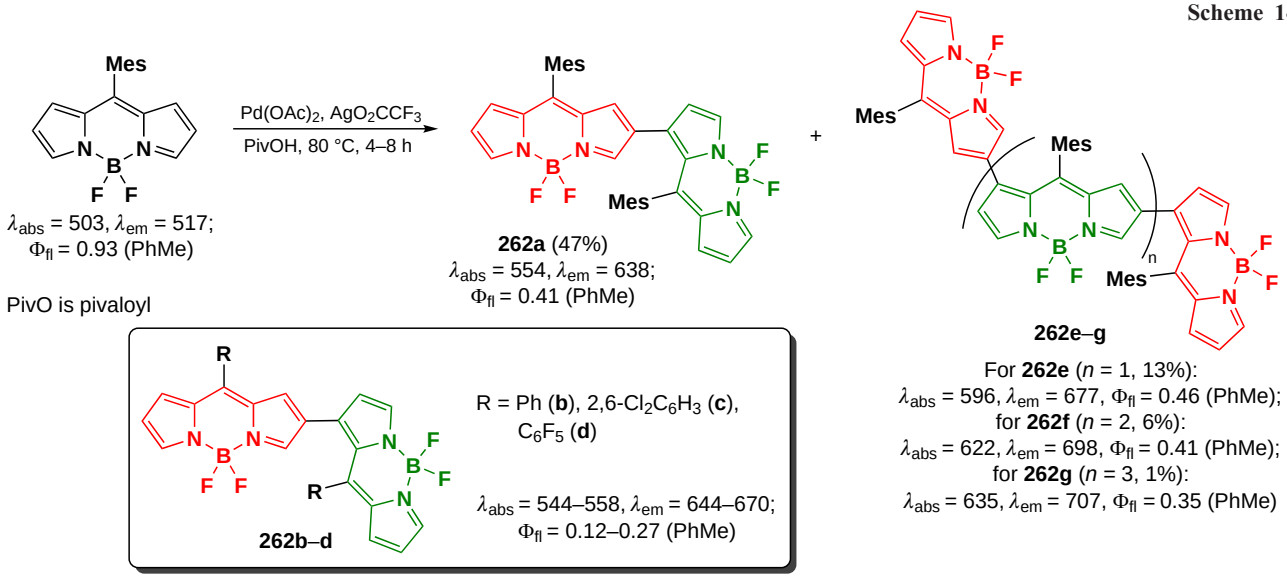

Scheme 148

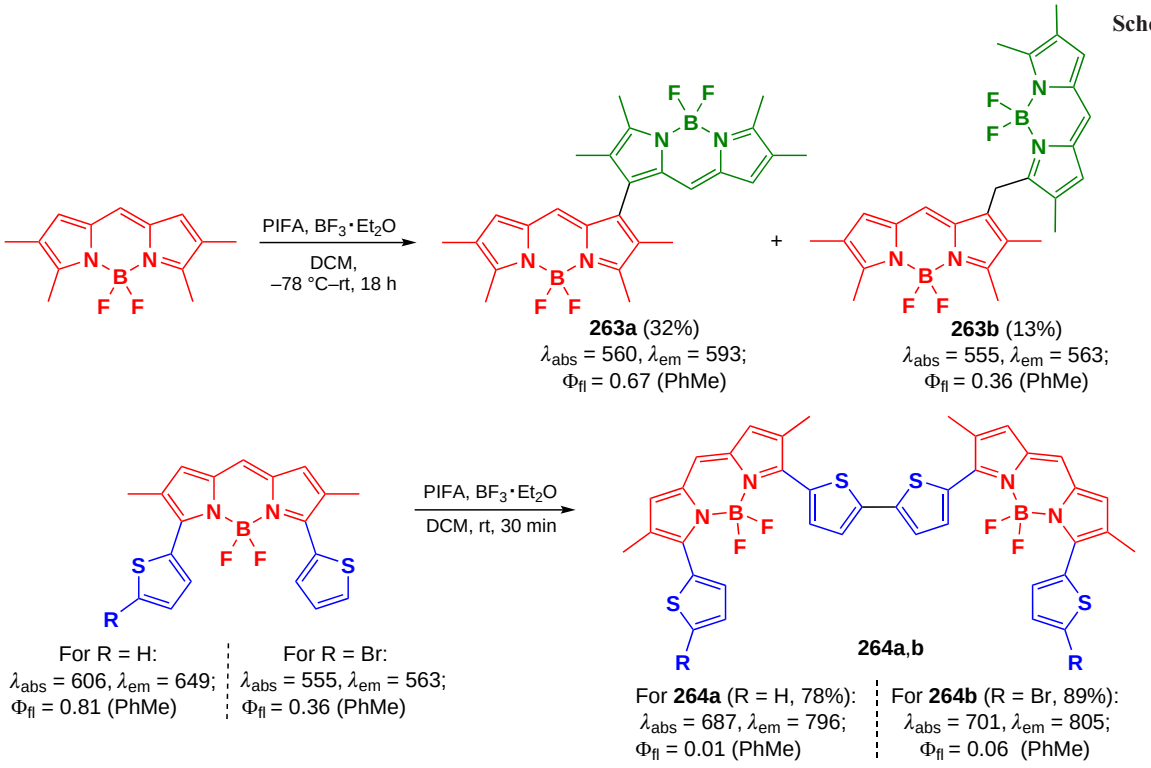

into the Knoevenagel condensation to form styryl- and distyryl-substituted BODIPY dimers **268a**–**d** (Scheme 150).

X-ray crystallography of dimer **267** showed that all aromatic rings lie in the same plane, from which only fluorine atoms and alkyl substituents de*via*te. A bathochromic shift was observed in the absorption spectra of dimer **267** and its styryl derivatives **268a**–**d** compared to the bands for the original BODIPY and the unconjugated dimer **266**. According to DFT calculations, the HOMO and LUMO were distributed over the two BODIPY cores; the calculated decrease in the energy gap between the HOMO and LUMO of the condensed dimer was consistent with the observed bathochromic shift.

In 2020, Wu *et al.*[294] described the synthesis of conformationally constrained BODIPY **269** dimers *via* intramolecular oxidative dimerization of unconjugated bis-BODIPYs under the action of $MoCl_5$. The products resulting from the oxidative combination exhibited a significant bathochromic shift of the absorption maxima coupled with an increase in fluorescence quantum yields (Scheme 151). The results of DFT calculations also showed decreased LUMO energy levels and increased HOMO energy levels for bis-BODIPY and fused-BODIPY, which was in good agreement with the bathochromic shift values. In addition, dimer **269a** exhibited fluorescence imaging ability in HeLa cells, in domestic cat muscle and in danio fish.

3.8.8. Dimers and oligomers with heteroatoms

In 2014, Shinokubo *et al.*[295] synthesized asymmetric trimers of BODIPY **270a**,**b** by oxidation of β-amino derivatives of DDQ (Scheme 152). Such trimers exhibited significant bathochromic shifts in the absorption spectra.

Scheme 149

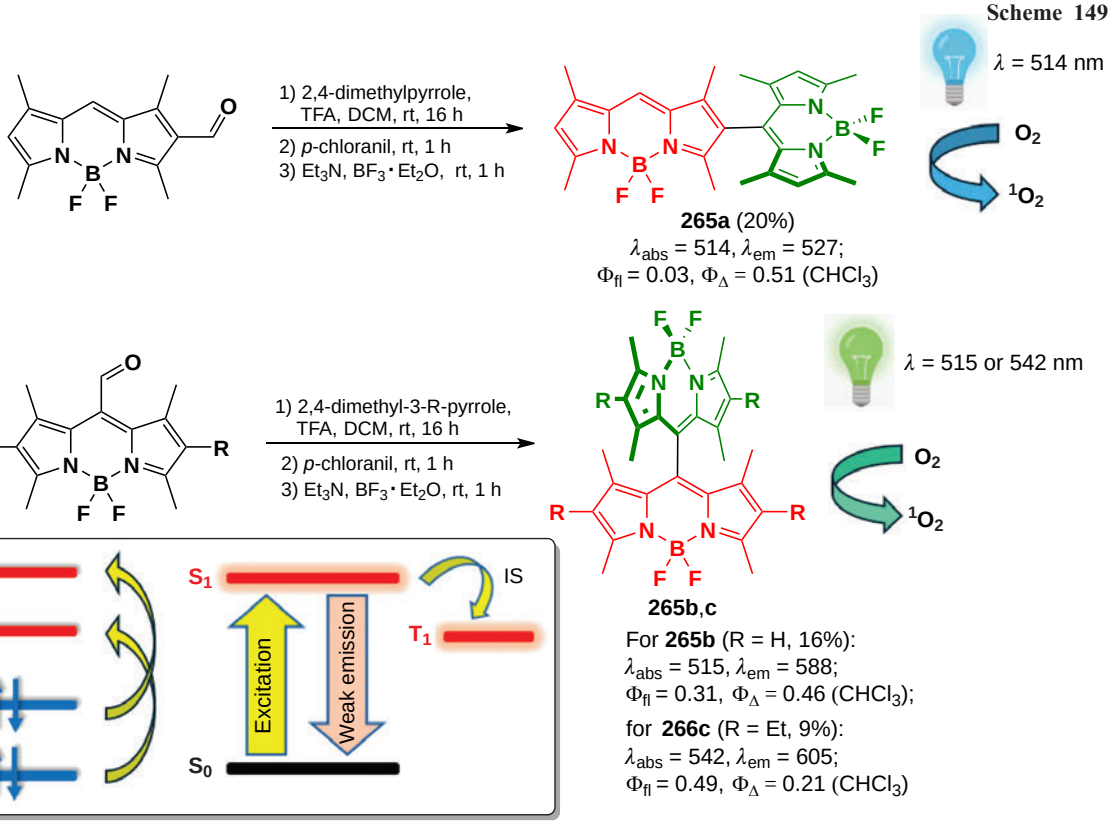

Scheme 150

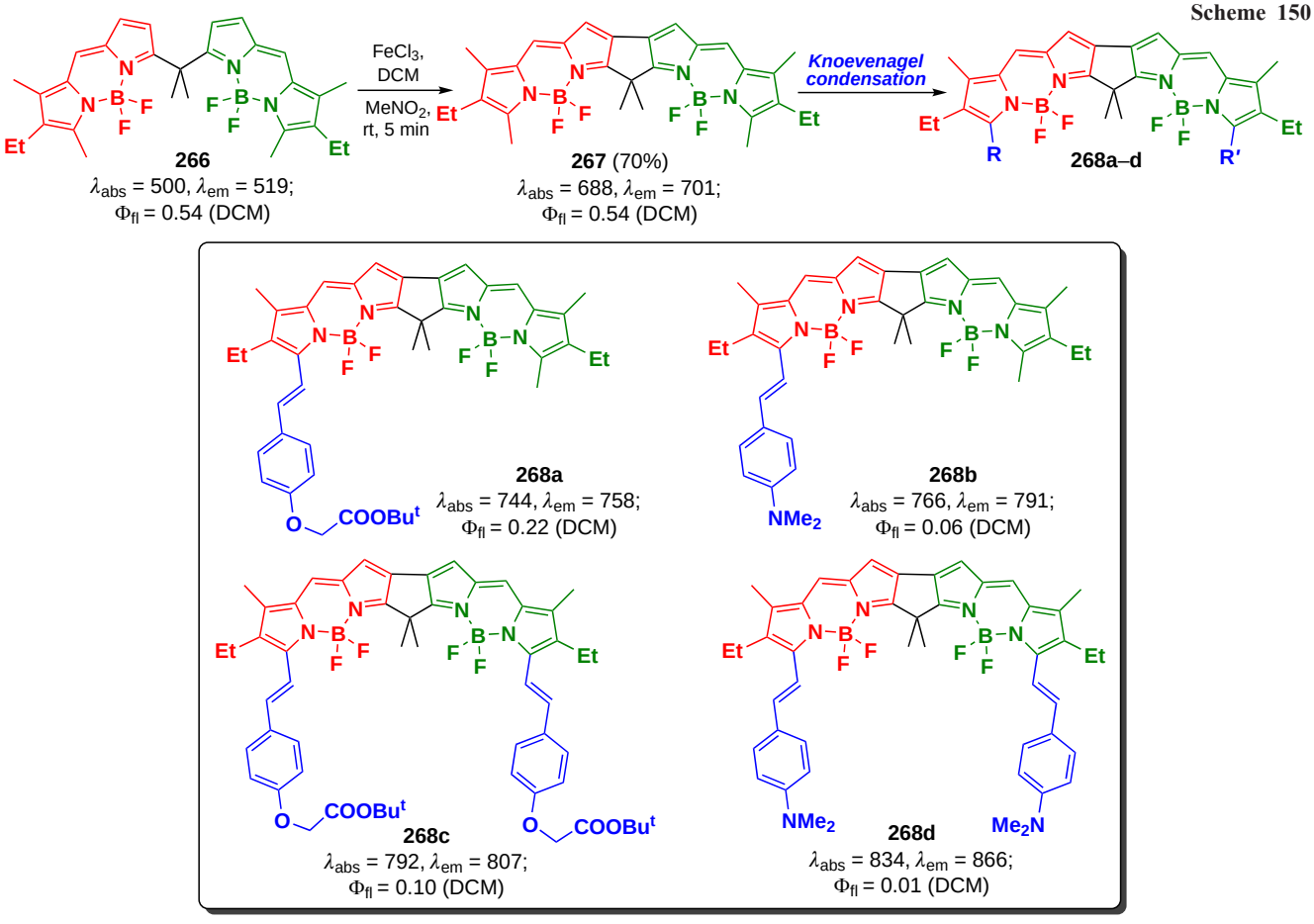

Scheme 151

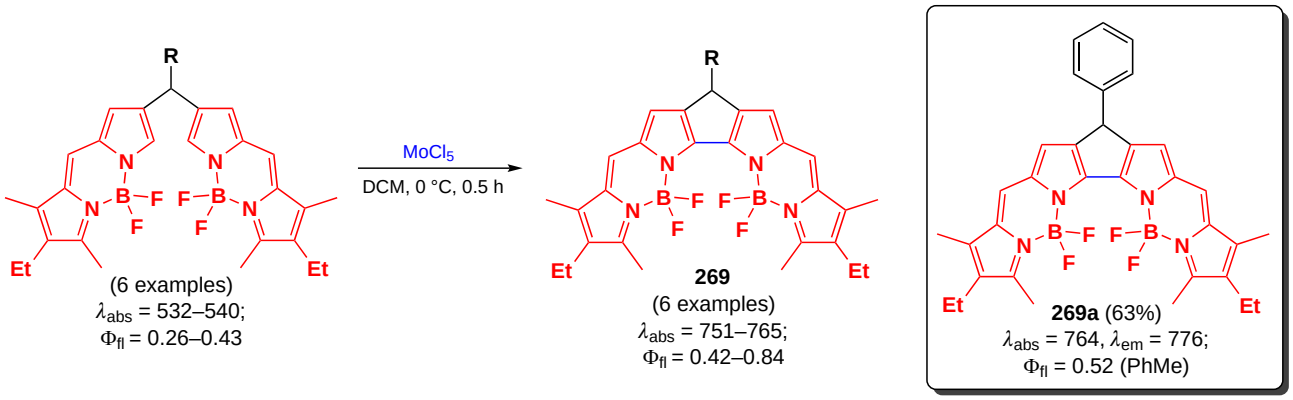

Scheme 152

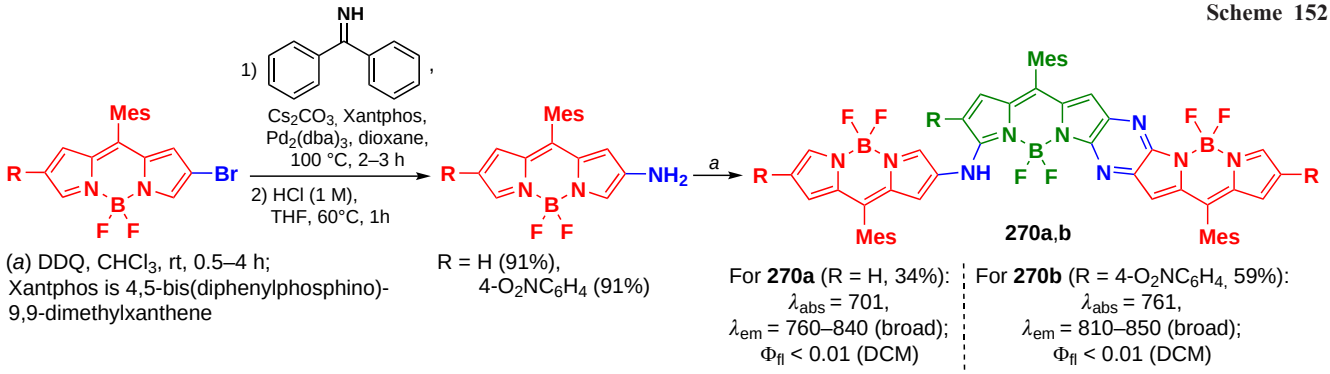

In 2021, Jiao *et al.*[296] reported the synthesis of dimers, trimers, and other BODIPY oligomers conjugated *via* a sulfide bridge using nucleophilic substitution reactions (Scheme 153). Conjugates **271**–**274** exhibited a bathochromic shift in both absorption and emission spectra. As the number of BODIPY links in oligomer increased, the fluorescence quantum yield decreased, and the ability to generate singlet oxygen increased due to the enhanced ICT effect. DFT calculations show LUMO

Scheme 153

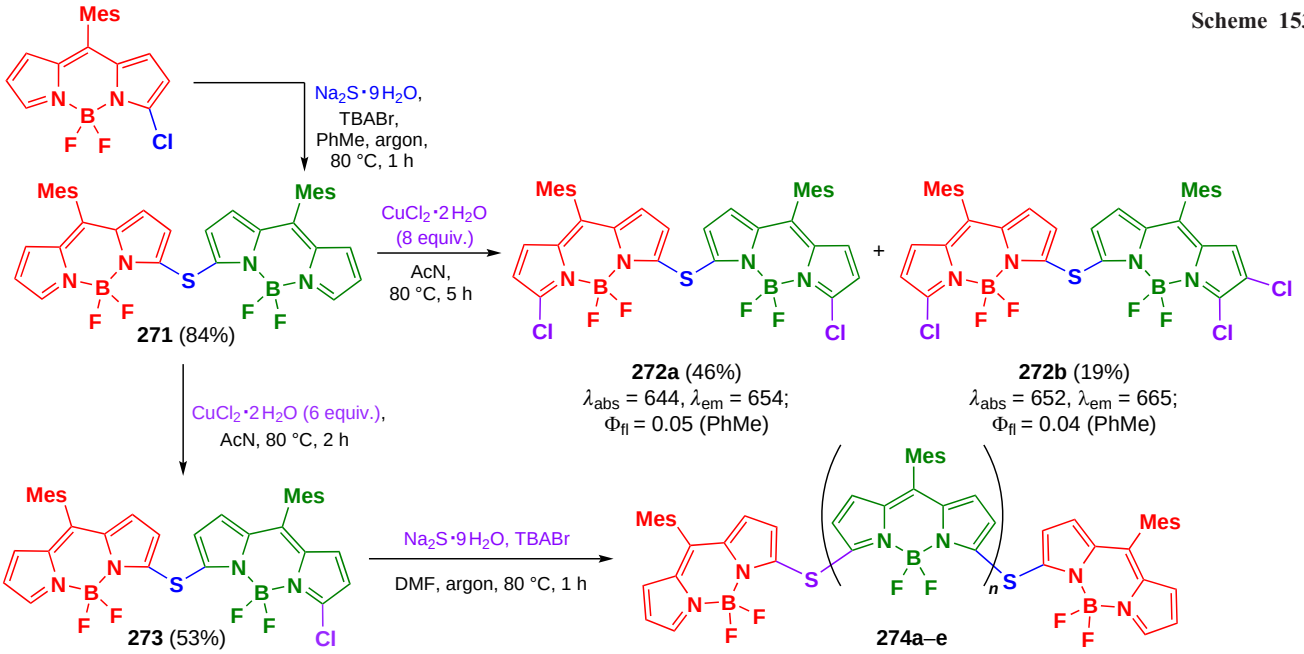

Conjugate	*n*	λ_{abs}, nm	λ_{em}, nm	Φ_{fl}
274a	0	627	640	0.06
274b	1	706, 662, 526	720	0.07
274c	2	730, 676, 607	769	0.03
274d	3	735, 636, 535	796	0.03
274e	4	734, 655	806	0.02

	HOMO, eV	LUMO, eV
274a	–5.59	–3.07
274b	–5.46	–3.18
274c	–5.39	–3.29 V

stabilization and HOMO destabilization as the number of BODIPY links in oligomers increases.

In 2021, Gong *et al.*[297] proposed an approach to synthesize thiophene-fused dimers of BODIPY **275**. This method involves nucleophilic substitution with sodium sulfide, and subsequent oxidation. Dimers **275** were obtained from the *in situ* formed unsubstituted (**271**), mono- (**273**) and dichloro-substituted (**272a**) disulfide dimers in the presence of excess $FeCl_3$. As the

Scheme 154

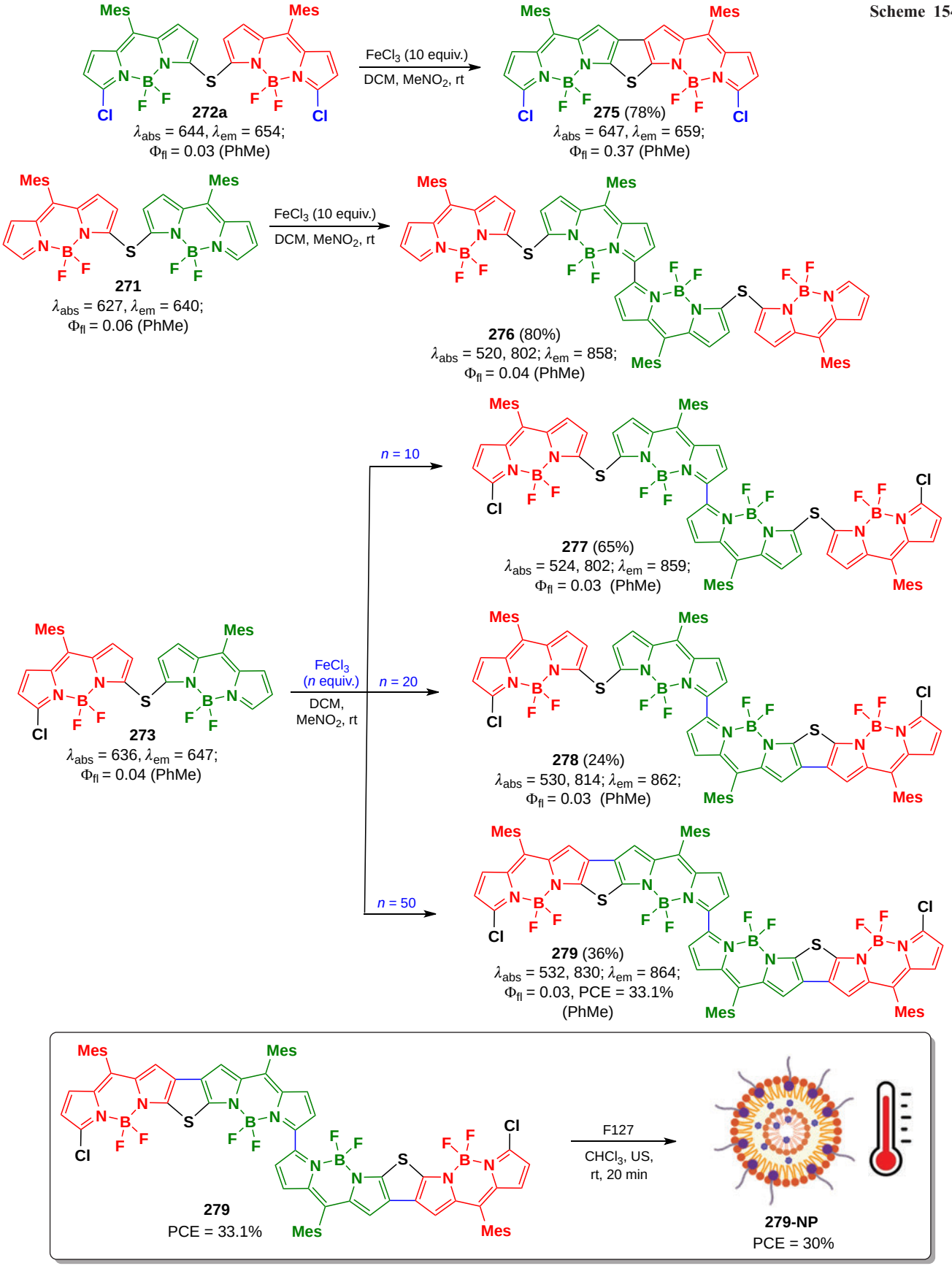

amount of $FeCl_3$ in the reaction mixture increased, the number of condensed links in the structure of the resulting tetramers **276**–**279** also increased (Scheme 154).

Disulfide oligomers **271**, **272a**, **273**, **276**, and **277** exhibited a significant bathochromic shift in the absorption spectrum (up to 130 nm), which increased further for the condensed dimer **275** and tetramers **278**, **279** (up to 200 and 300 nm). Due to the almost complete absence of fluorescence (Φ_{fl} = 0.03), BODIPY **279** exhibited photothermal properties; the PCE was 33.1%, and 30% for the NPs based on it.

In 2024, Werz *et al.*[298] presented N-complexed dimers **280**, trimers **281**, and tetramers of BODIPY **282** obtained by the Buchwald–Hartwig amination (Scheme 155). A bathochromic absorption shift and exciton splitting were observed in the electronic spectra of compounds **280** and **281**. Increasing the number of BODIPY links in the oligomer significantly decreased the fluorescence intensity, which was attributed to an increase in the contribution from radiation-free relaxation and a decrease in the S_1-level transient dipole moment for higher oligomers.

In 2024, Jiao *et al.*[299] described the synthesis of similar N-conjugated dimers and trimers of BODIPY *via* nucleophilic substitution reactions. Subsequent functionalization by the Suzuki reaction led to conjugates **284**, and reductive combination involving the trimer afforded products **285**–**288** (Scheme 156). Dimers **283**, **284**, and **289**, as well as trimers **285**, **287**, **288**, and **290** exhibited a bathochromic shift in the absorption spectrum and showed exciton coupling. DFT calculations showed that oligomerization *via* N-bridged links leads to higher HOMO energies. The fluorescence quantum yields decreased as the number of BODIPY links increased. Hexamer **286**-based nanoparticles showed high PTT efficiency.

3.8.9. Dimers and oligomers with an ethylene bridge

In 2017, Patalag *et al.*[300] synthesized BODIPY oligomers based on BODIPY subunits linked *via* an ethylene bridge. Due to a high flexibility, dimers were able to adopt a coplanar conformation favoring efficient J-aggregation.[8] Dimerization of 3-methyl-substituted BODIPY was carried out in the presence of lithium diisopropylamide (LDA) followed by iodination with ICl and nucleophilic substitution of the iodine atom by Li-BODIPY. The introduction of ethylene dimer **291a** with a methyl group at position 5 into the reaction under these conditions led to the formation of a mixture of tetramer **291b**, hexamer **291c** and octamer **291d** (Scheme 157). Crystal structure of the three dimers with different alkyl substituents showed that BODIPY subunits in the dimers were coplanar, and the slip angle was 36–44°, which was less than the maximum possible for the formation of J-aggregates. A significant narrowing of the emission bandwidth was observed for the J-aggregates of **291a**–**d** oligomers with increasing linker number, which makes them promising monochromatic emitters.

In 2021, Gong *et al.*[301] reported a method for the oxidative homocoupling of 3-methyl-BODIPY leading to the formation of ethylene bridge-coupled dimers and oligomers. When BODIPYs were oxidized with copper(I) iodide in the presence of Cs_2CO_3,

Scheme 155

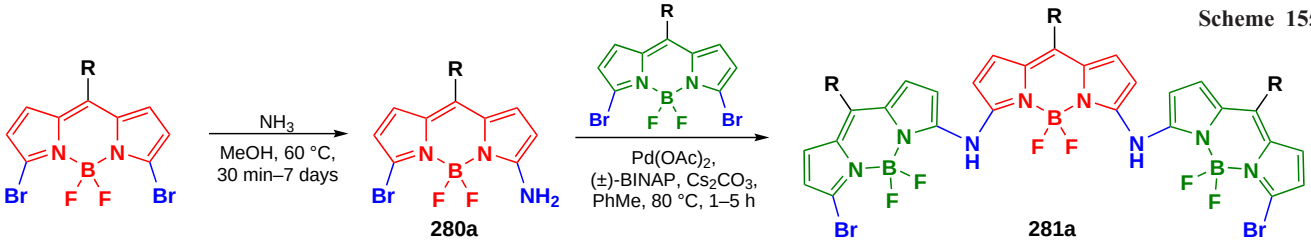

R = 4-Bu^{i}C$_6$H$_4$; BINAP is 2,2'-bis(diphenylphosphino)-1,1'-binaphthyl

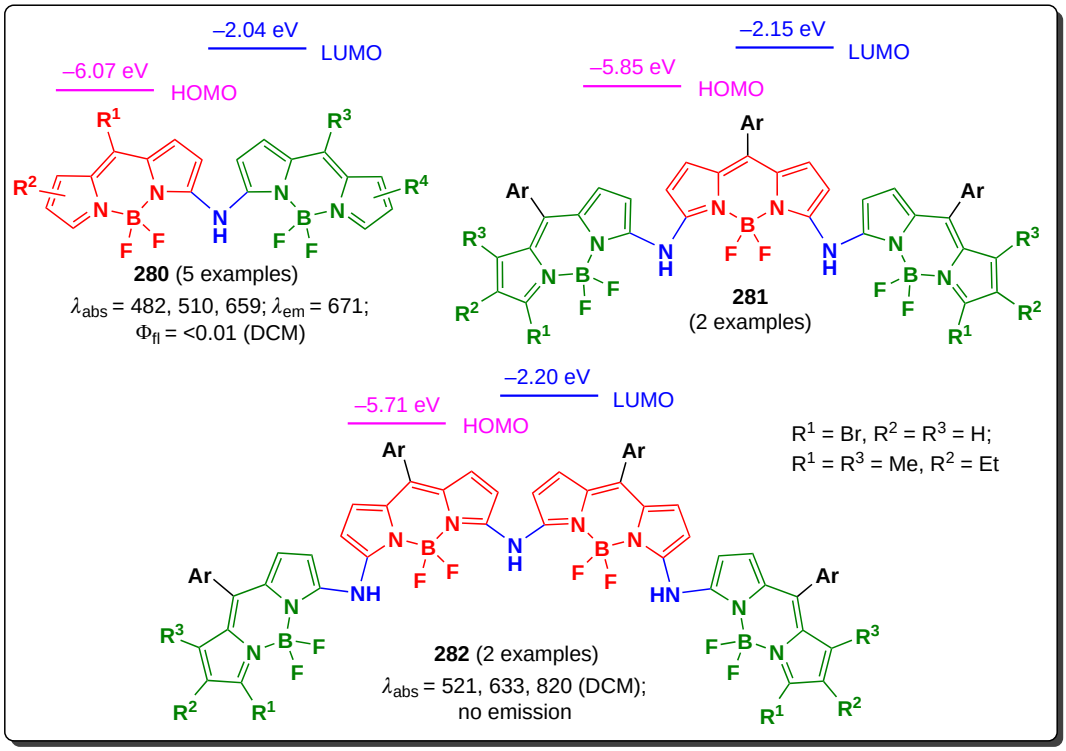

Scheme 156

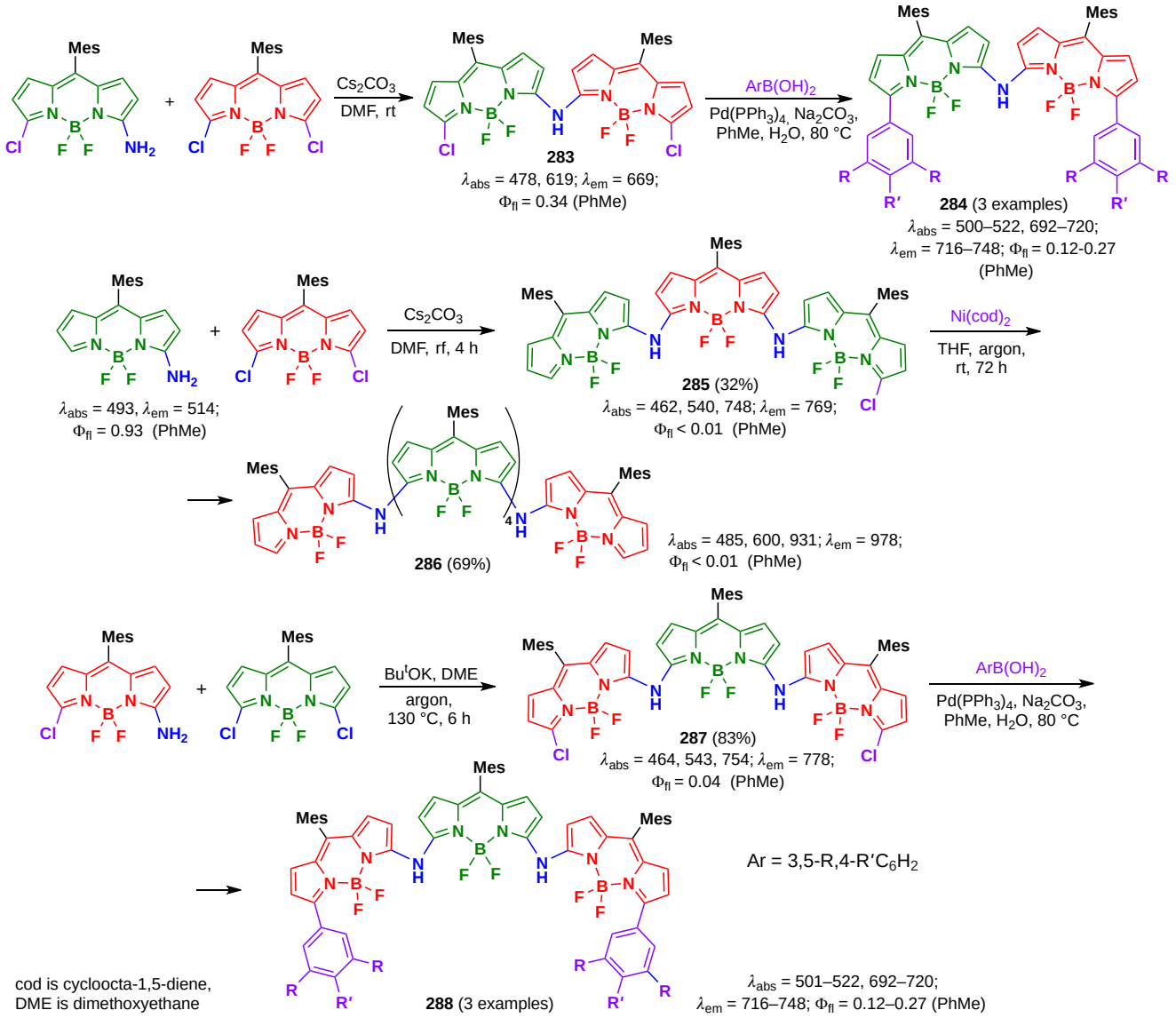

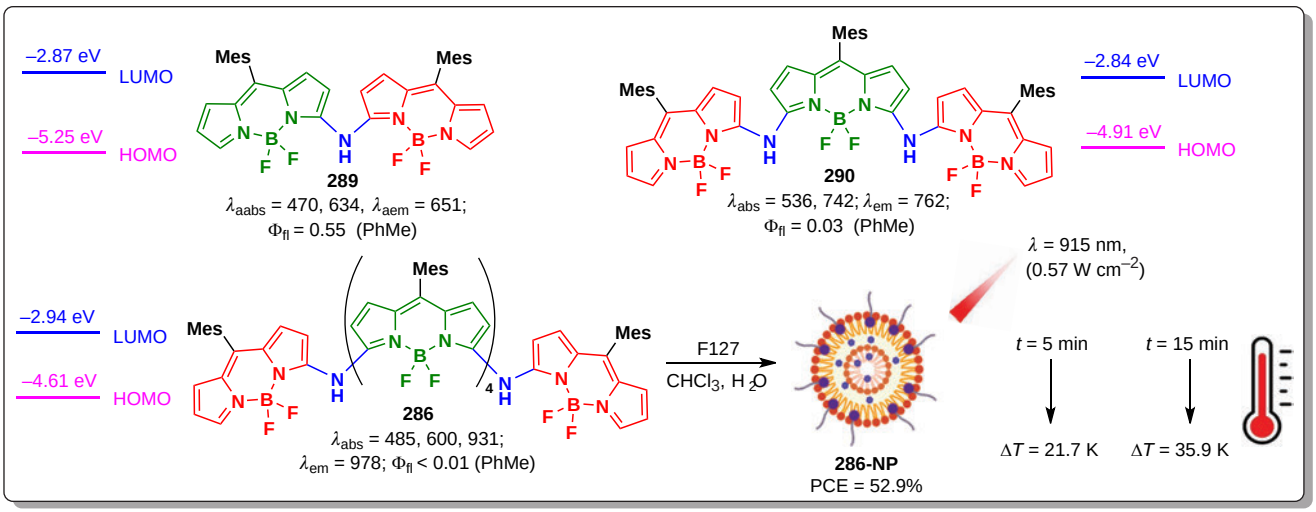

four dimers **292a–d** were obtained, and when the reaction time was increased to 18 h, trimers **292e,f** were also obtained (Scheme 158). Investigation of the reaction mechanism using radical 'traps' TEMPO and *N*-tret-butyl-α-phenyl nitrone (PBN), as well as EPR spectroscopy, confirmed the formation of the BODIPY cation radical. This cation radical was generated under the action of a base and reacted with a second substrate molecule to form a dimer. The dimers and trimers of **292** exhibited bathochromic shifts in the absorption spectrum and high molar extinction coefficients compared to those of the original monomers.

Scheme 157

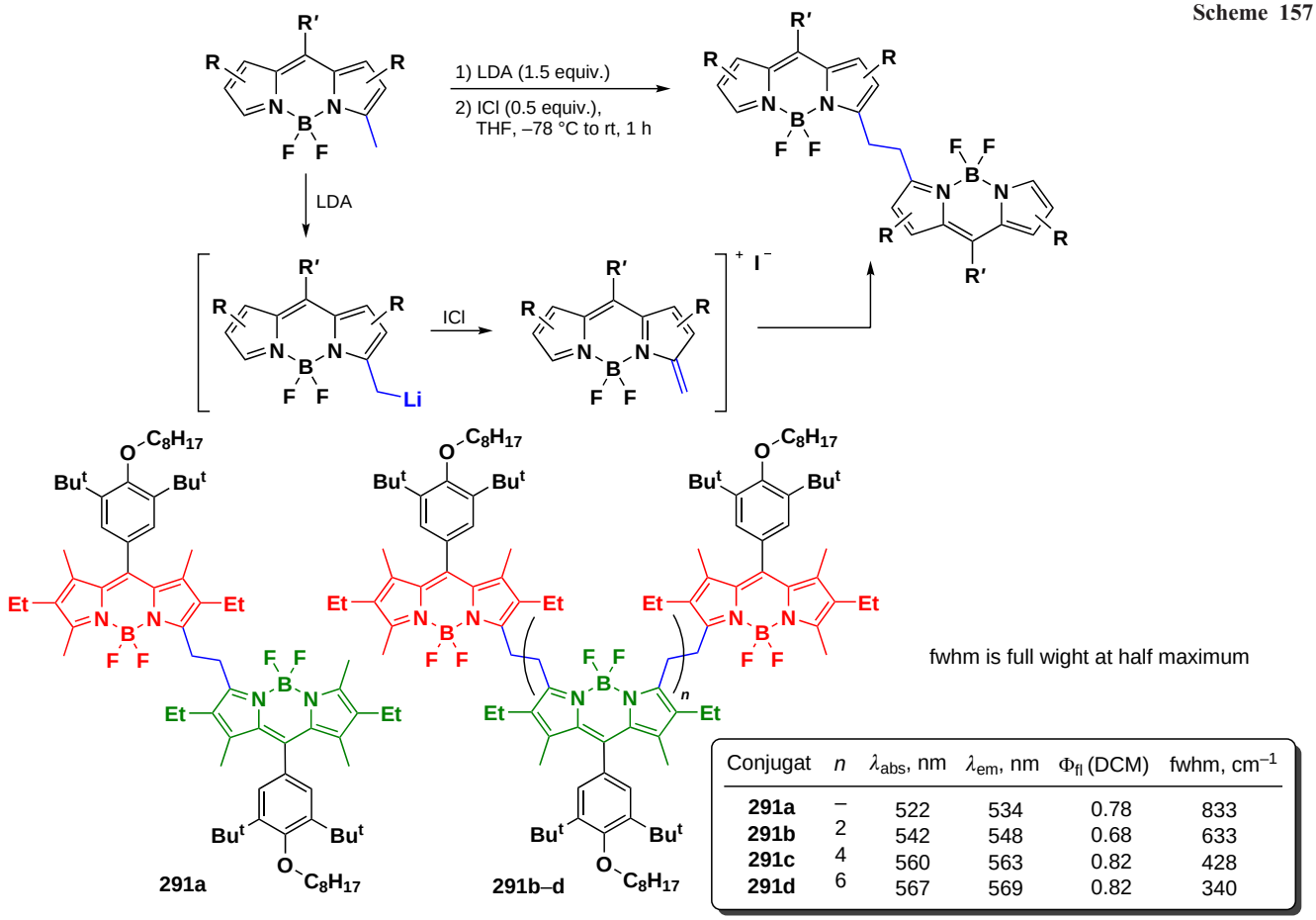

Conjugat	*n*	λ_{abs}, nm	λ_{em}, nm	Φ_{fl} (DCM)	fwhm, cm^{-1}
291a	–	522	534	0.78	833
291b	2	542	548	0.68	633
291c	4	560	563	0.82	428
291d	6	567	569	0.82	340

Scheme 158

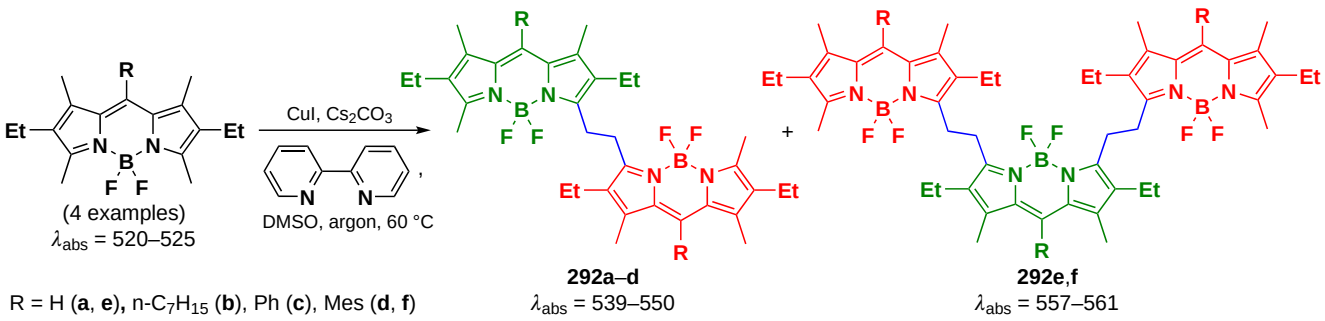

3.8.10. Double bonded dimers and oligomers

In 2020, Wu *et al.*[302] proposed an approach to synthesize coplanar π-conjugated dimers in which the BODIPY subunits were conjugated by a carbon-carbon double bond. Dimer **293** was synthesized by the Stille reaction from 3-chloro-BODIPY and *trans*-1,2-bis(tri-n-butylstannyl)ethene (ESn). Combining different α-chloro-BODIPY and stannates, trimer **294**, tetramer **295a**, pentamer **295b** and hexamer **295c** were obtained (Scheme 159).

The absorption maximum in oligomers **293**, **294**, and **295a–c** shifted significantly towards the NIR- and NIR-II-bands as the number of BODIPY links increased. The molar extinction coefficient varied nonlinearly with increasing link number, with the highest value observed for trimer **294**. The low fluorescence quantum yields of oligomers **294** and **295a–c** (< 1.5%) indicated the predominance of excitation-free relaxation pathways. For oligomers **294**, **295a**, and **295b**, the photothermal conversion efficiency (PCE) was 30–35%, with the PCE value increasing to 56.8% after encapsulation of the **294** trimer in NPs with pluronic F127.

In 2022, Wang *et al.*[88] designed an ethenylene-bridged BODIPYs as NIR-II-band absorbing FTT agents. BODIPYs **296a**,**b** (Fig. 27) were synthesized by the Stille coupling and their crystal structure was investigated. The slip angle between the monomers was 27° and they were linked by intermolecular π–π- and C–F interactions, which promoted a J-aggregation. Due to the presence of a meso-CF_3- group and a tetrahydroquinoxaline donor moieties, the absorption maximum of the D–A–π-A–D dimer **296a** was in the NIR-II region. In aqueous medium the absorption maximum shifted to an even longer wavelength region due to J-aggregation. **296a-NP** nanoparticles encapsulated in F127 exhibited high PCE (62%) and reduced the survival of HeLa cells under laser irradiation with c λ = 1208 nm (0.8 W cm^{-2}, 10 min) to 27% at a concentration of 30 μM. In *in vivo* experiments in mice with an orthotopic model of hepatocellular

Scheme 159

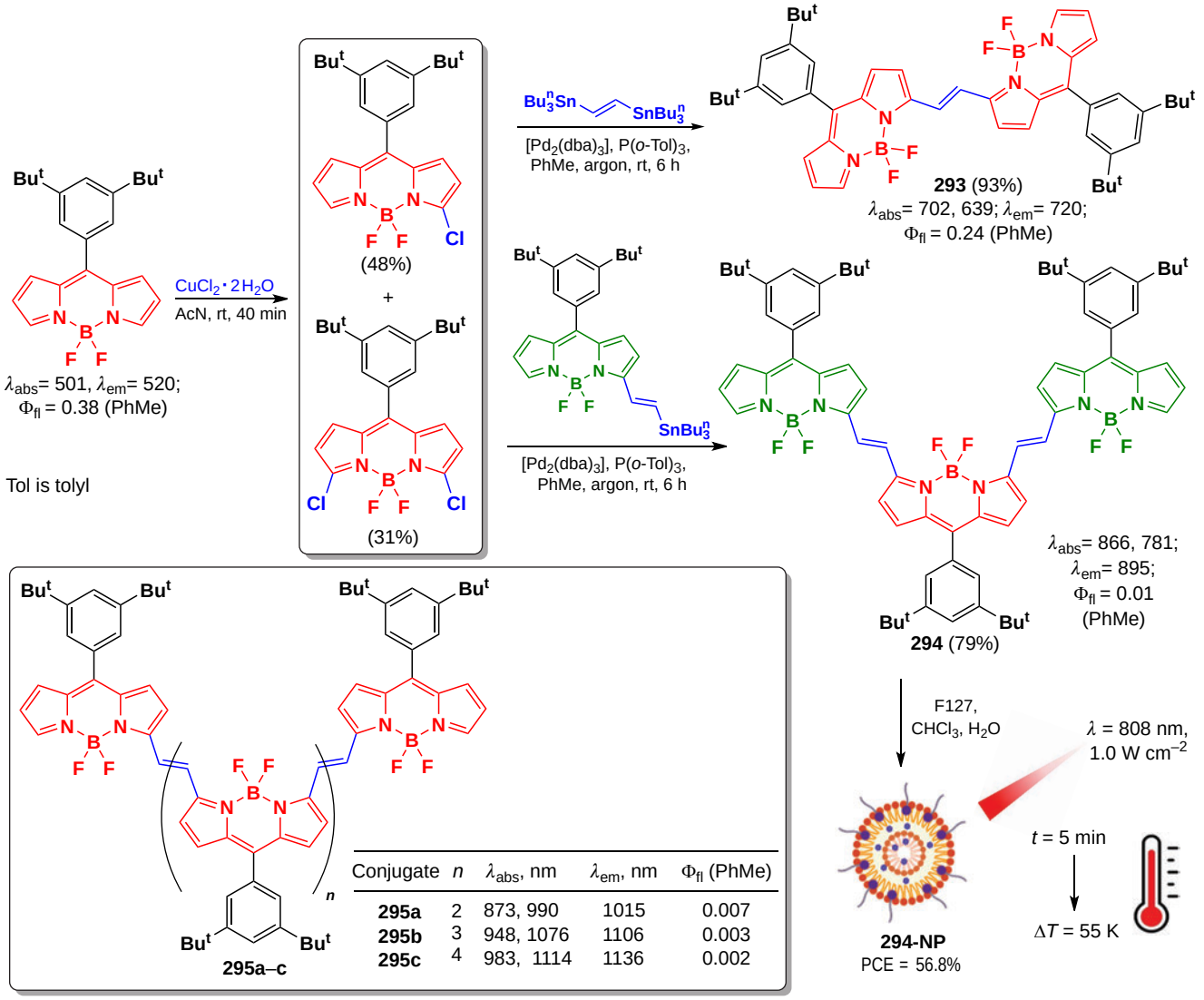

carcinoma, 6 h after intravenous injection of **296a-NP** particles, the maximum photoacoustic signal was observed in the tumor, which was 2–5 times more intense than in other organs. In the *in vivo* therapeutic efficacy study, complete remission was achieved in mice with $4T_1$ tumor after therapy with **296a-NP** and irradiation at λ = 1208 nm.

3.9. Modifications at the boron atom

BODIPY fluorophores discussed above almost always contained two fluoride ligands directly bonded to the boron atom. However, nucleophilic agents can also attack the boron centre to form BR_2 BODIPYs, which are the subject of this section. Although such modifications of the BODIPY core have been less thoroughly studied than the reactions of the pyrirromethene moiety, the functionalization of the boron atom is an important synthetic tool that allows significant modification of the physicochemical and photophysical properties of the products. The introduction of various nucleophilic agents onto the boron atom leads to a significant distortion of the three-dimensional structure of BODIPY and, consequently, to a change in a number of physicochemical properties, such as fluorescence quantum yield, redox potential, laser efficiency, chemical and photochemical stability, and aggregation properties.[10] In 2019, Bodio and Goze[12] published a review dedicated to the modification of BODIPY and its aza-analogues at the boron atom.

3.9.1. Lewis acid catalyzed synthesis of $B(OR)_2$-BODIPY

In 1999, Kim *et al.*[303] synthesized a chiral 4,4-diaryloxy-BODIPY **297** by intramolecular esterification in the presence of a Lewis acid boron tribromide (Scheme 160).

Scheme 160

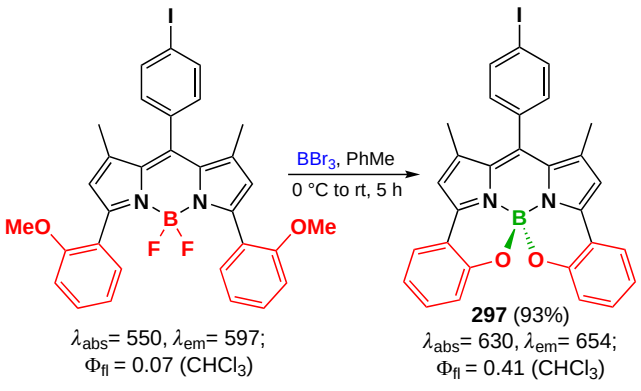

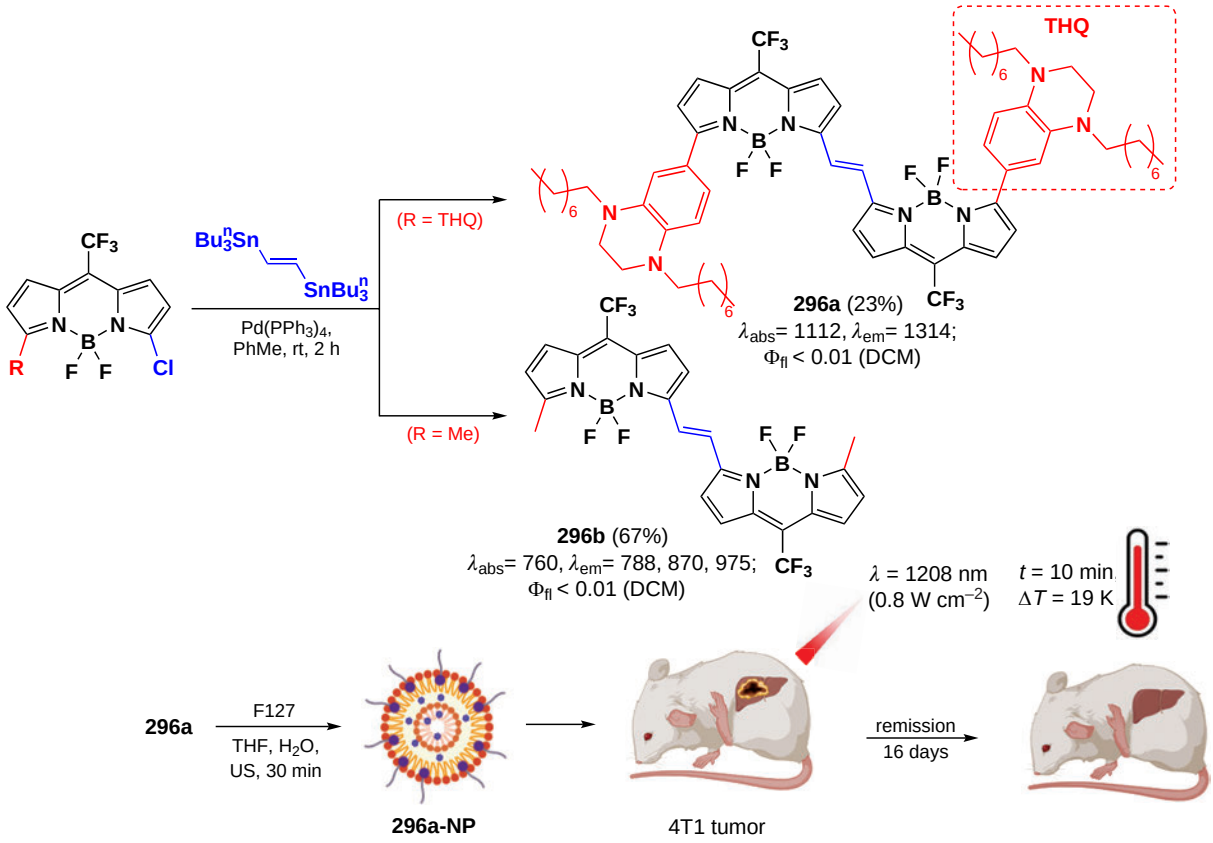

Figure 27. Schematic of the synthesis of BODIPY **296a–b** and the principle of action of **296a-NP** nanoparticles *in vivo*. Figure created by the authors based on the data of the publication[88].

Scheme 161

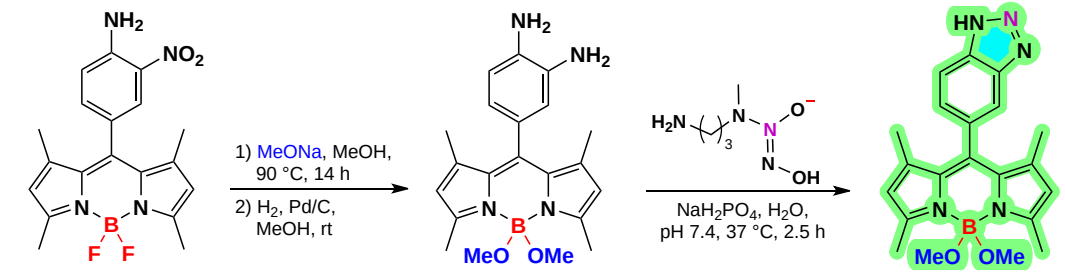

Scheme 162

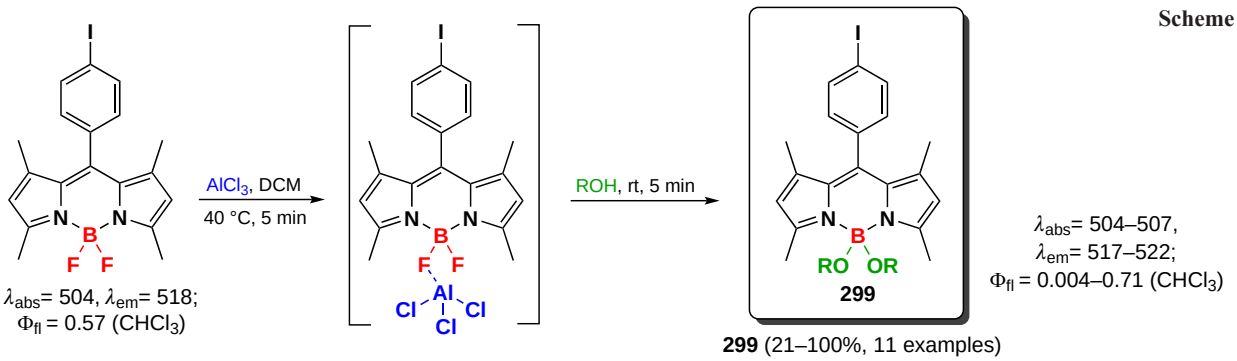

4,4-Dimethoxy-substituted BODIPY **298**, synthesized according to Scheme 161, has been proposed as a fluorescent probe for the detection of NO.[304]

In 2007, Tahtaoui *et al.*[167] proposed a method for the modification of BODIPY with alcohols by the activation of the B–F bond with a Lewis acid ($AlCl_3$), followed by nucleophilic substitution. This resulted in a large series of 4,4-dialkoxy or

Scheme 163

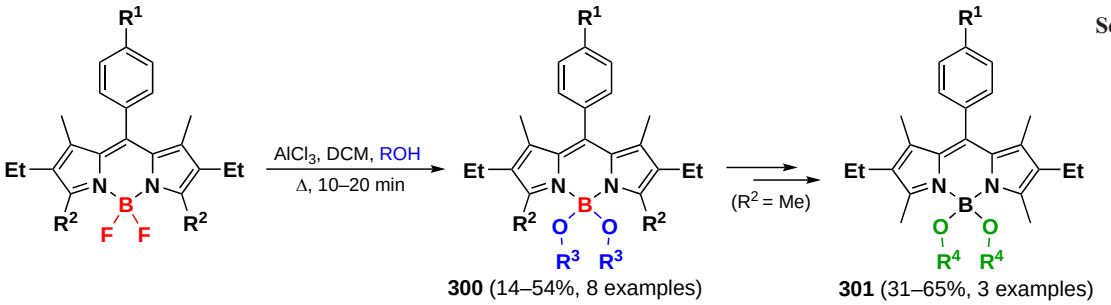

300 (14–54%, 8 examples)

301 (31–65%, 3 examples)

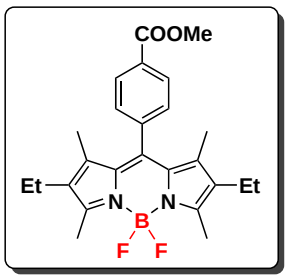

λ_{abs} = 525, λ_{em} = 550;
Φ_{fl} = 0.63 (THF)

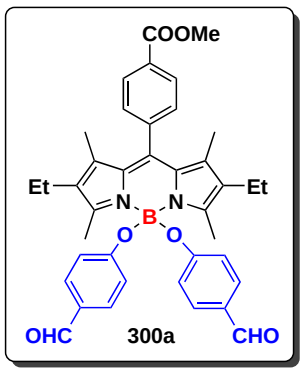

300a

λ_{abs} = 526, λ_{em} = 540;
Φ_{fl} = 0.5 (THF)

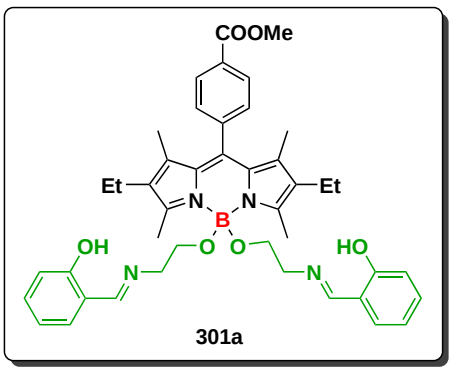

301a

λ_{abs} = 524, λ_{em} = 541;
Φ_{fl} = 0.67 (THF)

Scheme 164

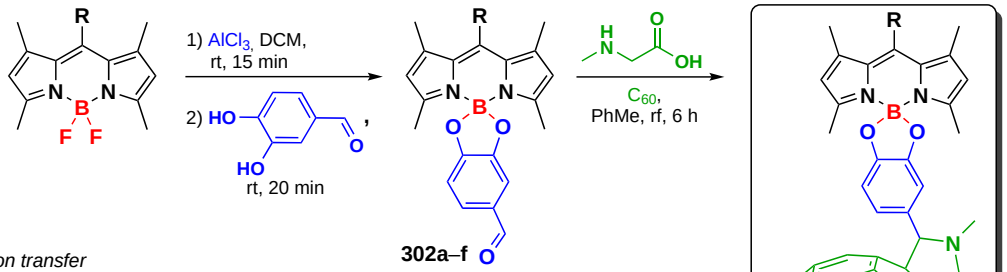

302a–f

303a–f

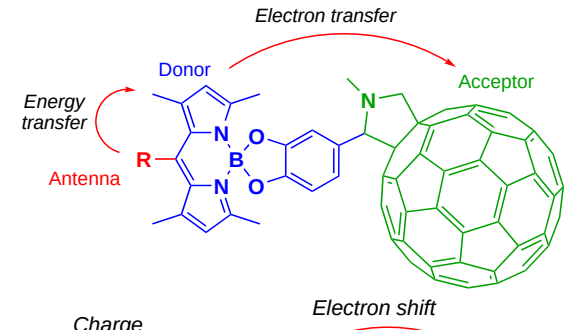

R =

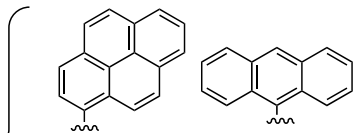

303b **303c**

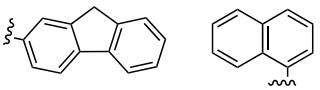

303d **303e**

N	λ_{abs} (PhCN)
303b	328, 350, 500
303c	389, 508
303d	305, 503
303e	312, 505

No emission

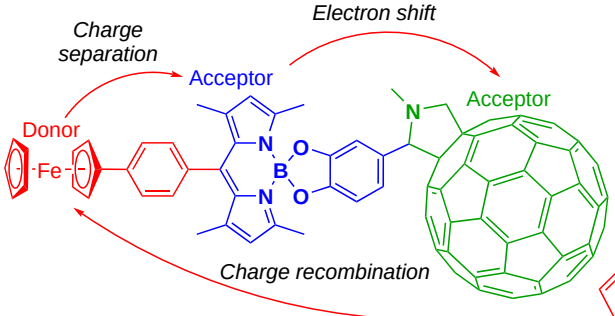

303a
λ_{abs} = 531, 433;
no emission (PhCN)

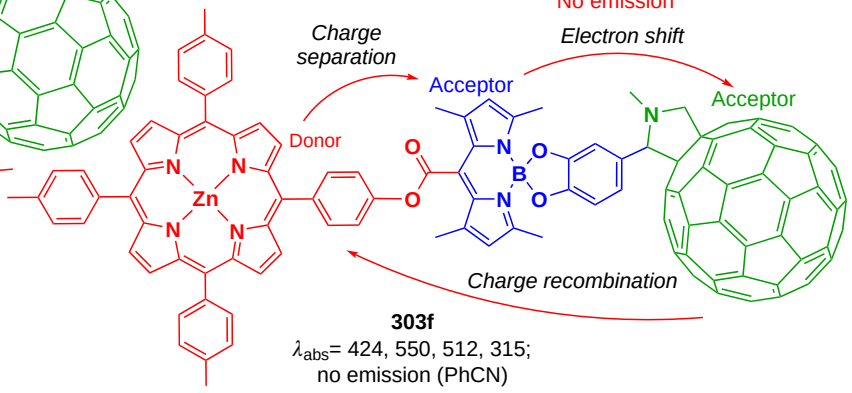

303f
λ_{abs}= 424, 550, 512, 315;
no emission (PhCN)

4,4-diaryloxy derivatives **299** (Scheme 162). This work initiated many subsequent Lewis acid-catalyzed modifications at the boron atom.

A few years later, Brizet *et al.*[307] reported an $AlCl_3$-catalyzed B–O-functionalization of BODIPY to form dialkoxy and diarylalkoxy derivatives **300**, which were then converted to water-soluble compounds **301a–c** (Scheme 163).

It is worth noting that boron-modified BODIPYs are of interest for the development of molecular switches. In 2010 and 2011, Wijesinghe *et al.*[306,307] created a donor–BODIPY–fullerene (**303a**) and an antenna–BODIPY–fullerene (**303b–e**) triads based on derivative **302**. Using femtosecond and nanosecond transition-state spectroscopy, the ability of such systems to form charge-separated particles was demonstrated: $Fc^{+\bullet}$–BDP–$[C_{60}]^{-\bullet}$ (Fc — ferrocenyl) for the triads **303a** and antenna–$BDP^{+\bullet}$–$[C_{60}]^{-\bullet}$ for the triads **303b–e**.

A similar triad donor–BODIPY–acceptor **303f** based on porphyrin (Por), BODIPY and fullerene was described by D'Souza *et al.*[14] in 2017 (Scheme 164). Using femtosecond and nanosecond flash photolysis, ultrafast energy transfer from the singlet excited state of BODIPY to the fullerene moiety was registered, along with the formation of the triad ZnPor–BODIPY–$^1[C_{60}]$* and then the triplet state ZnPor–BODIPY–$^3[C_{60}]$*. Selective excitation of the porphyrin fragment in the triad led to an electron transfer to the fullerene fragment, along with the formation of $ZnP^{+\bullet}$–BODIPY–$[C_{60}]^{-\bullet}$.

In 2012, Brizet *et al.*[308] presented dyads **304** and **305** consisting of BODIPY and porphyrin fragments capable of charge transfer from the former to the latter upon complexation with zinc (Scheme 165).

In 2014, Umeda *et al.*[309] proposed the use of aryloxy derivatives of BODIPYs **306** as photoremovable protecting groups. Photoactivated release of histamine from BODIPY **307** was observed under green light irradiation in HeLa cells (Scheme 166).

3.9.1.1. Synthesis of chiral $B(OR)_2$-BODIPY

Circularly polarized luminescence (CPL) is a differential emission of right- and left-circularly polarized light by chiral luminescent systems. CPL is quantitatively estimated by the luminescence dissymmetry coefficient g_{lum}, whose values range from –2 to +2 (right- and left-polarized emission).[310,311] Modification of BODIPY at the boron atom with chiral alcohols opens a way to the development of highly fluorescent CPL-active compounds.

The synthesis and chiroptical properties of chiral BODIPYs **308a**,**b** modified at the boron atom with (*R*)- and (*S*)-1,1′-bi-2-naphthols (BINOL) were first described by Moya *et al.*[312] in 2014 (Scheme 167). The ^{1}H nmR spectroscopy data indicated the diastereotopicity of the methylene group protons (ABX_3 spin system), and the CD spectra showed mirror dichroic signals at ~525 nm. The g_{lum} values were shown to be +0.00071 and −0.00085 for compounds **308a** and **308b**, respectively.

In 2015, Zhu *et al.*[313] presented similar BINOL-modified BODIPYs **309a**,**b** (Scheme 167). The CD spectra of the enantiomers contained mirror signals at 630 nm and g_{lum} values were ±0.002. In 2017, Moya *et al.*[314] studied the CPL for BINOL-substituted BODIPYs **310a**,**b**, which had higher fluorescence quantum yields than the previously described compounds **308a**,**b** and were able to produce circularly polarized laser emission.

In 2019, Moya *et al.*[315] demonstrated that ICT from the BINOL moiety to the BODIPY has a significant effect on the

Scheme 165

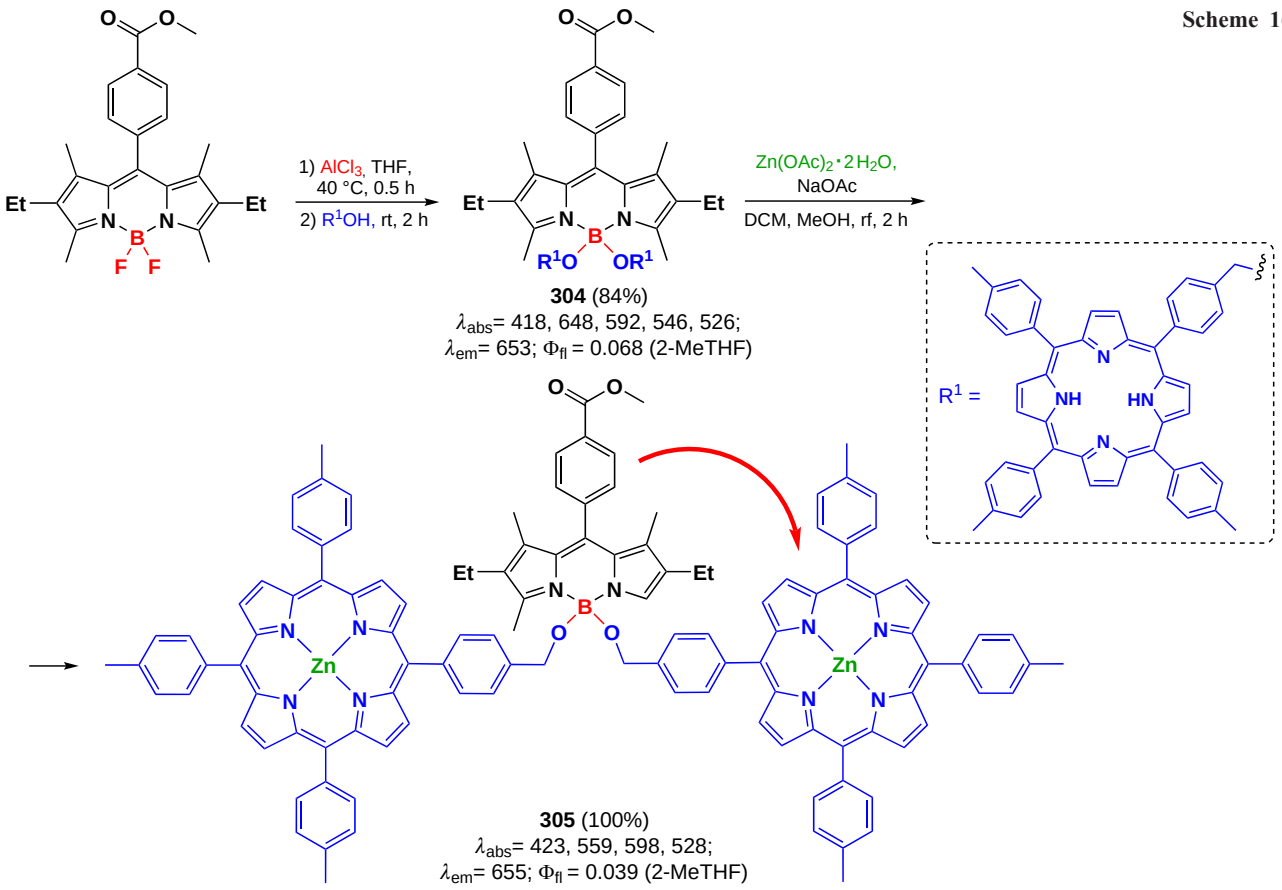

Scheme 166

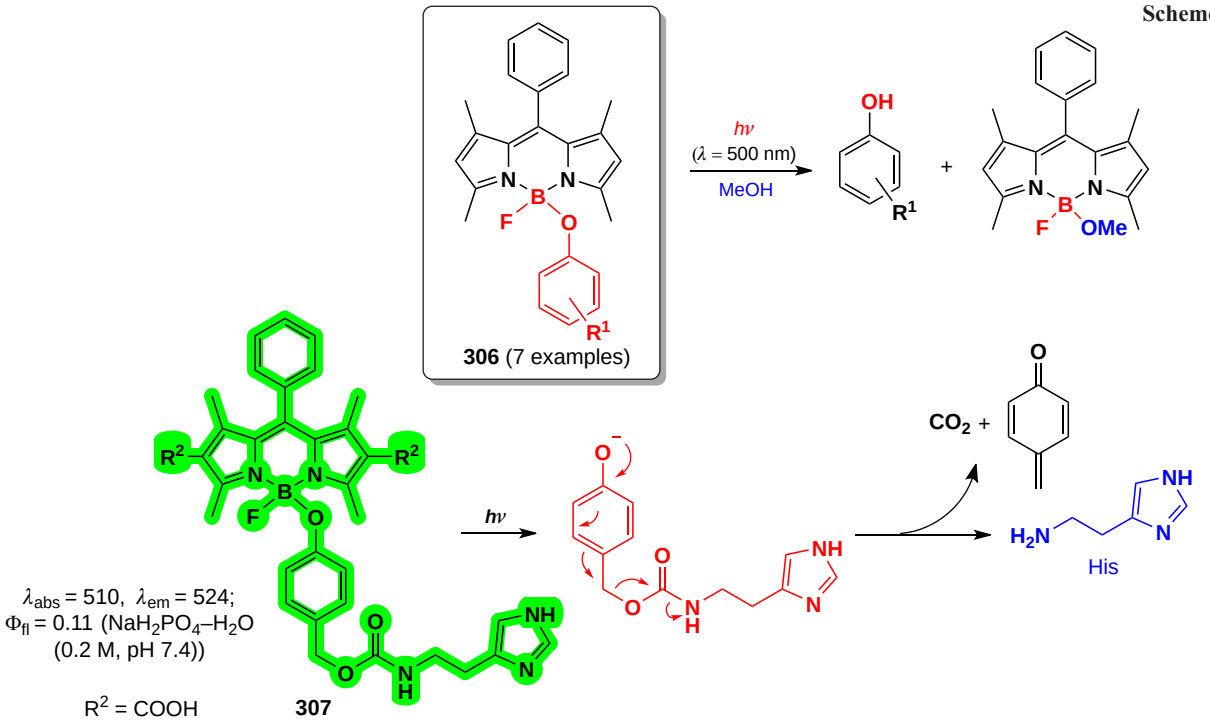

Scheme 167

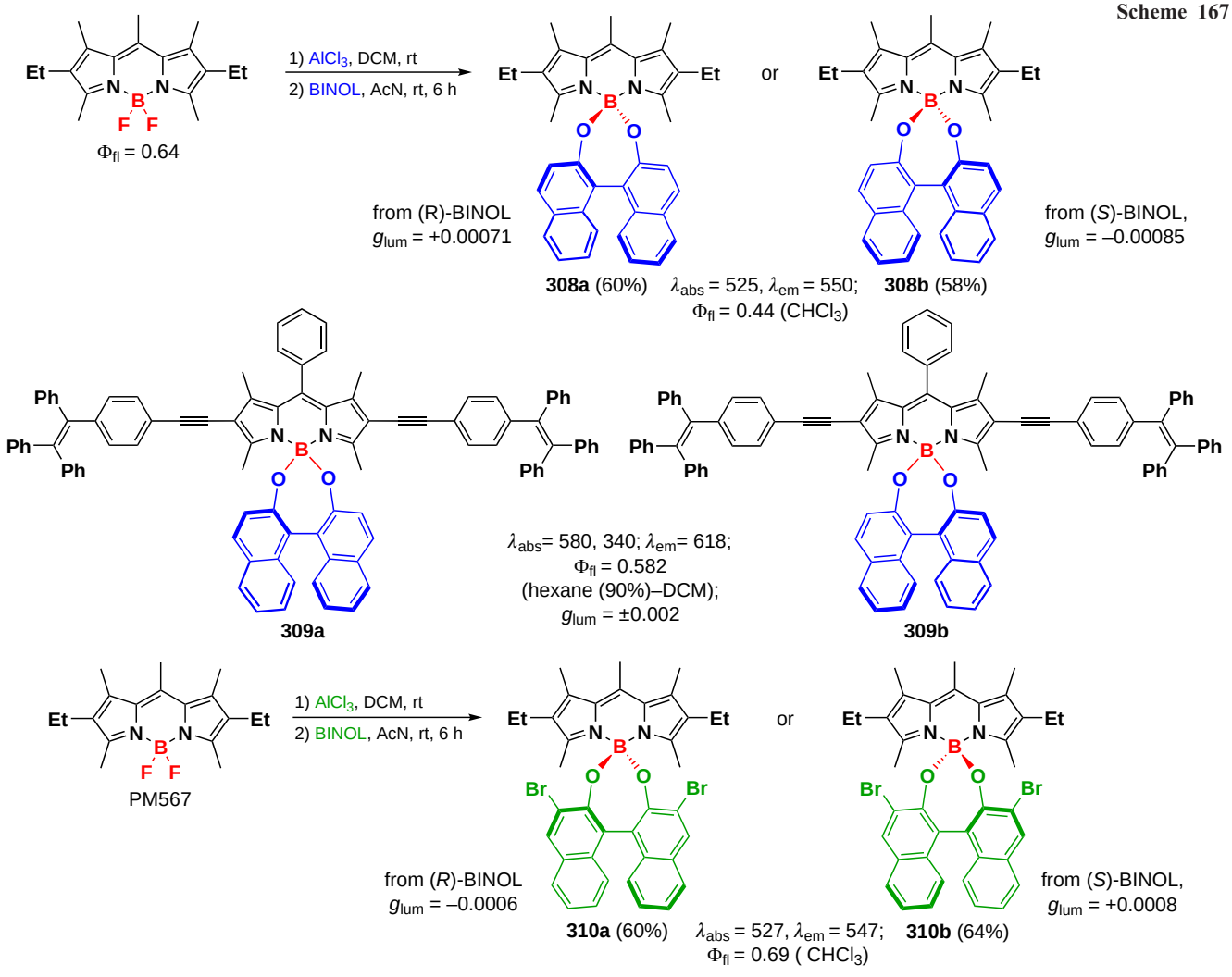

Scheme 168

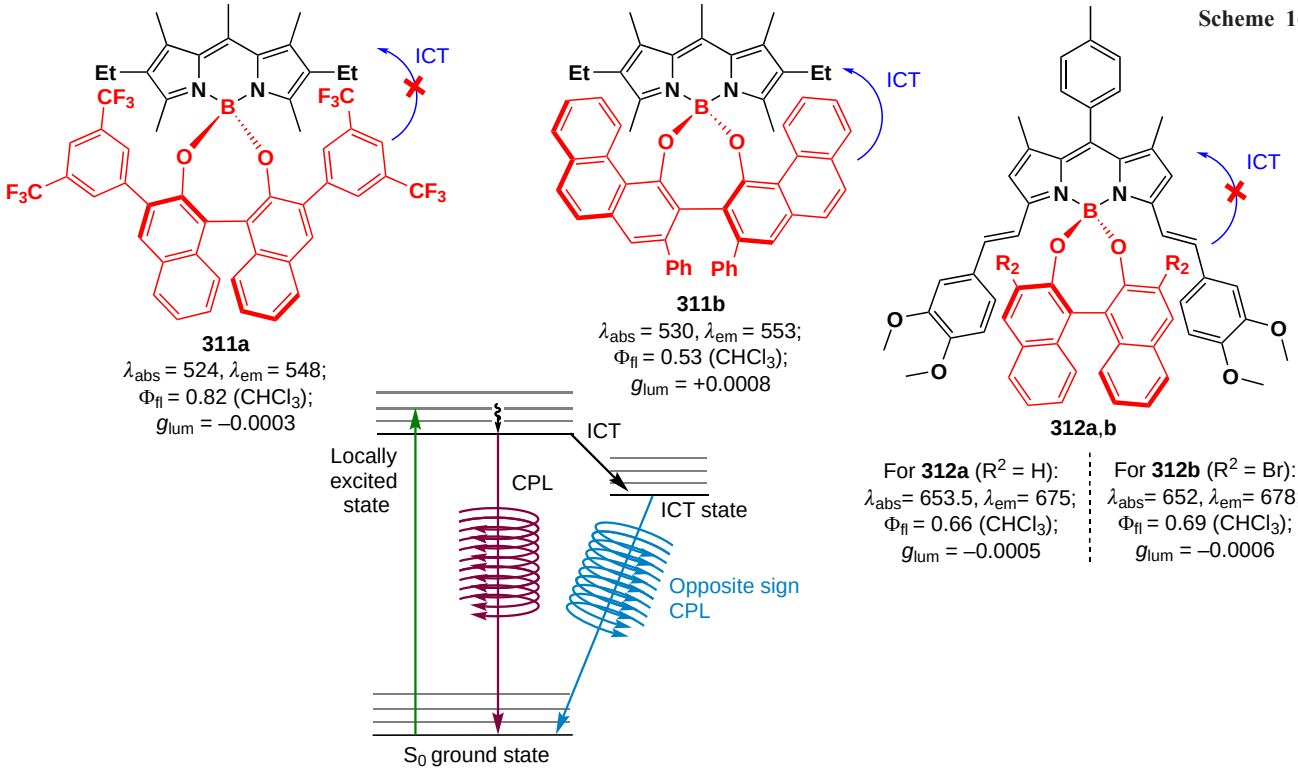

sign of CPL (Scheme 168). Thus, BODIPYs **308** and **310** show opposite g_{lum} values due to a strong ICT effect in BODIPY **308** and its absence in BODIPY **310** with BINOL containing a bromine atom substituent at the boron atom. A comparison was made of the chiroptical properties of BODIPY **311a** with trifluoromethyl groups, which is incapable of ICT, and BODIPY **311b** with a 2,2′-diphenyl-4-biphenanthrol (VAPOL) moiety, which is capable of ICT. The CD spectrum of compound **311a** contained a negative visible band in chloroform solution, and the spectrum of the derivative **311b** contained a positive visible band. At the same time, distyryl-BODIPYs **312a**,**b**, which are not capable of ICT due to the presence of electron-donating methoxy groups, had an identical negative sign in the CD and the CPL spectra.

As a follow-up to this study, in 2021, Moya *et al.*[316] described NIR-absorbing chiral BODIPYs **313a**,**b** with g_{lum} values +0.0016 (at λ = 780 nm) and –0.001, respectively (Scheme 169). Compound **314** showed a greater ICT effect than its analogue **313a** due to the presence of a quaternized nitrogen atom. ICT included a charge transfer from the BINOL moiety to the BODIPY.

In 2016, Hall *et al.*[317] synthesized chiral BODIPYs **315a,b** using the reaction sequence illustrated in Scheme 170. 3,5-di(2-methoxyphenyl) derivatives **316a,b** were synthesized using a cross-coupling reaction, and then the methoxy moieties were demethylated with BBr_3, resulting in the meso-aryl analogues **317a**,**b**. The luminescence dissymmetry factors $|g_{lum}|$ were shown to be 0.0033–0.0047 for BODIPYs **315a**,**b** and **317a**,**b**, and compound **315a** demonstrated a record high $|g_{lum}|$ value, along with bright fluorescence, equal to 0.0047 and 0.65, respectively.

Scheme 169

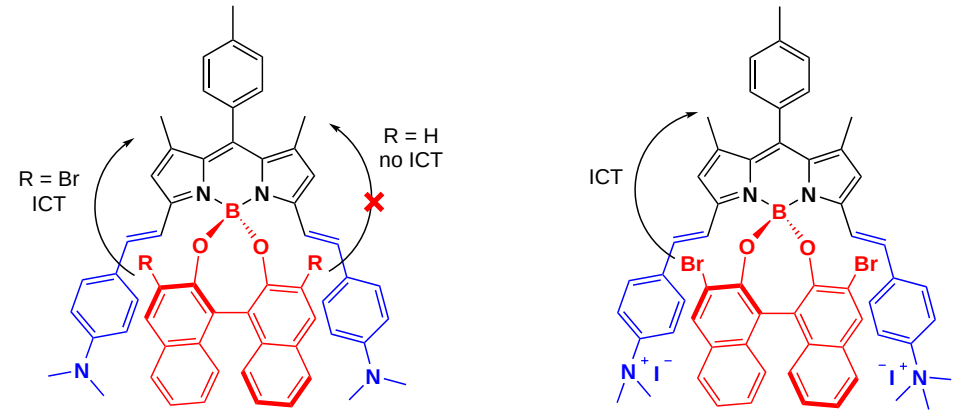

Scheme 170

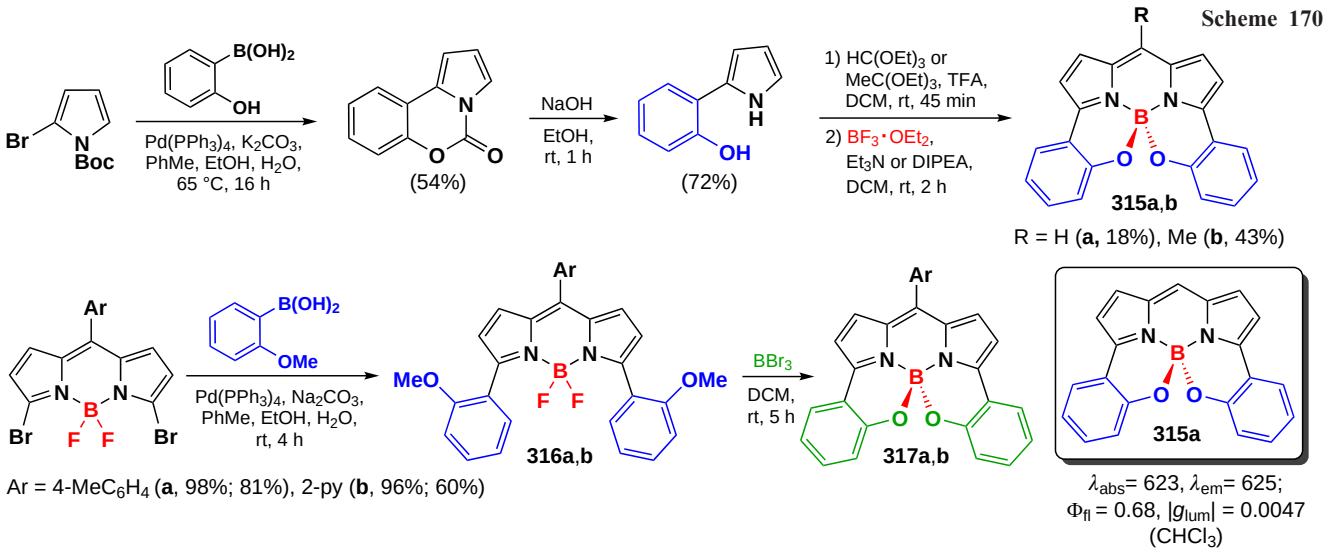

In 2017, Hall *et al.*[318] isolated an unexpected product **318′** while preparing a similar chiral BODIPY. Presumably, this compound is formed as a result of a sequence of transformations: substitution of the BF_2 group by the boron atom of (2-hydroxyphenyl)boronic acid, nucleophilic aromatic substitution (S_NAr) of the bromine to the phenolic hydroxy group, Suzuki coupling with a second equivalent of (2-hydroxyphenyl)boronic acid, and chelation of the boron atom by the free phenolic hydroxy group (Scheme 171). It is worth noting that the target BODIPY **318** can be prepared by another route (see Scheme 172 below).[319]

In 2023, the same research group[319] presented an optimized route to the synthesis of helical chiral N,N,O,C-BODIPY **319** from the corresponding dipyrromethenes (Scheme 172). It was also noted that Pd^{2+} is the key catalyst for the boron metathesis (see Scheme 171). The photophysical and chiroptical properties

Scheme 171

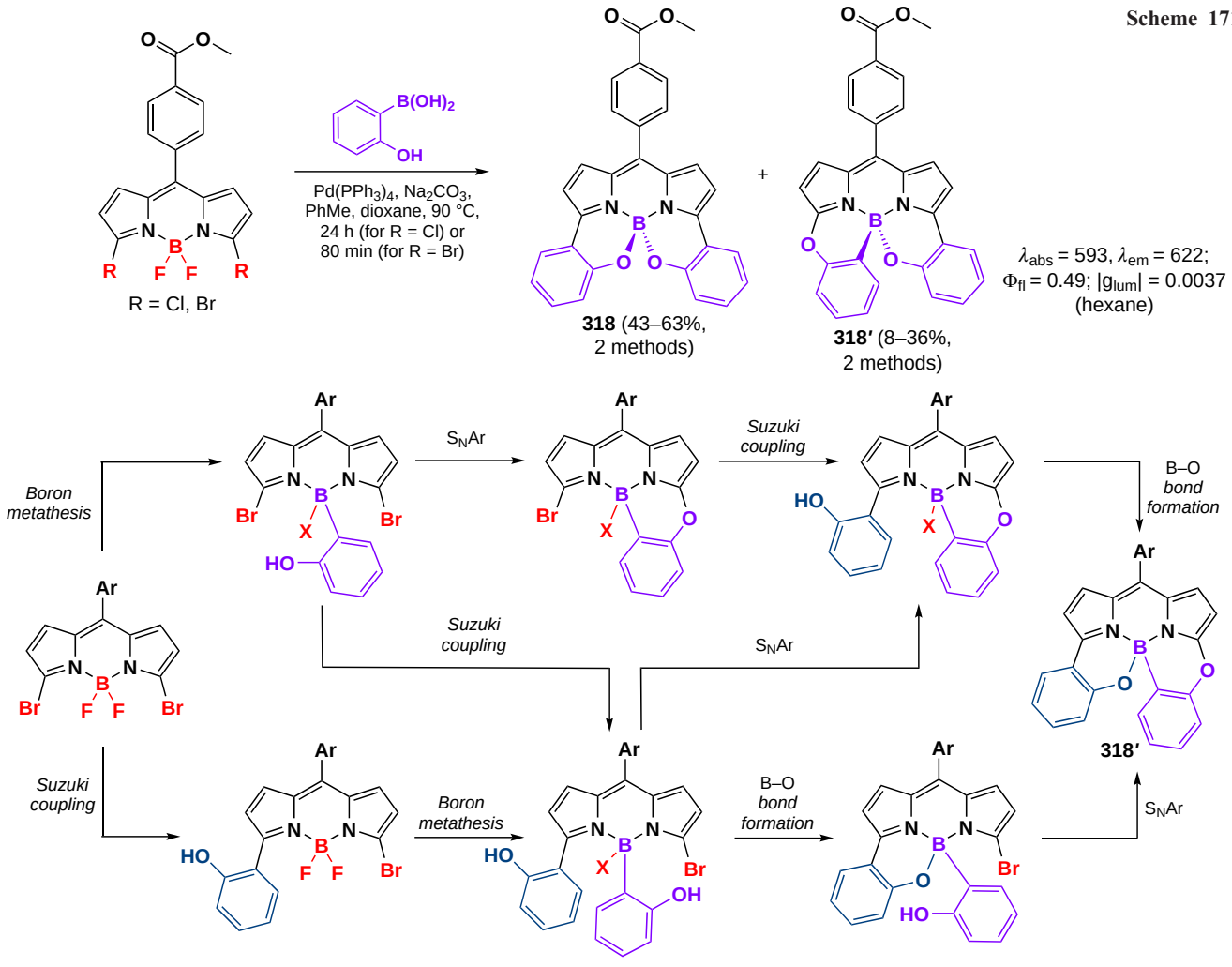

Scheme 172

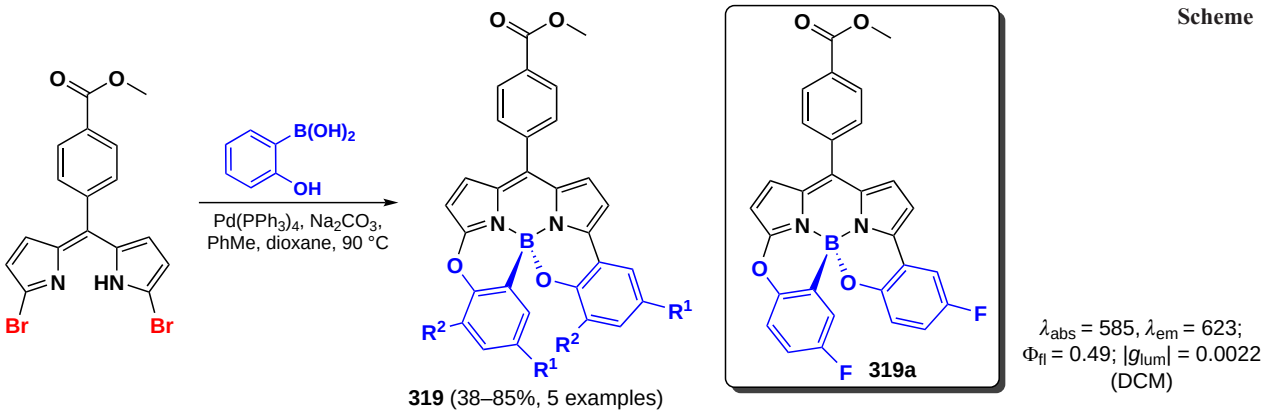

of this series of BODIPYs were almost identical to those of the previously described compound **318′**.

3.9.2. Synthesis of $B(OR)_2$- and ^{18}F-BODIPY using B(F)(OTf)-derivatives

In 2008, Hudnall and Gabbaï[320] suggested using boronium cations of BODIPY as sensors for the detection of fluoride anions (Scheme 173). The starting BODIPY (R = Me) was reacted with TMSOTf to form an unstable, moisture-sensitive salt **320a**, which rapidly reacted with 4-dimethylaminopyridine (DMAP) to give a stable monosubstituted salt **321**.

The salt **321** showed a 5-fold increase in fluorescence in the presence of fluoride anion with tetra-n-butylammonium fluoride due to the nucleophilic substitution of the DMAP moiety by the fluoride anion. However, the increase in fluorescence in the presence of chloride and bromide anions was significantly smaller (a 48% increase in fluorescence quantum yield was observed with bromide ions, and a 6% increase with chloride ions). The presence of iodide anion led to the fluorescence quenching due to the 'heavy atom' effect. Inspired by this result, Mazitschek *et al.*[321] in 2012 utilized the rapid exchange reaction of 4-dimethylaminopyridine with $^{18}F^-$ to obtain a labelled BODIPY **322a** proposed for fluorescence imaging and PET diagnostics (see Scheme 173). The authors proposed an alternative method in which TMSOTf efficiently displaced one fluoride anion of BODIPY in quantitative yield in less than 5 min at 0°C, and the subsequent addition of $^{18}F^-$ instantly converted the intermediate to the ^{18}F-labeled substrate **322a**. A ^{18}F-labeled NHS-activated ester **322** obtained by a similar procedure was used to label the antitumor drug trastuzumab, thereby demonstrating the potential of BODIPY derivatives for fluorescence imaging, PET diagnostics, and theranostics.

In 2014, Mazitschek *et al.*[322] applied their approach to the synthesis of water-soluble BODIPYs **323** to create highly fluorescent biological sensors (Scheme 174).

The resulting dyes were demonstrated to have the same optical properties as the starting BODIPYs, along with higher

Scheme 173

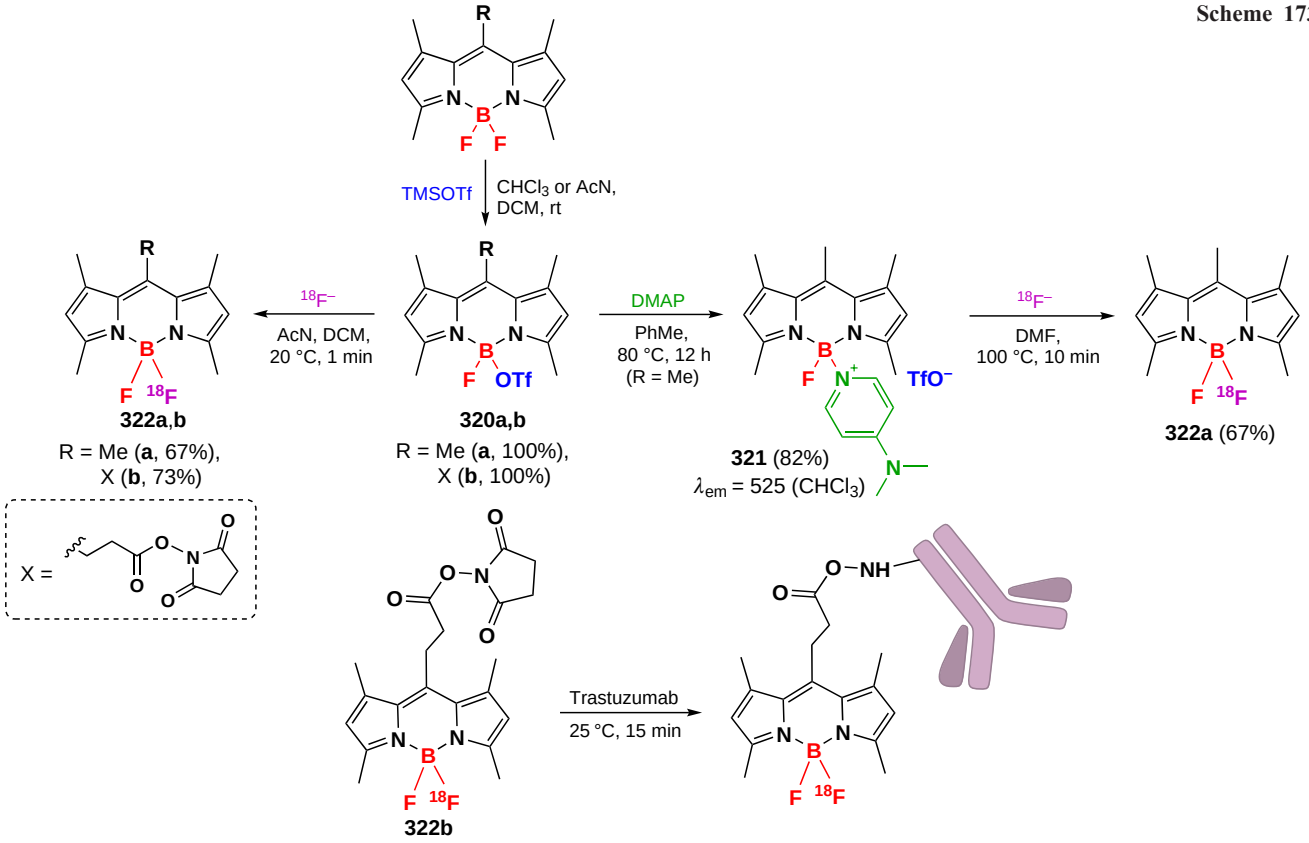

Scheme 174

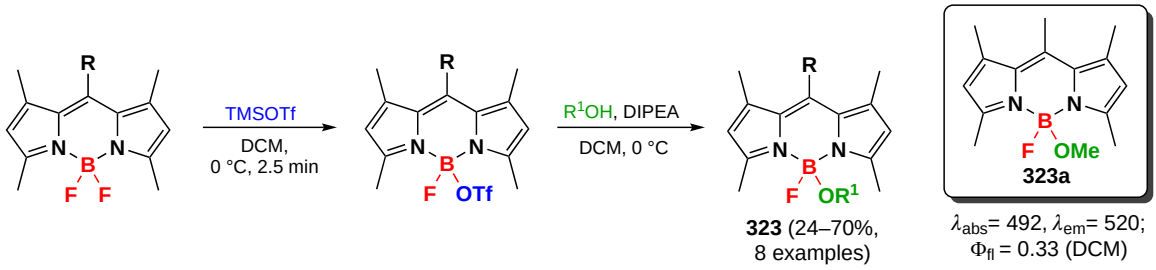

Scheme 175

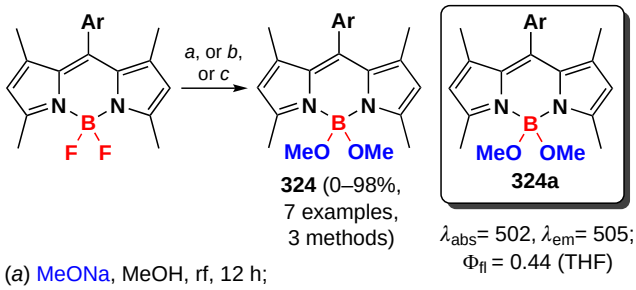

(*a*) MeONa, MeOH, rf, 12 h;
(*b*) 1) $AlCl_3$, DCM, rf, 15 min; 2) MeOH, rf, 15-30 min;
(*c*) 1) TMSOTf, PhMe, rf, 30 min; 2) MeOH, DIPEA, rt, 1 h;
Ar = Ph, 3,4-$(MeO)_2C_6H_3$, 4-$MeO_2CC_6H_4$

lipophilicity. Compounds **323** showed an increased cellular accumulation and cytotoxicity compared to the starting BODIPYs.

In 2015, Vicente *et al.*[50] used computer simulations to compare three approaches to the nucleophilic substitution at the boron atom to obtain products **324** (Scheme 175).

Since the substitution reactions involve the formation of the boronium cation, the Gibbs free energies of its formation from BODIPY under the conditions corresponding to each method were calculated using DFT modelling. For method *a*, direct dissociation of the fluoride ion from BODIPY was proposed. It occurs in methanol due to its high permittivity; the calculated energy barrier was 37 kcal mol^{-1}. For method *b*, the formation of a counterion, $AlCl_3F^-$, which stabilizes the boronium cation, was proposed. In the case of method *c*, fluoride elimination leading to a salt of the boronium cation with the triflate anion was suggested; the potential energy barrier of 25 kcal mol^{-1} for this reaction can be easily overcome by boiling the reactants in toluene.

3.9.3. Synthesis of BR_2-BODIPY *via* BCl_2-derivatives

In 2012, Lundrigan *et al.*[323,324] developed a method for the synthesis of 4,4-dichloro-BODIPY **325a**,**b** under an inert atmosphere with BCl_3. The corresponding dichloro-derivatives were stable under an inert atmosphere, and were found to undergo nucleophilic substitution reactions at the boron atom with both O- and C-nucleophiles under milder conditions. These conditions resulted in the formation of products **326**–**330** at a higher yield than that observed with the difluoro analogues. (Scheme 176).

Scheme 176

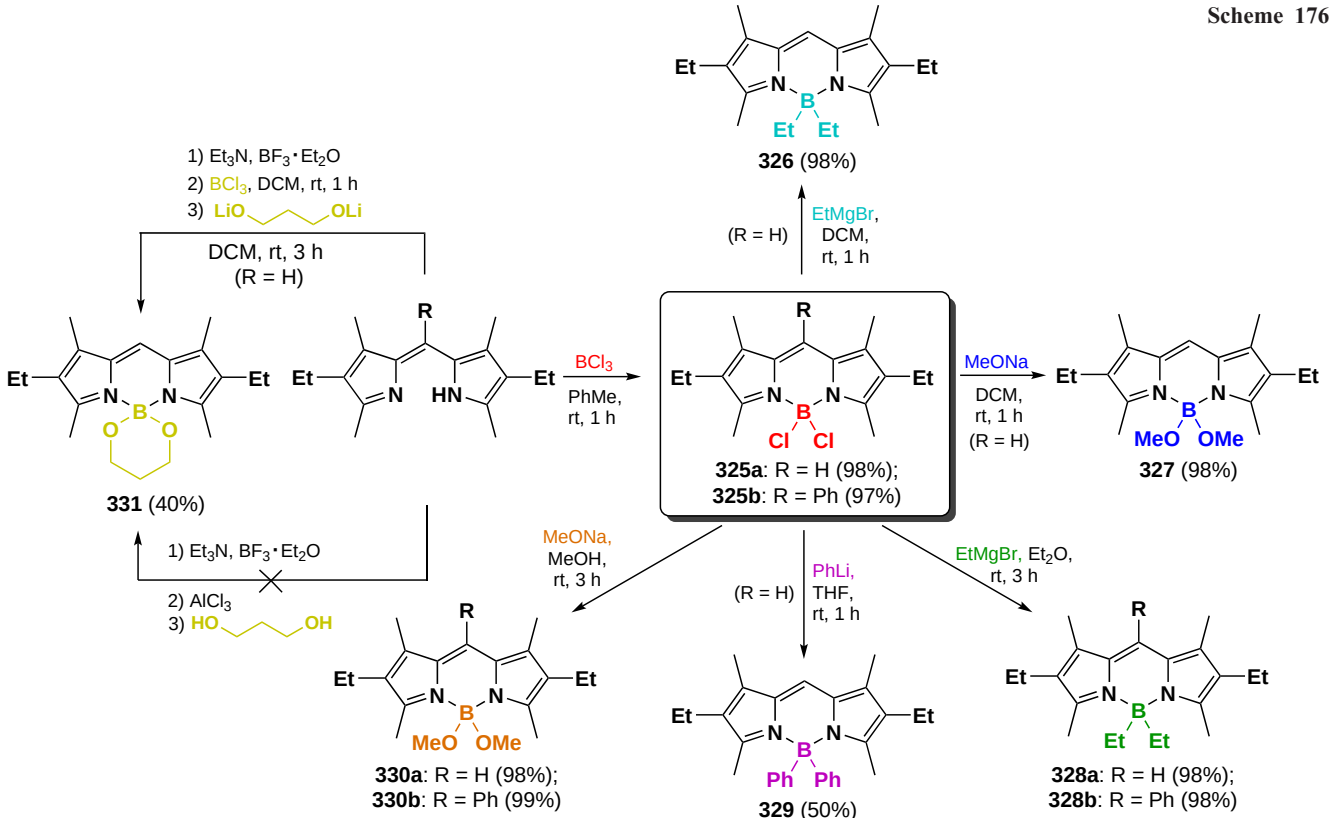

Scheme 177

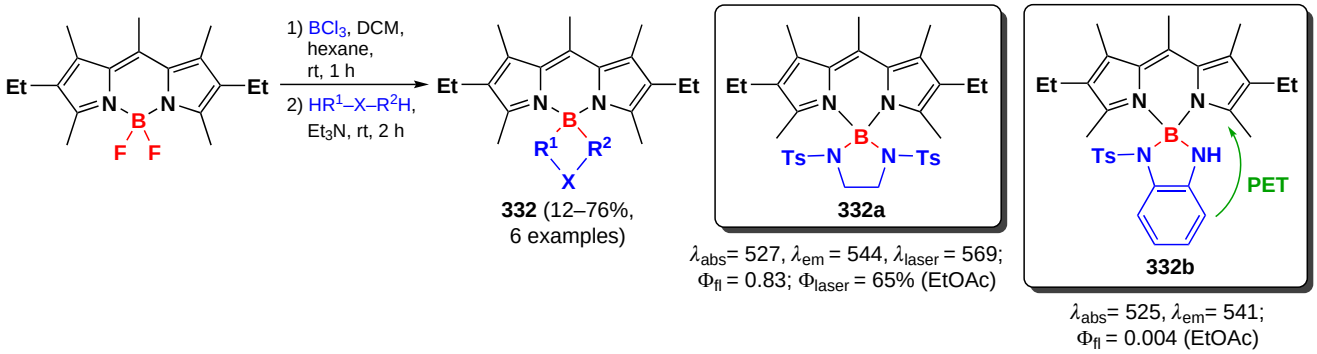

Scheme 178

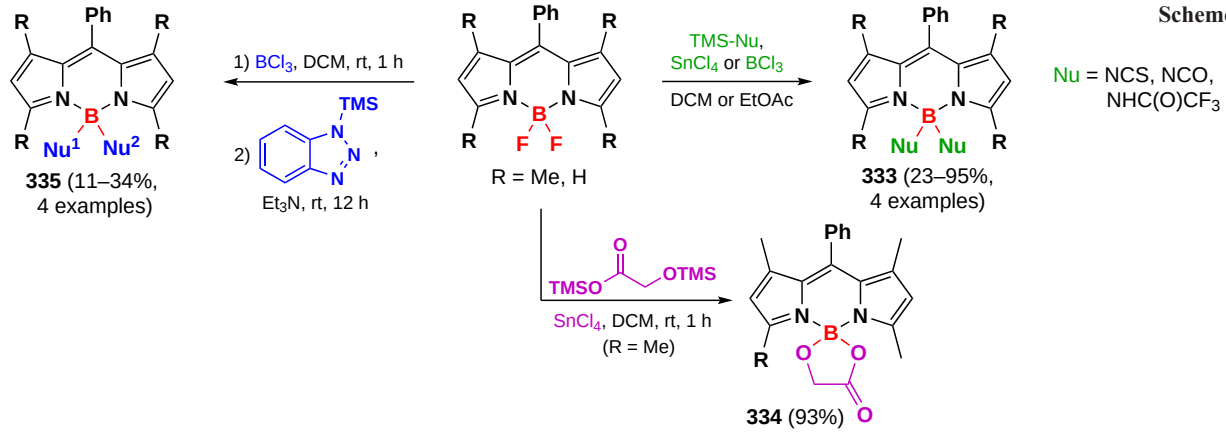

Nucleophilic attack by such a strong nucleophilic agent as a Grignard reagent occurred under the chosen conditions only at the boron atom, without affecting the substituted BODIPY core. A reaction with lithium dienolate was also carried out to obtain the *O*,*O*-ester BODIPY **331**. The direct synthesis of these compounds from the difluoro derivative under the previously proposed conditions[167] using aluminium chloride catalysis did not lead to the target molecule.

In 2017, Ray *et al.*[325] modified the boron atom of BODIPY with N- nucleophiles using a one-pot reaction with initial treatment of the substrate with BCl_3 (Scheme 177).

N,N-BODIPYs **332** exhibited bright fluorescence even in the solid state, as well as a noticeable laser efficiency exceeding that of the starting difluoro derivative. Compound **332b** showed a weak fluorescence due to PET. Since the chelation reaction of metal cations Co^{2+}, Fe^{2+}, Fe^{3+}, and Cr^{3+} led to the disruption of

Scheme 179

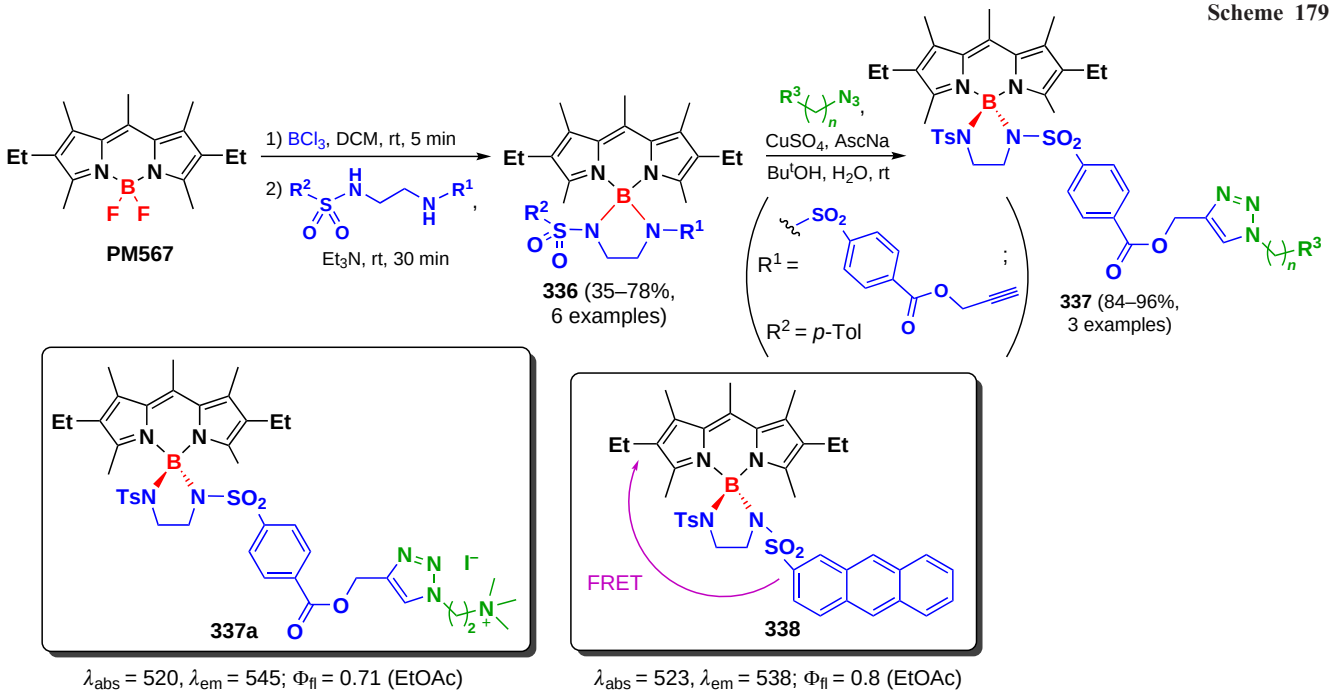

Scheme 180

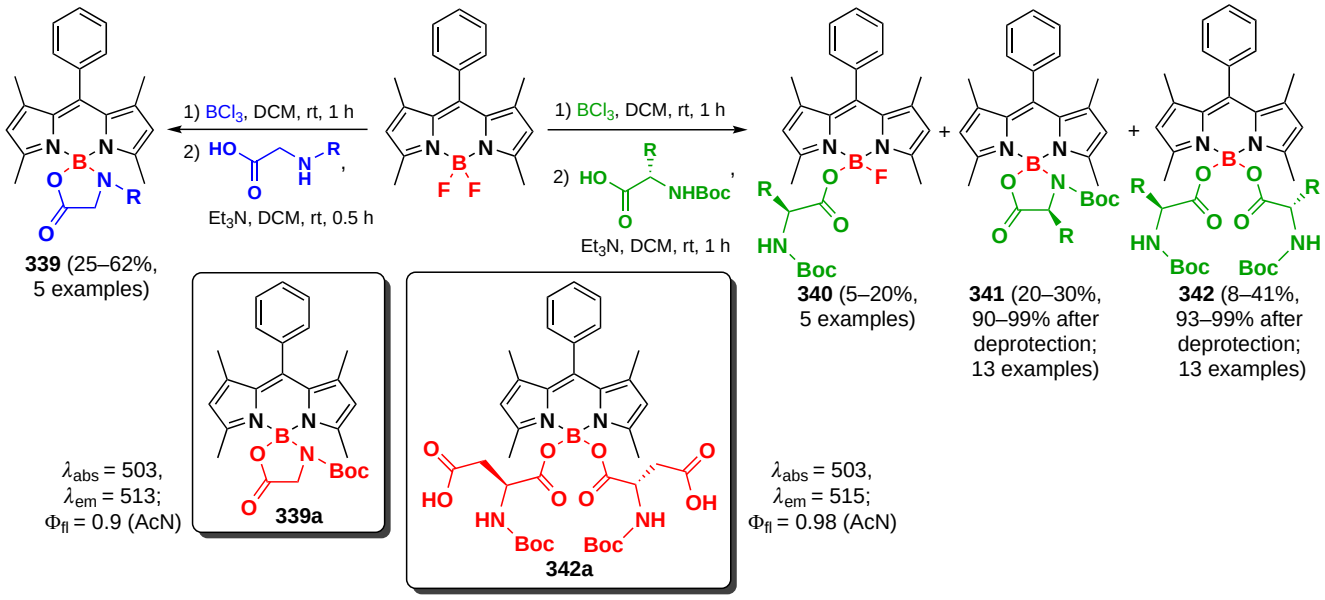

PET and to the enhancement of emission, BODIPY **332b** was suggested as a fluorescent cation sensor.

In 2018, Zhang *et al.*[326] proposed a modification at the boron atom with N- or O-TMS nucleophiles in the presence of Lewis acids. Using such reactions, which involve the *in situ* formation of BCl_2 derivatives, benzotriazole and trifluoroacetamide derivatives of BODIPYs **333**–**335** were obtained (Scheme 178).

In 2021, Ray *et al.*[327] described N,N-substituted boron BODIPYs **336** containing an alkynyl moiety, which allowed such compounds to be introduced into a click reaction to form BODIPY derivatives of triazoles **337** (Scheme 179). The ability to accumulate in the mitochondria of PANC-1 cells was shown for compound **337a**. In 2023, the same research group[328] presented unsymmetrical N,N-BODIPYs with naphthalene, camphor fragments, and morpholine fragments targeting lysosomes. The derivative **338** with an anthracene moiety exhibited FRET (fluorescence resonance energy transfer) with complete energy transfer from the anthracene moiety to the BODIPY, as indicated by absorption and fluorescence spectra.

In 2019, Wang *et al.*[329] introduced N-protected amino acid fragments to the boron atom of BODIPY by *in situ* formation of BCl_2-BODIPY (Scheme 180). Derivatives **339** and **340** had a slightly increased fluorescence quantum yield compared to that of the initial F,F-BODIPY due to the enhanced rigidity around the spirocyclic boron atom.

In 2021, the same research group synthesized B-spiro derivatives **341** and BODIPYs **342**, containing two amino acid fragments of histidine, lysine, arginine, aspartic acid, tyrosine, serine, glutamine and methionine, as well as tripeptide $(Gly)_3$-BODIPY (see Scheme 180). All synthesized α-amino acids with a BODIPY fragment demonstrated higher fluorescence quantum yields ($\Phi_{fl} \sim 0.9$) than the original BF_2-BODIPY ($\Phi_{fl} = 0.61$), and N,O-bidentate spiro-Arg- and spiro-His derivatives showed toxicity on human HEP2 cells ($IC_{50} \approx 22$ μM).[330]

In 2020, Moya *et al.*[331] proposed to use the *in situ* forming BCl_2-BODIPYs to synthesise carboxylate derivatives **343**. This approach made it possible to obtain the previously described BODIPYs in higher yields, to introduce different functional groups into the molecule, including the acceptor ones, and also to synthesize previously inaccessible *O*,*O*-spiro derivatives **344** (Scheme 181). Such BODIPYs demonstrated increased laser emission compared to the commercially available dye PM567.

3.9.4. Modification at the boron atom of BODIPY by C-nucleophiles

Modification at the boron atom by strong C-nucleophiles, such as Grignard reagents or organolithium compounds, was first described

Scheme 181

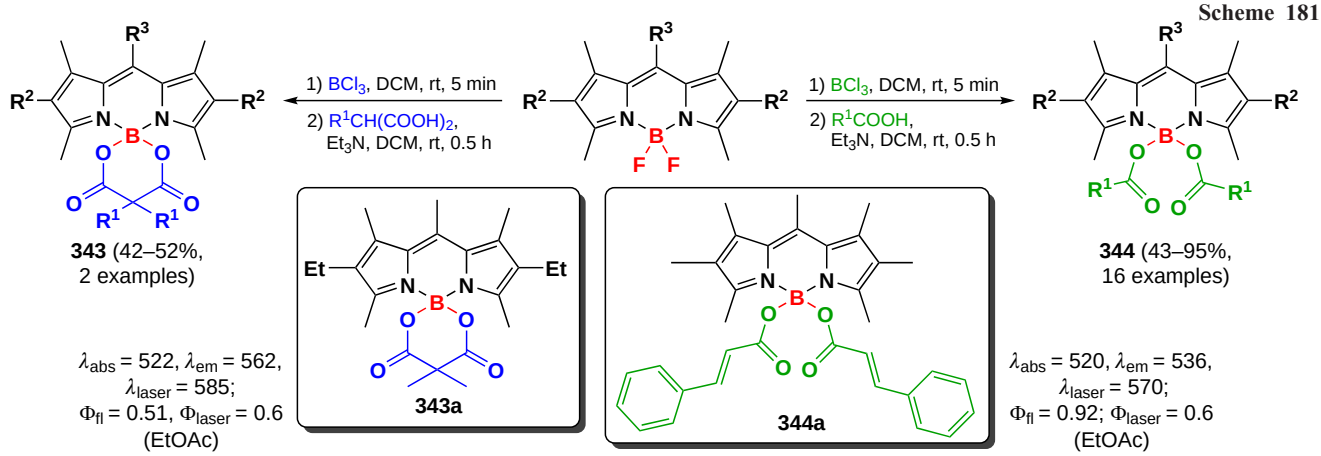

Scheme 182

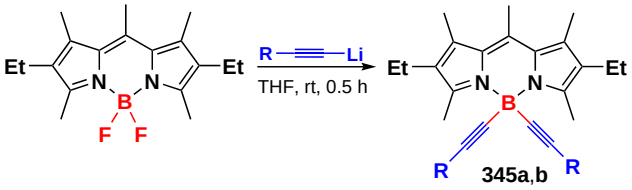

For **345a** (R = *p*-Tol, 62%): λ_{abs} = 516, λ_{em} = 537; Φ_{fl} = 0.95 (DCM)

For **345b** (R = 1-pyrenyl, 30%): λ_{abs} = 516, 371; λ_{em} = 535; Φ_{fl} = 0.94 (DCM)

in 2005. Ulrich *et al.*[332] reported reactions of BODIPY at the boron atom with 4-lithioethynyltoluene and 1-lithioethynylpyrene (Scheme 182). Products **345a**,**b** exhibited large Stokes shifts as well as minimal fluorescence quenching upon coupling with BSA.

In 2006, the same research group[333] demonstrated possibility of monoarylation reactions at the boron atom using 1 equiv. of a Grignard reagent to form compounds **346**, and also the possibility of substitution of both fluorine atoms using 2 equiv. of a Grignard reagent (products **347**). Biaryl derivatives **348** were obtained upon modification with organolithium carbanions. In the same year, dyads **349** capable of rapid energy transfer from the pyrene and the perylene fragments to the BODIPY were presented;[334] contributions from both chromophores were observed in the absorption spectrum of the dyads, while only the BODIPY signal was recorded in the fluorescence spectrum. In 2007, Goeb and Ziessel[335] also modified diisoindolodithienylpyrromethene at the B-center with alkynyl aryl-containing chromophores using a Grignard reagent. The resulting dyad **350a** exhibited a Stokes shift of 7800 cm^{-1} (Scheme 183).

Scheme 183

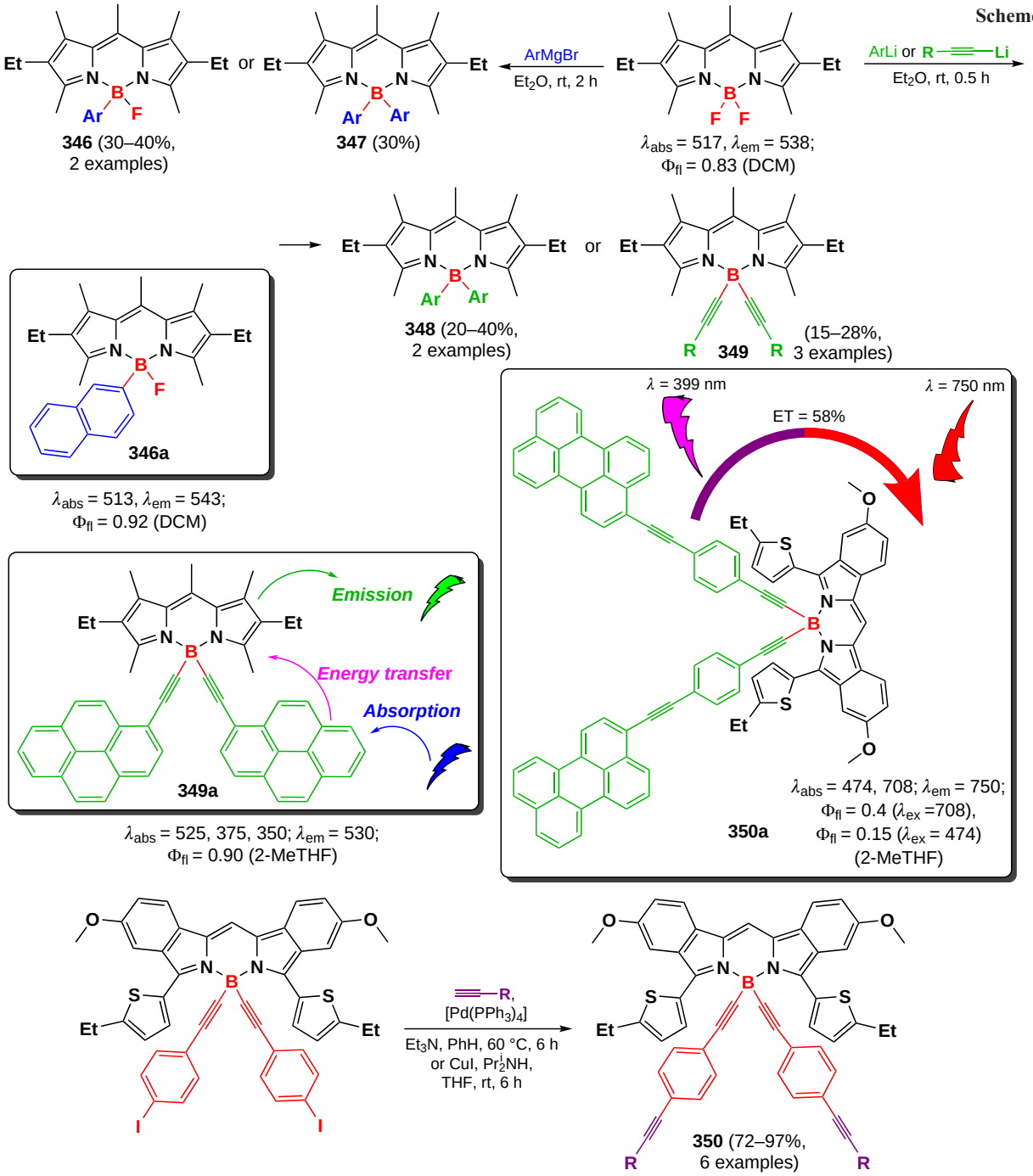

Scheme 184

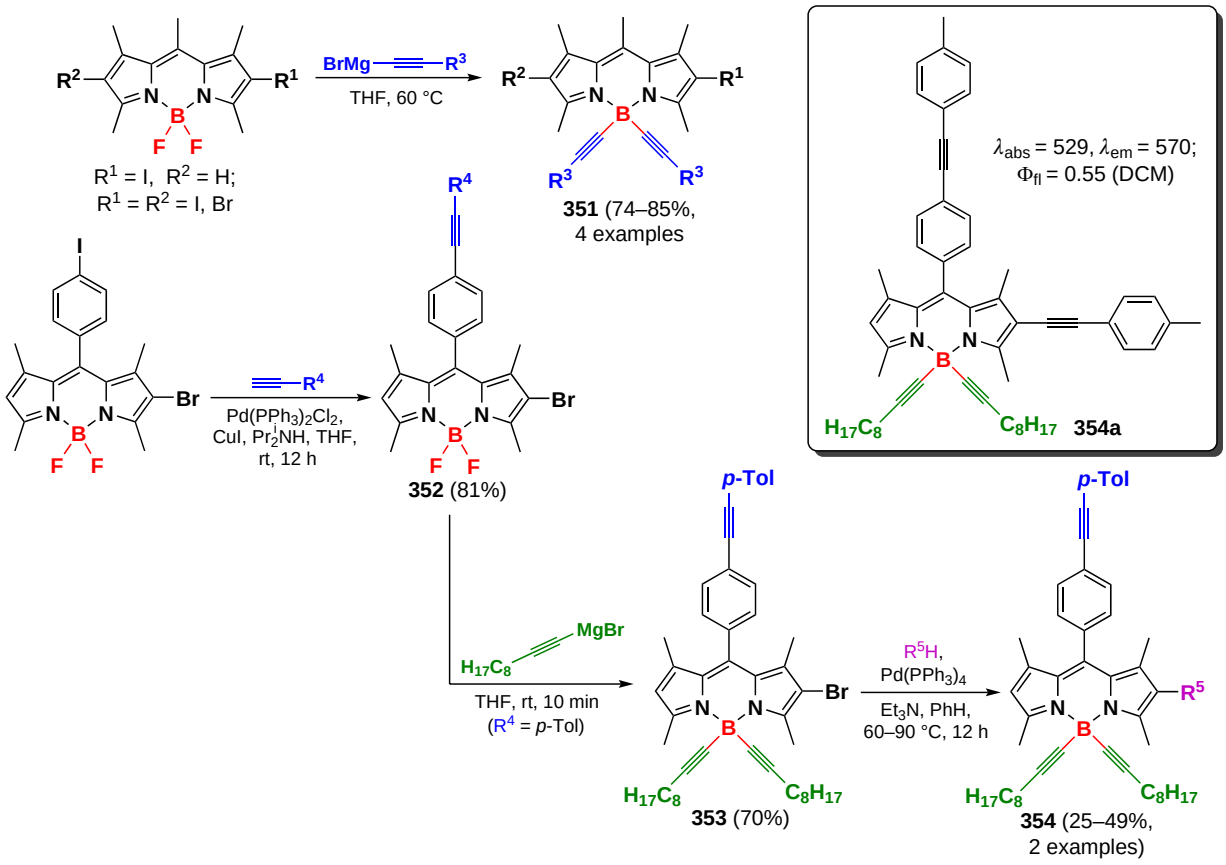

Scheme 185

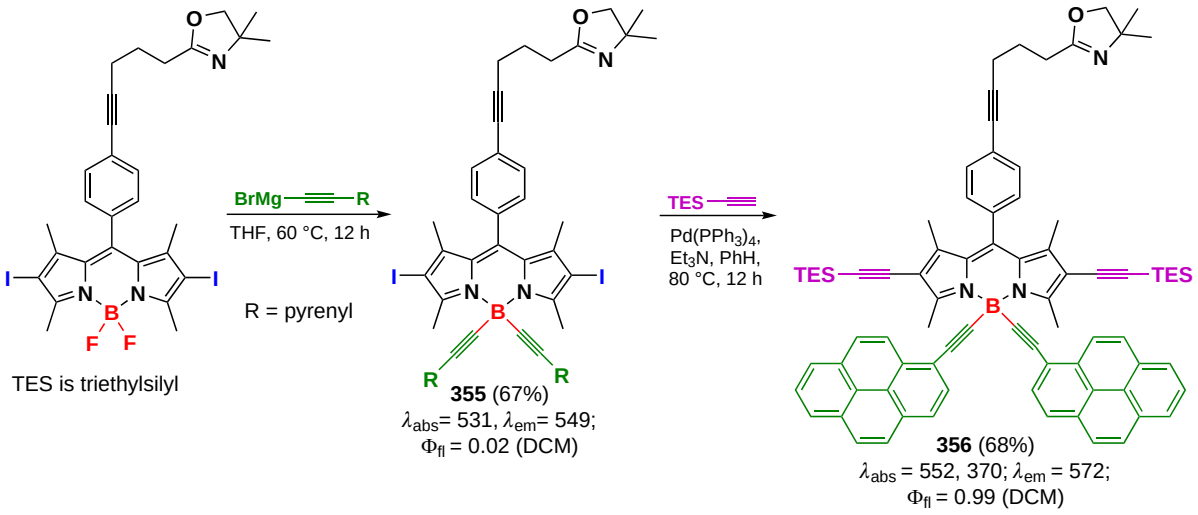

In 2008, the authors[336] proposed a method for the sequential introduction of C-nucleophiles at positions 2, 6, 8, and 4 of the BODIPY core using electrophilic halogenation reactions to form products **351**–**354**. Modification at the boron atom was also carried out using a Grignard reagent (Scheme 184). It is worth noting that the selective B–C-alkylation was successfully carried out even in the presence of halogen atoms in the BODIPY core (see Scheme 184, as well as the synthesis of compounds **355** and **356** in Scheme 185).

The interaction between a Grignard reagent and a boron atom of BODIPY has been successfully used by Niu *et al.*,[337,338] and by Bura and Ziessel[339] to create water-soluble fluorophores **357**.

In 2010, Ziessel *et al.*[340] presented chiral BODIPYs **358**–**360** modified at the boron atom with naphthalene (Scheme 186). Desymmetrization of the boron atom was achieved by the oxidation of 3-methyl group; hydrogen bonding between the fluorine atom and the proton of the aldehyde group in BODIPY **359** was proven by ^{1}H and ^{13}C nmR spectroscopy. The CD spectra of enantiomers **360a** and **360b** confirmed the persistence of both enantiomers.

In 2008, Li *et al.*[86] considered the competition of reaction centres in the BODIPY core when interacting with nucleophiles. Despite the presence of electrophilic centres in unsubstituted BODIPY, which are capable of interacting with hard

Structures 357

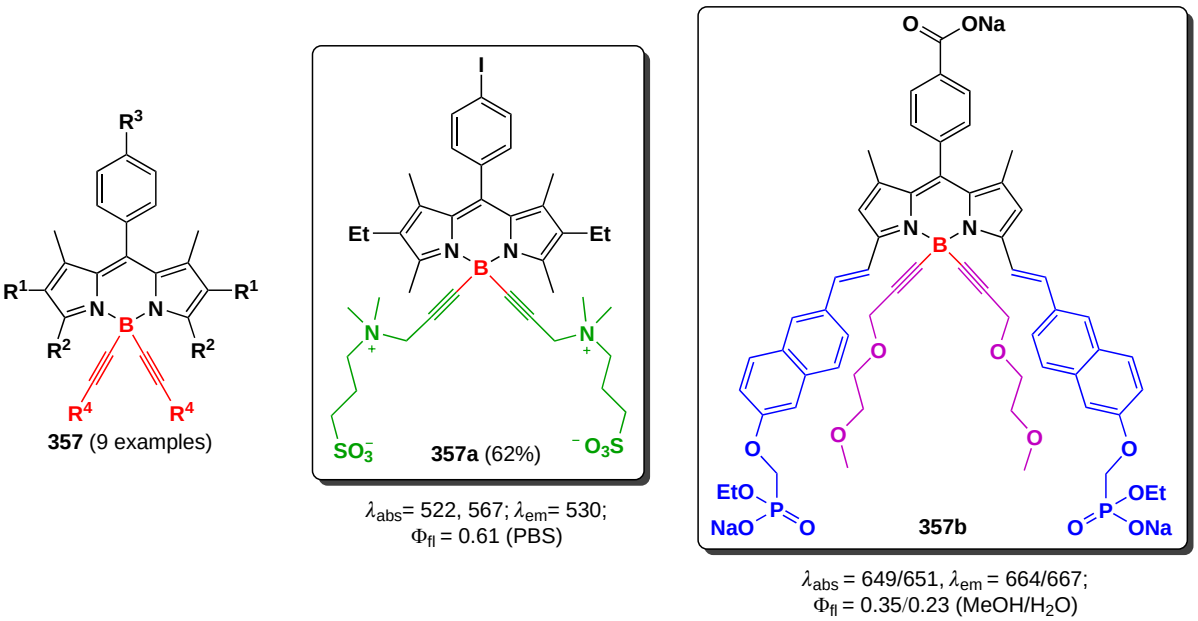

Scheme 186

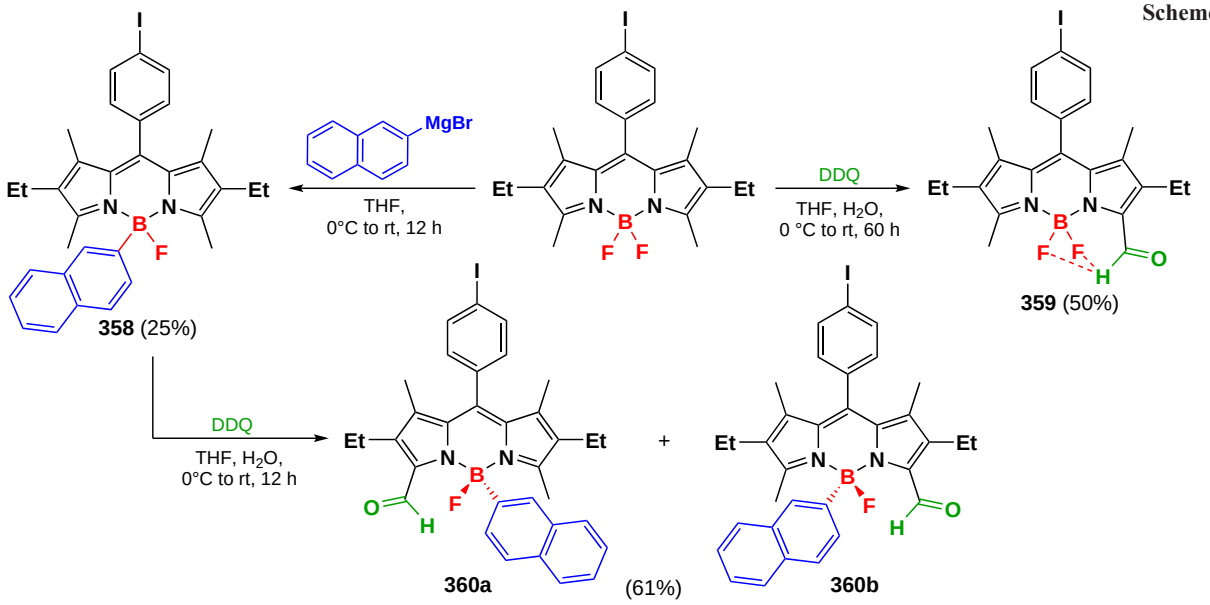

nucleophiles, the reaction at the B–F bond with the Grignard reagent was the fastest (product **361**). Further nucleophilic substitution in a reaction with piperidine derivative proceeded at the BODIPY core, affecting positions 3 and 5 as expected (product **362**) (Scheme 187).

In the reaction with a softer nucleophile, cyanide anion, the result of nucleophilic substitution is determined by the Lewis acid used. In the case of tin tetrachloride, the reaction proceeds selectively at the carbon atom to form compound **363**, whereas catalysis with boron trifluoride etherate promotes both types of substitution reactions, leading to tetracyanide **364** (Scheme 188).

In 2014, Chattopadhyay *et al.*[341] suggested using the ethylation reaction at the boron atom in BODIPY as a protecting group to carry out reactions at the BODIPY core with strong nucleophiles or reducing agents capable of affecting the BF_2 centre. The authors developed a convenient procedure for the substitution of fluorine atoms with ethyl groups under the use of Et_2AlCl to form Et_2B-BODIPY **365**. Regeneration of BF_2-BODIPY **366** was completed easily in the presence of $BF_3 \cdot Et_2O$. Moreover, the preparation of a similar ethyl substrate by direct reaction with a Grignard reagent or using *in situ* formed BCl_2-BODIPY either gave a lower yield of product **367** or required a longer time. The authors demonstrated the ability of Et_2B to act as a protecting group by performing the McMurry coupling reaction, impossible for BF_2-BODIPY, which resulted in the synthesis of β,β-dimer **368** with an ethynylene bridge (Scheme 189).

Modification at the boron atom can be carried out by using α-lithiated five-membered heterocycles. Thus, in 2023, Thompson *et al.*[342] presented the synthesis of BODIPYs **369a–d**, modified at the boron atom with chalcogenophenes (Scheme 190). These compounds were able to generate singlet oxygen and also acted as effective PDT agents on HeLa cells with moderate toxicity in the dark and nanomolar toxicity under irradiation.

Scheme 187

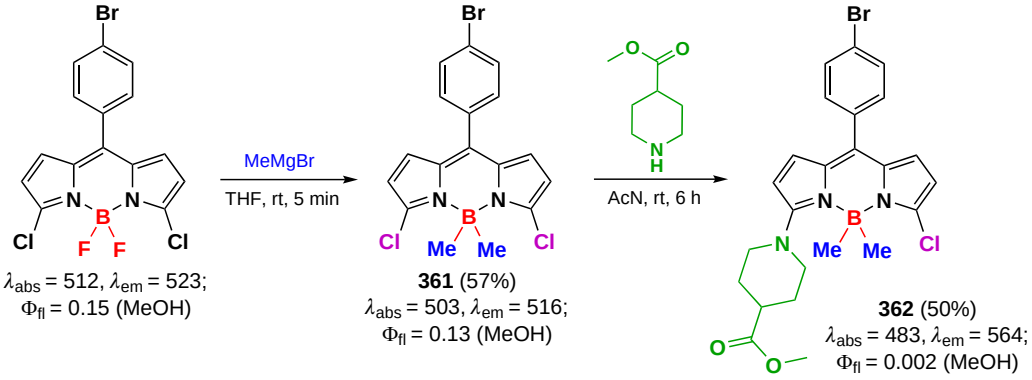

Scheme 188

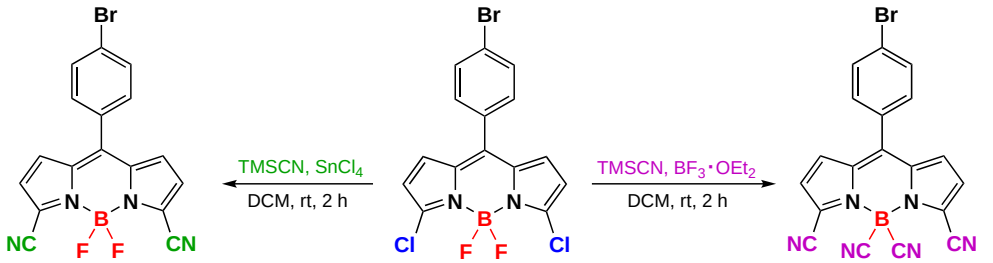

Scheme 189

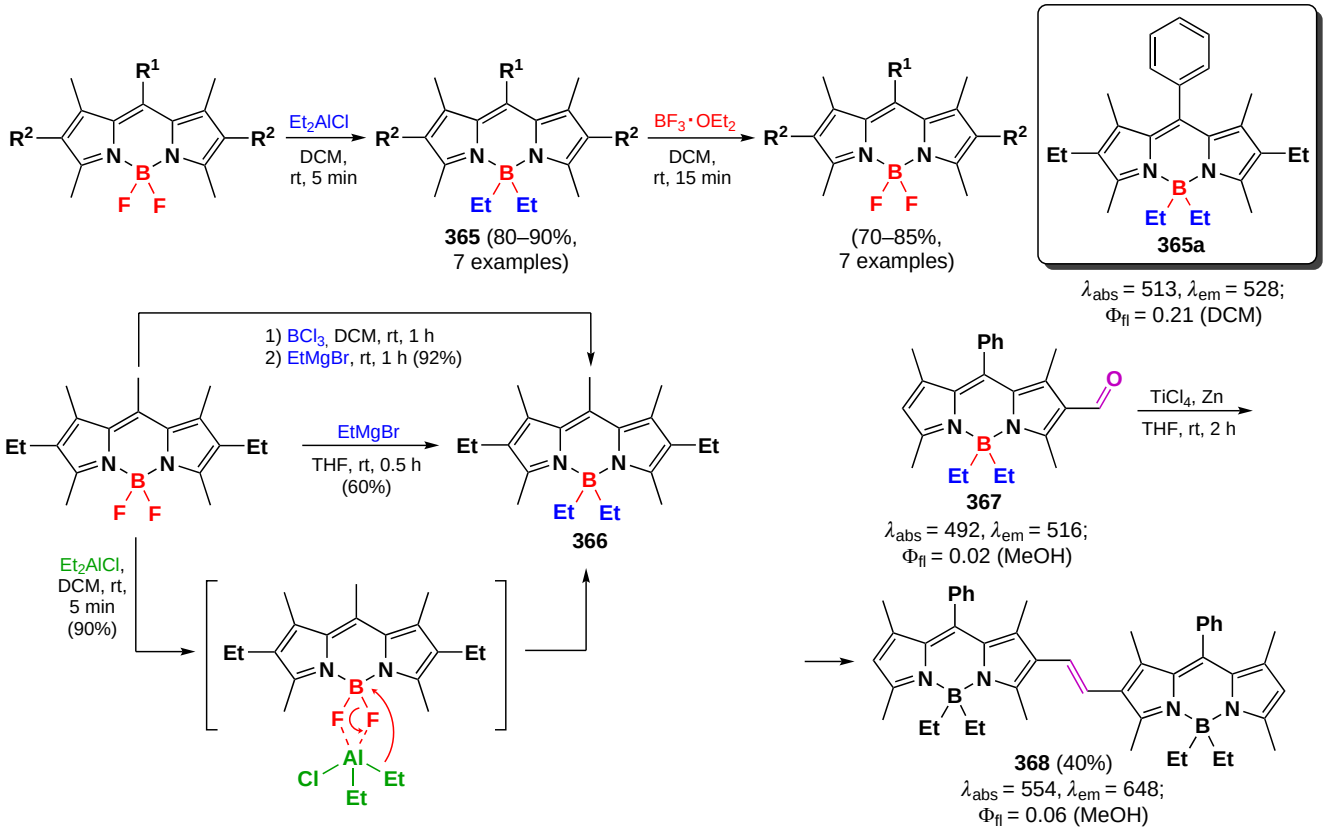

In the same year, Wang *et al.*[21] used $AlCl_3$ as a catalyst to modify BODIPY with chalcogenophenes, hypothesizing that conversion of (*N*,*N*-chelate)BF_2 to borenium cation [(*N*,*N*-chelate)BX]$^+$ or [(*N*,*N*-chelate)B]$^{2+}$ would allow boron metalation reactions with weak nucleophiles without affecting the pyrrole ring. Using this approach, reactions of arylstannanes with unsubstituted BODIPY in the presence of aluminium chloride were carried out to give BODIPYs **370**, **371**. This approach was proven to be convenient for nucleophilic substitution at the boron atom in aza-BODIPY **372** (Scheme 191).

3.9.5. Synthesis of B-acyloxy BODIPY derivatives

In 2012, Zhao *et al.*[343] synthesized alkoxycarbonyl BODIPYs **373** and **374** containing one or two acetoxy groups at the boron

Scheme 190

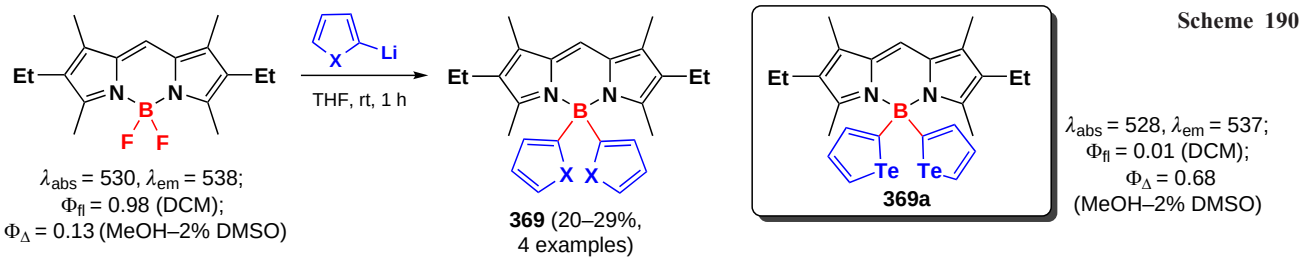

Scheme 191

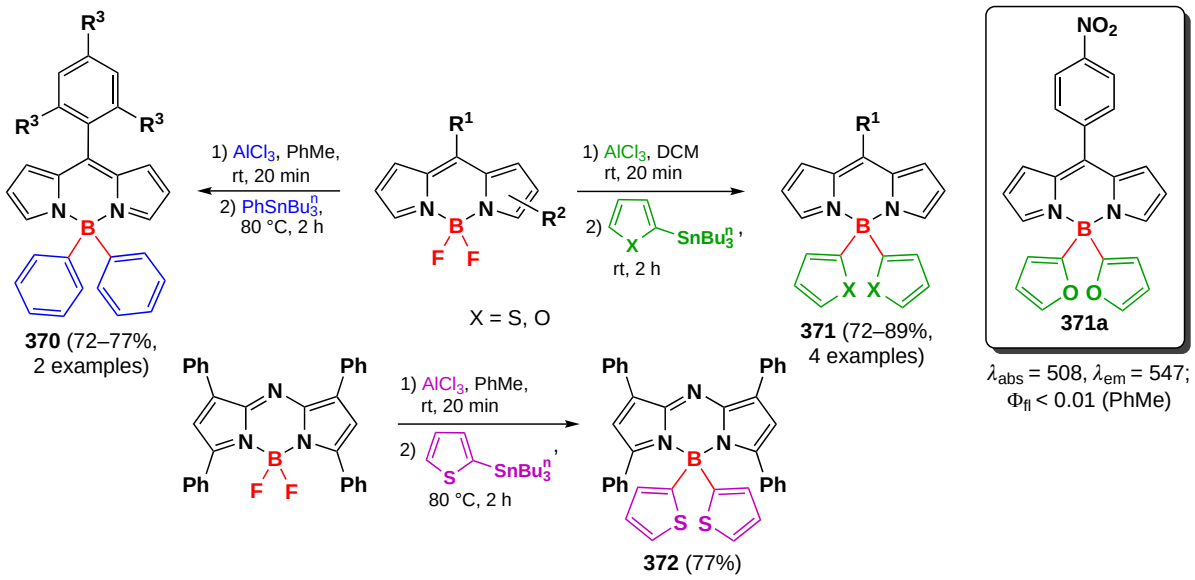

atom by nucleophilic substitution reaction at the boron atom using 20 equiv. of *in situ* generated trimethylsilyl acetate (Scheme 192). Derivatives **373** and **374** showed significantly improved aqueous solubility compared to the original BODIPY, while maintaining its photophysical properties, such as high fluorescence quantum yield and high photostability.

In 2013, Ortiz *et al.*[166] reported the synthesis of B-acyloxy-modified BODIPYs **375**–**377** by a reaction with 20 equiv TMSOAc in the presence of 3–4 equiv. $AlCl_3$ as a Lewis acid (Scheme 193, Method *A*). Furthermore, alternative routes were developed, including a reaction with *in situ* generated TMSOAc or $TMSOC(O)CF_3$ from the corresponding acid or TMSCl in the absence and presence of $AlCl_3$ (see Scheme 193, Methods *B*, *C*). The routes *B*, *C* were more efficient compared to Method *A*. The BODIPY derivatives exhibited laser efficiencies exceeding

Scheme 192

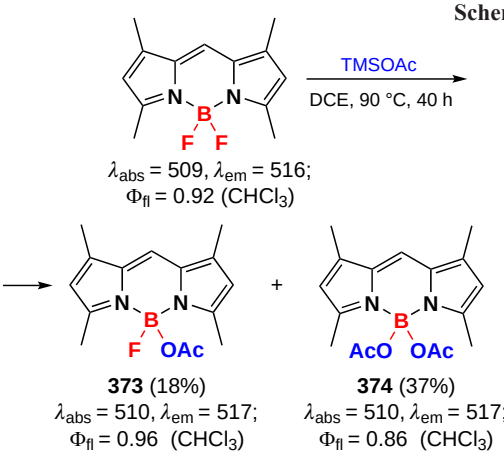

those of the starting difluoro-BODIPYs, the highest efficiency was observed for compound **377a** modified with trifluoroacetoxy groups.

In 2016, Chiara *et al.*[344] suggested using microwave irradiation to synthesize boron-modified BODIPYs **378** and **379** in high yields (Scheme 194).

Compounds **379** exhibited high laser efficiencies and good photostability. With increasing concentration of BODIPYs in solution, a second, bathochromically shifted laser emission band appeared in their spectra at 540–545 nm. The dependence of laser efficiency, as well as the ratio of the bichromatic emission bands on pump energy, indicated the formation of J-aggregates in organic solvents, which was also confirmed by molecular dynamics simulations.

4. Advances in boron-dipyrromethene research

BODIPY chemistry has been actively developed over the past 30 years, and has paved the way for new fluorophores with applications as fluorescent sensors, photocatalysts, photo-removable protecting groups, anti-tumor agents, laser dyes and light harvesting systems.

The main synthetic approaches to obtain the boron-dipyrromethene core were developed 10–30 years ago.[47,58,79,80] Currently, the known methods are being improved and new, more advanced methods are being developed. Thus, it is worth noting the direct synthesis of α-pyrrolyl-BODIPY 3 with absorption at ~600 nm[27] and the use of microwave radiation in the preparation of BODIPY from acid chlorohydrides, which significantly reduced the reaction time.[65] The expansion of the range of starting substrates for BODIPY synthesis has resulted

Scheme 193

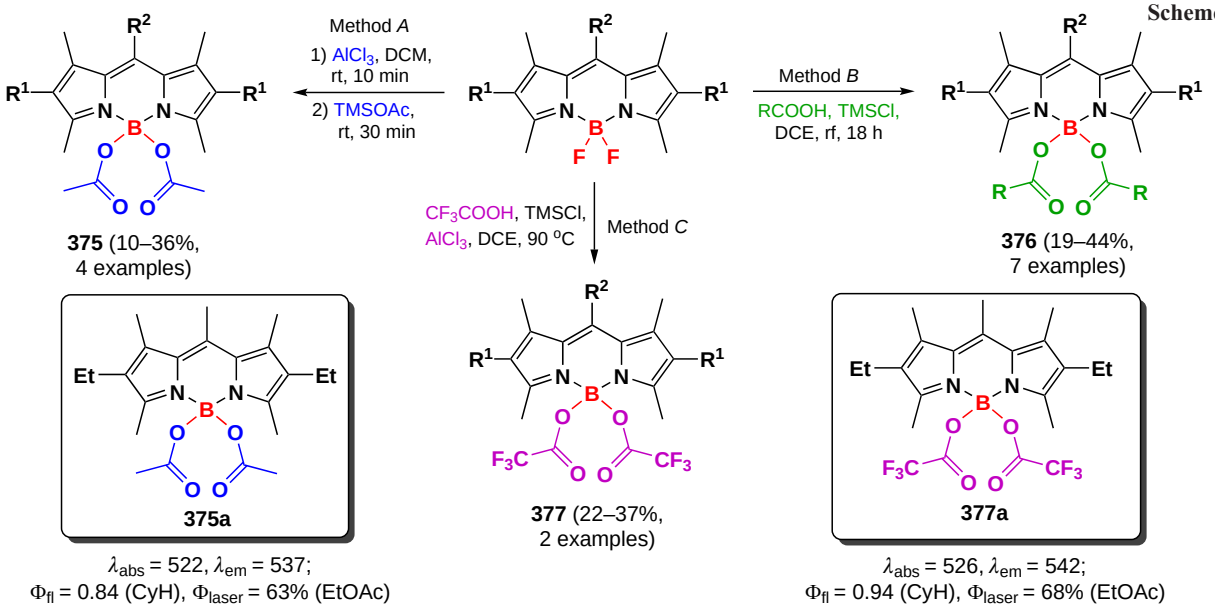

Scheme 194

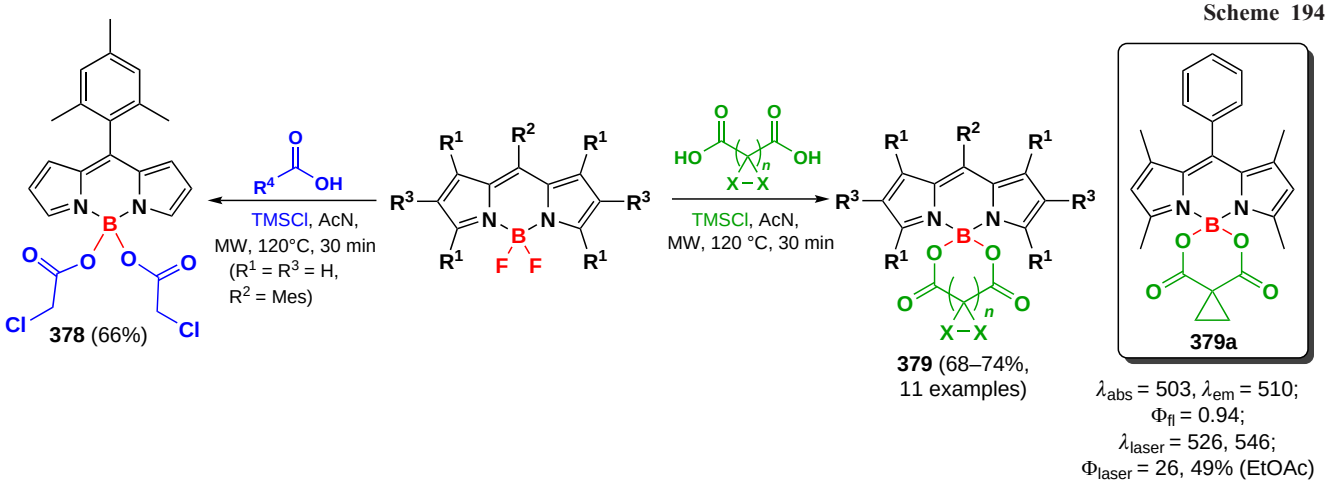

in the synthesis of new compound libraries. In particular, water-soluble α-glycosido-BODIPY **12** with bright fluorescence in aqueous media are formed from α-glycosidopyrroles.[22] The use of organoboron compounds as an alternative to boron trifluoride esterate allowed the direct synthesis of 4-substituted BODIPY **26**–**28**.[95,96]

An important advantage of 2,6-dihalogen-BODIPY was their ability to induce ISC and exhibit photosensitizing properties. 2,6-Dibromo-BODIPY **53** and **54**, which belong to both the type I and type II PDT agents, demonstrated high antiproliferative activity *in vivo*.[132] The 2,6-dibromo-BODIPY complex with copper **59-Cu** formed ROS not only as a photosensitizer but also *via* a copper-mediated mechanism. As a result, it exhibited cytotoxic activity under hypoxic conditions *in vitro,* and also significantly reduced tumor growth *in vivo*.[138] Monohalogenated BODIPYs can also act as PTT-agents. For example, 6-iodo-BODIPY **57a** was active in the nanomolar concentration range under low-power light due to the formation of PTT-active aggregates in the intracellular medium.[78]

Many new methods of modifying BODIPY *via* electrophilic substitution reactions have been developed in recent years. Thus, the interaction of BODIPY with 2-fluoropyridinium ethanide leads to the formation of a stable carbanion **97** with good water solubility.[171] Indium-catalyzed β-alkenylation of BODIPY allows the synthesis of 2,6-alkenyl-BODIPY **98**–**100**,[25] and 2- and 2,6-dipropargyl-BODIPY have been obtained by the Nicholas reaction involving BODIPY and the propargyl alcohol Co-complex **101**–**104**.[172]

New synthetic strategies for the modification of BODIPY, such as oxidative nucleophilic substitution, developed in the last few years have opened a direct route to the formation of α-seleno-BODIPYs **135**, **136** and α-cyano-BODIPY from unsubstituted analogs.[19,189] Photochemical synthesis of α-amino-BODIPY by reaction with aqueous ammonia proves the possibility of BODIPY modification by increasing its the reactivity in the excited state.[20]

The susceptibility of BODIPY to nucleophilic substitution reactions together with its sensitivity to the donor-acceptor properties of the substituent is widely used in the design of fluorescent probes for the detection of various organic and biological analytes. The fluorescent probes presented in this review act either through the nucleophilic substitution reaction of BODIPY with the analyte, which leads to a change in the photophysical or chemical properties of the probe due to differences in the electronic properties of the leaving group and the nucleophile, or by reducing PET-induced fluorescence quenching due to the reaction of the PET-donating scaffold with the analyte and the quenching of BODIPY fluorescence. Thus,

probes **122**, **130**, and **169** are able to selectively detect cysteine, homocysteine, or glutathione due to the different emission maxima of the nucleophilic substitution products of these biothiols.[177,185,207] Probes **123–125**, **128** and **129** have suppressed emission in the initial state, their reactions with different biothiols result in products with emission at different wavelengths, allowing selective detection of biothiols ratiometrically.[178–180,183] The mechanism of action of probe **126** is based on the emission properties not being affected after reaction with biothiols, but the resulting products differ from each other in polarity.[181]

Reduction of PET-induced fluorescence quenching as a result of specific reaction with the analyte is a preparatively convenient way to detect acids and other electrophiles due to the significant difference in fluorescence of the starting fluorophores and products. This principle was utilized in the development of sensors **119** and **120** sensitive to HClO, as well as sensors **167** and **173** for the detection of acyl chlorides and nitrite anions, respectively.[16,35,36,175,205] It should be noted that the analytical signal may be caused not only by the flaring of fluorescence due to the removal of the PET effect, but also by the quenching of emission due to ICT. This is the operating principle of the **131** sulfide-anion sensor.[186]

The CH-acidity of BODIPY methyl groups is widely used in a variety of synthetic approaches to tune the photophysical properties of fluorophores. In particular, the π-system expansion *via* the Knoevenagel condensation is a common approach to create NIR-absorbing BODIPY fluorophores. The suppression of BODIPY emission due to J-aggregation contributes to nonradiative decay, thus J-aggregates based on distyryl-BODIPY are promising PTT agents that have repeatedly proven their therapeutic efficacy *in vivo*. Thus, NIR-absorbing self-aggregating BODIPY **182** in nanoparticles have been developed, acting as combined PDT and PTT agents, which exhibit remarkable antitumor efficacy *in vivo*.[32] Styryl derivatives of 8-CF3-BODIPY **184** and **185** are of great interest as PTT agents due to the free rotation of the CF_3 group, for which the record high PCE of 88.3% and the possibility of photoacoustic imaging of tumor tissues in nanoparticle form have been shown.[31,34] Distyryl-BODIPY **190** can exhibit the properties of sonodynamic therapy agents and effectively inhibit tumor growth *in vivo* under ultrasound irradiation.[15] The ability of BODIPY **189**, containing electron-withdrawing substituents, to form J-aggregates allowed the development of a bioimaging agent with fluorescence in the NIR-II band, as demonstrated by real-time imaging of the mouse vascular system.[33]

The α-methyl groups of BODIPY can also be modified by various nucleophiles. For example, the oxidation of 4,4-dicyano-BODIPY by $Pb(OAc)_4$ followed by reaction with nucleophiles, described in 2022, allowed the synthesis of a library of more than 50 compounds and the introduction of a variety of O-, N-, and C-nucleophiles at the α-position of BODIPY *via* a methylene linker. This transformation opens up the possibility of easily modifying BODIPY by creating a new C–C bond that does not require metallocatalysis.[6]

Approaches to the modification of BODIPY by radical mechanism with the creation of C–C, C–S, and C–N bonds are being actively developed due to the ease of radical processes, the availability of reagents, and the possibility of introducing sterically loaded functional groups that are difficult to introduce by alternative nucleophilic substitution or cross-coupling reactions.[264] For example, the introduction of thiol groups into the α-position of BODIPY can be easily accomplished by the action of radical initiators such as tert-butylhydroperoxide[268] or under irradiation.[269] The use of radical reactions makes it possible to introduce sterically loaded functional groups into the BODIPY core. Thus, BODIPY **213′b** with cyclohexyl fragments at positions **3** and **5** was obtained, which exhibits solid-phase fluorescence.[264] An alternative synthetic route to create the C–C bond is the use of metallocatalysis or organometallic compounds, which require the introduction of protecting groups at the boron atom, which is prone to reactions with harsh C-nucleophiles (see Section 3.9.4).

Due to their excellent photochemical properties, BODIPYs have also been the subject of interest as photocatalysts. 2,6-Dihalogen-BODIPYs and BODIPYs devoid of heavy atoms are capable of functioning as photocatalysts in the singlet or triplet excited states, acting as both oxidants[275] and reducing agents.[273] BODIPYs have the ability to function as a source of singlet oxygen in oxidation reactions and as an electron donor or carrier, thereby facilitating the formation of C–C, C–N, C–P bonds.[272–275]

BODIPY derivatives prone to ISC, such as 8-SMe-BODIPY **16**, are employed as photocatalysts for the Beckmann rearrangement, facilitating the conversion of oximes to amides.[29] In recent years, an approach to the use of BODIPY as catalysts for ion-radical addition to multiple bonds has also been developed. Furthermore, 2,6-dihalogen-BODIPY **233** has been identified as a suitable photocatalyst for the ion-radical addition of α-halogenecarbonyl compounds to vinyl ethers, leading to the synthesis of several classes of organic compounds, including lactones, protected aldehydes, and others.[279] In regard to dyad **234a–b**, the potential for photocatalysis in the radical addition of malonic esters to the carbon-carbon double bond was demonstrated.[28]

The formation of dimers and oligomers from monomeric BODIPY is a topic of significant interest, given the distinctive photophysical properties exhibited by these higher-order structures, which are not observed in individual chromophores. The position at which dimerisation occurs has a significant impact on the properties of the resulting oligomers. To illustrate, α,α-dimers **235–239**, which exhibit a low degree of conjugation between BODIPY links, are characterized by exciton splitting of absorption maxima and high fluorescence quantum yields.[213,279,280] The α,α- and γ,γ-dimers **238** and **239** possess helical chirality and are a mixture of optically active aptoisomers. Planar α,α-dimers **240–246** exhibit a large bathochromic shift in the electronic spectrum with no exciton splitting.[282–284]

It has been demonstrated that dimers at the α,β-, α,γ-, β,γ- and *meso*,*meso*-positions, which do not contain heavy atoms in the structure, are capable of acting as PDT agent. The orthogonal α,γ-, β,γ-, β,*meso*- and *meso*,*meso*-dimers (*e.g.* compounds **241**, **262**, **265**) are predominantly type II PDT agents, producing singlet oxygen upon irradiation. In contrast, the β,*meso*-dimer **265a** has antiproliferative activity with EC50 values in the nanomolar range.[158,281,288] In contrast, α,β-dimers **247** are exclusively type I PDT agents and therefore exhibit high antiproliferative activity upon irradiation under both normoxic and hypoxic conditions.[285] The condensed oligomers **279** and **286**, which exhibit absorption in the near-infrared region, are regarded as prospective FTT agents. The emission of these compounds is suppressed due to the diminished energy gap between the HOMO and LUMO.[295,297] BODIPY oligomers **294** and **296a**, in which the BODIPY subunits are linked *via* an alkenyl linker, also display high FTT activity.[88,300] These oligomers are distinguished by a high PCE value (56–62%) and the additional property of emission in the NIR-II band.

The variation of substituents at the boron atom enables the enhancement of fluorescence quantum yields, the improvement of photostability, and the development of water-soluble BODIPY derivatives. BODIPYs with substituents at the boron atom have been identified as a promising class of light-harvesting systems. The incorporation of chiral substituents, such as BINOL, at the boron atom in BODIPY results in the formation of fluorophores exhibiting circularly polarised luminescence.[310,311] The BODIPY **314** synthesised by Moya *et al.*[316] represents the inaugural instance of a fluorophore exhibiting NIR-band CPL in an aqueous milieu. The ICT effect control permits the alteration of the sign of the circular polarisation.[315] Another example of light-gathering systems based on the change of substituents at the boron atom are BODIPY dyads and triads, which are created by the introduction of a fragment of ethynylene pyrylene, resulting in an energy transfer from the pyrene to the BODIPY core.[334] Moreover, in these light-gathering Stokes systems, the shift reaches values as low as 200 nm.[336] The functionalisation of BODIPYs can be achieved through the modification of substituents at the boron atom, while maintaining the photophysical properties of the molecule. This allows the generation of probes with bright fluorescence.[328] Boron-substituted BODIPYs are also promising agents for PDT, as exemplified by compound **379a**, modified at the boron atom by tellurophene and exhibiting nanomolar toxicity due to the 'heavy atom' effect.[342] The introduction of such chalcogenophenes is feasible not only with the corresponding organolithium derivatives, but also with arylstannanes in the presence of $AlCl_3$.[21]

This section presents an analysis of the most significant advances in the design and property studies of the various BODIPY derivatives considered in this review.

5. Conclusion

Boron-dipyrromethene dye-based fluorophores (BODIPY) are one of the most popular and widely used classes of fluorescent organic compounds. Over the past few decades, research into the development of BODIPY with tailored photochemical properties has led to many applications for such derivatives, such as bioimaging agents, fluorescent probes, antitumor agents, laser dyes, components of organic photovoltaic cells, and photocatalysts. Such a diversity of practical applications is due to the photophysical properties of BODIPY, as well as the ability to fine-tune the photophysical and photochemical properties of these fluorophores to suit the required tasks through simple structural modifications accessible by classical methods of organic synthesis. This paper systematizes information on the synthesis, modification and application of boron-dipyrromethene dyes, with an emphasis on studies published from 2017 to 2024.

Approaches to the creation of BODIPY fluorophores with specified photophysical properties and high biological activity are currently being actively developed. At the same time, significant progress has been made over the past 5 years in developing new methods for modifying the structure of BODIPYs and tuning their photophysical properties. A number of new synthetic and post-modification methods allow the target BODIPYs to be obtained under milder conditions, in higher yields, or in fewer steps. In particular, a significant reduction in process time can be achieved by using microwave radiation. Approaches to the creation of new methods for modifying BODIPY by electrophilic and nucleophilic substitution reactions, as well as by means of radical reactions, are also being actively developed. A number of methods, such as radical C–H-activation and oxidative nucleophilic substitution of the hydrogen atom, allow the introduction of target groups into the BODIPY core directly *via* the C–H bond and under mild conditions. Thus, further research into the chemical transformation of BODIPY can be aimed both at creating more efficient methods for the synthesis of already known BODIPY derivatives and at developing new ways to optimize the structure of boron-dipyrromethene dyes. The methods for modifying BODIPY developed in recent years can be further applied to the creation of new fluorescent probes, therapeutic and diagnostic agents, as well as laser dyes.

The use of BODIPY as imaging and detection tools has become attractive due to the high extinction coefficients and large fluorescence quantum yields of boron-dipyrromethene complexes. Over the past 5 years, methods for detecting a large number of objects, such as metal ions, hypochlorite and biothiols, have been improved. Fluorescent probes created in recent years make it possible to selectively determine target compounds in the nanomolar concentration range, including in living systems. Taking into account the wide variety of chemical properties of BODIPY derivatives, it is reasonable to expect that new probes based on them will be developed with sensitivity to metal ions, biomolecules and other objects. In addition, the creation of fluorescent probes with NIR emission for effective use in living systems, remains an urgent task. BODIPY fluorophores with emission in the NIR-II region have shown great promise for *in vivo* imaging, so it is reasonable to expect that the creation of new active fluorescent probes with NIR-II emission based on them.

PDT- and PTT-agents containing the BODIPY core are particularly attractive because they combine high antitumor activity under the influence of radiation with low toxicity in the absence of light. Due to the poor solubility of BODIPY in water and the shift of absorption and emission ranges to the NIR region, promising PDT- and PTT-agents are used in the form of J-aggregates, which form water-soluble nanoparticles in combination with polymers. The bathochromic shift resulting from J-aggregation enables NIR-II emission of BODIPY-based medications, opening up the possibility of their use as theranostic medications. In addition, recent advances in the development of PTT-active BODIPYs exhibiting activity in the nanomolar range of IC_{50} values demonstrate the still incompletely explored potential of BODIPYs as antitumor agents and prove the feasibility of searching for new structural modifications to enhance their effectiveness.

6. List of abbreviations

E_{red} — reduction potential,
E_{ox} — oxidation potential,
g_{lum} — luminescence asymmetry factor,
$|g_{lum}|$ — luminescence dissymmetry factor,
λ_{abs} — absorption wavelength,
λ_{em} — emission wavelength,
λ_{ex} — excitation wavelength,
λ_{laser} — lasing wavelength,
Φ_{fl} — quantum yield of fluorescence,
Φ_{Δ} — quantum yield of reactive oxygen species formation,
Φ_{laser} — quantum yield of laser irradiation,
A — acceptor,
AcN — acetonitrile,
AIEE — aggregation-induced emission,
ALDH1 — aldehyde dehydrogenase 1,
Ant — anthracenyl,

Asc — ascorbate,
AT — atom transfer,
BCN — spiro[2.3]hex-1-ene,
BHT — 2,6-di-tert-butyl-4-methylphenol,
BINAP — bis(diphenylphosphino)-1,1′-binaftyl,
BINOL — 1,1′-bi-2-naphthol (1,1′-bi-2-naphthol),
B2pin2 — bis(pinacolato)diboron,
Boc — tert-butoxycarbonyl,
BODIPY (BDP) — 4,4-difluoro-4-bora-3a,4a-diaza-*s*-indacene,
Brettphos — 2-dicyclohexylphosphino-3,6-dimethoxy-2′,4′,6′-triisopropyl-1,1′-biphenyl,
CAN — cerium(IV)-ammonium nitrate,
Cat — catalyst,
Cb — alicyclic carbocycle,
CD — circular dichroism,
CDT — chemodynamic therapy,
cod — cycloocta-1,5-diene,
Cp — cyclopentadienyl,
CPL — circularly polarized luminescence,
CS — charge separated state,
CVA — cyclic voltammetry,
Cy — cyclohexyl
Cys — cysteine,
D — donor,
dba — dibenzylideneacetone,
DBU — 1,8-diazabicyclo[5.4.0]undec-7-ene,
DCE — 1,2-dichloroethane,
DCM — dichloromethane,
DDQ — 2,3-dichloro-5,6-dicyano-1,4-benzoquinone,
DFT — density functional theory,
DIPEA — diisopropyl ethylamine,
DMAP — 4-(dimethylamino)pyridine,
DME — dimethoxyethane,
DMPO — 5,5-dimethyl-1-pyrroline-*N*-oxide,
dr — diastereomer ratio,
DSPE-PEG — 1,2-distearoyl-sn-glycero-3-phosphoethanolamine-*N*-[amino(polyethylene glycol)],
EC_{50} — half-maximal effective concentration,
ECM — exciton chirality method,
EDC — 1-ethyl-3-(3-dimethylaminopropyl)carbodiimide,
EnT — energy transfer,
ER — endoplasmic reticulum,
ESn — trans-1,2-bis(tributylstannyl)ethene,
ETA — ethanolamine,
EWG — electron-withdrawing group,
Fc — ferrocenyl,
FRET — fluorescence resonance energy transfer,
F127 — pluronic F127,
GSH — glutathione,
HAT — hydrogen atom transfer,
Hcy — homocysteine,
HEPES — 4-(2-hydroxyethyl)-1-piperazineethanesulfonic acid (buffer),
HFIP — hexafluoropropan-2-ol,
HOMO — highest occupied molecular orbital,
m-CPBA — m-chloroperoxybenzoic acid,
IC — internal conversion,
IC_{50} — half-maximal inhibition concentration,
ICT — intramolecular charge transfer,
ISC — intersystem crossing,
LDA — lithium diisopropylamide,
LED — light emitting diode,
LUMO — lowest unoccupied molecular orbital,
MES — 2-mercaptoethanesulfonate sodium,
Mes — 2,4,6-trimethylphenyl (mesityl),
MS — molecular sieves,
MW — microwave radiation,
NBS — *N*-bromosuccinimide,
NCS — *N*-chlorosuccinimide,
NHS — *N*-hydroxysuccinimide,
NIR — near infrared (spectrum),
NIS — *N*-iodosuccinimide,
NP — nanoparticles,
PA — photoacoustic,
PALM — photo-activated localization microscopy,
PBN — *N*-*tret*-butylphenylphenylnitron,
PBS — phosphate-salt buffer,
PCE — photothermal conversion efficiency,
PEDOT:PSS — poly(3,4-ethylenedioxythiophene) polystyrene sulfonate,
PDT — photodynamic therapy,
PEG — polyethylene glycol,
PEG-PCL — aminopoly(ethylene glycol)-*b*-poly(ε-caprolactone),
PET-photoinduced electron transfer,
phen — phenanthroline,
PIFA — bis(trifluoroacetoxy)iodbenzene,
PivO — pivaloyl,
por — porphyrin,
PS — proton sponge, 1,8-bis(dimethylamino)naphthalene),
PTT — photothermal therapy,
Py — pyridine,
py — pyridyl,
RET — resonance energy transfer,
ROS — reactive oxygen species,
rt — room temperature,
Selectfluor — bis(tetrafluoroborate)4-fluoro-1-chloromethyl diazonium-bicyclo[2.2.2.2]octane,
SET — single electron transfer,
SNAr — nucleophilic aromatic substitution,
SN1 — monomolecular nucleophilic substitution,
SOC — spin-orbit coupling,
SOCT-ISC — spin-orbit charge-transfer intersystem crossing,
TBA — tetra-*n*-butylammonium,
TBHP — *tret*-butyl-hydroperoxide,
TBPB — *tret*-butyl-peroxybenzoate,
TCBQ (*p*-chloranil) — tetrachloro-1,4-benzoquinone,
TC — thiophene-2-carboxylate,
TCE — 1,1,2-trichloroethane,
TCO — trans-cyclooctene,
TEBAC — benzyltriethylammonium chloride,
TEG — tetraethylene glycol,
TEMP — 2,2,6,6-tetramethylpiperidine,
TEMPO — 2,2,6,6,6-tetramethylpiperidine-N-oxyl,
terpy — terpyridine,
TES — triethylsilyl,
TFA — trifluoroacetic acid,
Tf — trifluoromethanesulfonyl (triflyl),
TFEA — 2,2,2,2-trifluethoethanol,
TFP — tri(2-furyl)phosphine,
TMS — trimethylsilyl,
Tol — tolyl,
TPP — *meso*-tetraphenylporphyrin,
Ts — *p*-toluenesulfonyl (tosyl),
TTEG — tetraethylene glycol,
US — ultrasound,

VAPOL — 2,2′-diphenyl-4-biphenanthrol,
Xantphos — 4,5-bis(diphenylphosphino)-9,9-dimethylxanthene,
X-Phos — 2-dicyclohexylphosphino-2′,4′,6′-triisopropylbiphenyl.

7. References

1. G.Ulrich, R.Ziessel, A.Harriman. *Angew. Chem., Int. Ed*., **47**, 1184 (2008); https://doi.org/10.1002/anie.200702070
2. J.Wang, Q.Gong, L.Wang, E.Hao, L.Jiao. *J. Porphyrins Phthalocyanines*, **24**, 603 (2020); https://doi.org/10.1142/S1088424619300234
3. X.Xing, K.Yang, B.Li, S.Tan, J.Yi, X.Li, E.Pang, B.Wang, X.Song, M.Lan. *J. Phys. Chem. Lett*., **13**, 7939 (2022); https://doi.org/10.1021/acs.jpclett.2c02122
4. P.De Bonfils, L.Péault, P.Nun, V.Coeffard. *Eur. J. Org. Chem*., 1809 (2021); https://doi.org/10.1002/ejoc.202001446
5. L.Chen, F.Li, Y.Li, J.Yang, Y.Li, B.He. *Chem. Commun*., **58**, 298 (2022); https://doi.org/10.1039/D1CC05863K
6. A.Blázquez-Moraleja, L.Maierhofer, E.Mann, R.Prieto-Montero, A.Oliden-Sánchez, L.Celada, V.Martínez-Martínez, M.-D.Chiara, J.L.Chiara. *Org. Chem. Front*., **9**, 5774 (2022); https://doi.org/10.1039/D2QO01099B
7. P.K.Singh, P.Majumdar, S.P.Singh. *Coord. Chem. Rev*., **449**, 214193 (2021); https://doi.org/10.1016/j.ccr.2021.214193
8. A.Harriman. *Chem. Commun*., **51**, 11745 (2015); https://doi.org/10.1039/C5CC03577E
9. A.Loudet, K.Burgess. *Chem. Rev*., **107**, 4891 (2007); https://doi.org/10.1021/cr078381n
10. N.Boens, B.Verbelen, M.J.Ortiz, L.Jiao, W.Dehaen. *Coord. Chem. Rev*., **399**, 213024 (2019); https://doi.org/10.1016/j.ccr.2019.213024
11. S.M.Waly, J.K.G.Karlsson, P.G.Waddell, A.C.Benniston, A.Harriman. *J. Phys. Chem. A*, **126**, 1530 (2022); https://doi.org/10.1021/acs.jpca.2c00035
12. E.Bodio, C.Goze. *Dyes Pigm*., **160**, 700 (2019); https://doi.org/10.1016/j.dyepig.2018.08.062
13. M.Saikawa, T.Nakamura, J.Uchida, M.Yamamura, T.Nabeshima. *Chem. Commun*., **52**, 10727 (2016); https://doi.org/10.1039/C6CC05439K
14. C.O.Obondi, G.N.Lim, P.Martinez, V.Swamy, F.D'Souza. *Nanoscale*, **9**, 18054 (2017); https://doi.org/10.1039/C7NR06687B
15. X.Li, X.Sun, H.Chen, X.Chen, Y.Li, D.Li, Z.Zhang, H.Chen, Y.Gao. *Eur. J. Med. Chem*., **264**, 116035 (2024); https://doi.org/10.1016/j.ejmech.2023.116035
16. X.-Z.Wei, Y.-L.Fu, M.-J.Xue, Q.-H.Song. *Org. Lett*., **21**, 9497 (2019); https://doi.org/10.1021/acs.orglett.9b03688
17. S.Guisán-Ceinos, A.R.Rivero, F.Romeo-Gella, S.Simón-Fuente, S.Gómez-Pastor, N.Calvo, A.H.Orrego, J.M.Guisán, I.Corral, F.Sanz-Rodriguez, M.Ribagorda. *J. Am. Chem. Soc*., **144**, 8185 (2022); https://doi.org/10.1021/jacs.2c01197
18. F.Lv, X.Guo, Z.-Y.Li, Q.Wu, J.Chen, C.Yu, L.Jiao, E.Hao. *Dyes Pigm*., **210**, 111030 (2023); https://doi.org/10.1016/j.dyepig.2022.111030
19. H.Zuo, Q.Wu, X.Guo, Z.Kang, J.Gao, Y.Wei, C.Yu, L.Jiao, E.Hao. *Org. Lett*., **25**, 8150 (2023); https://doi.org/10.1021/acs.orglett.3c03330
20. D.Wang, L.Wang, X.Guo, X.Zhang, J.Ma, Z.Kang, Z.-Y.Li, L.Jiao, E.Hao. *Org. Lett*., **25**, 7650 (2023); https://doi.org/10.1021/acs.orglett.3c02962
21. Z.Wang, X.Guo, Z.Kang, Q.Wu, H.Li, C.Cheng, C.Yu, L.Jiao, E.Hao. *Org. Lett*., **25**, 744 (2023); https://doi.org/10.1021/acs.orglett.2c04184
22. C.Uriel, D.Grenier, F.Herranz, N.Casado, J.Bañuelos, E.Rebollar, I.Garcia-Moreno, A.M.Gomez, J.C.López. *J. Org. Chem*., **89**, 4042 (2024); https://doi.org/10.1021/acs.joc.3c02907
23. A.Nagpal, N.Tyagi, P.P.Neelakandan. *Photochem. Photobiol. Sci*., **23**, 365 (2024); https://doi.org/10.1007/s43630-023-00524-z
24. R.V.Larkovich, V.E.Shambalova, S.A.Ponomarev, A.S.Aldoshin, B.N.Tarasevich, K.A.Lyssenko, V.G.Nenajdenko. *Dyes Pigm*., **221**, 111822 (2024); https://doi.org/10.1016/j.dyepig.2023.111822
25. A.Da Lama, J.Pérez Sestelo, L.A.Sarandeses, M.M.Martínez. *J. Org. Chem*., **89**, 4702 (2024); https://doi.org/10.1021/acs.joc.3c02951
26. Z.Chen, C.Li, K.Liu, L.-R.Wen, M.Li, L.-B.Zhang. *Org. Chem. Front*., **11**, 477 (2024); https://doi.org/10.1039/D3QO01616A
27. Z.Kang, W.Bu, X.Guo, L.Wang, Q.Wu, J.Cao, H.Wang, C.Yu, J.Gao, E.Hao, L.Jiao. *Inorg. Chem*., **63**, 3402 (2024); https://doi.org/10.1021/acs.inorgchem.3c04017
28. S.Abuhadba, M.Tsuji, T.Mani, T.V.Esipova. *ACS Omega*, **6**, 32809 (2021); https://doi.org/10.1021/acsomega.1c04724
29. X.Peng, Y.Liu, Q.Shen, D.Chen, X.Chen, Y.Fu, J.Wang, X.Zhang, H.Jiang, J.Li. *J. Org. Chem*., **87**, 11958 (2022); https://doi.org/10.1021/acs.joc.2c00813
30. J.Gao, T.Luan, J.Lv, M.Yang, H.Li, Z.Yuan. *J. Photochem. Photobiol. B*, **241**, 112666 (2023); https://doi.org/10.1016/j.jphotobiol.2023.112666
31. Y.Chen, Z.Wang, D.Zhang, X.Gong, J.Du, X.-D.Jiang, G.Wang. *Dyes Pigm*., **218**, 111500 (2023); https://doi.org/10.1016/j.dyepig.2023.111500
32. M.Jiang, J.Zhang, Y.Li, T.Shi, T.Ma, Y.Sun, H.Qiu, Y.Li, S.Yin. *Mater. Chem. Front*., **7**, 3668 (2023); https://doi.org/10.1039/D3QM00239J
33. Y.Zhu, P.Wu, S.Liu, J.Yang, F.Wu, W.Cao, Y.Yang, B.Zheng, H.Xiong. *Angew. Chem., Int. Ed*., **62**, e202313166 (2023); https://doi.org/10.1002/anie.202313166
34. D.Xi, M.Xiao, J.Cao, L.Zhao, N.Xu, S.Long, J.Fan, K.Shao, W.Sun, X.Yan, X.Peng. *Adv. Mater*., **32**, 1907855 (2020); https://doi.org/10.1002/adma.201907855
35. T.Yang, J.Fan, Y.He, Y.Han. *J. Photochem. Photobiol. A*, **447**, 115253 (2024); https://doi.org/10.1016/j.jphotochem.2023.115253
36. L.Zeng, Y.Ke, X.Yang, M.Lan, S.Zhao, B.Zhu. *Food Chem*., **438**, 138044 (2024); https://doi.org/10.1016/j.foodchem.2023.138044
37. Y.Ni, J.Wu. *Org. Biomol. Chem*., **12**, 3774 (2014); https://doi.org/10.1039/c3ob42554a
38. H.Lu, J.MacK, Y.Yang, Z.Shen. *Chem. Soc. Rev.*, **43**, 4778 (2014); https://doi.org/10.1039/c4cs00030g
39. K.Chen, Y.Dong, X.Zhao, M.Imran, G.Tang, J.Zhao, Q.Liu. *Front. Chem*., **7**, 821 (2019); https://doi.org/10.3389/fchem.2019.00821
40. M.Poddar, R.Misra. *Coord. Chem. Rev*., **421**, 213462 (2020); https://doi.org/10.1016/j.ccr.2020.213462
41. V.I.Martynov, A.A.Pakhomov. *Russ. Chem. Rev*., **90**, 1213 (2021); https://doi.org/10.1070/RCR4985
42. D.Wang, X.Wang, S.Zhou, P.Gu, X.Zhu, C.Wang, Q.Zhang. *Coord. Chem. Rev*., **482**, 215074 (2023); https://doi.org/10.1016/j.ccr.2023.215074
43. Y.Zhang, Y.Zheng, A.Tomassini, A.K.Singh, F.M.Raymo. *Molecules*, **28**, 2447 (2023); https://doi.org/10.3390/molecules28062447
44. R.G.Clarke, M.J.Hall. In *Advances in Heterocyclic Chemistry*. Vol. 128. (Amsterdam: Elsevier, 2019). P. 18; https://doi.org/10.1016/bs.aihch.2018.12.001
45. B.F.O.Nascimento, S.M.M.Lopes, M.Pineiro, T.M.V.D.Pinho e Melo. *Molecules*, **24**, 4348 (2019); https://doi.org/10.3390/molecules24234348
46. I.S.Yadav, R.Misra. *J. Mater. Chem. C*, **11**, 8688 (2023); https://doi.org/10.1039/D3TC00171G
47. R.W.Wagner, J.S.Lindsey. *Pure Appl. Chem*., **68**, 1373 (1996); https://doi.org/10.1351/pac199668071373

48. K.Yamada, T.Toyota, K.Takakura, M.Ishimaru, T.Sugawara. *New J. Chem*., **25**, 667 (2001); https://doi.org/10.1039/b100757m
49. J.Park, D.Feng, H.-C.Zhou. *J. Am. Chem. Soc*., **137**, 1663 (2015); https://doi.org/10.1021/ja5123528
50. A.L.Nguyen, P.Bobadova-Parvanova, M.Hopfinger, F.R.Fronczek, K.M.Smith, M.G.H.Vicente. *Inorg. Chem*., **54,** 3228 (2015); https://doi.org/10.1021/ic502821m
51. N.Li, Z.Huang, X.Zhang, X.Song, Y.Xiao. *Anal. Chem*., **91**, 15308 (2019); https://doi.org/10.1021/acs.analchem.9b04587
52. M.Jurášek, S.Rimpelová, E.Kmoníčková, P.Drašar, T.Ruml. *J. Med.Chem*., **57**, 7947 (2014); https://doi.org/10.1021/jm500690j
53. S.-R.Liu, S.-P.Wu. *Org. Lett*., **15,** 878 (2013); https://doi.org/10.1021/ol400011u
54. J.A.Levitt, M.K.Kuimova, G.Yahioglu, P.-H.Chung, K.Suhling, D.Phillips. *J. Phys. Chem. C*, **113**, 11634 (2009); https://doi.org/10.1021/jp9013493
55. P.-A.Faugeras, B.Boëns, P.-H.Elchinger, J.Vergnaud, K.Teste, R.Zerrouki. *Tetrahedron Lett*., **51**, 4630 (2010); https://doi.org/10.1016/j.tetlet.2010.06.122
56. S.Qi, N.Kwon, Y.Yim, V.-N.Nguyen, J.Yoon. *Chem. Sci*., **11**, 6479 (2020); https://doi.org/10.1039/D0SC01171A
57. G.Fan, N.Wang, J.Zhang, X.Ji, S.Qin, Y.Tao, W.Zhao. *Dyes Pigm*., **199**, 110073 (2022); https://doi.org/10.1016/j.dyepig.2021.110073
58. J.H.Boyer, A.M.Haag, G.Sathyamoorthi, M.Soong, K.Thangaraj, T.G.Pavlopoulos. *Heteroat. Chem*., **4**, 39 (1993); https://doi.org/10.1002/hc.520040107
59. C.Yu, Y.Gao, Yan.Zhang, J.Wang, Yuf.Zhang, J.Li, Xinx.Zhang, Z.Wu, Xing.Zhang. *Biomacromolecules*, **22**, 3704 (2021); https://doi.org/10.1021/acs.biomac.1c00461
60. P.Štacko, L.Muchová, L.Vítek, P.Klán. *Org. Lett*., **20**, 4907 (2018); https://doi.org/10.1021/acs.orglett.8b02043
61. M.Liras, S.Simoncelli, A.Rivas-Aravena, O.García, J.C.Scaiano, E.I.Alarcon, A.Aspée. *Org. Biomol. Chem*., **14**, 4023 (2016); https://doi.org/10.1039/C6OB00533K
62. Z.Li, E.Mintzer, R.Bittman. *J. Org. Chem*., **71**, 1718 (2006); https://doi.org/10.1021/jo052029x
63. D.Wang, J.Fan, X.Gao, B.Wang, S.Sun, X.Peng. *J. Org. Chem*., **74**, 7675 (2009); https://doi.org/10.1021/jo901149y
64. N.Z.Mhlongo, T.Ebenhan, C.H.S.Driver, G.E.M.Maguire, H.G.Kruger, T.Govender, T.Naicker. *Org. Biomol. Chem*., **18**, 7876 (2020); https://doi.org/10.1039/D0OB01415J
65. A.Da Lama, J.Pérez Sestelo, L.A.Sarandeses, M.M.Martínez. *Org. Biomol. Chem*., **20**, 9132 (2022); https://doi.org/10.1039/D2OB01349E
66. J.-S.Lee, N.Kang, Y.K.Kim, A.Samanta, S.Feng, H.K.Kim, M.Vendrell, J.H.Park, Y.-T.Chang. *J. Am. Chem. Soc*., **131**, 10077 (2009); https://doi.org/10.1021/ja9011657
67. A.Y.Kritskaya, M.B.Berezin, E.V.Antina, A.I.Vyugin. *J. Fluoresc*., **29**, 911 (2019); https://doi.org/10.1007/s10895-019-02403-2
68. E.V.Antina, M.B.Berezin, N.A.Dudina, S.L.Burkova, A.Y.Nikonova. *Russ. J. Inorg. Chem*., **59**, 1187 (2014); https://doi.org/10.1134/S0036023614100027
69. A.Wakamiya, N.Sugita, S.Yamaguchi. *Chem. Lett*., **37**, 1094 (2008); https://doi.org/10.1246/cl.2008.1094
70. J.Wang, Q.Wu, Y.Xu, C.Yu, Y.Wei, X.Mu, E.Hao, L.Jiao. *RSC Adv*., **6**, 52180 (2016); https://doi.org/10.1039/C6RA04412C
71. K.Gießler, H.Griesser, D.Göhringer, T.Sabirov, C.Richert. *Eur. J. Org. Chem*., 611 (2010); https://doi.org/10.1002/ejoc.201000210
72. A.V.Saura, M.I.Burguete, F.Galindo, S.V.Luis. *Org. Biomol. Chem*., **15**, 3013 (2017); https://doi.org/10.1039/C7OB00274B
73. A.Y.Bochkov, I.O.Akchurin, O.A.Dyachenko, V.F.Traven. *Chem. Commun*., **49**, 11653 (2013); https://doi.org/10.1039/c3cc46498a
74. A.Savoldelli, Q.Meng, R.Paolesse, F.R.Fronczek, K.M.Smith, M.G.H.Vicente. *J. Org. Chem*., **83**, 6498 (2018); https://doi.org/10.1021/acs.joc.8b00789
75. E.A.Yildiz, G.Sevinç, S.Tekin, A.Karatay, M.Hayvalı, A.Elmali. *Dyes Pigm*., **193**, 109522 (2021); https://doi.org/10.1016/j.dyepig.2021.109522
76. J.Li, Q.Zhang, J.Yin, C.Yu, K.Cheng, Y.Wei, E.Hao, L.Jiao. *Org. Lett*., **18**, 5696 (2016); https://doi.org/10.1021/acs.orglett.6b02924
77. C.Yu, Q.Wu, J.Wang, Y.Wei, E.Hao, L.Jiao. *J. Org. Chem*., **81**, 3761 (2016); https://doi.org/10.1021/acs.joc.6b00414
78. L.Schneider, M.Kalt, S.Koch, S.Sithamparanathan, V.Villiger, J.Mattiat, F.Kradolfer, E.Slyshkina, S.Luber, M.Bonmarin, C.Maake, B.Spingler. *J. Am. Chem. Soc*., **145**, 4534 (2023); https://doi.org/10.1021/jacs.2c11650
79. L.Wu, K.Burgess. *Chem. Commun*., 4933 (2008); https://doi.org/10.1039/b810503k
80. T.V.Goud, A.Tutar, J.-F.Biellmann. *Tetrahedron*, **62**, 5084 (2006); https://doi.org/10.1016/j.tet.2006.03.036
81. I.Esnal, I.Valois-Escamilla, C.F.A.Gómez-Durán, A.Urías-Benavides, M.L.Betancourt-Mendiola, I.López-Arbeloa, J.Bañuelos, I.García-Moreno, A.Costela, E.Peña-Cabrera. *ChemPhysChem*, **14**, 4134 (2013); https://doi.org/10.1002/cphc.201300818
82. V.Leen, P.Yuan, L.Wang, N.Boens, W.Dehaen. *Org. Lett*., **14**, 6150 (2012); https://doi.org/10.1021/ol3028225
83. B.Umasekhar, E.Ganapathi, T.Chatterjee, M.Ravikanth. *Dalton Trans*., **44**, 16516 (2015); https://doi.org/10.1039/C5DT02634B
84. M.Sekiya, K.Umezawa, A.Sato, D.Citterio, K.Suzuki. *Chem. Commun*., 3047 (2009); https://doi.org/10.1039/b903751a
85. V.P.Yakubovskyi, M.P.Shandura, Y.P.Kovtun. *Eur. J. Org. Chem*., 3237 (2009); https://doi.org/10.1002/ejoc.200900192
86. L.Li, B.Nguyen, K.Burgess. *Bioorg. Med. Chem. Lett*., **18**, 3112 (2008); https://doi.org/10.1016/j.bmcl.2007.10.103
87. L.N.Sobenina, A.M.Vasil'tsov, O.V.Petrova, K.B.Petrushenko, I.A.Ushakov, G.Clavier, R.Meallet-Renault, A.I.Mikhaleva, B.A.Trofimov. *Org. Lett*., **13**, 2524 (2011); https://doi.org/10.1021/ol200360f
88. X.Wang, Z.Jiang, Z.Liang, T.Wang, Y.Chen, Z.Liu. *Sci. Adv*., **8**, eadd5660 (2022); https://doi.org/10.1126/sciadv.add5660
89. S.Choi, J.Bouffard, Y.Kim. *Chem. Sci*., **5**, 751 (2014); https://doi.org/10.1039/C3SC52495G
90. Y.Tian, D.Yin, L.Yan. *WIREs Nanomed. Nanobiotechnol*., **15**, e1831 (2023); https://doi.org/10.1002/wnan.1831
91. X.Jiang, T.Fang, X.Liu, D.Xi. *Eur. J. Org. Chem*., 5074 (2017); https://doi.org/10.1002/ejoc.201700800
92. Y.Chen, J.Zhao, H.Guo, L.Xie. *J. Org. Chem*., **77**, 2192 (2012); https://doi.org/10.1021/jo202215x
93. S.S.Niu, C.Massif, G.Ulrich, P.-Y.P.Renard, A.Romieu, R.Ziessel. *Chem. – Eur. J*., **18**, 7229 (2012); https://doi.org/10.1002/chem.201103613
94. C.Bonnier, W.E.Piers, A.Al-Sheikh Ali, A.Thompson, M.Parvez. *Organometallics*, **28**, 4845 (2009); https://doi.org/10.1021/om900402e
95. K.Yuan, X.Wang, S.K.Mellerup, I.Kozin, S.Wang. *J. Org. Chem*., **82**, 13481 (2017); https://doi.org/10.1021/acs.joc.7b02602
96. Z.Wang, C.Cheng, Z.Kang, W.Miao, Q.Liu, H.Wang, E.Hao. *J. Org. Chem*., **84**, 2732 (2019); https://doi.org/10.1021/acs.joc.8b03145
97. E.M.Sánchez-Carnerero, A.R.Agarrabeitia, F.Moreno, B.L.Maroto, G.Muller, M.J.Ortiz, S.de la Moya. *Chem. – Eur. J*., **21**, 13488 (2015); https://doi.org/10.1002/chem.201501178
98. N.Shivran, S.Mula, T.K.Ghanty, S.Chattopadhyay. *Org. Lett*., **13**, 5870 (2011); https://doi.org/10.1021/ol202490p
99. M.J.Ortiz, A.R.Agarrabeitia, G.Duran-Sampedro, J.Bañuelos Prieto, T.A.Lopez, W.A.Massad, H.A.Montejano, N.A.García, I.Lopez Arbeloa. *Tetrahedron,* **68**, 1153 (2012); https://doi.org/10.1016/j.tet.2011.11.070

100. L.Jiao, W.Pang, J.Zhou, Y.Wei, X.Mu, G.Bai, E.Hao. *J. Org. Chem*., **76**, 9988 (2011); https://doi.org/10.1021/jo201754m
101. V.Leen, D.Miscoria, S.Yin, A.Filarowski, J.Molisho Ngongo, M.Van der Auweraer, N.Boens, W.Dehaen. *J. Org. Chem*., **76**, 8168 (2011); https://doi.org/10.1021/jo201082z
102. S.G.Awuah, Y.You. *RSC Adv*., **2**, 11169 (2012); https://doi.org/10.1039/c2ra21404k
103. X.-F.Zhang, X.Yang. *J. Phys. Chem. B*, **117**, 5533 (2013); https://doi.org/10.1021/jp4013812
104. E.Bassan, A.Gualandi, P.G.Cozzi, P.Ceroni. *Chem. Sci*., **12**, 6607 (2021); https://doi.org/10.1039/D1SC00732G
105. L.Jiao, C.Yu, J.Li, Z.Wang, M.Wu, E.Hao. *J. Org. Chem*., **74**, 7525 (2009); https://doi.org/10.1021/jo901407h
106. J.Yin, X.Jiang, G.Sui, Y.Du, E.Xing, R.Shi, C.Gu, X.Wen, Y.Feng, Z.Shan, S.Meng. *J. Mater. Chem. B*, **9**, 7461 (2021); https://doi.org/10.1039/d1tb01155c
107. G.Duran-Sampedro, A.R.Agarrabeitia, I.Garcia-Moreno, A.Costela, J.Bañuelos, T.Arbeloa, I.López Arbeloa, J.L.Chiara, M.J.Ortiz. *Eur. J. Org. Chem*., 6335 (2012); https://doi.org/10.1002/ejoc.201200946
108. R.P.Sabatini, T.M.McCormick, T.Lazarides, K.C.Wilson, R.Eisenberg, D.W.McCamant. *J. Phys. Chem. Lett*., **2**, 223 (2011); https://doi.org/10.1021/jz101697y
109. S.H.Lim, C.Thivierge, P.Nowak-Sliwinska, J.Han, H.van den Bergh, G.Wagnières, K.Burgess, H.B.Lee. *J. Med. Chem*., **53**, 2865 (2010); https://doi.org/10.1021/jm901823u
110. A.R.Sekhar, M.A.Kaloo, J.Sankar. *Chem. – Asian J*., **9**, 2422 (2014); https://doi.org/10.1002/asia.201402389
111. F.J.Frank, P.G.Waddell, M.J.Hall, J.G.Knight. *Org. Lett*., **23**, 8595 (2021); https://doi.org/10.1021/acs.orglett.1c03317
112. Z.Lou, Y.Hou, K.Chen, J.Zhao, S.Ji, F.Zhong, Y.Dede, B.Dick. *J. Phys. Chem. C*, **122**, 185 (2018); https://doi.org/10.1021/acs.jpcc.7b10466
113. Y.Hu, Y.Hou, Z.Wang, Y.Li, J.Zhao. *J. Chem. Phys*., **153**, 224304 (2020); https://doi.org/10.1063/5.0025224
114. X.-F.Wang, S.-S.Yu, C.Wang, D.Xue, J.Xiao. *Org. Biomol. Chem*., **14**, 7028 (2016); https://doi.org/10.1039/C6OB00736H
115. I.S.Turan, F.P.Cakmak, D.C.Yildirim, R.Cetin-Atalay, E.U.Akkaya. *Chem. – Eur. J*., **20**, 16088 (2014); https://doi.org/10.1002/chem.201405450
116. D.Zhang, Y.Wang, Y.Xiao, S.Qian, X.Qian. *Tetrahedron*, **65**, 8099 (2009); https://doi.org/10.1016/j.tet.2009.08.002
117. W.Miao, X.Guo, X.Yan, Y.Shang, C.Yu, E.Dai, T.Jiang, E.Hao, L.Jiao. *Chem.– Eur. J*., **29**, e202203832 (2023); https://doi.org/10.1002/chem.202203832
118. J.L.Belmonte-Vázquez, E.Avellanal-Zaballa, E.Enríquez-Palacios, L.Cerdán, I.Esnal, J.Bañuelos, C.Villegas-Gómez, I.López Arbeloa, E.Peña-Cabrera. *J. Org. Chem*., **84**, 2523 (2019); https://doi.org/10.1021/acs.joc.8b02933
119. N.Zhao, S.Xuan, F.R.Fronczek, K.M.Smith, M.G.H.Vicente. *J. Org. Chem*., **80**, 8377 (2015); https://doi.org/10.1021/acs.joc.5b01147
120. G.Zhang, M.Wang, C.Ndung'U, P.Bobadova-Parvanova, F.R.Fronczek, K.M.Smith, M.G.H.Vicente. *J. Porphyrins Phthalocyanines*, **24**, 869 (2020); https://doi.org/10.1142/S1088424619501967
121. G.Kubheka, J.Mack, N.Kobayashi, M.Kimura, T.Nyokong. *J. Porphyrins Phthalocyanines*, **21**, 523 (2017); https://doi.org/10.1142/S1088424617500511
122. L.Tang, D.Lin, N.Rehmat, M.Lu, Z.Mahmood, H.Liang, M.Li, Z.Zhao, Y.Huo, S.Ji. *Dyes Pigm*., **217**, 111392 (2023); https://doi.org/10.1016/j.dyepig.2023.111392
123. B.Yuan, H.Wu, H.Wang, B.Tang, J.Xu, X.Zhang. *Angew. Chem., Int. Ed*., **60**, 706 (2021); https://doi.org/10.1002/anie.202012477
124. D.Serrano-Molina, C.Montoro-García, M.J.Mayoral, A.de Juan, D.González-Rodríguez. *J. Am. Chem. Soc*., **144**, 5450 (2022); https://doi.org/10.1021/jacs.1c13295
125. Z.Ruan, W.Miao, P.Yuan, L.Le, L.Jiao, E.Hao, L.Yan. *Bioconjug. Chem*., **29**, 3441 (2018); https://doi.org/10.1021/acs.bioconjchem.8b00576
126. V.Lakshmi, M.Ravikanth. *J. Org. Chem*., **76**, 8466 (2011); https://doi.org/10.1021/jo2010022
127. X.Li, S.Huang, Y.Hu. *Org. Biomol. Chem*., **10**, 2369 (2012); https://doi.org/10.1039/c2ob07004a
128. N.Zhao, S.Xuan, B.Byrd, F.R.Fronczek, K.M.Smith, M.G.H.Vicente. *Org. Biomol. Chem*., **14**, 6184 (2016); https://doi.org/10.1039/C6OB00935B
129. Q.Huaulmé, A.Sutter, S.Fall, D.Jacquemin, P.Lévêque, P.Retailleau, G.Ulrich, N.Leclerc. *J. Mater. Chem. C*, **6**, 9925 (2018); https://doi.org/10.1039/C8TC03138J
130. X.Yan, M.Su, Y.Liu, Y.Zhang, H.Zhang, C.Li. *Adv. Funct. Mater*., **31**, 2008406 (2021); https://doi.org/10.1002/adfm.202008406
131. W.Zhang, W.Lin, C.Li, S.Liu, X.Hu, Z.Xie. *ACS Appl. Mater. Interfaces*, **11**, 32720 (2019); https://doi.org/10.1021/acsami.9b10713
132. M.Won, S.Koo, H.Li, J.L.Sessler, J.Y.Lee, A.Sharma, J.S.Kim. *Angew. Chem., Int. Ed.*, **60**, 3196 (2021); https://doi.org/10.1002/anie.202012687
133. J.Hu, Q.Lei, X.Zhang. *Prog. Mater. Sci*., **114**, 100685 (2020); https://doi.org/10.1016/j.pmatsci.2020.100685
134. S.Banfi, E.Caruso, S.Zaza, M.Mancini, M.B.Gariboldi, E.Monti. *J. Photochem. Photobiol. B*, **114**, 52 (2012); https://doi.org/10.1016/j.jphotobiol.2012.05.010
135. W.Krzemien, M.Rohlickova, M.Machacek, V.Novakova, J.Piskorz, P.Zimcik. *Molecules*, **26**, 4194 (2021); https://doi.org/10.3390/molecules26144194
136. I.W.Badon, J.-P.Jee, T.P.Vales, C.Kim, S.Lee, J.Yang, S.K.Yang, H.-J.Kim. *Pharmaceutics*, **15**, 1512 (2023); https://doi.org/10.3390/pharmaceutics15051512
137. Y.Tian, Q.Cheng, H.Dang, H.Qian, C.Teng, K.Xie, L.Yan. *Dyes Pigm*., **194**, 109611 (2021); https://doi.org/10.1016/j.dyepig.2021.109611
138. H.S.Jung, S.Koo, M.Won, S.An, H.Park, J.L.Sessler, J.Han, J.S.Kim. *Chem. Sci*., **14**, 1808 (2023); https://doi.org/10.1039/D2SC03945A
139. X.Zhou, C.Yu, Z.Feng, Y.Yu, J.Wang, E.Hao, Y.Wei, X.Mu, L.Jiao. *Org. Lett*., **17**, 4632 (2015); https://doi.org/10.1021/acs.orglett.5b02383
140. F.Frank, L.M.Alice, P.Mauker, A.A.Alsimaree, P.G.Waddell, M.R.Probert, T.J.Penfold, J.G.Knight, M.J.Hall. *Tetrahedron*, **76**, 131113 (2020); https://doi.org/10.1016/j.tet.2020.131113
141. T.Rohand, M.Baruah, W.Qin, N.Boens, W.Dehaen. *Chem. Commun*., 266 (2006); https://doi.org/10.1039/B512756D
142. V.Leen, E.Braeken, K.Luckermans, C.Jackers, M.Van der Auweraer, N.Boens, W.Dehaen. *Chem. Commun*., 4515 (2009); https://doi.org/10.1039/b906164a
143. S.Debnath, S.Singh, A.Bedi, K.Krishnamoorthy, S.S.Zade. *J. Polym. Sci., Part A: Polym. Chem*., **54**, 1978 (2016); https://doi.org/10.1002/pola.28064
144. T.Jiang, P.Zhang, C.Yu, J.Yin, L.Jiao, E.Dai, J.Wang, Y.Wei, X.Mu, E.Hao. *Org. Lett*., **16**, 1952 (2014); https://doi.org/10.1021/ol500507f
145. A.M.Huynh, J.Menges, M.Vester, T.Dier, V.Huch, D.A.Volmer, G.Jung. *ChemPhysChem*, **17**, 433 (2016); https://doi.org/10.1002/cphc.201500869
146. A.R.Mazzotti, M.G.Campbell, P.Tang, J.M.Murphy, T.Ritter. *J. Am. Chem. Soc*., **135**, 14012 (2013); https://doi.org/10.1021/ja405919z
147. Z.Köstereli, K.Severin. *Org. Biomol. Chem*., **13**, 252 (2015); https://doi.org/10.1039/C4OB02095B
148. J.Kim, Y.Kim. *Analyst*, **139**, 2986 (2014); https://doi.org/10.1039/C4AN00466C
149. D.Kand, P.Liu, M.X.Navarro, L.J.Fischer, L.Rousso-Noori, D.Friedmann-Morvinski, A.H.Winter, E.W.Miller, R.Weinstain. *J. Am. Chem. Soc*., **142**, 4970 (2020); https://doi.org/10.1021/jacs.9b13219
150. M.Gupta, S.Mula, M.Tyagi, T.K.Ghanty, S.Murudkar, A.K.Ray, S.Chattopadhyay. *Chem. – Eur. J*., **19**, 17766 (2013); https://doi.org/10.1002/chem.201302359

151. M.Koli, S.Mula. *Synlett*, **35**, 84 (2024); https://doi.org/10.1055/a-2086-0530
152. I.Esnal, J.Bañuelos, I.López Arbeloa, A.Costela, I.Garcia-Moreno, M.Garzón, A.R.Agarrabeitia, M.José Ortiz. *RSC Adv.*, **3**, 1547 (2013); https://doi.org/10.1039/C2RA22916A
153. C.Ndung'U, P.Bobadova-Parvanova, D.J.La Master, D.Goliber, F.R.Fronczek, M.da G.H.Vicente. *Molecules*, **28**, 4581 (2023); https://doi.org/10.3390/molecules28124581
154. K.Renault, C.Sabot, P.Renard. *Eur. J. Org. Chem*., 7992 (2015); https://doi.org/10.1002/ejoc.201501140
155. S.M.Gil de Melo, L.C.D.de Rezende, R.Petrilli, R.F.Vianna Lopez, M.O.F.Goulart, F.da Silva Emery. *Dyes Pigm*., **173**, 107885 (2020); https://doi.org/10.1016/j.dyepig.2019.107885
156. Y.Wang, J.Yang, Q.Chen, J.Su, W.-J.Shi, L.Zhang, C.Xia, J.Yan. *ACS Appl. Bio Mater*., **5**, 3049 (2022); https://doi.org/10.1021/acsabm.2c00335
157. C.N.Paulson, X.Guan, A.M.Ayoub, A.Chan, R.M.Karim, W.C.K.Pomerantz, E.Schönbrunn, G.I.Georg, J.E.Hawkinson. *ACS Med. Chem. Lett*., **9**, 1223 (2018); https://doi.org/10.1021/acsmedchemlett.8b00380
158. Y.Cakmak, S.Kolemen, S.Duman, Y.Dede, Y.Dolen, B.Kilic, Z.Kostereli, L.T.Yildirim, A.L.Dogan, D.Guc, E.U.Akkaya. *Angew. Chem., Int. Ed*., **50**, 11937 (2011); https://doi.org/10.1002/anie.201105736
159. Z.Yang, D.H.Kang, H.Lee, J.Shin, W.Yan, B.Rathore, H.-R.Kim, S.J.Kim, H.Singh, L.Liu, J.Qu, C.Kang, J.S.Kim. *Bioconjug. Chem*., **29**, 1446 (2018); https://doi.org/10.1021/acs.bioconjchem.8b00128
160. M.Tsuchiya, R.Sakamoto, M.Shimada, Y.Yamanoi, Y.Hattori, K.Sugimoto, E.Nishibori, H.Nishihara. *Chem. Commun*., **53**, 7509 (2017); https://doi.org/10.1039/C7CC03279J
161. F.Suárez-Blas, M.Martínez-Fernández, A.Prieto-Castañeda, A.García-Fernández, J.I.Martínez, M.M.Ramos, M.J.Ortiz, R.Martínez-Máñez, J.L.Segura. *Dyes Pigm*., **219**, 111561 (2023); https://doi.org/10.1016/j.dyepig.2023.111561
162. S.Madhu, M.R.Rao, M.S.Shaikh, M.Ravikanth. *Inorg. Chem*., **50**, 4392 (2011); https://doi.org/10.1021/ic102499h
163. J.M.Ganley, M.Christensen, Y.Lam, Z.Peng, A.R.Angeles, C.S.Yeung. *Org. Lett*., **20**, 5752 (2018); https://doi.org/10.1021/acs.orglett.8b02453
164. F.Lv, Y.Yu, E.Hao, C.Yu, H.Wang, N.Boens, L.Jiao. *Org. Biomol. Chem*., **17**, 5121 (2019); https://doi.org/10.1039/C9OB00927B
165. M.Yu, J.K.-H.Wong, C.Tang, P.Turner, M.H.Todd, P.J.Rutledge. *Beilstein J. Org. Chem*., **11**, 37 (2015); https://doi.org/10.3762/bjoc.11.6
166. G.Durán-Sampedro, A.R.Agarrabeitia, L.Cerdán, M.E.Pérez-Ojeda, A.Costela, I.García-Moreno, I.Esnal, J.Bañuelos, I.L.Arbeloa, M.J.Ortiz. *Adv. Funct. Mater*., **23**, 4195 (2013); https://doi.org/10.1002/adfm.201300198
167. C.Tahtaoui, C.Thomas, F.Rohmer, P.Klotz, G.Duportail, Y.Mély, D.Bonnet, M.Hibert. *J. Org. Chem*., **72**, 269 (2007); https://doi.org/10.1021/jo061567m
168. G.Mirri, D.C.Schoenmakers, P.H.J.Kouwer, P.Veranič, I.Muševič, B.Štefane. *ChemistryOpen*, **5**, 450 (2016); https://doi.org/10.1002/open.201600067
169. F.de Jong, J.Pokorny, B.Manshian, B.Daelemans, J.Vandaele, J.B.Startek, S.Soenen, M.Van der Auweraer, W.Dehaen, S.Rocha, G.Silveira-Dorta. *Dyes Pigm*., **176**, 108200 (2020); https://doi.org/10.1016/j.dyepig.2020.108200
170. J.A.González-Vera, F.Lv, D.Escudero, A.Orte, X.Guo, E.Hao, E.M.Talavera-Rodriguez, L.Jiao, N.Boens, M.J.Ruedas-Rama. *Dyes Pigm*., **182**, 108510 (2020); https://doi.org/10.1016/j.dyepig.2020.108510
171. H.Yanai, S.Hoshikawa, Y.Moriiwa, A.Shoji, A.Yanagida, T.Matsumoto. *Angew. Chem., Int. Ed*., **60**, 5168 (2021); https://doi.org/10.1002/anie.202012764
172. C.Uriel, A.M.Gómez, E.García Martínez de la Hidalga, J.Bañuelos, I.Garcia-Moreno, J.C.López. *Org. Lett*., **23**, 6801 (2021); https://doi.org/10.1021/acs.orglett.1c02380
173. J.Ventura, C.Uriel, A.M.Gómez, E.Avellanal-Zaballa, J.Bañuelos, E.Rebollar, I.Garcia-Moreno, J.C.López. *Org. Lett*., **25**, 2588 (2023); https://doi.org/10.1021/acs.orglett.3c00476
174. E.Fron, E.Coutiño-Gonzalez, L.Pandey, M.Sliwa, M.Van der Auweraer, F.C.De Schryver, J.Thomas, Z.Dong, V.Leen, M.Smet, W.Dehaen, T.Vosch. *New J. Chem*., **33**, 1490 (2009); https://doi.org/10.1039/b900786e
175. S.Bi, T.Yang, K.An, B.Zhou, Y.Han. *Spectrochim. Acta, Part A*, **299**, 122860 (2023); https://doi.org/10.1016/j.saa.2023.122860
176. Y.Mei, Z.Li, K.Rong, Z.Hai, W.Tang, Q.-H.Song. *Chem. Commun*., **59**, 12775 (2023); https://doi.org/10.1039/D3CC03914E
177. L.-Y.Niu, Y.-S.Guan, Y.-Z.Chen, L.-Z.Wu, C.-H.Tung, Q.-Z.Yang. *J. Am. Chem. Soc.*, **134**, 18928 (2012); https://doi.org/10.1021/ja309079f
178. L.-Y.Niu, Y.-S.Guan, Y.-Z.Chen, L.-Z.Wu, C.-H.Tung, Q.-Z.Yang. *Chem. Commun.*, **49**, 1294 (2013); https://doi.org/10.1039/c2cc38429a
179. L.-Y.Niu, Q.-Q.Yang, H.-R.Zheng, Y.-Z.Chen, L.-Z.Wu, C.-H.Tung, Q.-Z.Yang. *RSC Adv.*, **5**, 3959 (2015); https://doi.org/10.1039/C4RA13526A
180. F.Wang, L.Zhou, C.Zhao, R.Wang, Q.Fei, S.Luo, Z.Guo, H.Tian, W.-H.Zhu. *Chem. Sci*., **6**, 2584 (2015); https://doi.org/10.1039/C5SC00216H
181. M.-Y.Jia, L.-Y.Niu, Y.Zhang, Q.-Z.Yang, C.-H.Tung, Y.-F.Guan, L.Feng. *ACS Appl. Mater. Interfaces*, **7**, 5907 (2015); https://doi.org/10.1021/acsami.5b00122
182. Y.Liu, L.-Y.Niu, Y.-Z.Chen, Q.-Z.Yang. *J. Photochem. Photobiol. A*, **355**, 311 (2018); https://doi.org/10.1016/j.jphotochem.2017.08.042
183. F.Wang, Z.Guo, X.Li, X.Li, C.Zhao. *Chem. – Eur. J.*, **20**, 11471 (2014); https://doi.org/10.1002/chem.201403450
184. D.Gong, S.-C.Han, A.Iqbal, J.Qian, T.Cao, Wei Liu, Weis.Liu, W.Qin, H.Guo. *Anal. Chem*., **89**, 13112 (2017); https://doi.org/10.1021/acs.analchem.7b02311
185. X.-L.Liu, L.-Y.Niu, Y.-Z.Chen, M.-L.Zheng, Y.Yang, Q.-Z.Yang. *Org. Biomol. Chem.*, **15**, 1072 (2017); https://doi.org/10.1039/C6OB02407F
186. D.Gong, X.Zhu, Y.Tian, S.-C.Han, M.Deng, A.Iqbal, W.Liu, W.Qin, H.Guo. *Anal. Chem*., **89**, 1801 (2017); https://doi.org/10.1021/acs.analchem.6b04114
187. V.Leen, V.Z.Gonzalvo, W.M.Deborggraeve, N.Boens, W.Dehaen. *Chem. Commun*., **46**, 4908 (2010); https://doi.org/10.1039/c0cc00568a
188. M.Zhang, E.Hao, J.Zhou, C.Yu, G.Bai, F.Wang, L.Jiao. *Org. Biomol. Chem*., **10**, 2139 (2012); https://doi.org/10.1039/c2ob06689k
189. B.S.Cugnasca, F.Wodtke, A.A.Dos Santos. *Curr. Chem. Biol*., **15**, 215 (2021); https://doi.org/10.2174/2212796815666210504084205
190. V.Leen, M.Van der Auweraer, N.Boens, W.Dehaen. *Org. Lett*., **13**, 1470 (2011); https://doi.org/10.1021/ol200148u
191. J.G.Knight, R.B.Alnoman, P.G.Waddell. *Org. Biomol. Chem*., **13**, 3819 (2015); https://doi.org/10.1039/C4OB02626H
192. T.Ozdemir, Z.Kostereli, R.Guliyev, S.Yalcin, Y.Dede, E.U.Akkaya. *RSC Adv*., **4**, 14915 (2014); https://doi.org/10.1039/C4RA00989D
193. R.Lincoln, L.E.Greene, K.Krumova, Z.Ding, G.Cosa. *J. Phys. Chem. A*, **118**, 10622 (2014); https://doi.org/10.1021/jp5059148
194. C.F.A.Gómez-Durán, I.García-Moreno, A.Costela, V.Martin, R.Sastre, J.Bañuelos, F.López Arbeloa, I.López Arbeloa, E.Peña-Cabrera. *Chem. Commun*., **46**, 5103 (2010); https://doi.org/10.1039/c0cc00397b
195. J.Bañuelos, V.Martín, C.F.A.Gómez-Durán, I.J.A.Córdoba, E.Peña-Cabrera, I.García-Moreno, Á.Costela, M.E.Pérez-Ojeda, T.Arbeloa, Í.L.Arbeloa. *Chem. – Eur. J*., **17**, 7261 (2011); https://doi.org/10.1002/chem.201003689

196. C.A.Osorio-Martínez, A.Urías-Benavides, C.F.A.Gómez-Durán, J.Bañuelos, I.Esnal, I.López Arbeloa, E.Peña-Cabrera. *J. Org. Chem.*, **77**, 5434 (2012); https://doi.org/10.1021/jo300724m
197. R.I.Roacho, A.Metta-Magaña, M.M.Portillo, E.Peña-Cabrera, K.H.Pannell. *J. Org. Chem*., **78**, 4245 (2013); https://doi.org/10.1021/jo302758a
198. B.D.Gutiérrez-Ramos, J.Bañuelos, T.Arbeloa, I.L.Arbeloa, P.E.González-Navarro, K.Wrobel, L.Cerdán, I.García-Moreno, A.Costela, E.Peña-Cabrera. *Chem. – Eur. J*., **21**, 1755 (2015); https://doi.org/10.1002/chem.201405233
199. R.I.Roacho, A.Metta-Magaña, E.Peña-Cabrera, K.Pannell. *Org. Biomol. Chem*., **13**, 995 (2015); https://doi.org/10.1039/C4OB01892C
200. I.Esnal, A.Urías-Benavides, C.F.A.Gómez-Durán, C.A.Osorio-Martínez, I.García-Moreno, A.Costela, J.Bañuelos, N.Epelde, I.López Arbeloa, R.Hu, B.Zhong Tang, E.Peña-Cabrera. *Chem. Asian J.*, **8**, 2691 (2013); https://doi.org/10.1002/asia.201300760
201. A.Yagishita, T.Ueno, K.Tsuchihara, Y.Urano. *Bioconjug. Chem*., **32**, 234 (2021); https://doi.org/10.1021/acs.bioconjchem.0c00565
202. W.Shi, J.Li, X.He, S.Zhou, H.Sun, H.Wu. *Org. Lett*., **24**, 3368 (2022); https://doi.org/10.1021/acs.orglett.2c01118
203. N.Boens, L.Wang, V.Leen, P.Yuan, B.Verbelen, W.Dehaen, M.Van der Auweraer, W.D.De Borggraeve, L.Van Meervelt, J.Jacobs, D.Beljonne, C.Tonnelé, R.Lazzaroni, M.J.Ruedas-Rama, A.Orte, L.Crovetto, E.M.Talavera, J.M.Alvarez-Pez. *J. Phys. Chem. A*, **118**, 1576 (2014); https://doi.org/10.1021/jp412132y
204. R.Misra, B.Dhokale, T.Jadhav, S.M.Mobin. *New J. Chem*., **38**, 3579 (2014); https://doi.org/10.1039/C4NJ00354C
205. S.Popov, H.Plenio. *Eur. J. Inorg. Chem*., e202200335 (2022); https://doi.org/10.1002/ejic.202200335
206. L.Zeng, T.Chen, B.Zhu, S.Koo, Y.Tang, W.Lin, T.D.James, J.S.Kim. *Chem. Sci*., **13**, 4523 (2022); https://doi.org/10.1039/D2SC00299J
207. X.-H.Xu, C.Liu, Y.Mei, Q.-H.Song. *J. Mater. Chem. B*, **7**, 6861 (2019); https://doi.org/10.1039/C9TB01641D
208. D.H.Ma, D.Kim, E.Seo, S.-J.Lee, K.H.Ahn. *Analyst*, **140**, 422 (2015); https://doi.org/10.1039/C4AN01791A
209. X.Ji, N.Wang, J.Zhang, S.Xu, Y.Si, W.Zhao. *Dyes Pigm.*, **187**, 109089 (2021); https://doi.org/10.1016/j.dyepig.2020.109089
210. X.Yang, J.Wang, Z.Zhang, B.Zhang, X.Du, J.Zhang, J.Wang. *Food Chem*., **416**, 135730 (2023); https://doi.org/10.1016/j.foodchem.2023.135730
211. D.Kim, K.Yamamoto, K.H.Ahn. *Tetrahedron*, **68**, 5279 (2012); https://doi.org/10.1016/j.tet.2012.01.091
212. Y.Chen, L.Wan, D.Zhang, Y.Bian, J.Jiang. *Photochem. Photobiol. Sci*., **10**, 1030 (2011); https://doi.org/10.1039/c1pp00001b
213. T.Slanina, P.Shrestha, E.Palao, D.Kand, J.A.Peterson, A.S.Dutton, N.Rubinstein, R.Weinstain, A.H.Winter, P.Klán. *J. Am. Chem. Soc*., **139**, 15168 (2017); https://doi.org/10.1021/jacs.7b08532
214. A.B.Nepomnyashchii, M.Bröring, J.Ahrens, A.J.Bard. *J. Am. Chem. Soc*., **133**, 19498 (2011); https://doi.org/10.1021/ja207545t
215. K.Rurack, M.Kollmannsberger, J.Daub. *Angew. Chem., Int. Ed.*, **40**, 385 (2001); https://doi.org/10.1002/1521-3773(20010119)40:2<385::AID-ANIE385>3.0.CO;2-F
216. O.Buyukcakir, O.A.Bozdemir, S.Kolemen, S.Erbas, E.U.Akkaya. *Org. Lett*., **11**, 4644 (2009); https://doi.org/10.1021/ol9019056
217. J.Zou, P.Wang, Y.Wang, G.Liu, Y.Zhang, Q.Zhang, J.Shao, W.Si, W.Huang, X.Dong. *Chem. Sci.*, **10**, 268 (2019); https://doi.org/10.1039/C8SC02443J
218. N.Boens, V.Leen, W.Dehaen. *Chem. Soc. Rev*., **41**, 1130 (2012); https://doi.org/10.1039/c1cs15132k
219. N.A.Bumagina, E.V.Antina, A.A.Ksenofontov, L.A.Antina, A.A.Kalyagin, M.B.Berezin. *Coord. Chem. Rev*., **469**, 214684 (2022); https://doi.org/10.1016/j.ccr.2022.214684
220. T.Bura, N.Leclerc, S.Fall, P.Lévêque, T.Heiser, P.Retailleau, S.Rihn, A.Mirloup, R.Ziessel. *J. Am. Chem. Soc*., **134**, 17404 (2012); https://doi.org/10.1021/ja3072513
221. C.L.Teoh, D.Su, S.Sahu, S.-W.Yun, E.Drummond, F.Prelli, S.Lim, S.Cho, S.Ham, T.Wisniewski, Y.-T.Chang. *J. Am. Chem. Soc*., 137, 13503 (2015); https://doi.org/10.1021/jacs.5b06190
222. C.Duan, M.Won, P.Verwilst, J.Xu, H.S.Kim, L.Zeng, J.S.Kim. *Anal. Chem.*, **91**, 4172 (2019); https://doi.org/10.1021/acs.analchem.9b00224
223. L.Huang, J.Zhao, S.Guo, C.Zhang, J.Ma. *J. Org. Chem*., **78**, 5627 (2013); https://doi.org/10.1021/jo400769u
224. L.Huang, X.Yu, W.Wu, J.Zhao. *Org. Lett*., **14**, 2594 (2012); https://doi.org/10.1021/ol3008843
225. S.Kaya, Y.A.Ismaiel, N.Kwon, G.Kim, J.L.Bila, J.Yoon, O.Seven, E.U.Akkaya. *Dyes Pigm.*, **188**, 109158 (2021); https://doi.org/10.1016/j.dyepig.2021.109158
226. J.Yang, C.H.Devillers, P.Fleurat-Lessard, H.Jiang, S.Wang, C.P.Gros, G.Gupta, G.D.Sharma, H.Xu. *Dalton Trans.*, **49**, 5606 (2020); https://doi.org/10.1039/D0DT00637H
227. A.B.Nepomnyashchii, M.Bröring, J.Ahrens, A.J.Bard. *J. Am. Chem. Soc*., **133**, 8633 (2011); https://doi.org/10.1021/ja2010219
228. Y.Liu, J.Gao, H.Li, M.Yang, J.Lv, Y.Zhou, Z.Yuan, X.Li. *Org. Biomol. Chem*., **21**, 4672 (2023); https://doi.org/10.1039/D3OB00465A
229. H.Xiong, H.Zuo, Y.Yan, G.Occhialini, K.Zhou, Y.Wan, D.J.Siegwart. *Adv. Mater*., **29**, 1700131 (2017); https://doi.org/10.1002/adma.201700131
230. X.Kong, L.Di, Y.Fan, Z.Zhou, X.Feng. *Chem. Commun*., **55**, 11567 (2019); https://doi.org/10.1039/c9cc04416g
231. O.Karaman, T.Almammadov, M.Emre Gedik, G.Gunaydin, S.Kolemen, G.Gunbas. *ChemMedChem,* **14**, 1879 (2019); https://doi.org/10.1002/cmdc.201900380
232. S.Duman, Y.Cakmak, S.Kolemen, E.U.Akkaya, Y.Dede. *J. Org. Chem*., **77**, 4516 (2012); https://doi.org/10.1021/jo300051v
233. H.Xiong, K.Zhou, Y.Yan, J.B.Miller, D.J.Siegwart. *ACS Appl. Mater. Interfaces*, **10**, 16335 (2018); https://doi.org/10.1021/acsami.8b04710
234. V.Ramu, S.Gautam, A.Garai, P.Kondaiah, A.R.Chakravarty. *Inorg. Chem*., **57**, 1717 (2018); https://doi.org/10.1021/acs.inorgchem.7b02249
235. V.Ramu, S.Gautam, P.Kondaiah, A.R.Chakravarty. *Inorg. Chem.*, **58**, 9067 (2019); https://doi.org/10.1021/acs.inorgchem.9b00567
236. J.Ma, X.Yuan, B.Küçüköz, S.Li, C.Zhang, P.Majumdar, A.Karatay, X.Li, H.Gul Yaglioglu, A.Elmali, J.Zhao, M.Hayvali. *J. Mater. Chem. C*, **2**, 3900 (2014); https://doi.org/10.1039/C3TC32456G
237. A.Aguiar, J.Farinhas, W.da Silva, M.E.Ghica, C.M.A.Brett, J.Morgado, A.J.F.N.Sobral. *Dyes Pigm*., **168**, 103 (2019); https://doi.org/10.1016/j.dyepig.2019.04.031
238. S.Ma, S.Du, G.Pan, S.Dai, B.Xu, W.Tian. *Aggregate*, **2**, e96 (2021); https://doi.org/10.1002/agt2.96
239. X.Hu, Z.Fang, C.Zhu, Y.Yang, Z.Yang, W.Huang. *Adv. Funct. Mater*., **34**, 2401325 (2024); https://doi.org/10.1002/adfm.202401325
240. M.Su, Q.Han, X.Yan, Y.Liu, P.Luo, W.Zhai, Q.Zhang, L.Li, C.Li. *ACS Nano*, **15**, 5032 (2021); https://doi.org/10.1021/acsnano.0c09993
241. V.-N.Nguyen, Y.Yan, J.Zhao, J.Yoon. *Acc. Chem. Res*., **54**, 207 (2021); https://doi.org/10.1021/acs.accounts.0c00606
242. Z.Lei, F.Zhang. *Angew. Chem., Int. Ed*., **60**, 16294 (2021); https://doi.org/10.1002/anie.202007040
243. M.Bayda, F.Dumoulin, G.L.Hug, J.Koput, R.Gorniak, A.Wojcik. *Dalton Trans*., **46**, 1914 (2017); https://doi.org/10.1039/C6DT02651F

244. H.Dang, Y.Tian, Q.Cheng, C.Teng, K.Xie, L.Yan. *J. Colloid Interface Sci*., **612**, 287 (2022); https://doi.org/10.1016/j.jcis.2021.12.177
245. X.Guo, J.Yang, M.Li, F.Zhang, W.Bu, H.Li, Q.Wu, D.Yin, L.Jiao, E.Hao. *Angew. Chem., Int. Ed*., **61**, e202211081 (2022); https://doi.org/10.1002/anie.202211081
246. M.Yang, C.Ji, M.Yin. *WIREs Nanomed. Nanobiotechnol*., **16**, e1960 (2024); https://doi.org/10.1002/wnan.1960
247. H.S.Jung, P.Verwilst, A.Sharma, J.Shin, J.L.Sessler, J.S.Kim. *Chem. Soc. Rev*., **47**, 2280 (2018); https://doi.org/10.1039/C7CS00522A
248. L.Huang, Z.Li, Y.Zhao, J.Yang, Y.Yang, A.I.Pendharkar, Y.Zhang, S.Kelmar, L.Chen, W.Wu, J.Zhao, G.Han. *Adv. Mater*., **29**, 1604789 (2017); https://doi.org/10.1002/adma.201604789
249. M.Su, X.Yan, X.Guo, Q.Li, Y.Zhang, C.Li. *Chem. – Eur. J*., **26**, 4505 (2020); https://doi.org/10.1002/chem.202000462
250. J.Zou, Z.Yin, P.Wang, D.Chen, J.Shao, Q.Zhang, L.Sun, W.Huang, X.Dong. *Chem. Sci*., **9**, 2188 (2018); https://doi.org/10.1039/C7SC04694D
251. S.Ansteatt, A.Meares, M.Ptaszek. *J. Org. Chem.*, **86**, 8755 (2021); https://doi.org/10.1021/acs.joc.1c00586
252. J.Zhang, M.Yang, W.Mazi, K.Adhikari, M.Fang, F.Xie, L.Valenzano, A.Tiwari, F.-T.Luo, H.Liu. *ACS Sensors*, **1**, 158 (2016); https://doi.org/10.1021/acssensors.5b00065
253. W.Hu, X.Miao, H.Tao, A.Baev, C.Ren, Q.Fan, T.He, W.Huang, P.N.Prasad. *ACS Nano*, **13**, 12006 (2019); https://doi.org/10.1021/acsnano.9b06208
254. E.Palao, A.R.Agarrabeitia, J.Bañuelos-Prieto, T.A.Lopez, I.Lopez-Arbeloa, D.Armesto, M.J.Ortiz. *Org. Lett*., **15**, 4454 (2013); https://doi.org/10.1021/ol401993p
255. S.Chibani, B.Le Guennic, A.Charaf-Eddin, A.D.Laurent, D.Jacquemin. *Chem. Sci*., **4**, 1950 (2013); https://doi.org/10.1039/c3sc22265a
256. C.Yu, Y.Xu, L.Jiao, J.Zhou, Z.Wang, E.Hao. *Chem. – Eur. J*., **18**, 6437 (2012); https://doi.org/10.1002/chem.201200398
257. M.P.Shandura, V.P.Yakubovskyi, Y.P.Kovtun. *J. Heterocycl. Chem*., **46**, 1386 (2009); https://doi.org/10.1002/jhet.263
258. G.Ulrich, R.Ziessel, A.Haefele. *J. Org. Chem*., **77**, 4298 (2012); https://doi.org/10.1021/jo3002408
259. G.Sathyamoorthi, L.T.Wolford, A.M.Haag, J.H.Boyer. *Heteroat. Chem*., **5**, 245 (1994); https://doi.org/10.1002/hc.520050309
260. Q.Wu, J.Zhou, Y.Wu, C.Yu, E.Hao, L.Jiao. *New J. Chem*., **40**, 1387 (2016); https://doi.org/10.1039/C5NJ02346G
261. A.L.Nguyen, M.Wang, P.Bobadova-Parvanova, Q.Do, Z.Zhou, F.R.Fronczek, K.M.Smith, M.G.H.Vicente. *J. Porphyrins Phthalocyanines*, **20**, 1409 (2016); https://doi.org/10.1142/S108842461650125X
262. M.Wang, M.G.H.Vicente, D.Mason, P.Bobadova-Parvanova. *ACS Omega*, **3**, 5502 (2018); https://doi.org/10.1021/acsomega.8b00404
263. B.Verbelen, S.Boodts, J.Hofkens, N.Boens, W.Dehaen. *Angew. Chem., Int. Ed*., **54**, 4612 (2015); https://doi.org/10.1002/anie.201410853
264. B.Verbelen, L.Cunha Dias Rezende, S.Boodts, J.Jacobs, L.Van Meervelt, J.Hofkens, W.Dehaen. *Chem. – Eur. J*., **21**, 12667 (2015); https://doi.org/10.1002/chem.201500938
265. X.Zhou, Q.Wu, Y.Yu, C.Yu, E.Hao, Y.Wei, X.Mu, L.Jiao. *Org. Lett*., **18**, 736 (2016); https://doi.org/10.1021/acs.orglett.5b03706
266. Y.Yu, L.Jiao, J.Wang, H.Wang, C.Yu, E.Hao, N.Boens. *Chem. Commun*., **53**, 581 (2017); https://doi.org/10.1039/C6CC08098G
267. H.Zhang, X.Chen, J.Lan, Y.Liu, F.Zhou, D.Wu, J.You. *Chem. Commun*., **54**, 3219 (2018); https://doi.org/10.1039/C8CC00238J
268. F.Lv, B.Tang, E.Hao, Q.Liu, H.Wang, L.Jiao. *Chem. Commun*., **55**, 1639 (2019); https://doi.org/10.1039/C8CC09821B
269. F.Ma, L.Zhou, Q.Liu, C.Li, Y.Xie. *Org. Lett*., **21**, 733 (2019); https://doi.org/10.1021/acs.orglett.8b03954
270. W.Li, Z.Xie, X.Jing. *Catal. Commun*., **16**, 94 (2011); https://doi.org/10.1016/j.catcom.2011.09.007
271. W.Li, W.Zhang, X.Dong, L.Yan, R.Qi, W.Wang, Z.Xie, X.Jing. *J. Mater. Chem*., **22**, 17445 (2012); https://doi.org/10.1039/c2jm32778c
272. C.Zhang, J.Zhao, S.Wu, Z.Wang, W.Wu, J.Ma, S.Guo, L.Huang. *J. Am. Chem. Soc*., **135**, 10566 (2013); https://doi.org/10.1021/ja405170j
273. L.Huang, J.Zhao. *RSC Adv*., **3**, 23377 (2013); https://doi.org/10.1039/c3ra43299h
274. S.Guo, H.Zhang, L.Huang, Z.Guo, G.Xiong, J.Zhao. *Chem Commun*., **49**, 8689 (2013); https://doi.org/10.1039/c3cc44486d
275. S.Guo, R.Tao, J.Zhao. *RSC Adv*., **4**, 36131 (2014); https://doi.org/10.1039/C4RA03631J
276. X.-Z.Wang, Q.-Y.Meng, J.-J.Zhong, X.-W.Gao, T.Lei, L.-M.Zhao, Z.-J.Li, B.Chen, C.-H.Tung, L.-Z.Wu. *Chem. Commun*., **51**, 11256 (2015); https://doi.org/10.1039/C5CC03421C
277. R.Rajmohan, P.Nisha, P.Vairaprakash. *ACS Omega*, **4**, 14458 (2019); https://doi.org/10.1021/acsomega.9b01407
278. G.Magagnano, A.Gualandi, M.Marchini, L.Mengozzi, P.Ceroni, P.G.Cozzi. *Chem. Commun*., **53**, 1591 (2017); https://doi.org/10.1039/C6CC09387F
279. W.H.García-Santos, J.Ordóñez-Hernández, M.Farfán-Paredes, H.M.Castro-Cruz, N.A.Macías-Ruvalcaba, N.Farfán, A.Cordero-Vargas. *J. Org. Chem*., **86**, 16315 (2021); https://doi.org/10.1021/acs.joc.1c01598
280. M.Bröring, R.Krüger, S.Link, C.Kleeberg, S.Köhler, X.Xie, B.Ventura, L.Flamigni. *Chem. – Eur. J*., **14**, 2976 (2008); https://doi.org/10.1002/chem.200701912
281. T.Bruhn, G.Pescitelli, S.Jurinovich, A.Schaumlöffel, F.Witterauf, J.Ahrens, M.Bröring, G.Bringmann. *Angew. Chem., Int. Ed*., **53**, 14592 (2014); https://doi.org/10.1002/anie.201408398
282. D.Wang, Q.Wu, X.Zhang, W.Wang, E.Hao, L.Jiao. *Org. Lett*., **22**, 7694 (2020); https://doi.org/10.1021/acs.orglett.0c02895
283. Z.Kang, Q.Wu, X.Guo, L.Wang, Y.Ye, C.Yu, H.Wang, E.Hao, L.Jiao. *Chem. Commun*., **57**, 9886 (2021); https://doi.org/10.1039/D1CC04098G
284. Q.Gong, X.Zhang, W.Li, X.Guo, Q.Wu, C.Yu, L.Jiao, Y.Xiao, E.Hao. *J. Am. Chem. Soc.*, **144**, 21992 (2022); https://doi.org/10.1021/jacs.2c08947
285. K.Teng, W.Chen, L.Niu, W.Fang, G.Cui, Q.Yang. *Angew. Chem., Int. Ed*., **60**, 19912 (2021); https://doi.org/10.1002/anie.202106748
286. Y.Hayashi, S.Yamaguchi, W.Y.Cha, D.Kim, H.Shinokubo. *Org. Lett*., **13**, 2992 (2011); https://doi.org/10.1021/ol200799u
287. S.Rihn, M.Erdem, A.De Nicola, P.Retailleau, R.Ziessel. *Org. Lett*., **13**, 1916 (2011); https://doi.org/10.1021/ol200189y
288. I.J.Arroyo-Córdoba, R.Sola-Llano, N.Epelde-Elezcano, I.L.Arbeloa, V.Martínez-Martínez, E.Peña-Cabrera. *J. Org. Chem*., **83**, 10186 (2018); https://doi.org/10.1021/acs.joc.8b01429
289. L.Wang, Q.Wu, Z.Kang, X.Guo, W.Miao, Z.Li, H.Zuo, H.Wang, H.Si, L.Jiao, E.Hao. *Org. Lett*., **25**, 5055 (2023); https://doi.org/10.1021/acs.orglett.3c01755
290. Z.Kang, F.Lv, Q.Wu, H.Li, Z.Li, F.Wu, Z.Wang, L.Jiao, E.Hao. *Org. Lett*., **23**, 7986 (2021); https://doi.org/10.1021/acs.orglett.1c02996
291. A.Poirel, A.De Nicola, P.Retailleau, R.Ziessel. *J. Org. Chem*., **77**, 7512 (2012); https://doi.org/10.1021/jo301300b
292. L.Salem, C.Rowland. *Angew. Chem., Int. Ed.*, **11**, 92 (1972); https://doi.org/10.1002/anie.197200921
293. C.Yu, L.Jiao, T.Li, Q.Wu, W.Miao, J.Wang, Y.Wei, X.Mu, E.Hao. *Chem. Commun*., **51**, 16852 (2015); https://doi.org/10.1039/C5CC07304A

294. Q.Wu, G.Jia, B.Tang, X.Guo, H.Wu, C.Yu, E.Hao, L.Jiao. *Org. Lett*., **22**, 9239 (2020); https://doi.org/10.1021/acs.orglett.0c03441
295. H.Yokoi, N.Wachi, S.Hiroto, H.Shinokubo. *Chem. Commun*., **50**, 2715 (2014); https://doi.org/10.1039/C3CC48738E
296. Q.Gong, Q.Wu, X.Guo, W.Li, L.Wang, E.Hao, L.Jiao. *Org. Lett*., **23**, 7220 (2021); https://doi.org/10.1021/acs.orglett.1c02622
297. Q.Gong, Q.Wu, X.Guo, H.Li, W.Li, C.Yu, E.Hao, L.Jiao. *Org. Lett*., **23**, 7661 (2021); https://doi.org/10.1021/acs.orglett.1c02926
298. S.H.Röttger, L.J.Patalag, F.Hasenmaile, L.Milbrandt, B.Butschke, P.G.Jones, D.B.Werz. *Org. Lett*., **26**, 3020 (2024); https://doi.org/10.1021/acs.orglett.4c00827
299. L.Wang, C.Cheng, Z.-Y.Li, X.Guo, Q.Wu, E.Hao, L.Jiao. *Org. Lett*., **26**, 3026 (2024); https://doi.org/10.1021/acs.orglett.4c00669
300. L.J.Patalag, L.P.Ho, P.G.Jones, D.B.Werz. *J. Am. Chem. Soc*., **139**, 15104 (2017); https://doi.org/10.1021/jacs.7b08176
301. Q.Gong, K.Cheng, Q.Wu, W.Li, C.Yu, L.Jiao, E.Hao. *J. Org. Chem*., **86**, 15761 (2021); https://doi.org/10.1021/acs.joc.1c01824
302. Q.Wu, Z.Kang, Q.Gong, X.Guo, H.Wang, D.Wang, L.Jiao, E.Hao. *Org. Lett*., **22**, 7513 (2020); https://doi.org/10.1021/acs.orglett.0c02704
303. H.Kim, A.Burghart, M.B.Welch, J.Reibenspies, K.Burgess. *Chem. Commun*., 1889 (1999); https://doi.org/10.1039/a905739k
304. Y.Gabe, T.Ueno, Y.Urano, H.Kojima, T.Nagano. *Anal. Bio Anal. Chem*., **386**, 621 (2006); https://doi.org/10.1007/s00216-006-0587-y
305. B.Brizet, C.Bernhard, Y.Volkova, Y.Rousselin, P.D.Harvey, C.Goze, F.Denat. *Org. Biomol. Chem*., **11**, 7729 (2013); https://doi.org/10.1039/c3ob41370e
306. C.A.Wijesinghe, M.E.El-Khouly, J.D.Blakemore, M.E.Zandler, S.Fukuzumi, F.D'Souza. *Chem. Commun*., **46**, 3301 (2010); https://doi.org/10.1039/c000565g
307. C.A.Wijesinghe, M.E.El-Khouly, N.K.Subbaiyan, M.Supur, M.E.Zandler, K.Ohkubo, S.Fukuzumi, F.D'Souza. *Chem. – Eur. J*., **17**, 3147 (2011); https://doi.org/10.1002/chem.201002446
308. B.Brizet, A.Eggenspiller, C.P.Gros, J.-M.Barbe, C.Goze, F.Denat, P.D.Harvey. *J. Org. Chem.*, **77**, 3646 (2012); https://doi.org/10.1021/jo3000833
309. N.Umeda, H.Takahashi, M.Kamiya, T.Ueno, T.Komatsu, T.Terai, K.Hanaoka, T.Nagano, Y.Urano. *ACS Chem. Biol*., **9**, 2242 (2014); https://doi.org/10.1021/cb500525p
310. H.Tanaka, Y.Inoue, T.Mori. *ChemPhotoChem*, **2**, 386 (2018); https://doi.org/10.1002/cptc.201800015
311. Y.Zhang, S.Yu, B.Han, Y.Zhou, X.Zhang, X.Gao, Z.Tang. *Matter*, **5**, 837 (2022); https://doi.org/10.1016/j.matt.2022.01.001
312. E.M.Sánchez-Carnerero, F.Moreno, B.L.Maroto, A.R.Agarrabeitia, M.J.Ortiz, B.G.Vo, G.Muller, S.de la Moya. *J. Am. Chem. Soc*., **136**, 3346 (2014); https://doi.org/10.1021/ja412294s
313. S.Zhang, Y.Wang, F.Meng, C.Dai, Y.Cheng, C.Zhu. *Chem. Commun*., **51**, 9014 (2015); https://doi.org/10.1039/C5CC01994J
314. J.Jiménez, L.Cerdán, F.Moreno, B.L.Maroto, I.García-Moreno, J.L.Lunkley, G.Muller, S.de la Moya. *J. Phys. Chem. C*, **121**, 5287 (2017); https://doi.org/10.1021/acs.jpcc.7b00654
315. J.Jiménez, F.Moreno, B.L.Maroto, T.A.Cabreros, A.S.Huy, G.Muller, J.Bañuelos, S.de la Moya. *Chem. Commun*., **55**, 1631 (2019); https://doi.org/10.1039/C8CC09401B
316. J.Jiménez, C.Díaz-Norambuena, S.Serrano, S.C.Ma, F.Moreno, B.L.Maroto, J.Bañuelos, G.Muller, S.de la Moya. *Chem. Commun*., **57**, 5750 (2021); https://doi.org/10.1039/D1CC01255J
317. R.B.Alnoman, S.Rihn, D.C.O'Connor, F.A.Black, B.Costello, P.G.Waddell, W.Clegg, R.D.Peacock, W.Herrebout, J.G.Knight, M.J.Hall. *Chem. – Eur. J*., **22**, 93 (2016); https://doi.org/10.1002/chem.201504484
318. R.Clarke, K.L.Ho, A.A.Alsimaree, O.J.Woodford, P.G.Waddell, J.Bogaerts, W.Herrebout, J.G.Knight, R.Pal, T.J.Penfold, M.J.Hall. *ChemPhotoChem*, **1**, 513 (2017); https://doi.org/10.1002/cptc.201700106
319. R.G.Clarke, J.Weatherston, R.A.Taj-Aldeen, P.G.Waddell, W.McFarlane, T.J.Penfold, J.Bogaerts, W.Herrebout, L.E.Mackenzie, R.Pal, M.J.Hall. *ChemPhotoChem*, **7**, e202200194 (2023); https://doi.org/10.1002/cptc.202200194
320. T.W.Hudnall, F.P.Gabbaï. *Chem. Commun*., 4596 (2008); https://doi.org/10.1039/b808740g
321. J.A.Hendricks, E.J.Keliher, D.Wan, S.A.Hilderbrand, R.Weissleder, R.Mazitschek. *Angew. Chem., Int. Ed*., **51**, 4603 (2012); https://doi.org/10.1002/anie.201107957
322. A.M.Courtis, S.A.Santos, Y.Guan, J.A.Hendricks, B.Ghosh, D.M.Szantai-Kis, S.A.Reis, J.V.Shah, R.Mazitschek. *Bioconjug. Chem*., **25**, 1043 (2014); https://doi.org/10.1021/bc400575w
323. T.Lundrigan, S.M.Crawford, T.S.Cameron, A.Thompson. *Chem. Commun*., **48**, 1003 (2012); https://doi.org/10.1039/C1CC16351E
324. T.Lundrigan, A.Thompson. *J. Org. Chem*., **78**, 757 (2013); https://doi.org/10.1021/jo302277d
325. C.Ray, L.Díaz-Casado, E.Avellanal-Zaballa, J.Bañuelos, L.Cerdán, I.García-Moreno, F.Moreno, B.L.Maroto, Í.López-Arbeloa, S.de la Moya. *Chem. – Eur. J*., **23**, 9383 (2017); https://doi.org/10.1002/chem.201701350
326. G.Zhang, M.Wang, F.R.Fronczek, K.M.Smith, M.G.H.Vicente. *Inorg. Chem*., **57**, 14493 (2018); https://doi.org/10.1021/acs.inorgchem.8b02775
327. C.Ray, A.García-Sampedro, C.Schad, E.Avellanal-Zaballa, F.Moreno, M.J.Ortiz, J.Bañuelos, A.Villanueva, P.Acedo, B.L.Maroto, S.de la Moya. *Chem. Proc*., **3** (1), 15 (2021); https://doi.org/10.3390/ecsoc-24-08374
328. C.Ray, E.Avellanal-Zaballa, M.Muñoz-Úbeda, J.Colligan, F.Moreno, G.Muller, I.López-Montero, J.Bañuelos, B.L.Maroto, S.de la Moya. *Org. Chem. Front*., **10**, 5834 (2023); https://doi.org/10.1039/D3QO01561K
329. M.Wang, G.Zhang, P.Bobadova-Parvanova, A.N.Merriweather, L.Odom, D.Barbosa, F.R.Fronczek, K.M.Smith, M.G.H.Vicente. *Inorg. Chem*., **58**, 11614 (2019); https://doi.org/10.1021/acs.inorgchem.9b01474
330. M.Wang, G.Zhang, P.Bobadova-Parvanova, K.M.Smith, M.G.H.Vicente. *J. Org. Chem.*, **86**, 18030 (2021); https://doi.org/10.1021/acs.joc.1c02328
331. C.Ray, C.Schad, F.Moreno, B.L.Maroto, J.Bañuelos, T.Arbeloa, I.García-Moreno, C.Villafuerte, G.Muller, S.de la Moya. *J. Org. Chem*., **85**, 4594 (2020); https://doi.org/10.1021/acs.joc.9b03059
332. G.Ulrich, C.Goze, M.Guardigli, A.Roda, R.Ziessel. *Angew. Chem., Int. Ed*., **44**, 3694 (2005); https://doi.org/10.1002/anie.200500808
333. C.Goze, G.Ulrich, L.J.Mallon, B.D.Allen, A.Harriman, R.Ziessel. *J. Am. Chem. Soc*., **128**, 10231 (2006); https://doi.org/10.1021/ja062405a
334. A.Harriman, G.Izzet, R.Ziessel. *J. Am. Chem. Soc*., **128**, 10868 (2006); https://doi.org/10.1021/ja0631448
335. S.Goeb, R.Ziessel. *Org. Lett*., **9**, 737 (2007); https://doi.org/10.1021/ol0627404
336. L.Bonardi, G.Ulrich, R.Ziessel. *Org. Lett*., **10**, 2183 (2008); https://doi.org/10.1021/ol800560b
337. S.L.Niu, G.Ulrich, R.Ziessel, A.Kiss, P.-Y.Renard, A.Romieu. *Org. Lett*., **11**, 2049 (2009); https://doi.org/10.1021/ol900302n
338. S.Niu, C.Massif, G.Ulrich, P.Renard, A.Romieu, R.Ziessel. *Chem. – Eur. J*., **18**, 7229 (2012); https://doi.org/10.1002/chem.201103613
339. T.Bura, R.Ziessel. *Org. Lett*., **13**, 3072 (2011); https://doi.org/10.1021/ol200969r
340. A.Haefele, C.Zedde, P.Retailleau, G.Ulrich, R.Ziessel. *Org. Lett*., **12**, 1672 (2010); https://doi.org/10.1021/ol100109j

341. A.B.More, S.Mula, S.Thakare, N.Sekar, A.K.Ray, S.Chattopadhyay. *J. Org. Chem*., **79**, 10981 (2014); https://doi.org/10.1021/jo502028g
342. J.W.Campbell, M.T.Tung, K.N.Robertson, A.A.Beharry, A.Thompson. *J. Org. Chem*., **88**, 10655 (2023); https://doi.org/10.1021/acs.joc.3c00708
343. X.-D.Jiang, J.Zhang, T.Furuyama, W.Zhao. *Org. Lett*., **14**, 248 (2012); https://doi.org/10.1021/ol2030229
344. H.Manzano, I.Esnal, T.Marqués-Matesanz, J.Bañuelos, I.López-Arbeloa, M.J.Ortiz, L.Cerdán, A.Costela, I.García-Moreno, J.L.Chiara. *Adv. Funct. Mater.*, **26**, 2756 (2016); https://doi.org/10.1002/adfm.201505051